AD-A190 567 PARAMETER-ADAPTIVE MODEL-FOLLOWING FOR IN-FLIGHT SIMULATION(U) AIR FORCE INST OF TECH WRIGHT-PATTERSON AFB OH SCHOOL OF ENGINEERING L A PINEIRO DEC 87 AFIT/GE/ENG/87D-74 1/4

UNCLASSIFIED F/G 1/3.3 NL

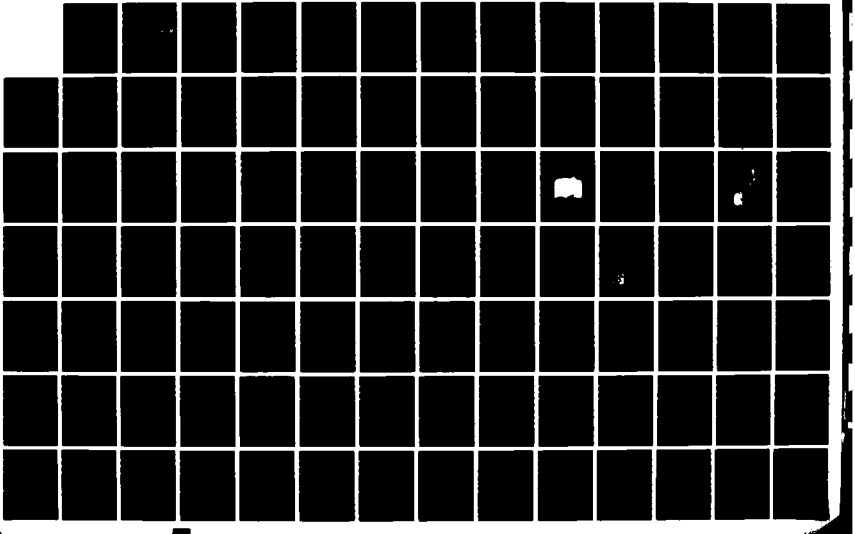

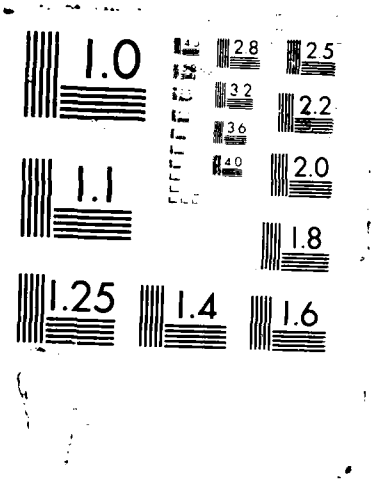
1.0
1.1
1.25
1.4
1.6
1.8
2.0
2.2
2.5
2.8
3.2
3.6
4.0

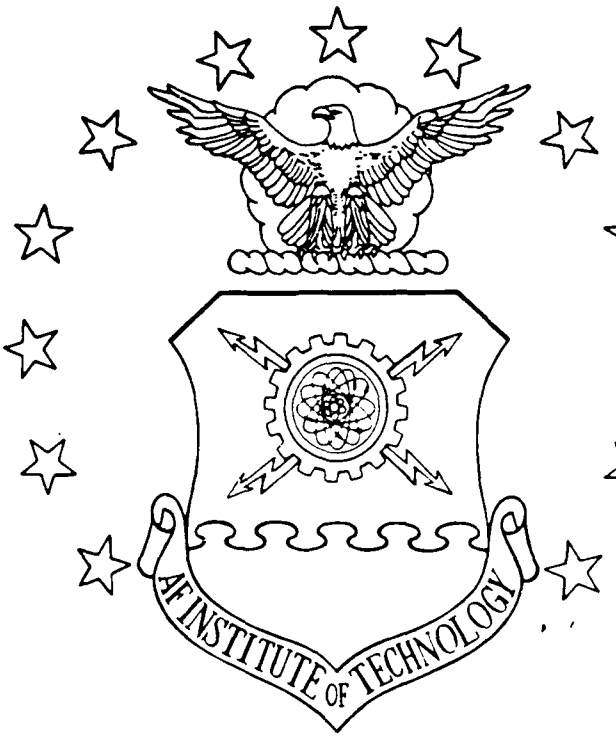

PARAMETER-ADAPTIVE MODEL-FOLLOWING FOR IN-FLIGHT SIMULATION

THESIS

Luis A. Pineiro
Capt. USAF

AFIT/GE/ENG/87D-74

DEPARTMENT OF THE AIR FORCE
AIR UNIVERSITY
AIR FORCE INSTITUTE OF TECHNOLOGY

Wright-Patterson Air Force Base, Ohio

AFIT/GE/ENG/87D-74

PARAMETER-ADAPTIVE MODEL-FOLLOWING FOR IN-FLIGHT SIMULATION

THESIS

Luis A. Pineiro
Capt. USAF

AFIT/GE/ENG/87D-74

AFIT/GE/ENG/87D-74

PARAMETER-ADAPTIVE MODEL-FOLLOWING FOR IN-FLIGHT SIMULATION

THESIS

Presented to the Faculty of the School of Engineering

of the Air Force Institute of Technology

Air University

In Partial Fulfillment of the

Requirements for the Degree of

Master of Science in Electrical Engineering

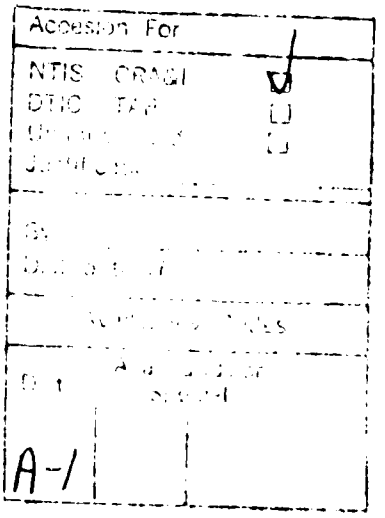

Luis A. Pimeiro, B. S. E. E.

Captain, USAF

December 1987

Aproved for public release; distribution unlimited

Preface

This thesis investigates the development of preliminary designs for parameter-adaptive longitudinal flight control laws for possible application in model-following variable stability systems for in-flight simulations. The control law theorethical background is based on techniques developed by Professor Brian Porter from the University of Salford, England, while the recursive identification theory is based on techniques develped by Tore Hagglung from the Lund Institute of Technology in Sweden.

I wish to thank the personnel of the Variable stability In-flight Simulator Test Aircraft Program Office of the Flight Dynamics Laboratory for sponsoring this effort. I would like also to thank Capt. Joe Anderson and Mr. Fred Unfried from the Control Synthesis Branch in the Flight Dynamics Laboratory for their assistance in obtaining modeling data for the AFTI/F-16 aircraft which is used in this investigation.

My special thanks are extended to my thesis advisor LT. Col. Daniel J. Biezad, commitee members Professor John J. D'azzo and LT. Col Zdzislaw H. Lewantowicz from the AFIT faculty, Prof. Brian Porter from the University of Salford, England, and Capt. Robert Eslinger from the Control Systems Development Branch in the Flight Dynamics Laboratory, for their invaluable assistance and guidance during this study.

Finally, I want to express my love and deep appreciation to my wife, Ruth, for her patience and understanding during this endeavor. I would also like to thank my parents for all their love and support, and Maj. Douglas Porter, for his encouragement during my early stages of graduate work.

— Capt. Luis A. Pineiro

Table of Content

		Page
Preface		ii
List of Figures		vi
List of Tables		xxvi
List of Symbols		xxvii
Abstract		xxxii
I.	Introduction	1
	1.1 Background	1
	1.2 Problem Description	3
	1.3 Approach	7
	1.4 Problem Statement	8
	1.5 Scope	9
	1.6 Overview	12
II.	Control Law Development	14
	2.1 Introduction	14
	2.2 Summary of Current Model-Folowing Techniques	16
	2.3 Porter's Method	21
	2.3.1 Fixed Gain Control Law	21
	2.3.2 Adaptive Control Law	27
III.	Recursive Identification	28
	3.1 Introduction	28
	3.2 Input-output model specification	29
	3.3 Recursive Least Squares Algorithm	35
	3.4 Hagglund's Algorithm	45
IV.	Design Process	62
	4.1 Introduction	62
	4.2 Aircraft Model	63
	4.3 Control Law Design	76
	4.3.1 Mathematical Background	76
	4.3.2 Design Variables	80
	4.3.3 Command Maneuver	85
	4.3.4 Design Simulations	85
	4.3.5 Parameter Variation and Sensor Noise	117
	4.4 Parameter Identifier Design	117
	4.4.1 Design Variables	117
	4.4.2 Parameter Estimate Variance	118

4.4.3 Fault Detector Design 119
4.4.4 Noise Variance Estimator Design 120
4.4.5 Practical Signal Processing Considerations 121

V. Results 132

5.1 Introduction 132
5.2 Fixed Gain Controller Responses 132
5.2.1 Plant Parameter Change 132
5.2.2 Plant Parameter Change and Sensor Noise 138
5.3 Parameter-Adaptive Controller 147
5.3.1 Fixed Plant Dynamics 147
5.3.2 Fixed Plant Dynamics and Sensor Noise . 158
5.3.3 Plant Parameter Change 168
5.3.4 Plant Parameter Change and Sensor Noise 178
5.3.5 Identification of Entire Parameter Vector with Full, and Reduced Order Models . . 198

VI. Conclusions and Recommendations 237

6.1 Design Results 237
6.2 Proposed Future Work 237

Appendix A: AFTI F-16 Aircraft Data 244
State Space and Difference Equation Model Data 245

Appendix B: Equivalence Between the Step-Response Matrix and the Difference Equation Model's Matrix Coefficient B_1 247

Appendix C: Implementation Details of the Recursive Identification Algorithm 250

Appendix D: Root-Locus Analysis and Time Response Checks with Regards to Functional Controllability 259

Bibliography 280

Vita 284

List of Figures

Figure		Page
1-1	NT-33 In-Flight Simulator	2
1-2	VISTA/F-16 Configuration	4
1-3	VISTA/F-16 Features	5
1-4	VISTA/F-16 Flight/Simulation Envelope	6
1-5	Parameter-Adaptive Control System	8
1-6	Initial VISTA/F-16 Configuration	10
1-7	AFTI/F-16 Aircraft	11
2-1	Response Feedback Concept	15
2-2	Model Following Concept	17
2-3	Explicit Model Following System	18
2-4	Improved Explicit Model Following System	19
3-1	Effect of Forgetting Factor in Transient Response of Parameter Estimates	41
3-2	Parameter-Adaptive Control System with Supervision Functions	44
3-3	The Error Frequency f_f Versus the Threshold r_0	54
3-4	Possible Choice of the Eigenvalue $\nu(kT)$	56
4-1	Aircraft Axis System	64
4-2	Aircraft Dynamics Representation	67
4-3	Gain Scheduler Function for the Aircraft's A Matrix	68
4-4	Gain Scheduler Function for the Aircraft's B Matrix	69
4-5	Actuator Model Representation	70
4-6	Limited Integrator Function Representation	71

4-7 Definition of Positive Control Surface Deflections . . 74

4-8 Sensor Measurement Noise Representation 75

4-9 Control Law Representation 83

4-10 Closed-Loop System Representation 84

4-11 Model-Following Simulation Geometry 86

4-12 Flight Path Command Maneuver (deg) 87

4-13 Pitch Rate Command Maneuver (deg/sec) 87

4-14 Flight Path Angle Command and Response (deg)
Σ = diag{ 0.1, 0.7 }, ρ = 0.8 89

4-15 Flight Path Angle Tracking Performance Index (deg)
Σ = diag{ 0.1, 0.7 }, ρ = 0.8 89

4-16 Pitch Rate Command and Response (deg/sec)
Σ = diag{ 0.1, 0.7 }, ρ = 0.8 90

4-17 Pitch Rate Tracking Performance Index (deg/sec)
Σ = diag{ 0.1, 0.7 }, ρ = 0.8 90

4-18 Elevator Deflection (deg)
Σ = diag{ 0.1, 0.7 }, ρ = 0.8 91

4-19 Elevator Deflection Rate (deg/sec)
Σ = diag{ 0.1, 0.7 }, ρ = 0.8 91

4-20 Flaperon Deflection (deg)
Σ = diag{ 0.1, 0.7 }, ρ = 0.8 92

4-21 Flaperon Deflection Rate (deg/sec)
Σ = diag{ 0.1, 0.7 }, ρ = 0.8 92

4-22 Flight Path Angle Command and Response (deg)
Σ = diag{ 0.3, 0.7 }, ρ = 0.8 93

4-23 Flight Path Angle Tracking Performance Index (deg)
Σ = diag{ 0.3, 0.7 }, ρ = 0.8 93

4-24 Pitch Rate Command and Response (deg/sec)
Σ = diag{ 0.3, 0.7 }, ρ = 0.8 94

4-25 Pitch Rate Tracking Performance Index (deg/sec)
Σ = diag{ 0.3, 0.7 }, ρ = 0.8 94

4-26 Elevator Deflection (deg)
Σ = diag{ 0.3, 0.7 }, ρ = 0.8 95

4-27 Elevator Deflection Rate (deg/sec)
Σ = diag{ 0.3, 0.7 }, ρ = 0.8 95

4-28 Flaperon Deflection (deg)
Σ = diag{ 0.3, 0.7 }, ρ = 0.8 96

4-29 Flaperon Deflection Rate (deg/sec)
Σ = diag{ 0.3, 0.7 }, ρ = 0.8 96

4-30 Flight Path Angle Command and Response (deg)
Σ = diag{ 0.5, 0.7 }, ρ = 0.8 97

4-31 Flight Path Angle Tracking Performance Index (deg)
Σ = diag{ 0.5, 0.7 }, ρ = 0.8 97

4-32 Pitch Rate Command and Response (deg/sec)
Σ = diag{ 0.5, 0.7 }, ρ = 0.8 98

4-33 Pitch Rate Tracking Performance Index (deg/sec)
Σ = diag{ 0.5, 0.7 }, ρ = 0.8 98

4-34 Elevator Deflection (deg)
Σ = diag{ 0.5, 0.7 }, ρ = 0.8 99

4-35 Elevator Deflection Rate (deg/sec)
Σ = diag{ 0.5, 0.7 }, ρ = 0.8 99

4-36 Flaperon Deflection (deg)
Σ = diag{ 0.5, 0.7 }, ρ = 0.8 100

4-37 Flaperon Deflection Rate (deg/sec)
Σ = diag{ 0.5, 0.7 }, ρ = 0.8 100

4-38 Flight Path Angle Command and Response (deg)
Σ = diag{ 0.3, 0.5 }, ρ = 0.8 101

4-39 Flight Path Angle Tracking Performance Index (deg)
Σ = diag{ 0.3, 0.5 }, ρ = 0.8 101

4-40 Pitch Rate Command and Response (deg/sec)
Σ = diag{ 0.3, 0.5 }, ρ = 0.8 102

4-41 Pitch Rate Tracking Performance Index (deg/sec)
Σ = diag{ 0.3, 0.5 }, ρ = 0.8 102

4-42 Elevator Deflection (deg)
Σ = diag{ 0.3, 0.5 }, ρ = 0.8 103

4-43 Elevator Deflection Rate (deg/sec)
Σ = diag{ 0.3, 0.5 }, ρ = 0.8 103

4-44 Flaperon Deflection (deg)
Σ = diag{ 0.3, 0.5 }, ρ = 0.8 104

4-45 Flaperon Deflection Rate (deg/sec)
Σ = diag{ 0.3, 0.5 }, ρ = 0.8 104

4-46 Flight Path Angle Command and Response (deg)
Σ = diag{ 0.3, 0.8 }, ρ = 0.8 105

4-47 Flight Path Angle Tracking Performance Index (deg)
Σ = diag{ 0.3, 0.8 }, ρ = 0.8 105

4-48 Pitch Rate Command and Response (deg/sec)
Σ = diag{ 0.3, 0.8 }, ρ = 0.8 106

4-49 Pitch Rate Tracking Performance Index (deg/sec)
Σ = diag{ 0.3, 0.8 }, ρ = 0.8 106

4-50 Elevator Deflection (deg)
Σ = diag{ 0.3, 0.8 }, ρ = 0.8 107

4-51 Elevator Deflection Rate (deg/sec)
Σ = diag{ 0.3, 0.8 }, ρ = 0.8 107

4-52 Flaperon Deflection (deg)
Σ = diag{ 0.3, 0.8 }, ρ = 0.8 108

4-53 Flaperon Deflection Rate (deg/sec)
Σ = diag{ 0.3, 0.8 }, ρ = 0.8 108

4-54 Flight Path Angle Command and Response (deg)
Σ = diag{ 0.3, 0.7 }, ρ = 0.6 109

4-55 Flight Path Angle Tracking Performance Index (deg)
Σ = diag{ 0.3, 0.7 }, ρ = 0.6 109

4-56 Pitch Rate Command and Response (deg/sec)
Σ = diag{ 0.3, 0.7 }, ρ = 0.6 110

4-57 Pitch Rate Tracking Performance Index (deg/sec)
Σ = diag{ 0.3, 0.7 }, ρ = 0.6 110

4-58 Elevator Deflection (deg)
Σ = diag{ 0.3, 0.7 }, ρ = 0.6 111

4-59 Elevator Deflection Rate (deg/sec)
Σ = diag{ 0.3, 0.7 }, ρ = 0.6 111

4-60 Flaperon Deflection (deg)
Σ = diag{ 0.3, 0.7 }, ρ = 0.6 112

4-61 Flaperon Deflection Rate (deg/sec)
Σ = diag{ 0.3, 0.7 }, ρ = 0.6 112

4-62 Flight Path Angle Command and Response (deg)
Σ = diag{ 0.3, 0.7 }, ρ = 1.0 113

4-63 Flight Path Angle Tracking Performance Index (deg)
Σ = diag{ 0.3, 0.7 }, ρ = 1.0 113

4-64 Pitch Rate Command and Response (deg/sec)
Σ = diag{ 0.3, 0.7 }, ρ = 1.0 114

4-65 Pitch Rate Tracking Performance Index (deg/sec)
Σ = diag{ 0.3, 0.7 }, ρ = 1.0 114

4-66 Elevator Deflection (deg)
Σ = diag{ 0.3, 0.7 }, ρ = 1.0 115

4-67 Elevator Deflection Rate (deg/sec)
Σ = diag{ 0.3, 0.7 }, ρ = 1.0 115

4-68 Flaperon Deflection (deg)
Σ = diag{ 0.3, 0.7 }, ρ = 1.0 116

4-69 Flaperon Deflection Rate (deg/sec)
Σ = diag{ 0.3, 0.7 }, ρ = 1.0 116

4-70 Identification Algorithm implementation in $MATRIX_X$ . . 129

4-71 Performance Index Calculation 130

5-1 Flight Path Angle Command and Response (deg)
Fixed Gain Control Law. Plant Parameter Change 134

5-2 Flight Path Angle Tracking Performance Index (deg)
Fixed Gain Control Law. Plant Parameter Change 134

5-3 Pitch Rate Command and Response (deg/sec)
Fixed Gain Control Law. Plant Parameter Change 135

5-4 Pitch Rate Tracking Performnace Index (deg/sec)
Fixed Gain Control Law. Plant Parameter Change 135

5-5 Elevator Deflection (deg)
Fixed Gain Control Law. Plant Parameter Change 136

5-6 Elevator Deflection Rate (deg/sec)
Fixed Gain Control Law. Plant Parameter Change 136

5-7 Flaperon Deflection (deg)
Fixed Gain Control Law. Plant Parameter Change 137

5-8 Flaperon Deflection Rate (deg/sec)
Fixed Gain Control Law. Plant Parameter Change 137

5-9 Flight Path Angle Command and Response (deg)
Fixed Gain Control Law. Plant Parameter Change
and Sensor Noise (std. dev. = 0.0573 deg) 139

5-10 Flight Path Angle Tracking Performance Index (deg)
Fixed Gain Control Law. Plant Parameter Change
and Sensor Noise (std. dev. = 0.0573 deg) 139

5-11 Pitch Rate Command and Response (deg/sec)
Fixed Gain Control Law. Plant Parameter Change
and Sensor Noise (std. dev. = 0.0573 deg/sec) 140

5-12 Pitch Rate Tracking Performnace Index (deg/sec)
Fixed Gain Control Law. Plant Parameter Change
and Sensor Noise (std. dev. = 0.0573 deg/sec) 140

5-13 Elevator Deflection (deg)
Fixed Gain Control Law. Plant Parameter Change
and Sensor Noise (std. dev. = 0.0573 deg (deg/sec)) . . 141

5-14 Elevator Deflection Rate (deg/sec)
Fixed Gain Control Law. Plant Parameter Change
and Sensor Noise (std. dev. = 0.0573 deg (deg/sec)) . . 141

5-15 Flaperon Deflection (deg)
Fixed Gain Control Law. Plant Parameter Change
and Sensor Noise (std. dev. = 0.0573 deg (deg/sec)) . . 142

5-16 Flaperon Deflection Rate (deg/sec)
Fixed Gain Control Law. Plant Parameter Change
and Sensor Noise (std. dev. = 0.0573 deg (deg/sec)) . . 142

5-17 Flight Path Angle Command and Response (deg)
Fixed Gain Control Law. Plant Parameter Change
and Sensor Noise (std. dev. = 0.314 deg) 143

5-18 Flight Path Angle Tracking Performance Index (deg)
Fixed Gain Control Law. Plant Parameter Change
and Sensor Noise (std. dev. = 0.314 deg) 143

5-19 Pitch Rate Command and Response (deg/sec)
Fixed Gain Control Law. Plant Parameter Change
and Sensor Noise (std. dev. = 0.314 deg/sec) 144

5-20 Pitch Rate Tracking Performnace Index (deg/sec)
Fixed Gain Control Law. Plant Parameter Change
and Sensor Noise (std. dev. = 0.314 deg/sec) 144

5-21 Elevator Deflection (deg)
Fixed Gain Control Law. Plant Parameter Change
and Sensor Noise (std. dev. = 0.314 deg (deg/sec)) . . 145

5-22 Elevator Deflection Rate (deg/sec)
Fixed Gain Control Law. Plant Parameter Change
and Sensor Noise (std. dev. = 0.314 deg (deg/sec)) . . 145

5-23 Flaperon Deflection (deg)
Fixed Gain Control Law. Plant Parameter Change
and Sensor Noise (std. dev. = 0.314 deg (deg/sec)) . . 146

5-24 Flaperon Deflection Rate (deg/sec)
Fixed Gain Control Law. Plant Parameter Change
and Sensor Noise (std. dev. = 0.314 deg (deg/sec)) . . 146

5-25 Flight Path Angle Command and Response (deg)
Adaptive Control Law. No Plant Parameter Change 148

5-26 Flight Path Angle Tracking Performance Index (deg)
Adaptive Control Law. No Plant Parameter Change 148

5-27 Pitch Rate Command and Response (deg/sec)
Adaptive Control Law. No Plant Parameter Change 149

5-28 Pitch Rate Tracking Performnace Index (deg/sec)
Adaptive Control Law. No Plant Parameter Change 149

5-29 Elevator Deflection (deg)
Adaptive Control Law. No Plant Parameter Change 150

5-30 Elevator Deflection Rate (deg/sec)
Adaptive Control Law. No Plant Parameter Change 150

5-31 Flaperon Deflection (deg)
Adaptive Control Law. No Plant Parameter Change 151

5-32 Flaperon Deflection Rate (deg/sec)
Adaptive Control Law. No Plant Parameter Change 151

5-33 Fault Detector Test Signal 152

5-34 Estimate of Step-Response Matrix Element $h_{11}(kT)$ . . . 153

5-35 Covariance Matrix Element $p_{11}(kT)$ 153

5-36 Estimate of Step-Response Matrix Element $h_{12}(kT)$ . . . 154

5-37 Covariance Matrix Element $p_{22}(kT)$ 154

5-38 Estimate of Step-Response Matrix Element $h_{21}(kT)$ . . . 155

5-39 Covariance Matrix Element $p_{33}(kT)$ 155

5-40 Estimate of Step-Response Matrix Element $h_{22}(kT)$ . . . 156

5-41 Covariance Matrix Element $p_{44}(kT)$ 156

5-42 Flight Path Angle Command and Response (deg)
Adaptive Control Law. No Plant Parameter Change
and Sensor Noise (std. dev. = 0.00181 deg) 159

5-43 Flight Path Angle Tracking Performance Index (deg)
Adaptive Control Law. No Plant Parameter Change
and Sensor Noise (std. dev. = 0.00181 deg) 159

5-44 Pitch Rate Command and Response (deg/sec)
Adaptive Control Law. No Plant Parameter Change
and Sensor Noise (std. dev. = 0.00181 deg/sec) 160

5-45 Pitch Rate Tracking Performnace Index (deg/sec)
Adaptive Control Law. No Plant Parameter Change
and Sensor Noise (std. dev. = 0.00181 deg/sec) 160

5-46 Elevator Deflection (deg)
Adaptive Control Law. No Plant Parameter Change
and Sensor Noise (std. dev. = 0.00181 deg (deg/sec)) . 161

5-47 Elevator Deflection Rate (deg/sec)
Adaptive Control Law. No Plant Parameter Change
and Sensor Noise (std. dev. = 0.00181 deg (deg/sec.)) . 161

5-48 Flaperon Deflection (deg)
Adaptive Control Law. No Plant Parameter Change
and Sensor Noise (std. dev. = 0.00181 deg (deg/sec)) . 162

5-49 Flaperon Deflection Rate (deg/sec)
Adaptive Control Law. No Plant Parameter Change
and Sensor Noise (std. dev. = 0.00181 deg (deg/sec)) . 162

5-50 Fault Detector Test Signal with Sensor Noise
(std. dev. = 0.00181 deg (deg/sec)) 163

5-51 Estimate of Step-Response Matrix Element $h_{11}(kT)$ with
Sensor Noise. (std. dev. = 0.00181 deg (deg/sec)) . . . 164

5-52 Covariance Matrix Element $p_{11}(kT)$ with Sensor Noise
(std. dev. = 0.00181 deg (deg/sec)) 164

5-53 Estimate of Step-Response Matrix Element $h_{12}(kT)$ with
Sensor Noise. (std. dev. = 0.00181 deg (deg/sec)) . . . 165

5-54 Covariance Matrix Element $p_{22}(kT)$ with Sensor Noise
(std. dev. = 0.00181 deg (deg/sec)) 165

5-55 Estimate of Step-Response Matrix Element $h_{21}(kT)$ with Sensor Noise. (std. dev. = 0.00181 deg (deg/sec)) . . . 166

5-56 Covariance Matrix Element $p_{33}(kT)$ with Sensor Noise (std. dev. = 0.00181 deg (deg/sec)) 166

5-57 Estimate of Step-Response Matrix Element $h_{22}(kT)$ with Sensor Noise. (std. dev. = 0.00181 deg (deg/sec)) . . . 167

5-58 Covariance Matrix Element $p_{44}(kT)$ with Sensor Noise (std. dev. = 0.00181 deg (deg/sec)) 167

5-59 Flight Path Angle Command and Response (deg) Adaptive Control Law. Plant Parameter Change 169

5-60 Flight Path Angle Tracking Performance Index (deg) Adaptive Control Law. Plant Parameter Change 169

5-61 Pitch Rate Command and Response (deg/sec) Adaptive Control Law. Plant Parameter Change 170

5-62 Pitch Rate Tracking Performnace Index (deg/sec) Adaptive Control Law. Plant Parameter Change 170

5-63 Elevator Deflection (deg) Adaptive Control Law. Plant Parameter Change 171

5-64 Elevator Deflection Rate (deg/sec) Adaptive Control Law. Plant Parameter Change 171

5-65 Flaperon Deflection (deg) Adaptive Control Law. Plant Parameter Change 172

5-66 Flaperon Deflection Rate (deg/sec) Adaptive Control Law. Plant Parameter Change 172

5-67 Fault Detector Test Signal Plant Parameter Change 173

5-68 Estimate of Step-Response Matrix Element $h_{11}(kT)$ Plant Parameter Change 174

5-69 Covariance Matrix Element $p_{11}(kT)$ Plant Parameter Change 174

5-70 Estimate of Step-Response Matrix Element $h_{12}(kT)$ Plant Parameter chnage 175

5-71 Covariance Matrix Element $p_{22}(kT)$ Plant Parameter Change 175

5-72 Estimate of Step-Response Matrix Element $h_{21}(kT)$ Plant Parameter chnage 176

5-73 Covariance Matrix Element $p_{33}(kT)$ Plant Parameter Change 176

5-74 Estimate of Step-Response Matrix Element $h_{22}(kT)$ Plant Parameter Change 177

5-75 Covariance Matrix Element $p_{44}(kT)$ Plant Parameter Change 177

5-76 Flight Path Angle Command and Response (deg) Adaptive Control Law. Plant Parameter Change and Sensor Noise (std. dev. = 0.00181 deg) 179

5-77 Flight Path Angle Tracking Performance Index (deg) Adaptive Control Law. Plant Parameter Change and Sensor Noise (std. dev. = 0.00181 deg) 179

5-78 Pitch Rate Command and Response (deg/sec) Adaptive Control Law. Plant Parameter Change and Sensor Noise (std. dev. = 0.00181 deg/sec) 180

5-79 Pitch Rate Tracking Performnace Index (deg/sec) Adaptive Control Law. Plant Parameter Change and Sensor Noise (std. dev. = 0.00181 deg/sec) 180

5-80 Elevator Deflection (deg) Adaptive Control Law. Plant Parameter Change and Sensor Noise (std. dev. = 0.00181 deg (deg/sec)) . 181

5-81 Elevator Deflection Rate (deg/sec) Adaptive Control Law. Plant Parameter Change and Sensor Noise (std. dev. = 0.00181 deg (deg/sec)) . 181

5-82 Flaperon Deflection (deg) Adaptive Control Law. Plant Parameter Change and Sensor Noise (std. dev. = 0.00181 deg (deg/sec)) . 182

5-83 Flaperon Deflection Rate (deg/sec) Adaptive Control Law. Plant Parameter Change and Sensor Noise (std. dev. = 0.00181 deg (deg/sec)) . 182

5-84 Fault Detector Test Signal with Plant Parameter Change and Sensor Noise (std. dev. = 0.00181 deg (deg/sec)) . 183

5-85 Estimate of Step-Response Matrix Element $h_{11}(kT)$ with Sensor Noise (std. dev. = 0.00181 deg (deg/sec)) . . . 184

5-86 Covariance Matrix Element $p_{11}(kT)$ with Sensor Noise (std. dev. = 0.00181 deg (deg/sec)) 184

5-87 Estimate of Step-Response Matrix Element $h_{12}(kT)$ with Sensor Noise (std. dev. = 0.00181 deg (deg/sec)) . . . 185

5-88 Covariance Matrix Element $p_{22}(kT)$ with Sensor Noise (std. dev. = 0.00181 deg (deg/sec)) 185

5-89 Estimate of Step-Response Matrix Element $h_{21}(kT)$ with Sensor Noise. (std. dev. = 0.00181 deg (deg/sec)) . . . 186

5-90 Covariance Matrix Element $p_{33}(kT)$ with Sensor Noise (std. dev. = 0.00181 deg (deg/sec)) 186

5-91 Estimate of Step-Response Matrix Element $h_{22}(kT)$ with Sensor Noise. (std. dev. = 0.00181 deg (deg/sec)) . . . 187

5-92 Covariance Matrix Element $p_{44}(kT)$ with Sensor Noise (std. dev. = 0.00181 deg (deg/sec)) 187

5-93 Flight Path Angle Command and Response (deg) Adaptive Control Law. Plant Parameter Change and Sensor Noise (std. dev. = 0.00181 deg) Scaled Algorithm (SF = 100) 189

5-94 Flight Path Angle Tracking Performance Index (deg) Adaptive Control Law. Plant Parameter Change and Sensor Noise (std. dev. = 0.00181 deg) Scaled Algorithm (SF = 100) 189

5-95 Pitch Rate Command and Response (deg/sec) Adaptive Control Law. Plant Parameter Change and Sensor Noise (std. dev. = 0.00181 deg/sec) Scaled Algorithm (SF = 100) 190

5-96 Pitch Rate Tracking Performnace Index (deg/sec) Adaptive Control Law. Plant Parameter Change and Sensor Noise (std. dev. = 0.00181 deg/sec) Scaled Algorithm (SF = 100) 190

5-97 Elevator Deflection (deg) Adaptive Control Law. Plant Parameter Change and Sensor Noise (std. dev. = 0.00181 deg (deg/sec)) Scaled Algorithm (SF = 100) 191

5-98 Elevator Deflection Rate (deg/sec) Adaptive Control Law. Plant Parameter Change and Sensor Noise (std. dev. = 0.00181 deg (deg/sec.)) Scaled Algorithm (SF = 100) 191

5-99 Flaperon Deflection (deg) Adaptive Control Law. Plant Parameter Change and Sensor Noise (std. dev. = 0.00181 deg (deg/sec)) Scaled Algorithm (SF = 100) 192

5-100 Flaperon Deflection Rate (deg/sec)
Adaptive Control Law. Plant Parameter Change and
Sensor Noise (std. dev. = 0.00181 deg (deg/sec))
Scaled Algorithm (SF = 100) 192

5-101 Fault Detector Test Signal with Sensor Noise
(std. dev. = 0.00181 deg (deg/sec))
Scaled Algorithm (SF = 100) 193

5-102 Estimate of Step-Response Matrix Element $h_{11}(kT)$ with
Sensor Noise. (std. dev. = 0.00181 deg (deg/sec))
Scaled Algorithm (SF = 100) 194

5-103 Covariance Matrix Element $p_{11}(kT)$ with Sensor Noise
(std. dev. = 0.00181 deg (deg/sec))
Scaled Algorithm (SF = 100) 194

5-104 Estimate of Step-Response Matrix Element $h_{12}(kT)$ with
Sensor Noise. (std. dev. = 0.00181 deg (deg/sec))
Scaled Algorithm (SF = 100) 195

5-105 Covariance Matrix Element $p_{22}(kT)$ with Sensor Noise
(std. dev. = 0.00181 deg (deg/sec))
Scaled Algorithm (SF = 100) 195

5-106 Estimate of Step-Response Matrix Element $h_{21}(kT)$ with
Sensor Noise. (std. dev. = 0.00181 deg (deg/sec))
Scaled Algorithm (SF = 100) 196

5-107 Covariance Matrix Element $p_{33}(kT)$ with Sensor Noise
(std. dev. = 0.00181 deg (deg/sec))
Scaled Algorithm (SF = 100) 196

5-108 Estimate of Step-Response Matrix Element $h_{22}(kT)$ with
Sensor Noise. (std. dev. = 0.00181 deg (deg/sec))
Scaled Algorithm (SF = 100) 197

5-109 Covariance Matrix Element $p_{44}(kT)$ with Sensor Noise
(std. dev. = 0.00181 deg (deg/sec))
Scaled Algorithm (SF = 100) 197

5-110 Flight Path Angle Command and Response (deg)
Adaptive Control Law. Plant Parameter Change and
Sensor Noise (std. dev. = 0.00573 deg)
Scaled Algorithm (SF = 100) 199

5-111 Flight Path Angle Tracking Performance Index (deg)
Adaptive Control Law. Plant Parameter Change and
Sensor Noise (std. dev. = 0.00573 deg)
Scaled Algorithm (SF = 100) 199

5-112 Pitch Rate Command and Response (deg/sec)
Adaptive Control Law. Plant Parameter Change and
Sensor Noise (std. dev. = 0.00573 deg/sec)
Scaled Algorithm (SF = 100) 200

5-113 Pitch Rate Tracking Performnace Index (deg/sec)
Adaptive Control Law. Plant Parameter Change and
Sensor Noise (std. dev. = 0.00573 deg/sec)
Scaled Algorithm (SF = 100) 200

5-114 Elevator Deflection (deg)
Adaptive Control Law. Plant Parameter Change and
Sensor Noise (std. dev. = 0.00573 deg (deg/sec))
Scaled Algorithm (SF = 100) 201

5-115 Elevator Deflection Rate (deg/sec)
Adaptive Control Law. Plant Parameter Change and
Sensor Noise (std. dev. = 0.00573 deg (deg/sec.))
Scaled Algorithm (SF = 100) 201

5-116 Flaperon Deflection (deg)
Adaptive Control Law. Plant Parameter Change and
Sensor Noise (std. dev. = 0.00573 deg (deg/sec))
Scaled Algorithm (SF = 100) 202

5-117 Flaperon Deflection Rate (deg/sec)
Adaptive Control Law. Plant Parameter Change and
Sensor Noise (std. dev. = 0.00573 deg (deg/sec))
Scaled Algorithm (SF = 100) 202

5-118 Fault Detector Test Signal with Sensor Noise
(std. dev. = 0.00573 deg (deg/sec))
Scaled Algorithm (SF = 100) 203

5-119 Estimate of Step-Response Matrix Element $h_{11}(kT)$ with
Sensor Noise. (std. dev. = 0.00573 deg (deg/sec))
Scaled Algorithm (SF = 100) 204

5-120 Covariance Matrix Element $p_{11}(kT)$ with Sensor Noise
(std. dev. = 0.00573 deg (deg/sec))
Scaled Algorithm (SF = 100) 204

5-121 Estimate of Step-Response Matrix Element $h_{12}(kT)$ with
Sensor Noise. (std. dev. = 0.00573 deg (deg/sec))
Scaled Algorithm (SF = 100) 205

5-122 Covariance Matrix Element $p_{22}(kT)$ with Sensor Noise
(std. dev. = 0.00573 deg (deg/sec))
Scaled Algorithm (SF = 100) 205

5-123 Estimate of Step-Response Matrix Element $h_{21}(kT)$ with Sensor Noise. (std. dev. = 0.00573 deg (deg/sec)) Scaled Algorithm (SF = 100) 206

5-124 Covariance Matrix Element $p_{33}(kT)$ with Sensor Noise (std. dev. = 0.00573 deg (deg/sec)) Scaled Algorithm (SF = 100) 206

5-125 Estimate of Step-Response Matrix Element $h_{22}(kT)$ with Sensor Noise. (std. dev. = 0.00573 deg (deg/sec)) Scaled Algorithm (SF = 100) 207

5-126 Covariance Matrix Element $p_{44}(kT)$ with Sensor Noise (std. dev. = 0.00573 deg (deg/sec)) Scaled Algorithm (SF = 100) 207

5-127 Flight Path Angle Command and Response (deg) Adaptive Control Law. Plant Parameter Change Identification of Full 4th Order Model 209

5-128 Flight Path Angle Tracking Performance Index (deg) Adaptive Control Law. Plant Parameter Change Identification of Full 4th Order Model 209

5-129 Pitch Rate Command and Response (deg/sec) Adaptive Control Law. Plant Parameter Change Identification of Full 4th Order Model 210

5-130 Pitch Rate Tracking Performnace Index (deg/sec) Adaptive Control Law. Plant Parameter Change Identification of Full 4th Order Model 210

5-131 Elevator Deflection (deg) Adaptive Control Law. Plant Parameter Change Identification of Full 4th Order Model 211

5-132 Elevator Deflection Rate (deg/sec) Adaptive Control Law. Plant Parameter Change Identification of Full 4th Order Model 211

5-133 Flaperon Deflection (deg) Adaptive Control Law. Plant Parameter Change Identification of Full 4th Order Model 212

5-134 Flaperon Deflection Rate (deg/sec) Adaptive Control Law. Plant Parameter Change Identification of Full 4th Order Model 212

5-135 Fault Detector Test Signal Identification of Full 4th Order Model 213

5-136 Estimate of Step-Response Matrix Element $h_{11}(kT)$
Identification of Full 4th Order Model 214

5-137 Covariance Matrix Element $p_{11}(kT)$
Identification of Full 4th Order Model 214

5-138 Estimate of Step-Response Matrix Element $h_{12}(kT)$
Identification of Full 4th Order Model 215

5-139 Covariance Matrix Element $p_{22}(kT)$
Identification of Full 4th Order Model 215

5-140 Estimate of Step-Response Matrix Element $h_{21}(kT)$
Identification of Full 4th Order Model 216

5-141 Covariance Matrix Element $p_{33}(kT)$
Identification of Full 4th Order Model 216

5-142 Estimate of Step-Response Matrix Element $h_{22}(kT)$
Identification of Full 4th Order Model 217

5-143 Covariance Matrix Element $p_{44}(kT)$
Identification of Full 4th Order Model 217

5-144 Flight Path Angle Command and Response (deg)
Adaptive Control Law. Plant Parameter Change
Identification of Full 3rd Order Model 218

5-145 Flight Path Angle Tracking Performance Index (deg)
Adaptive Control Law. Plant Parameter Change
Identification of Full 3rd Order Model 218

5-146 Pitch Rate Command and Response (deg/sec)
Adaptive Control Law. Plant Parameter Change
Identification of Full 3rd Order Model 219

5-147 Pitch Rate Tracking Performnace Index (deg/sec)
Adaptive Control Law. Plant Parameter Change
Identification of Full 3rd Order Model 219

5-148 Elevator Deflection (deg)
Adaptive Control Law. Plant Parameter Change
Identification of Full 3rd Order Model 220

5-149 Elevator Deflection Rate (deg/sec)
Adaptive Control Law. Plant Parameter Change
Identification of Full 3rd Order Model 220

5-150 Flaperon Deflection (deg)
Adaptive Control Law. Plant Parameter Change
Identification of Full 3rd Order Model 221

5-151 Flaperon Deflection Rate (deg/sec)
Adaptive Control Law. Plant Parameter Change
Identification of Full 3rd Order Model 221

5-152 Fault Detector Test Signal
Identification of Full 3rd Order Model 222

5-153 Estimate of Step-Response Matrix Element $h_{11}(kT)$
Identification of Full 3rd Order Model 223

5-154 Covariance Matrix Element $p_{11}(kT)$
Identification of Full 3rd Order Model 223

5-155 Estimate of Step-Response Matrix Element $h_{12}(kT)$
Identification of Full 3rd Order Model 224

5-156 Covariance Matrix Element $p_{22}(kT)$
Identification of Full 3rd Order Model 224

5-157 Estimate of Step-Response Matrix Element $h_{21}(kT)$
Identification of Full 3rd Order Model 225

5-158 Covariance Matrix Element $p_{33}(kT)$
Identification of Full 3rd Order Model 225

5-159 Estimate of Step-Response Matrix Element $h_{22}(kT)$
Identification of Full 3rd Order Model 226

5-160 Covariance Matrix Element $p_{44}(kT)$
Identification of Full 3rd Order Model 226

5-161 Flight Path Angle Command and Response (deg)
Adaptive Control Law. Plant Parameter Change
Identification of Full 2nd Order Model 227

5-162 Flight Path Angle Tracking Performance Index (deg)
Adaptive Control Law. Plant Parameter Change
Identification of Full 2nd Order Model 227

5-163 Pitch Rate Command and Response (deg/sec)
Adaptive Control Law. Plant Parameter Change
Identification of Full 2nd Order Model 228

5-164 Pitch Rate Tracking Performnace Index (deg/sec)
Adaptive Control Law. Plant Parameter Change
Identification of Full 2nd Order Model 228

5-165 Elevator Deflection (deg)
Adaptive Control Law. Plant Parameter Change
Identification of Full 2nd Order Model 229

5-166 Elevator Deflection Rate (deg/sec)
Adaptive Control Law. Plant Parameter Change
Identification of Full 2nd Order Model 229

5-167 Flaperon Deflection (deg)
Adaptive Control Law. Plant Parameter Change
Identification of Full 2nd Order Model 230

5-168 Flaperon Deflection Rate (deg/sec)
Adaptive Control Law. Plant Parameter Change
Identification of Full 2nd Order Model 230

5-169 Fault Detector Test Signal
Identification of Full 2nd Order Model 231

5-170 Estimate of Step-Response Matrix Element $h_{11}(kT)$
Identification of Full 2nd Order Model 232

5-171 Covariance Matrix Element $p_{11}(kT)$
Identification of Full 2nd Order Model 232

5-172 Estimate of Step-Response Matrix Element $h_{12}(kT)$
Identification of Full 2nd Order Model 233

5-173 Covariance Matrix Element $p_{22}(kT)$
Identification of Full 2nd Order Model 233

5-174 Estimate of Step-Response Matrix Element $h_{21}(kT)$
Identification of Full 2nd Order Model 234

5-175 Covariance Matrix Element $p_{33}(kT)$
Identification of Full 2nd Order Model 234

5-176 Estimate of Step-Response Matrix Element $h_{22}(kT)$
Identification of Full 2nd Order Model 235

5-177 Covariance Matrix Element $p_{44}(kT)$
Identification of Full 2nd Order Model 235

D-1 Flight Path Angle Command and Response (deg)
"Clipped" Flight Path Command 263

D-2 Flight Path Angle Tracking Performance Index (deg)
"Clipped" Flight Path Command 263

D-3 Pitch Rate Command and Response (deg/sec)
"Clipped" Flight Path Command 264

D-4 Pitch Rate Tracking Performnace Index (deg/sec)
"Clipped" Flight Path Command 264

D-5 Elevator Deflection (deg)
"Clipped" Flight Path Command 265

D-6 Elevator Deflection Rate (deg/sec)
"Clipped" Flight Path Command 265

D-7 Flaperon Deflection (deg)
"Clipped" Flight Path Command 266

D-8 Flaperon Deflection Rate (deg/sec)
"Clipped" Flight Path Command 266

D-9 Flight Path Angle Command and Response (deg)
Flight Path Command = 0 deg
No Integrator Limiter in Control Law 267

D-10 Flight Path Angle Tracking Performance Index (deg)
Flight Path Command = 0 deg
No Integrator Limiter in Control Law 267

D-11 Pitch Rate Command and Response (deg/sec)
Flight Path commnad = 0 deg
No Integrator Limiter in Control Law 268

D-12 Pitch Rate Tracking Performnace Index (deg/sec)
Flight Path Command = 0 deg
No Integrator Limiter in Control Law 268

D-13 Elevator Deflection (deg)
Flight Path Command = 0 deg
No Integrator Limiter in Control Law 269

D-14 Elevator Deflection Rate (deg/sec)
Flight Path Command = 0 deg
No Integrator Limiter in Control Law 269

D-15 Flaperon Deflection (deg)
Flight Path Command = 0 deg
No Integrator Limiter in Control Law 270

D-16 Flaperon Deflection Rate (deg/sec)
Flight Path Command = 0 deg
No Integrator Limiter in Control Law 270

D-17 Flight Path Angle Command and Response (deg)
Flight Path Command = 0 deg
Control Law with Integrator Limiter 271

D-18 Flight Path Angle Tracking Performance Index (deg)
Flight Path Command = 0 deg
Control Law with Integrator Limiter 271

D-19 Pitch Rate Command and Response (deg/sec)
Flight Path commnad = 0 deg
Control Law with Integrator Limiter 272

D-20 Pitch Rate Tracking Performnace Index (deg/sec)
Flight Path Command = 0 deg
Control Law with Integrator Limiter 272

D-21 Elevator Deflection (deg)
Flight Path Command = 0 deg
Control Law with Integrator Limiter 273

D-22 Elevator Deflection Rate (deg/sec)
Flight Path Command = 0 deg
Control Law with Integrator Limiter 273

D-23 Flaperon Deflection (deg)
Flight Path Command = 0 deg
Control Law with Integrator Limiter 274

D-24 Flaperon Deflection Rate (deg/sec)
Flight Path Command = 0 deg
Control Law with Integrator Limiter 274

D-25 Flight Path Angle Command and Response (deg)
Pitch Rate Command = 0 deg/sec
Control Law with Integrator Limiter 275

D-26 Flight Path Angle Tracking Performance Index (deg)
Pitch Rate Command = 0 deg/sec
Control Law with Integrator Limiter 275

D-27 Pitch Rate Command and Response (deg/sec)
Flight Path commnad = 0 deg
Control Law with Integrator Limiter 276

D-28 Pitch Rate Tracking Performnace Index (deg/sec)
Pitch Rate Command = 0 deg/sec
Control Law with Integrator Limiter 276

D-29 Elevator Deflection (deg)
Pitch Rate Command = 0 deg/sec
Control Law with Integrator Limiter 277

D-30 Elevator Deflection Rate (deg/sec)
Pitch Rate Command = 0 deg/sec
Control Law with Integrator Limiter 277

D-31 Flaperon Deflection (deg)
Pitch Rate Command = 0 deg/sec
Control Law with Integrator Limiter 278

D-32 Flaperon Deflection Rate (deg/sec)
Pitch Rate Command = 0 deg/sec
Control Law with Integrator Limiter 278

List of Tables

Table		Page
4-1	Control Surface Position and Rate Limits	73
4-2	Final Control Law Design Parameters	88
4-3	Final Estimation Algorithm Design Parameters	131
A-1	AFTI/F-16 Aircraft Data	244
A-2	AFTI/F-16 Aircraft Data for 0.9 Mach, 10,000 ft.	245
A-3	AFTI/F-16 Aircraft Data for 0.3 Mach, 10,000 ft.	246
D-1	Root-Locus Analysis, σ_1 Gain Sweep ($\sigma_2 = 0.7$, $\rho = 0.8$) . .	259
D-2	Root-Locus Analysis, σ_2 Gain Sweep ($\sigma_1 = 0.3$, $\rho = 0.8$) . .	260
D-3	Root-Locus Analysis, ρ Gain Sweep ($\sigma_1 = 0.3$, $\sigma_2 = 0.7$) . .	260

List of Symbols

A, A_p	Continuous-time host aircraft plant matrix
A_m	Model plant matrix
A_e	Error dynamics matrix
a	Desired variance of the parameter estimates
α	Angle of attack
$\alpha(kT)$	Discounting factor
B	Continuous-time input matrix
$\beta(kT)$	Fault detector's contribution to P
b	Wing span
C	Output matrix
C	Unit circle
c	Mean aerodynamic chord
cg	Center of gravity
deg	Degree
D(kT)	Diagonal matrix
$\delta(kT)$	Discounting factor
δ_e	Elevator deflection
δ_f	Flaperon deflection
e(t)	Continuous-time error vector
e(kT)	Discrete tracking error vector
$\varepsilon(kT)$	Discrete equation error vector
$\bar{\varepsilon}(kT)$	Prediction error
ft	Feet
f	Sampling frequency

f_f	error frequency
G(z)	Discrete transfer function matrix
$\Gamma(z)$	Discrete asymptotic transfer matrix
$\gamma 1, \gamma 2$	Desing parameters for fault detector
$\gamma 3$	Design parameter for noise variance estimator
γ	Flight path angle
H(T)	Step-response matrix
I_{xx}	Moment of inertia about x-axis
Iyy	Moment of inertia about y-axis
I_{zz}	Moment of inertia about z-axis
I_{xz}	Product of inertia about xz-axes
I	Identity matrix
I_m	Identity matrix of dimension m
J	Cost function
K	Control law anti-windup compensation gain
$K_1, \bar{K}_1$	Control law proportional gain matrix
$K_2, \bar{K}_2$	Control law integral gain matrix
K1	Model state rate multiplier matrix
K2	Model state multiplier matrix
K_p	Plant feedback matrix
lbs	pounds
M'_θ	Dimensional variation of pitching moment with pitch angle
M'_u	Dimensional variation of pitching moment with velocity
M'_α	Dimensional variation of pitching moment with angle of attack
M'_q	Dimensional variation of pitching moment with pitch rate
$M'_{\delta e}$	Dimensional variation of pitching moment with elevator deflection

$M'_{\delta f}$	Dimensional variation of pitching moment with flaperon deflection
M_C	Controllability matrix
M_O	Observability matrix
m	model aircraft, number of inputs and outputs
N	Order of difference equation model
$\mathcal{N}$	Total number of measurements
n	number of states
ν	Eigenvalue of estimation algorithm
$\Omega(kT)$	product of "fixed" portion of parameter vector, times its corresponding delayed measurements
ω	Filter corner frequency
P	Parameter covariance matrix
P[x]	Probability of x
Π	Control law anti-windup tuning matrix
ρ	Ratio of proportional to integral gain
Φ	Discrete plant matrix
Ψ	Discrete input matrix
q	Pitch rate
$\bar{q}$	Dynamic pressure
R(kT)	Information matrix
$r(kT)$	reference vector
r(kT)	Fault detector test signal
r_0, r_1	Fault detector thresholds
S	Surface area
s	Laplace operator
sec	Seconds

SF	Scale factor
σ	Elements of the Sigma (Σ) matrix, std. deviation
Σ	Control law gain weighting matrix
ξ	Input-output perturbation filter design constant
Ξ	Parameter estimate rate limiter constant
T	Sampling period
τ	Time delay, dummy integration variable
U(z)	Z transform of plant input vector
U(kT)	Upper diagonal matrix
u	Perturbation velocity along x-axis
u	Plant input vector
V	Noise signals
v(kT)	Estimate of the noise variance at time kT
W(kT)	Weighting function, estimate of average direction of parameter estimate updates
X'_θ	Dimensional variation of x-force with pitch angle
X'_u	Dimensional variation of x-force with velocity
X'_α	Dimensional variation of x-force with angle of attack
X'_q	Dimensional variation of x-force with pitch rate
$X'_{\delta e}$	Dimensional variation of x-force with elevator deflection
$X'_{\delta f}$	Dimensional variation of x-force with flaperon deflection
X, x	Aircraft states
Y(z)	Z transform of output vector
y	output vector
y_{model}	outputs from model aircraft
Z'_θ	Dimensional variation of z-force with pitch angle
Z'_u	Dimensional variation of z-force with velocity

Z'_{α}	Dimensional variation of z-force with angle of attack
Z'_{q}	Dimensional variation of z-force with pitch rate
$Z'_{\delta e}$	Dimensional variation of z-force with elevator deflection
$Z'_{\delta e}$	Dimensional variation of z-force with flaperon deflection
$\mathcal{Z}$	Z transform
$\mathcal{Z}_1, \mathcal{Z}_2, \mathcal{Z}_3$	Sets of closed-loop system roots
z	Z transform operator
$Z(kT)$	Discrete integral of the tracking error vector
θ	Pitch angle
Θ	Parameter vector
Θ'	Subset of Θ containing the elements of H(T)
$\hat{\Theta}$	Estimate of Θ
Υ	Input-output data measurements matrix
υ_i	Columns of Υ
λ	Forgetting factor

Abtract

In-flight simulations are normally accomplished by using model-following control laws which depend on accurate knowledge of the stability derivatives of the host aircraft. Degraded simulation performance may result if the stability derivatives deviate considerably from their presumed values. Gain scheduling is often employed to compensate for plant parameter variations, but this form of open-loop compensation usually requires extensive flight testing for proper fine tuning. This thesis implements an adaptive, fast-sampling control law to compensate for changing aircraft parameters. The step-response matrix which is required for this implementation is identified recursively using a recently developed technique which does not require special "test" signals and which automatically discounts old data depending on the input excitation detected. Tracking fidelity is maintained despite parameter changes which occur either abruptly or slowly. Simulations are conducted, using a model of the AFTI/F-16 aircraft and the control design package $MATRIX_X$, to test the resulting adaptive system. Actuator position and rate limits are discussed. The performance of the resulting system is excellent and demonstrates the relative advantages of adaptive controllers for in-flight simulation. Recommendations are made for future analysis including the use of moving-bank estimators.

PARAMETER-ADAPTIVE MODEL-FOLLOWING FOR IN-FLIGHT SIMULATION

I. Introduction

1.1 Background

Flight simulation plays an essential role in the development of modern day aircraft as well as pilot training. It can be conducted in a ground based simulator, or in actual flight, with a special class of aircraft called in-flight simulators. An in-flight simulator is an aircraft whose stability, feel, and flying characteristics can be changed to match those of another aircraft. This is accomplished by interfacing the pilot to the aircraft by means of a "fly-by-wire" variable stability flight control system and a programmable artificial feel system. As the pilot moves the controls, the aircraft responds as the simulated vehicle would. The pilot experiences the real flight motions and handling qualities of the simulated aircraft (29:38). In-flight simulators are essential tools in the research and development process that provide the capability to realistically and safely evaluate new or modified aircraft and weapon systems before first-flight and before committing to production (9). They have been used in the development of the F-16, YF-17, F-18, A-10, B-1, and Space Shuttle. Other uses invole many types of generic research, especially handling qualities, and for several types of specialized training, particularly at the Air Force and Navy Test Pilot Schools (29:38).

An NT-33A in-flight simulator (Figure 1-1), owned by the Flight Dynamics Laboratory at Wright-Patterson AFB and operated under contract by the CALSPAN corporation, has served effectively as a research tool for over 28 years. As new aircraft concepts become more complex, the limitation of the NT-33A to provide an in-flight simulation capability have become apparent. The NT-33A is becoming deficient in three areas: basic performance limitations, variable stability system limitations, and logistic supportability (8).

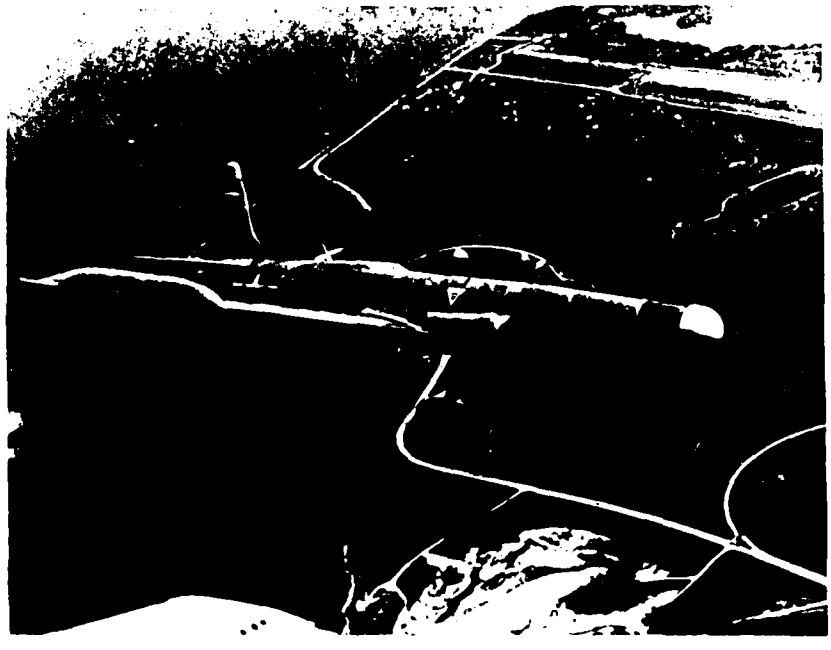

Figure 1-1. NT-33 In-Flight Simulator

A new in-flight simulator, which is based on present-day technology, will eliminate the mentioned areas of deficiency, and inherently accommodate the requirements of the foreseeable future. This advanced in-flight simulator, called VISTA (Variable stability In-flight

Simulator Test Aircraft), will meet future research needs by providing upgraded simulation capabilities (Figure 1-2). This will be accomplished by modifying a modern, high performance fighter aircraft with variable stability controls and a reprogrammable cockpit (Figure 1-3).

1.2 Problem Description

The dominant performance features of the VISTA/F-16 are likely to be a wide range of operating conditions in an expanded flight envelope (Figure 1-4), and large amplitude maneuvering (8,42). Both of these situations produce large variations in the stability derivatives of the host aircraft. This variation of parameters, coupled with initial uncertainty on their exact values, may adversely affect the fidelity of in-flight simulations (given a fixed parameter control law). The fidelity of an in-flight simulation is highly dependent on the ability of the variable stability system to either complement the natural stability derivatives of the host aircraft until they match those of the simulated vehicle (response feedback mode), or to establish a unity transfer function between the responses of a computer model of the simulated vehicle and the responses of the host aircraft (model-following mode) (39). In both cases it is necessary to have detailed knowledge of the host aircraft stability derivatives to perform a satisfactory simulation (39,42). Although gain scheduling is often used to alleviate plant parameter variation problems, this can at best be considered open-loop compensation which may require extensive flight testing for proper fine tuning.

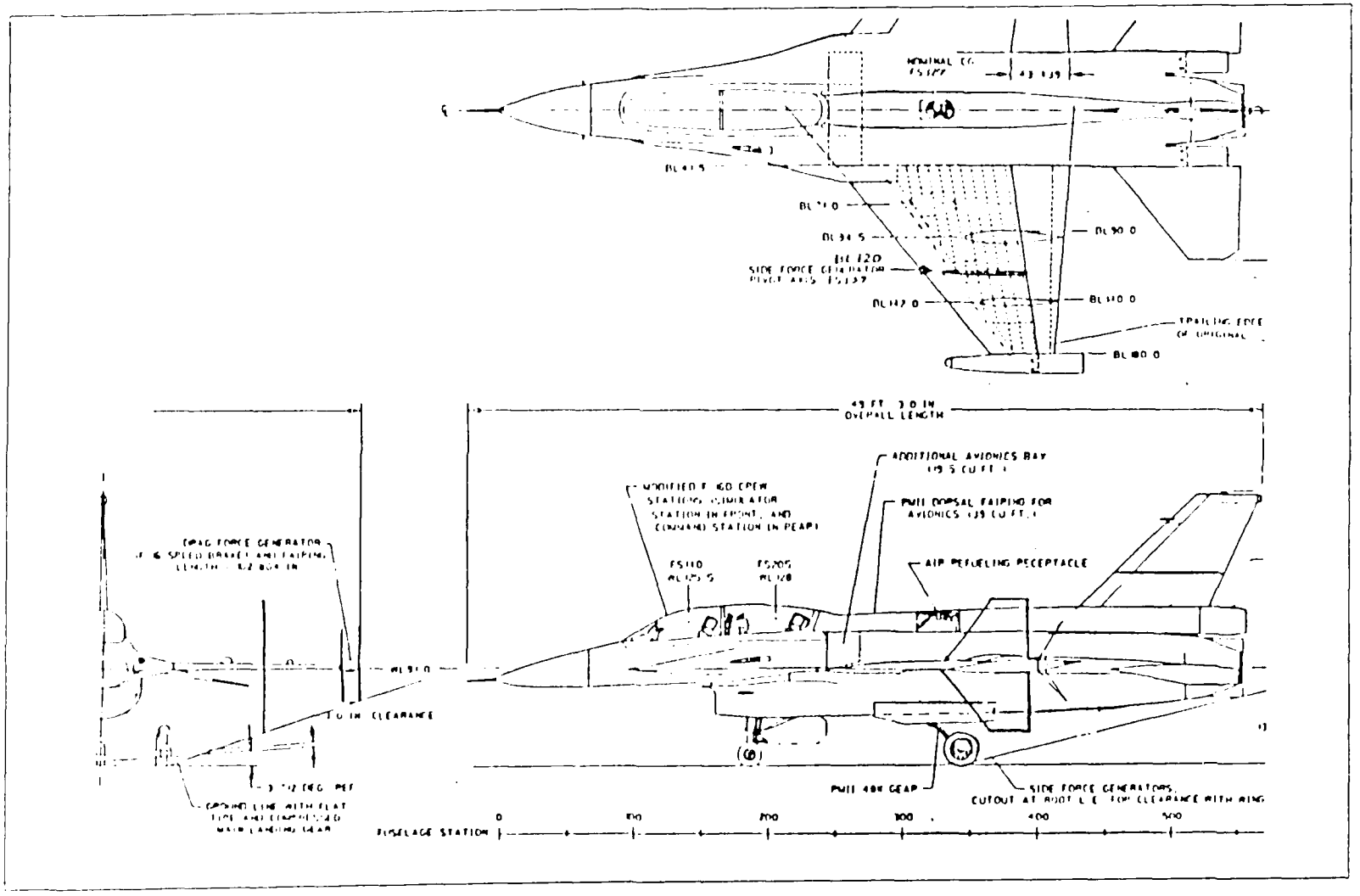

Figure 1-2. VISTA/F-16 Configuration

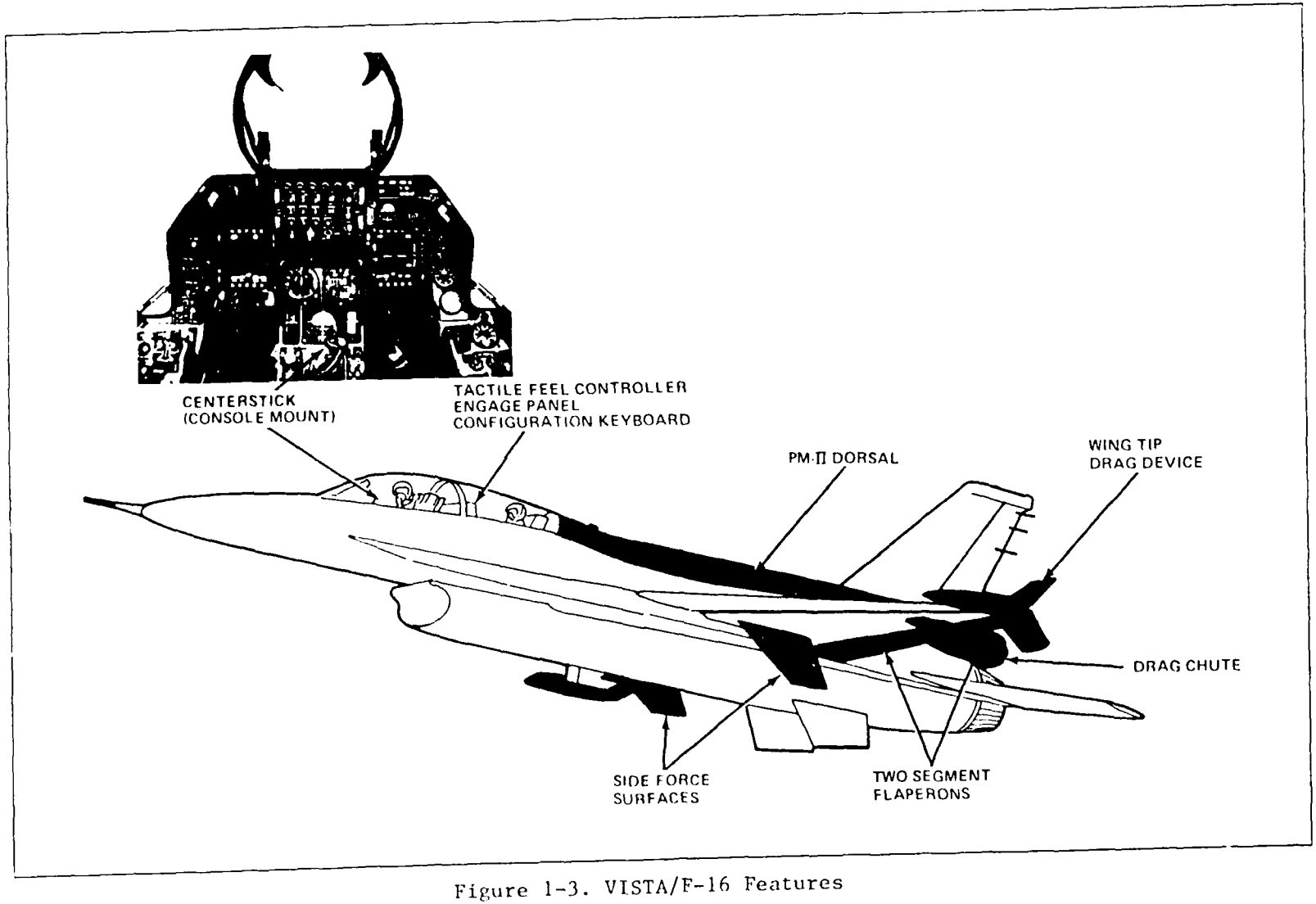

Figure 1-3. VISTA/F-16 Features

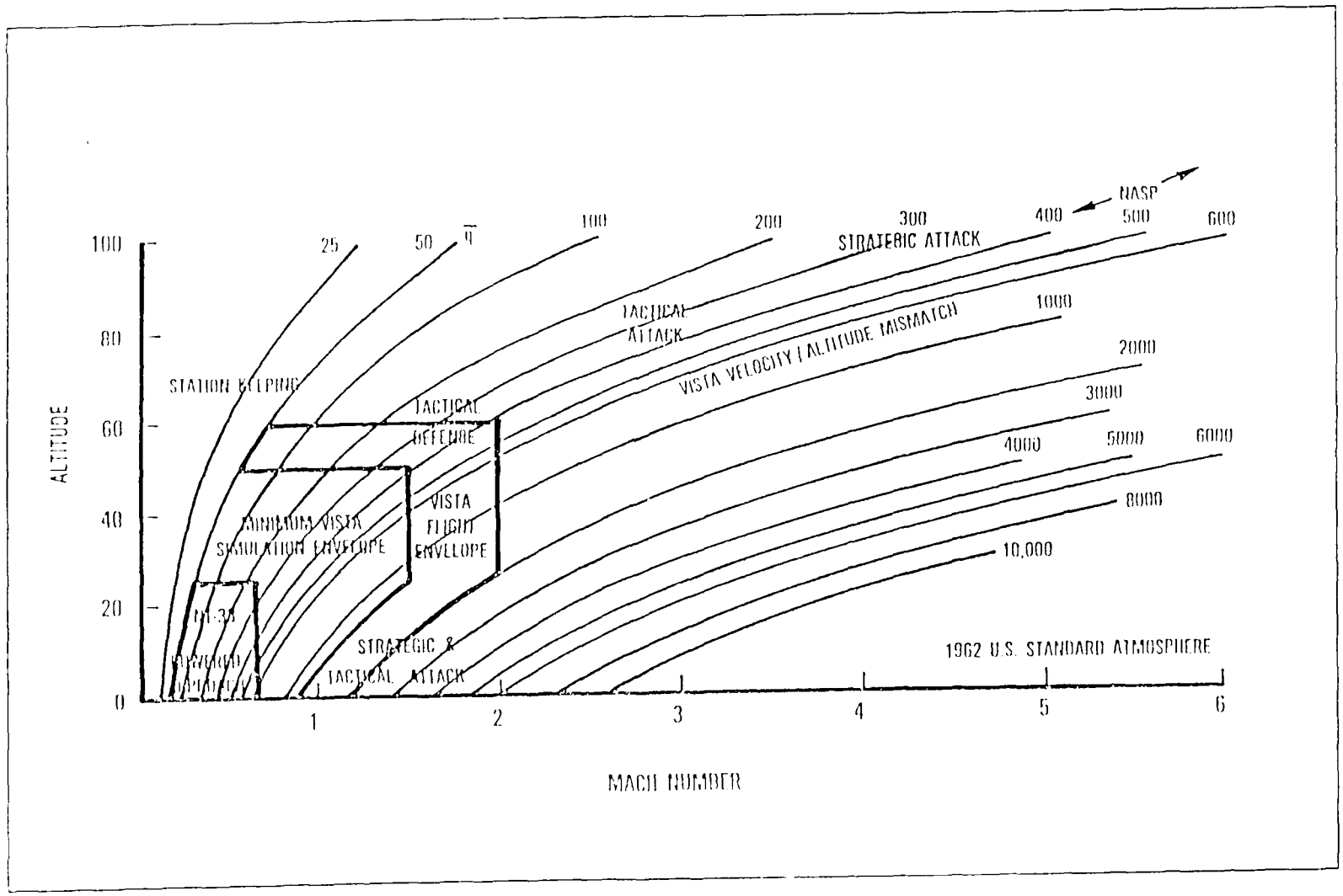

Figure 1-4. VISTA/F-16 Flight/Simulation Envelope

1.3 Approach

Adaptive control is a promising approach to deal with the problem of maintaining a specified level of tracking performance, and therefore simulation fidelity, throughout the operating envelope. The primary reason for considering the use of an adaptive controller for the VISTA/F-16 is the wide range of dynamic characteristics assumed as the operating point changes. Rather than designing off-line, fixed point control strategies, i.e. control strategies designed for a specific operating condition, and attempting to chose the appropriate strategy to meet the current conditions, the basic idea is to perform on-line system identification and control design simultaneously. As the operating conditions change, so does the system being identified, and appropriate changes are made to the control law. Thus, the control system is adapting to the changing environment. The identification subsystem uses the inputs and outputs of the plant in order to identify an equivalent input-output model for the aircraft dynamics. The identified parameters are then used to calculate a set of time-varying controller gains, which in turn are used to compute the current control inputs to the plant. The structure of such a system is shown in Figure 1-5.

Much effort has been devoted recently to the investigation of adaptive control laws based on the application of recursive parameter identification algorithms. Positive results have been reported in the literature on the use of such adaptive control schemes for aerospace applications (20,41,48). New theoretical developments in the area of parameter identification (19), and advances in microprocessor technology (1,12,26,47), make the alternative of parameter-adaptive control

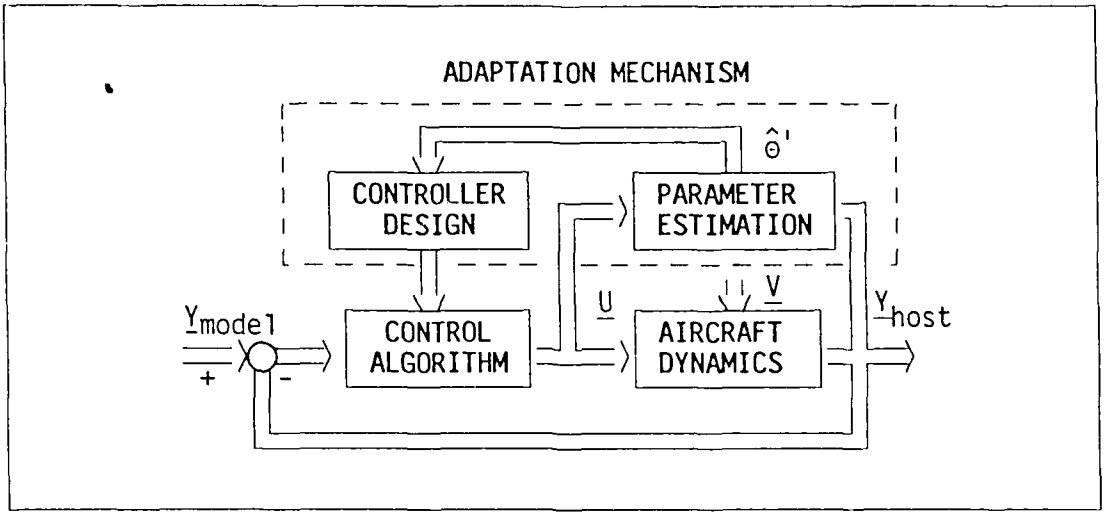

Figure 1-5. Parameter-adaptive control system. Y_m, model motions; V noise signals.

increasingly viable.

1.4 Problem Statement

The purpose of this thesis is to test the effectiveness of digital parameter-adaptive control laws in maintaining tracking performance for an in-flight simulator, despite plant parameter changes. The use of parameter-adaptive control laws will alleviate the requirement for accurate knowledge of the stability derivatives of the host aircraft and offer the potential of increased fidelity for in-flight simulations. The design techniques of Professor Brian Porter (31-38), are used to develop longitudinal control laws for a model-following application. These new techniques use on-line, recursive, step-response matrix identifiers to update the control law gains as needed to account for plant parameter variations. A parameter identification algorithm recently developed by T. Hagglund (19) is

chosen for this implementation. This algorithm allows for identification during general aircraft maneuvering by updating the parameter estimates only when adequate input-output activity is present.

1.5 Scope

Because of budgetary constraints, the initial VISTA will be developed without side-force surfaces and wingtip speed brakes, in a configuration such as the one depicted in Figure 1-6. Since aerodynamic data is not yet available for the VISTA/F-16, and because of the similarity between its proposed physical configuration and that of the Advanced Technology Integration F-16 (AFTI/F-16, Figure 1-7), this thesis adresses the development of adaptive multivariable tracker control laws using the AFTI/F-16 as the host aircraft. The investigation is limited to the linearized, longitudinal, rigid body dynamics of the AFTI/F-16 using perturbation equations of motion at a nominal flight condition of Mach 0.9 at 10,000 ft MSL.

This thesis accomplishes the following objectives:

1. Successful control of the linear aircraft model including actuator dynamics with position and rate limits.
2. Determines the feasibility of using fast-sampling multivariable tracker control laws in a model-following configuration for in-flight simulation.
3. Successful implementation of state-of-the-art recursive identification algorithm for on-line tunning of control law gains.

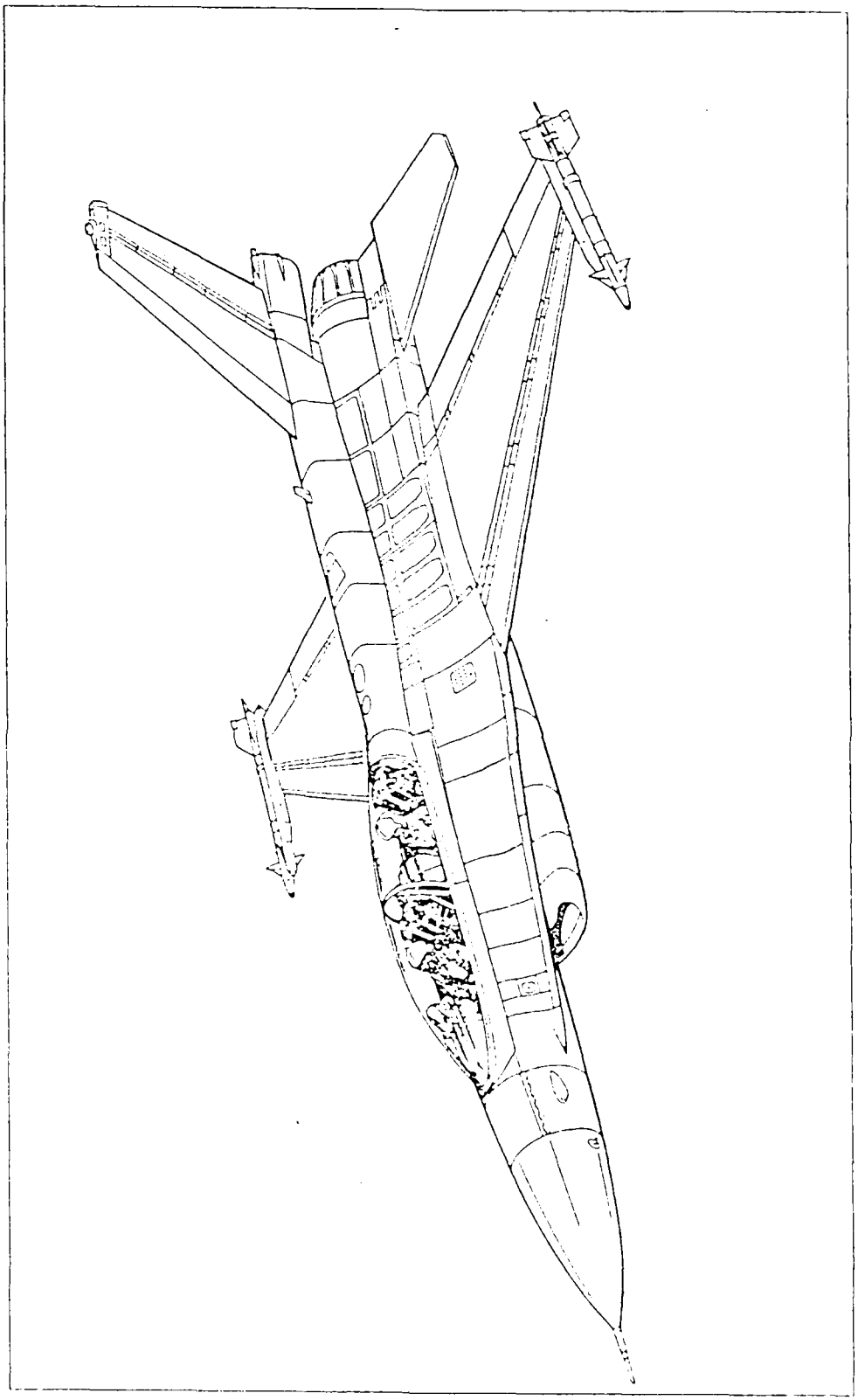

Figure 1-6. Initial VISTA/F-16 Configuration

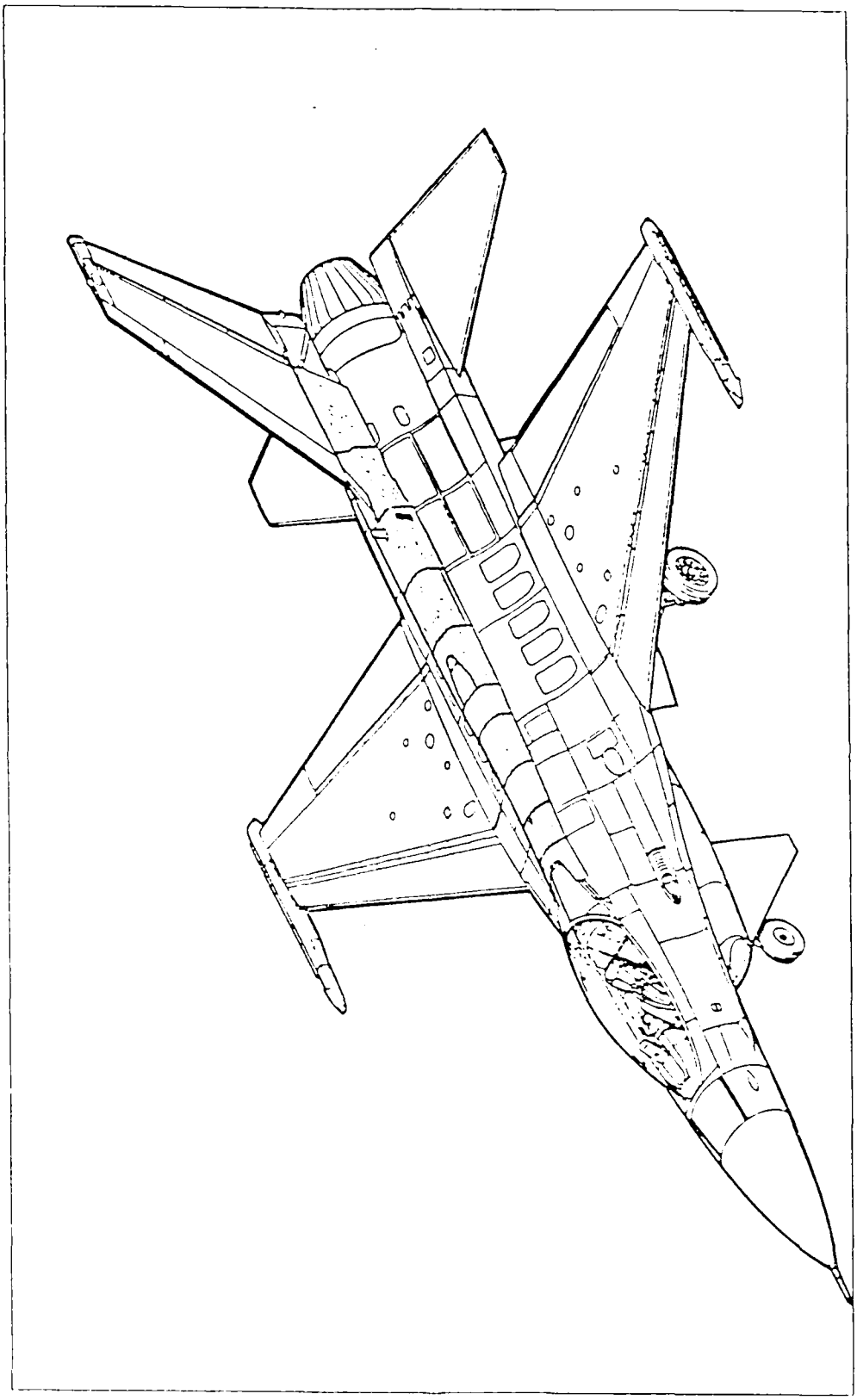

Figure 1-7. AFTI/F-16 Aircraft

4. Assesses the improvement in tracking performance and simulation fidelity by using an adaptive system.

5. Studies closed-loop system performance under simulated output measurement noise conditions

1.6 Overview

The material in this thesis consists of a brief summary of current model-following techniques presented in Chapter II. This chapter also provides a description of the multivariable design theory developed by Professor Brian Porter of the University of Salford, England, presented here as an alternate approach to the model-following problem. Chapter III then discusses the recursive technique used to identify the step-response matrix elements required by the control law. Chapter IV presents details of the design procedure used in the development of the control law and recursive identification algorithm, as well as a description of the simulation setup in which the parameter identifier is coupled with the control law to form an adaptive system. The capability of the model-following system to adjust itself to changing conditions is analyzed through the use of the $MATRIX_X$ software package (23). Chapter V presents simulation results and compares the performance of the adaptive controller to that of a fixed gain system. Finally, a summary of the simulation results, as well as conclusions and recommendations for further studies are presented in Chapter VI. Four appendices are included as supplementary material to the body of the thesis. Appendix A provides data for the state space and difference equation models representing the equations of motion of the AFTI/F-16 aircraft. Appendix B details the equivalence between the step-response

matrix and the matrix coefficient B_1 of the vector difference equation describing the input-output dynamics of the plant. Appendix C covers implementation details of the recursive parameter identification algorithm, and Appendix D presents the results of a root-locus analysis and some of the time responses used for assesing the implications of functional uncontrollability on the closed-loop system.

II. Control Law Development

2.1 Introduction (39:21-22)

The concept of using a stability augmentation system to modify the dynamic characteristics of an airplane is not a new one. The same concept can be used to adjust the terms in the equations of motion of the variable stability airplane to match the corresponding terms in the equations of motion of the simulated airplane. This technique is known as the "response feedback" approach to in-flight simulation. A response feedback variable stability system can be described as a generalized stability augmentation system which has wide ranges of adjustment so that large variations in airplane response characteristics can be produced (Figure 2-1). A response feedback system operates by adding to or substracting from the airplane's natural stability and control characteristics. Thus it is necessary to know accurately the stability and control characteristics of the host airplane at all flight conditions of interest. Also, it is difficult to calculate exactly in advance the variable stability system gain settings which will simultaneously produce correct values of the many parameters which define the aircraft dynamics. Thus in-flight calibration of the configurations that are to be evaluated is generaly necessary for fine-tuning of the system in order to match the motions of the simulated aircraft.

A different approach to in-flight simulation uses the idea of "model-following". In this type of system, the signals coming from the

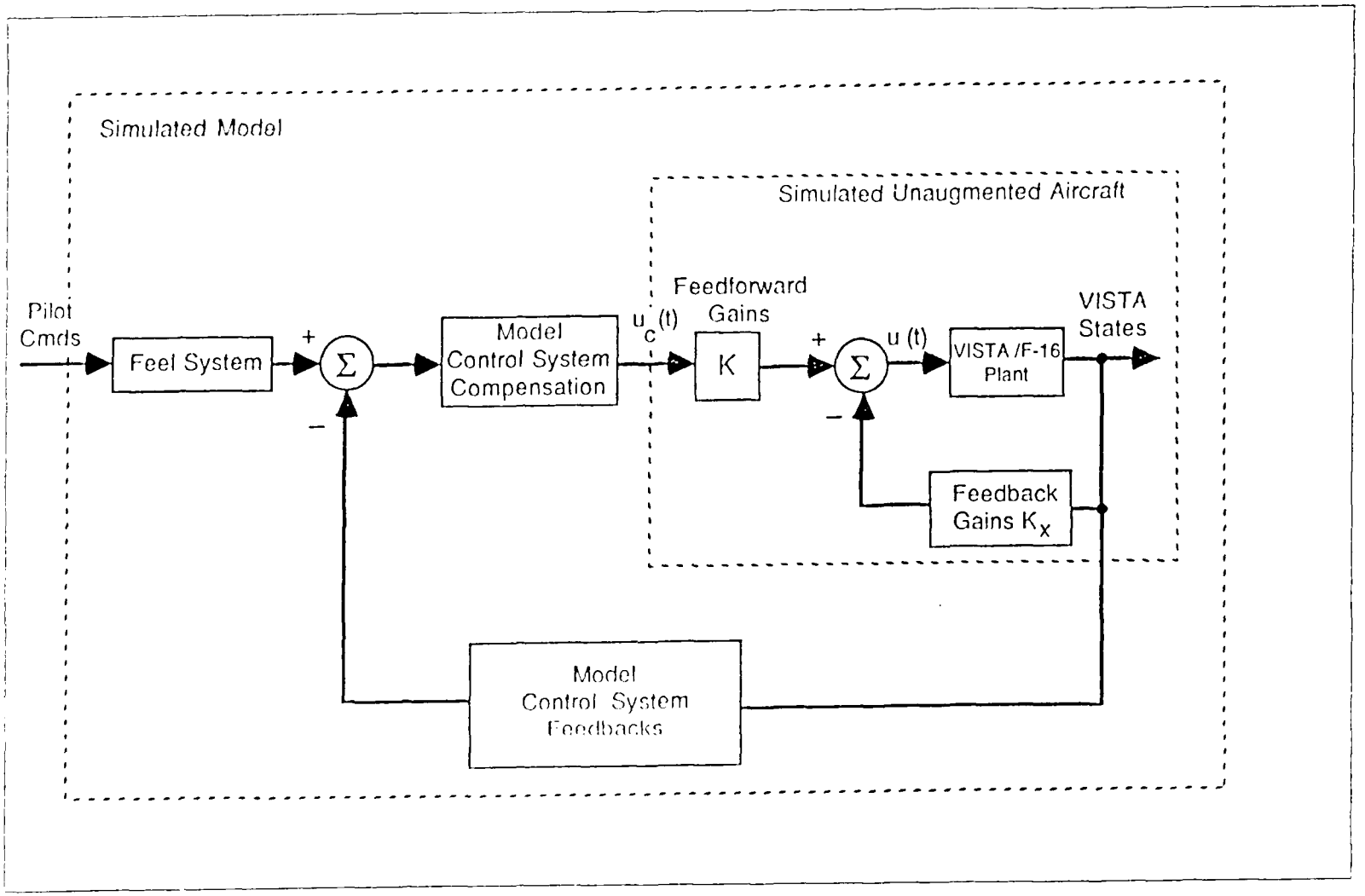

Figure 2-1. Response Feedback Concept

evaluation pilot's cockpit are fed as inputs to a computer which has in it the equations of motion of the airplane to be simulated. The output of this computer is a set of time histories describing the motion of the simulated airplane to the inputs applied by the pilot. The task of the variable stability system then is to automaticaly operate the control surfaces of the host airplane in such a way that its motions (at the pilot's station) duplicate those of the modeled airplane. The model-following concept is illustrated in Figure 2-2. The model-follwing approach permits the computer that defines the simulated aircraft to be set up and checked out on the ground prior to flight. Although less sensitive to host airplane parameter variations than the response feedback technique, the model following approach still requires an accurate knowlwdge of the host airplane's stability derivatives for good model-following performance as is shown next.

2.2 Summary of current model-following techniques (39:21-28)

Under the assumptions presented in Etkin (15:121-189) the host vehicle dynamics at a particular flight condition can be represented by a linear matrix differential equation of the form

$$\dot{X}_p(t) = A_p X_p(t) + B_p u_p(t) \qquad (2\text{-}1)$$

and the dynamics of the simulated vehicle by the linear matrix differential equation

$$\dot{X}_m(t) = A_m X_m(t) + B_m u_m(t) \qquad (2\text{-}2)$$

where A_p, A_m, B_p, B_m are matrices of stability derivatives, X_p and X_m

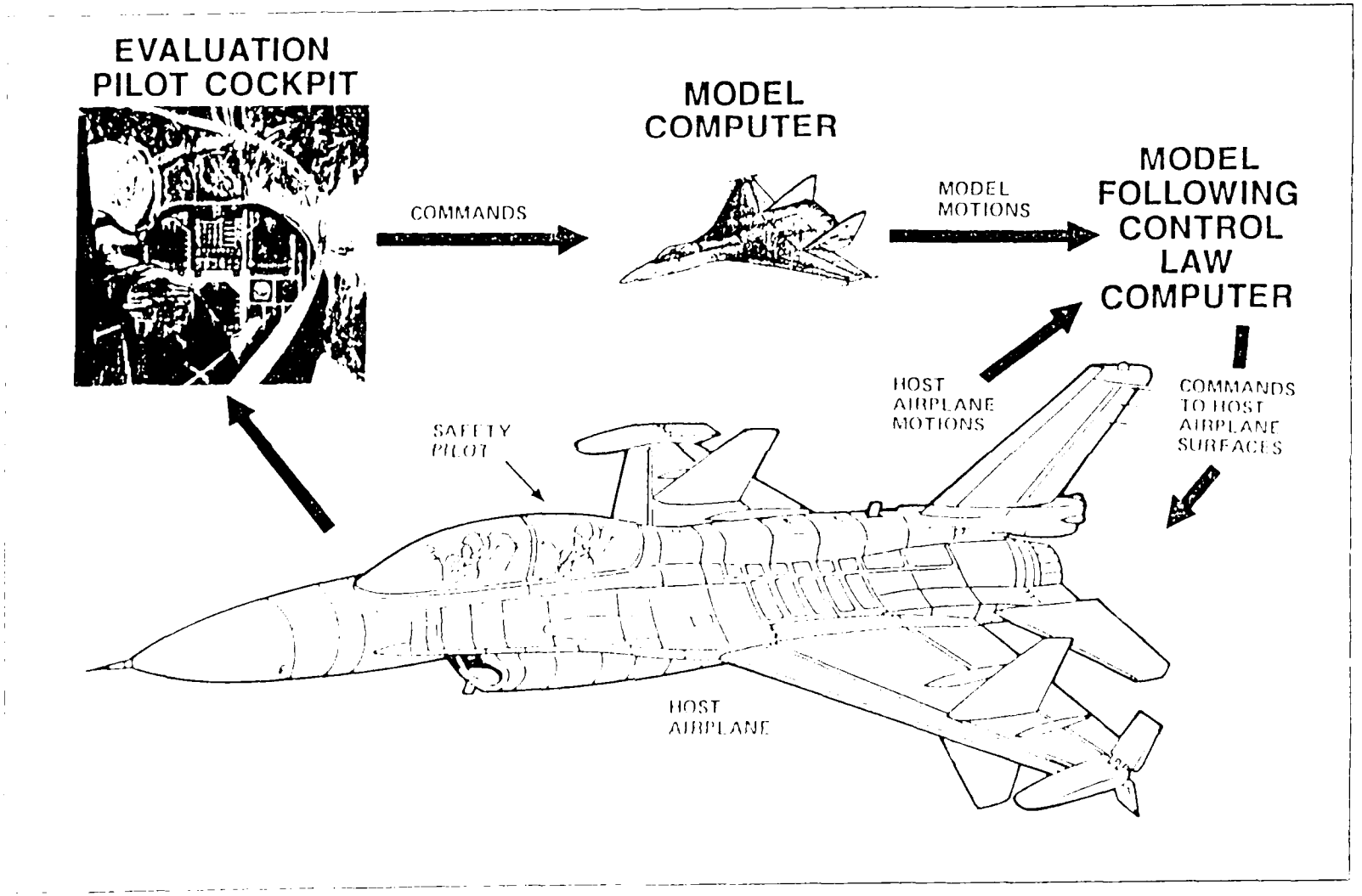

Figure 2-2. Model Following Concept

are the states, u_p and u_m are control surface deflections and the subscripts p and m denote the plant (host) and model airplane respectively. Assuming that the simulation is started with the host and the simulated aircraft at the same initial conditions, a control law for exact model-following can then be obtained by simply substituting the state, and rate of change of the state, of the model into Eqn (2-1) and solving for the control input $u_p(t)$:

$$\dot{X}_m(t) = A_p X_m(t) + B_p u_p(t) \qquad (2\text{-}3)$$

or

$$u_p(t) = B_p^{-1} \dot{X}_m(t) - B_p^{-1} A_p X_m(t) \qquad (2\text{-}4)$$

$$u_p(t) = K_1 \dot{X}_m(t) - K_2 X_m(t) \qquad (2\text{-}5)$$

Equations (2-4) and (2-5) define the control inputs to the host aircraft in terms of the model states and rate of change of those states. Both of them are available from the equations of motion of the simulated vehicle that are contained in the variable stability system's simulation computer (Figure 2-3).

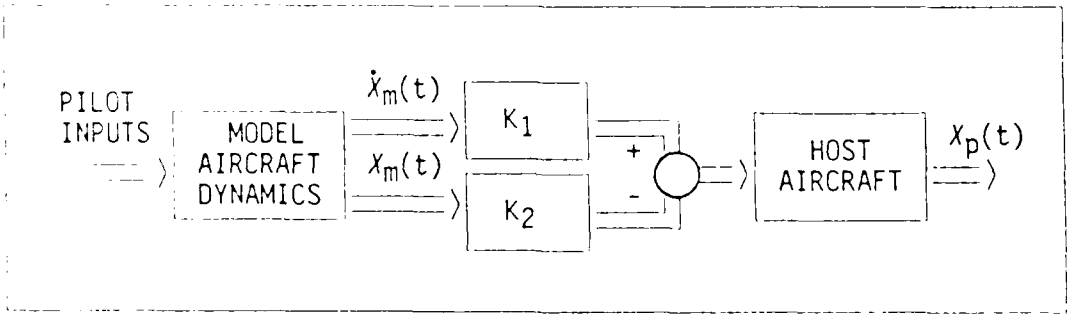

Figure 2-3. Explicit Model Following System

Equation (2-4) also demonstrates the requirement for accurate knowledge of the stability derivatives of the host aircraft.

To reduce the sensitivity of this control scheme to plant parameter variations, a feedback loop is introduced around the plant with a gain matrix K_p (Figure 2-4).

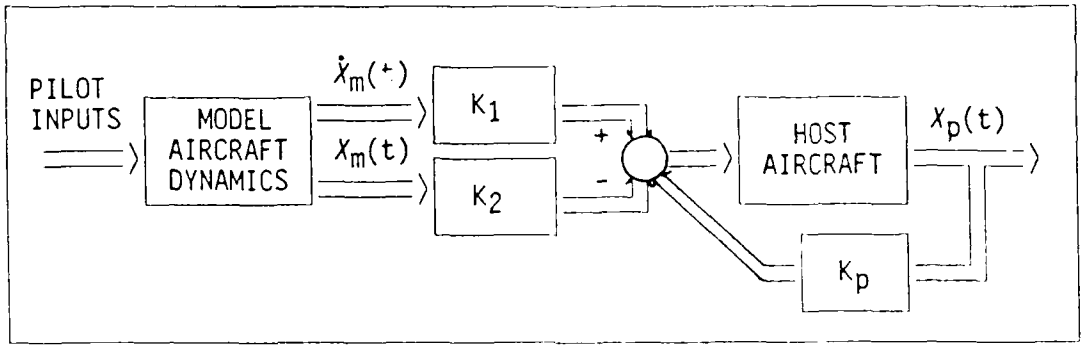

Figure 2-4. Improved Explicit Model Following System

The feedforward gains are now determined as follows:

$$K_1 = B_p^{-1} \tag{2-6}$$

$$K_2 = B_p^{-1} A_p - K_p \tag{2-7}$$

The feedback around the plant is arbitrary, subject to the requirement that the regulator loop must be stable. It can be shown that by selecting K_2 as in Eqn (2-7), the dynamics of the tracking error become

$$\dot{e}(t) = (A_p - B_p K_p)\, e(t) \tag{2-8a}$$

$$= A_e\, e(t) \tag{2-8b}$$

If A_e is stable, the error is driven to zero. By selecting large values for the gains in the matrix K_p the regulator loop becomes increasingly tight, making the system less dependent on the gain matrix K_1 and reducing its sensitivity to plant parameter variations. This reduces the requirement for accurate knowledge of the plant's stability derivatives. In practice, concerns for closed-loop stability, sensor noise, structural limitations, etc. determine how high the feedback gains can be, thus restricting the amount of desensitization (to plant parameter variations) that can be provided.

The feedback gains can be selected based on the maximum gain available that will not significantly compromise closed-loop stability or result in undesirable control surface rates of motion which could place excessive demands on the hydraulic system used to actuate the control surfaces of the plant. Usually they are designed as constants to reduce system complexity, however, it important to note that the effect on the output of the control surfaces is a function of dynamic pressure since the actual control effectiveness of the surface is also a function of dynamic pressure. Thus the aerodynamic gain will vary with flight condition. This increases the actual feedback gain as dynamic pressure increases and could result in closed-loop instabilities. This condition can be minimized if the feedback gains are selected at the highest dynamic pressure to be encountered in the simulation, although this may compromise performance at flight conditions characterized by low dynamic pressure. An alternate solution is simply to use gain scheduling, but this approach may require extensive flight testing to determine an appropriate schedule for the large number of possible

flight conditions likely to be encountered during simulations.

2.3 Porter's Method

2.3.1 Fixed Gain Control Law. One of the many alternatives for achieving model following is the use of fast-sampling multivarible control laws in a configuration similar to a command generator/tracker. Control laws such as the ones developed by Prof. B. Porter can be used to make the plant follow the time histories generated by a computer model of the simulated vehicle.

The basic longitudinal equations of motion of the host aircraft in this thesis are assummed to be completely controllable and observable, and described by state and output equations of the form

$$\dot{X}(t) = A\,X(t) + B\,u(t) \qquad (2\text{-}1)$$

$$y(t) = C\,X(t) \qquad (2\text{-}9)$$

where the subscript p has been droped for notational convenience, and A is (n x n), B is (n x m) and has rank "m", C is (m x n), $y(t)$ and $u(t)$ are (m x 1).

The A, B, and C matrices are partitioned according to the control input matrix (B) to yield the following equations:

$$\begin{bmatrix} \dot{x}_1(t) \\ \dot{x}_2(t) \end{bmatrix} = \begin{bmatrix} A_{11} & A_{12} \\ A_{21} & A_{22} \end{bmatrix} \begin{bmatrix} x_1(t) \\ x_2(t) \end{bmatrix} + \begin{bmatrix} 0 \\ B_2 \end{bmatrix} u(t) \qquad (2\text{-}10)$$

and

$$y(t) = \begin{bmatrix} C_1 & C_2 \end{bmatrix} \begin{bmatrix} x_1(t) \\ x_2(t) \end{bmatrix} \qquad (2\text{-}11)$$

where $x_1(t)$ is (p x 1), $x_2(t)$ is (n-p x 1) and B_2 is (n-p x m) with rank "m". The equations defining $\dot{x}_1(t)$ are kinematic relationships with no forcing function present. For the aircraft longitudinal equations of motion the kinematic equation is $\dot{\theta} = q$, where θ is the pitch angle and q is pitch rate. The resulting state vector has the form:

$$x_1 = [\ \theta\ ] \text{ deg} \tag{2-12}$$

$$x_2 = [\ u\ \ \alpha\ \ q\ ]^T \text{ fps, deg, deg/sec} \tag{2-13}$$

The plant is considered "regular" or "irregular" depending on whether or not the first Markov parameter , CB, has full rank equal to "m". For "regular" plants (rank(CB) = m) with stable transmision zeros, the control law is a discrete proportional-plus-integral (PI) output feedback control law expressed as

$$u(kT) = (1/T)\ [\ K_1\ e(kT) + K_2\ Z(kT)\ ] \tag{2-14}$$

and

$$u(t) = u(kT) \text{ for } t\in[kT,\ (k+1)T) \tag{2-15}$$

where

k = integer

T = 1/f is the sampling period,

K_1 and K_2 are (m x m) controller gain matrices,

$e(kT) = r(kT) - y(kT)$ is the (m x 1) error vector

$r(kT) = y_{model}(kT)$ is the reference vector

$Z(kT)$ is the digital integral of the error vector, defined as

$$Z[(k+1)T] = Z(kT) + T\ e(kT) \tag{2-16}$$

For "irregular" plants, a proportional plus integral plus derivative (PID) controller structure can be used as described in References (31), (32) and (33). The input-output configuration in this thesis provides for a "regular" design.

The plant state and output equations may be discretized for the sampling period T using the relationships

$$\begin{bmatrix} \Phi_{11} & \Phi_{12} \\ \Phi_{21} & \Phi_{21} \end{bmatrix} = \exp\left\{ \begin{bmatrix} A_{11} & A_{12} \\ A_{21} & A_{22} \end{bmatrix} T \right\} \qquad (2\text{-}17)$$

and

$$\begin{bmatrix} \Psi_1 \\ \Psi_2 \end{bmatrix} = \int_0^T \exp\left\{ \begin{bmatrix} A_{11} & A_{12} \\ A_{21} & A_{22} \end{bmatrix} t \right\} \begin{bmatrix} 0 \\ B_2 \end{bmatrix} dt \qquad (2\text{-}18)$$

The resulting sampled data state and output equations for the plant are

$$\begin{bmatrix} x_1\{(k+1)T\} \\ x_2\{(k+1)T\} \end{bmatrix} = \begin{bmatrix} \Phi_{11} & \Phi_{12} \\ \Phi_{21} & \Phi_{21} \end{bmatrix} \begin{bmatrix} x_1(kT) \\ x_2(kT) \end{bmatrix} + \begin{bmatrix} \Psi_1 \\ \Psi_2 \end{bmatrix} u(kT) \qquad (2\text{-}19)$$

$$y(kT) = \begin{bmatrix} C_1 & C_2 \end{bmatrix} \begin{bmatrix} x_1(kT) \\ x_2(kT) \end{bmatrix} \qquad (2\text{-}20)$$

The augmented closed-loop state and output equations for the control law of Eqn (2-12) are given by (36)

$$\begin{bmatrix} Z\{(k+1)T\} \\ x_1\{(k+1)T\} \\ x_2\{(k+1)T\} \end{bmatrix} = \begin{bmatrix} I_m & -TC_1 & -TC_2 \\ f\Psi_1 K_2 & \Phi_{11}-f\Psi_1 K_1 C_1 & \Phi_{12}-f\Psi_1 K_1 C_2 \\ f\Psi_2 K_2 & \Phi_{21}-f\Psi_2 K_1 C_1 & \Phi_{22}-f\Psi_2 K_1 C_2 \end{bmatrix} \begin{bmatrix} Z(kT) \\ x_1(kT) \\ x_2(kT) \end{bmatrix}$$

$$+ \begin{bmatrix} TI_m \\ f\Psi_1 K_1 \\ f\Psi_2 K_1 \end{bmatrix} r(kT) \quad (2\text{-}21)$$

and

$$y(kT) = \begin{bmatrix} 0 & C_1 & C_2 \end{bmatrix} \begin{bmatrix} Z(kT) \\ x_1(kT) \\ x_2(kT) \end{bmatrix} \quad (2\text{-}22)$$

where f is the sampling frequency. A transformation is introduced (27) which block diagonalizes the state and output equations so that they assume the form

$$\begin{bmatrix} \bar{x}_1\{(k+1)T\} \\ \bar{x}_2\{(k+1)T\} \end{bmatrix} = \begin{bmatrix} \bar{A}_1 & 0 \\ 0 & \bar{A}_4 \end{bmatrix} \begin{bmatrix} \bar{x}_1(kT) \\ \bar{x}_2(kT) \end{bmatrix} + \begin{bmatrix} \bar{B}_1 \\ \bar{B}_2 \end{bmatrix} r(kT) \quad (2\text{-}23)$$

$$y(kT) = \begin{bmatrix} \bar{C}_1 & \bar{C}_2 \end{bmatrix} \begin{bmatrix} \bar{x}_1(kT) \\ \bar{x}_2(kT) \end{bmatrix} \quad (2\text{-}24)$$

where

$$\bar{x}_1(kT) = \begin{bmatrix} Z(kT) \\ x_1(kT) \end{bmatrix} \quad (2\text{-}25)$$

$$\bar{x}_2(kT) = x_2(kT) \quad (2\text{-}26)$$

$$\bar{C}_1 = \begin{bmatrix} K_1^{-1}K_2 & , & 0 \end{bmatrix} \quad (2\text{-}27)$$

$$\bar{C}_2 = C_2 \quad (2\text{-}28)$$

$$\bar{A}_1 = \begin{bmatrix} I_m - TK_1^{-1}K_2 & , & 0 \\ TA_{12}C_2^{-1}K_1^{-1}K_2 & , & I_{n-m} + A_{11}T - TA_{12}C_2^{-1}C_1 \end{bmatrix} \quad (2\text{-}29)$$

$$\bar{B}_1 = \begin{bmatrix} 0 \\ T A_{12} C_2^{-1} \end{bmatrix} \tag{2-30}$$

$$\bar{A}_4 = I_m - B_2 K_1 C_2 \tag{2-31}$$

$$\bar{B}_2 = B_2 K_1 \tag{2-32}$$

As the sampling frequency is increased ($f \to \infty$), the closed-loop transfer function assumes the asymptotic form (37)

$$\Gamma(z) = \Gamma_1(z) + \Gamma_2(z) \tag{2-33}$$

where z is the discrete transform operator and

$$\Gamma_1(z) = \bar{C}_1(zI_n - I_n - TA_0)^{-1}TB_0 \tag{2-34}$$

$$\Gamma_2(z) = \bar{C}_2(zI_m - I_m - A_4)^{-1}B_4 \tag{2-35}$$

with

$$A_0 = \begin{bmatrix} K_1^{-1}K_2 & 0 \\ A_{12}C_2^{-1}K_1^{-1}K_2 & A_{11} - A_{12}C_2^{-1}C_1 \end{bmatrix} \tag{2-36}$$

$$B_0 = \begin{bmatrix} 0 \\ A_{12}C_2^{-1} \end{bmatrix} \tag{2-37}$$

$$A_4 = -B_2 K_1 C_2 \tag{2-38}$$

$\Gamma_1(z)$ and $\Gamma_2(z)$ are the slow and fast mode transfer functions respectively. The slow modes can be grouped into two sets Z_1 and Z_2 and are given by

$$Z_1 = \{z \in C: |zI_m - I_m + TK_1^{-1}K_2| = 0\} \quad (2\text{-}39)$$

and

$$Z_2 = \{z \in C: |zI_{n-m} - I_{n-m} - TA_{11} + TA_{12}C_2^{-1}C_1| = 0\} \quad (2\text{-}40)$$

The fast modes are given by

$$Z_3 = \{z \in C: |zI_m - I_m + C_2B_2K_1| = 0\} \quad (2\text{-}41)$$

Because of the form of A_0, B_0, and $\bar{C}_1$, the eigenvalues of A_0 are uncontrollable or unobservable. Thus, as the sampling frequency increases, the slow transfer function asymptotically approaches zero and the overall system transfer function contains only the fast modes, as given by $\Gamma_2(z)$ which can be put in the equivalent form

$$\Gamma(z) = \Gamma_2(z) = (zI_m - I_m + C_2B_2K_1)^{-1}C_2B_2K_1 \quad (2\text{-}42)$$

The controller matrices K_1 and K_2 are then given by

$$K_1 = [C_2B_2]^{-1}\Sigma \quad (2\text{-}43)$$

$$K_2 = \rho K_1 \quad (2\text{-}44)$$

where ρ is any positive scalar greater than zero, and Σ is a diagonal tuning matrix. Both ρ and Σ are chosen by the designer to achieve the desired tracking characteristics.

Although the method just outlined provides robust control

characteristics, some degradation of performance is inevitable when faced with large parameter variations in the plant. To avoid this performance degradation, adaptive control techniques may be used to adjust the control law parameters as necessary and maintain tracking performance.

2.3.2 Adaptive Control Law. An alternate way of defining the control law gain matrices of Eqns (2-43) and (2-44) is by the use of the step-response matrix (34) defined as

$$H(T) = \int_0^T C \exp(A(t-\tau))\, B\, d\tau \qquad (2\text{-}45)$$

For small sampling periods $H(T) \cong TCB$, and the control law can be expressed as

$$u(kT) = \bar{K}_1 e(kT) + \bar{K}_2 Z(kT) \qquad (2\text{-}46)$$

where

$$\bar{K}_1 = H^{-1}(T)\Sigma \qquad (2\text{-}47)$$

$$\bar{K}_2 = \rho \bar{K}_1 \qquad (2\text{-}48)$$

The significance of using $H(T)$ is that it can be obtained from real-time input-output measurements to reflect the current characteristics of the plant (31,32), thus forming the basis for an adaptive system. In order to do this, an autoregressive difference equation is used to represent the open-loop dynamics of the host aircraft. This is accomplished in the next chapter.

III. Recursive Identification

3.1 Introduction

In recent years numerous new developments for parameter-adaptive control algorithms based on parameter estimation techniques have taken place. Recursive Least Squares identification algorithms play a crucial role for many problems, not only in adaptive control, but also for adaptive signal processing, and for general model building and monitoring problems. Today, with the aid of an on-line digital computer, it is possible to use an empirical model to represent a non-linear plant in a sequential manner. Specifically, a low order linear model can be selected to represent the dynamics of the system. By use of the proper estimation algorithm, the computer is able to provide updated parameter estimates for the empirical model at each sample instant. This quasi-linearization procedure permits the use of advanced control techniques such as the self-adaptive strategy, which uses the information about the empirical model to update control law parameters, thus allowing improved performance over a wide range of system parameter variations. This chapter presents a short description of the procedure and algorithms used to carry out the identification part of the adaptation mechanism.

The identification problem considered in this thesis is the following:

Given a discrete input-output time history of the airplane longitudinal dynamics, determine the parameters of a suitable linear

model that best describes the characteristics of the airplane (according to a given criterion) at its current operating condition. Furthermore, the identification must be done "on-line" with a minimal amount of data storage (recursive algorithm implementation), and using only the normal control inputs to the plant.

Section 3.2 of this chapter describes the process of selecting the structure of the input-output model used in the identification procedure. Section 3.3 then sumarizes the commonly used Recursive Least Squares identification algorithm, its characteristics, and some of its limitations. This leads the way to Section 3.4 which sumarizes a modified version of the Least Squres algorithm developed by Hagglund (19) which overcomes some of the limitations of the basic Least Squares approach. For this investigation, it will be assumed that the computational time involved in the execution of the control and identification algorithms is sufficiently short (compared to the sampling time, and variation of plant parameters) as to introduce negligible time delay effects. This assumption is justified by the availability of sophisticated microproccesors such as the ones described in References (12), (26), and (47) which may allow for fast execution of these algorithms.

3.2 Input-output Model Specification

The first step of the identification problem is the specification of an algebraic structure between the input and output variables to describe the behavior of the plant. This model is postulated a priori and can be based upon knowledge of the underlying theory governing the dynamics of the plant. The discrete nature of the

control laws being considered here, in which input-output data is gathered by the on-line computer for the control process, suggests that the most convenient model is in the form of difference equations.

One of the posibilities for the derivation of a difference equation model for the open-loop longitudinal dynamics of the host airplane is based on the discrete state and output relationships given in Eqns (2-17) and (2-18). These equations can provide the desired input-output relationship by simply taking their Z Transform and obtaining a transfer function model (22) as follows:

$$X\{(k+1)T\} = \Phi\, X(kT) + \Psi\, u(kT) \tag{3-1}$$

$$y(kT) = C\, X(kT) \tag{3-2}$$

$$Y(z) = [\, C\,[zI - \Phi]^{-1}\, \Psi\,]\, U(z) = G(z)\, U(z) \tag{3-3}$$

The m x 1 vector Y(z), the m x m matrix G(z), and the m x 1 vector U(z) are given by:

$$Y(z) = \begin{bmatrix} Y_1(z) \\ Y_2(z) \\ \vdots \\ Y_m(z) \end{bmatrix} \tag{3-4}$$

$$G(z) = \begin{bmatrix} G_{11}(z) & G_{12}(z) & \cdots & G_{1m}(z) \\ G_{21}(z) & G_{22}(z) & \cdots & G_{2m}(z) \\ \cdots & \cdots & \cdots & \cdots \\ G_{m1}(z) & G_{m2}(z) & \cdots & G_{mm}(z) \end{bmatrix} \tag{3-5}$$

$$U(z) = \begin{bmatrix} U_1(z) \\ U_2(z) \\ \vdots \\ U_m(z) \end{bmatrix} \qquad (3\text{-}6)$$

where $G_{ij}(z)$ is the transfer function relating the output Y_i to the control input U_j and is of the form

$$G_{ij}(z) = \frac{b_1 z^w + b_2 z^{w-1} + \cdots + b_w z + b_{w+1}}{z^n + a_1 z^{n-1} + \cdots + a_{n-1} z + a_n} \qquad (w < n) \quad (3\text{-}7)$$

By dividing each numerator and denominator in $G(z)$ by z^n the transfer matrix $G(z)$ is transformed into the delay operator form

$$G_{ij}(z) = \frac{b_1 z^{w-n} + b_2 z^{w-n-1} + \ldots + b_{w+1} z^{-n}}{1 + a_1 z^{-1} + \ldots + a_{n-1} z^{-n+1} + a_n z^{-n}} \qquad (w < n) \quad (3\text{-}8)$$

At this point, the input-output relationship of the open-loop plant may be obtained by grouping the coeficients with the same amount of delay in every transfer function $G_{ij}(z)$, and taking the inverse Z transform to yield the following N^{th} order vector difference equation model

$$y(kT) = B_1 u\{(k-1)T\} - A_1 y\{(k-1)T\} + \ldots + B_n u\{(k-N)T\} - A_n y\{(k-N)T\} + \varepsilon(kT) \qquad (3\text{-}9)$$

or equivalently

$$y(kT) = \Upsilon^T(kT)\,\Theta + \varepsilon(kT) \quad \in R^m \qquad (3\text{-}10)$$

where

$\varepsilon(kT)$ is an equation error term assumed to be a zero mean Gaussian white-noise vector with elements of variance σ^2_i, added to account for modeling errors that may arise from applying a linear model structure to a possibly nonlinear plant, or mismatch between the real system order "n" and the difference equation order "N"

$\Upsilon^T(kT) \in R^{mxl}$ is a matrix of past values of $\{y(kT)\}$ and $\{u(kT)\}$

the matrices $A_i \in R^{mxm}$ ($i = 1,2,\ldots,N$), $B_i \in R^{mxm}$ ($i = 1,2,\ldots,N$) and the vector $\Theta \in R^{lxl}$ are the parameters of the N^{th} order difference equation

By defintion of the step-response matrix it can be shown (Appendix B) that

$$H(T) = B_1 \cong TCB \qquad (3\text{-}11)$$

thus, by identifying the matrix coefficient B_1 in real-time from input-output data, and invoking the certainty equivalence principle (6), updated step-response matrix estimates can be provided for the control law design calculations (Eqn (2-47)) (31,32,34).

It is important to note that all the parameters of Eqn (3-9) must be identified to obtain the step-response matrix denoted by B_1. Ideally, in the case a transfer matrix model reduced to the same denominator, the

order "N" should be the same as the discretized plant model order "n" (Eqns (2-17) and (2-18)) to avoid biases in the estimates resulting from trying to fit a reduced order transfer function model to the plant dynamics (this assumes of course that a model of order "n" is true). A model in which "N" is large however may represent a problem, since the computational effort and the convergence time of the identification algorithm depends, among other factors, on the number of parameters to be identified. It is important therefore to keep the number of identified parameters to a minimun. This fact seems to oppose the desire of having "N" equal to "n", favoring the use of reduced order models. A reduced order model may be appropriate for certain situations depending upon the tracking performance required and desired gain margins. Compensation for biases in the step-response matrix can be introduced by increasing the overall loop gain of the system. However, it is highly desirable to achieve the desired tracking behavior with the lowest amount of gain possible in order to provide satisfactory gain margins in the system. A solution is then needed that permits the reduction of biases in the parameter estimates associated with reduced order modeling, while also providing for a small amount of parameters to be identified. It is recognized that a diference equation model derived from a transfer matrix does not provide for a minimal number of parameters to represent a system (17,18), however, it facilitates the identification procedure by providing for decoupled equation error terms which in turn allow for a simple scalar measurement update procedure (10, 30, 43, Appendix C).

Since only B_1 (= H(T)) is required for the control law calculation

of Eqn (2-47), a possible approach to solve the aforementioned problems is to identify only the elements of B_1 leaving the rest of the parameters in the full order model (N = n) fixed. It is assummed for this investigation that the appropriate parameters for the fixed portion of the model of Eqns (3-9) and (3-10) (representative of the current flight condition) are available for use in calculating the plant's output predictions and residuals needed in the identification algorithm. This approach is justified in light of the results obtained in references (3), (21), and (46), where multiple models are employed for identification based on a-priori data. This a-priori data can be provided from information gathered by stability and control derivative prediction methods, wind tunnel tests, and preliminary flight test data. Selection of the best performing model could then be based upon on-line calculation of a probability of correctness associated with each model. Furthermore, the same input-output data used in updating the estimates of the step response-matrix elements can be used to update a full order model that may be evaluated on a background proccesing mode. This information can eventually be used in refining the models selected a-priori for improved performance. The computational effort involved in the multiple model approach is easily accomodated by pararallel processing techniques and should not produce any significant computational time delays.

The procedure of identifying only B_1 causes the following partition of Eqn (3-10)

$$y(kT) = \bar{r}^T(kT)\, o' + \Omega(kT) + \epsilon(kT) \quad \in R^m \qquad (3\text{-}12)$$

in which the known or fixed parameters in o have been deleted to form

Θ'. This is also done with the corresponding elements in $\Upsilon(kT)$. These non identified parameters and appropriate delayed measurements are then collected into the vector $\Omega(kT)$. The vector Θ' thus contains only the elements of B_1 and $\Upsilon'(kT)$ the corresponding elements of $\Upsilon(kT)$. Additional details are given in Appendix C.

Having settled upon a model structure to represent the plant dynamics, it is now necessary to choose a recursive algorithm to identify the required elements of the step-response matrix. Sections 3.3 and 3.4 are devoted to this subject.

3.3 Recursive Least Squares Identification [1] (28)

Given a linear model of the structure described by Eqn (3-9), our goal is to find an estimate of the parameter vector Θ such that it minimizes the following weighted quadratic cost criterion on the parameter vector estimate

$$J = \sum_{k=0}^{\bar{N}} \{ [y(kT) - \Upsilon^T(kT) \Theta]^2 \} \qquad (3\text{-}13)$$

where $\bar{N}$ represents the total number of measurements, and the quantity within the brackets is the error between the measurement of the actual output of the system and the predicted output based on the current estimate of Θ. Differentiating the cost function with respect to the

---

1 This discussion pertains to a single-input single-output difference equation model although the multiple-input multiple-output case can be easily accomodated by performing a scalar measurement update procedure [(10), (28), Appendix C].

parameter vector (Θ) and after some derivations (28), the recursive least-squares (RLS) identification algorithm is obtained

$$R(kT) = R\{(k-1)T\} + \frac{1}{kT} [\ \Upsilon(kT)\ \Upsilon(kT)^T - R\{(k-1)T\}\ ] \quad (3\text{-}14)$$

$$\bar{\varepsilon}(kT) = y(kT) - \Upsilon(kT)^T\ \Theta\{(k-1)T\} \quad (3\text{-}15)$$

$$\hat{\Theta}(kT) = \hat{\Theta}\{(k-1)T\} + \frac{1}{kT} R(kT)^{-1}\ \Upsilon(kT)\ \bar{\varepsilon}(kT) \quad (3\text{-}16)$$

where $R(kT)$ is the information matrix, and $\bar{\varepsilon}(kT)$ is the prediction error. Though these equations are recursive, they are not well suited for on-line implementation since at each step a matrix inverse is required. However, taking the advantage of the fact that the update to the information matrix ($R(kT)$) is of rank one, the matrix inversion lemma can be used to exchange the matrix inverse for a scalar division in the propagation of the parameter covariance matrix as shown in Eqn (3-17)

$$P(kT) = P\{(k-1)T\} - \frac{P\{(k-1)T\}\ \Upsilon(kT)\ \Upsilon^T(kT)\ P\{(k-1)T\}}{1 + \Upsilon^T(kT)\ P\{(k-1)T\}\ \Upsilon(kT)} \quad (3\text{-}17)$$

where

$P(kT) = \frac{1}{kT} R^{-1}(kT)$ is the parameter covariance matrix

The parameter update equation is

$$\hat{\Theta}(kT) = \hat{\Theta}\{(k-1)T\} + P(kT)\ \Upsilon(kT)\ \bar{\varepsilon}(kT) \qquad (3\text{-}18a)$$

$$= \hat{\Theta}\{(k-1)T\} + \frac{P\{(k-1)T\}\ \Upsilon(kT)\ \bar{\varepsilon}(kT)}{1 + \Upsilon^T(kT)\ P\{(k-1)T\}\ \Upsilon(kT)} \qquad (3\text{-}18b)$$

The previous equations weight each measurement equally and assume that the parameters and measurement noise levels are constant over time, though the estimate $\hat{\Theta}(kT)$ is certainly a time-varying quantity. The interpretation given to $\hat{\Theta}(kT)$ is that of the best estimate of the constant parameter vector given all the past information up to time kT.

A more realistic approach allows for time varying noise levels and/or parameter vector. Such is the case in the weighted least-squares approach where the cost function is modified as follows:

$$J = \sum_{k=0}^{\bar{N}} \frac{1}{W(kT)} \{ [\ y(kT) - \Upsilon^T(kT)\ \Theta\ ]^2 \} \qquad (3\text{-}19)$$

where the weights $W(kT)$ are to be selected in such a way as to indicate the degree of confidence that can be placed on the individual measurements, or equivalently, the amount of uncertainty associated with a particular measurement. A desirable choice for the weights $W(kT)$ would be the variances of the corresponding measurements. A key problem in identification of time-varying systems is, however, the lack of knowledge of these variances (19:21).

Assuming that an estimate of the noise variance is available, the RLS algorithm is given by:

$$\hat{\Theta}(kT) = \hat{\Theta}\{(k-1)T\} + \frac{P\{(k-1)T\}\ \Upsilon(kT)\ \bar{\varepsilon}(kT)}{v(kT) + \Upsilon^T(kT)\ P\{(k-1)T\}\ \Upsilon(kT)} \qquad (3\text{-}20)$$

$$P(kT) = P\{(k-1)T\} - \frac{P\{(k-1)T\}\ \Upsilon(kT)\ \Upsilon^T(kT)\ P\{(k-1)T\}}{v(kT) + \Upsilon^T(kT)\ P\{(k-1)T\}\ \Upsilon(kT)} \qquad (3\text{-}21)$$

where $v(kT) = W(kT)$ is an estimate of the noise variance at time kT. Although this algorithm still assumes that the parameters are constant, it allows for time varying noise characteristics.

In order to allow for time-varying parameters, past information must somehow be deweighted and greater emphasis placed on more recent information.

A common and simple way to accomplish this goal is by modifying the cost function to include a "forgetting factor" to cause an exponential deweighting of data and place more emphasis on recent measurements. The cost function then becomes:

$$J = \sum_{k=0}^{\bar{N}} \frac{1}{v(kT)} \{ [\ y(kT) - \Upsilon^T(kT)\ \Theta\ ]^2\ \lambda^{\bar{N}-k}\ \} \qquad (3\text{-}22)$$

where $0 < \lambda \leq 1$ is the forgetting factor. This cost function leads to one of the most commonly used version of the RLS algorithm:

$$\hat{\Theta}(kT) = \hat{\Theta}\{(k-1)T\} + \frac{P\{(k-1)T\}\ \Upsilon(kT)\ \bar{\varepsilon}(kT)}{\lambda\ v(kT) + \Upsilon^T(kT)\ P\{(k-1)T\}\ \Upsilon(kT)} \qquad (3\text{-}23)$$

$$P(kT) = \frac{1}{\lambda}\left[P\{(k-1)T\} - \frac{P\{(k-1)T\}\ \Upsilon(kT)\ \Upsilon^T(kT)\ P\{(k-1)T\}}{\lambda\ v(kT) + \Upsilon^T(kT)\ P\{(k-1)T\}\ \Upsilon(kT)} \right] \qquad (3\text{-}24)$$

The use of the RLS algorithm is subject to a number of preconditions and limitations. A principal assumption is that the time variations of the parameters, and noise level, are slow and/or seldom compared with the time constants of the system (19:25); in other words, that large step-like changes in the parameters may not occur frequently.

An important requirement is that of "presistency of excitation" of the input data. To estimate a model of the plant dynamics that is satisfactory, the input signals to the plant must have sufficient energy and rich frequency content within the control bandwidth of interest. The conditions on persistency of excitation are related to the complexity of the estimated model. This implies that the requirements on the input signal become more severe if the model order (or the number of identified parameters) is increased (45). Since the input signals to the plant are generated by feedback there is no guarantee that these signals will be persistently exciting. On the contrary, good regulation may give a poor excitation (5, 45) since the algorithms usually extract information from the perturbations of the input-output signals around the nominal set-points. In that case the perturbations can be small, unless the command signals themselves are dynamic enough to provide the necessary control activity. This however is not always possible or practical.

To track parameter variations it is necessary to discount old data by means of the forgeting factor in Eqns (3-22) and (3-24). The choice of a suitable forgetting factor is usually the result of a compromise between fast adaptation and high stationary accuracy of the parameter estimates. If the forgetting factor is small, old data is discounted quickly and the estimated parameters will converge rapidly towards the new values. However, the accuracy of the estimates will decrease. A high value for the forgrtting factor ($\lambda \approx 1$) on the other hand will make it impossible to track rapid parameter variations (Figure 3-1). The final selection of a forgeting factor then reflects the compromise between the demands on convergence rate and long term quality of the parameter estimates. This trade-off is not always satisfactory (19:17). It is desirable to discount old data quickly when the plant is changing or has just changed and to discount data slowly when the parameters are relatively constant.

Another problem that may occur when a constant forgetting factor less than one is used is that of instabilities in the estimation algorithm commonly refered to as "estimator wind-up" (2). Exponential forgetting works well only if the plant is properly excited all the time. This may not be the case if the main source of excitation are changes in the set-points. Then there may be long periods with no excitation, the estimator will continue to discount old information and the uncertainty of the parameters will grow. The effect can be seen analytically. It can be shown that Eqn (3-24) is equivalent to:

$$P(kT) = [\ v^{-1}(kT)\ \bar{r}(kT)\ \bar{r}^{T}(kT) + \lambda\ P^{-1}\{(k-1)T\}\ ]^{-1} \qquad (3\text{-}25)$$

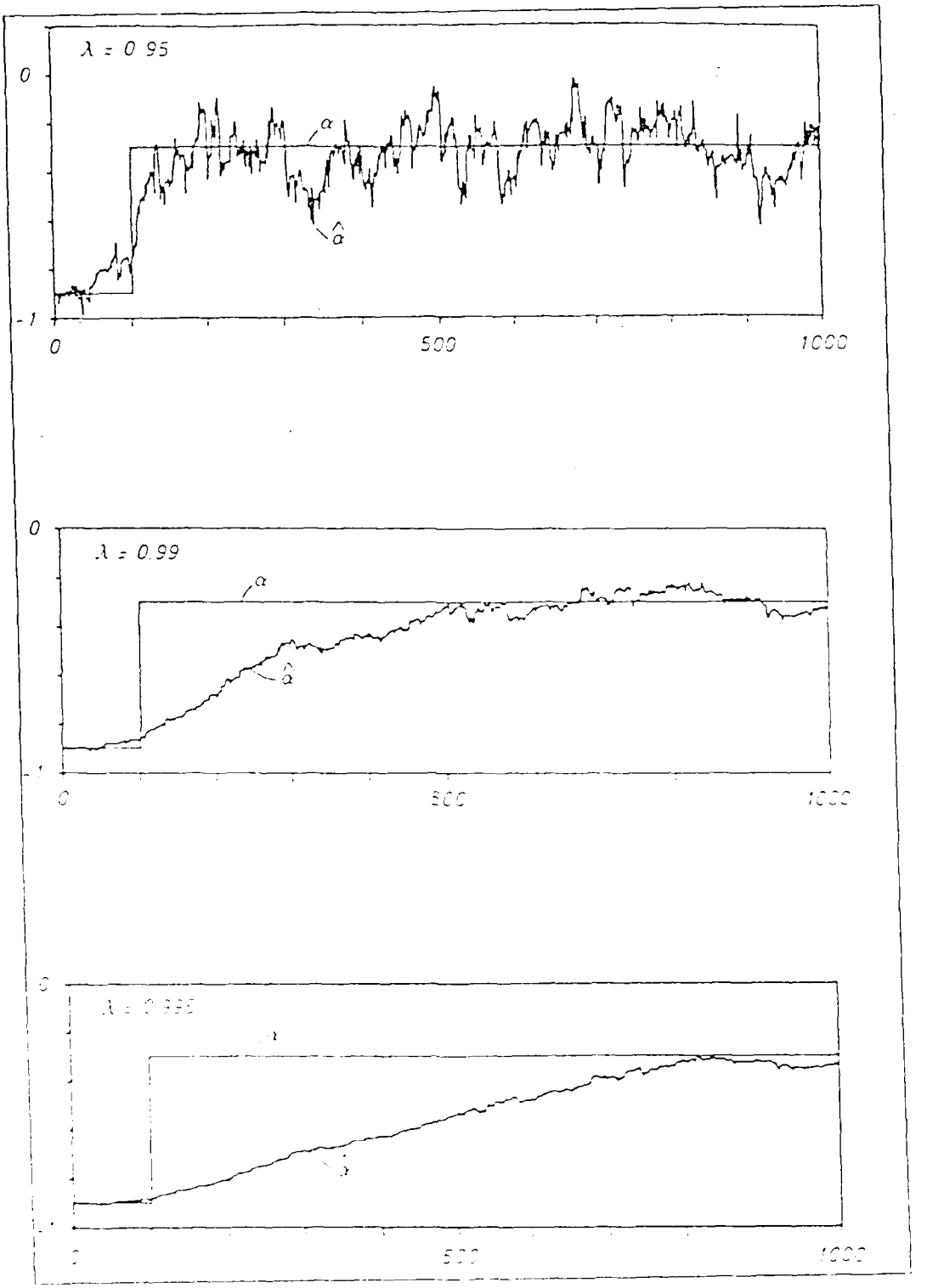

Figure 3-1. Effect of Forgetting Factor in transient response of parameter estimates (19:18)

If the plant is poorly excited, the input $u(kT)$ and the output $y(kT)$ are small. Since the components of the vector $\tau(kT)$ are delayed values of the input and output the vector $\tau(kT)$ will be also small. In the extreme case when $\tau(kT)$ is zero Eqn (3-25) leads to

$$P(kT) = \frac{P\{(k-1)T\}}{\lambda} \qquad (3\text{-}26)$$

indicating that the matrixx $P(kT)$ grows exponentially. If there is no excitation for a long period of time then $P(kT)$ may become very large and the estimator becomes unstable. Since $P(kT)$ is the gain in Eqns (3-18a) and (3-23), small prediction errors can produce large variations in the parameter estimates. This in turn may drive the closed-loop system unstable.

Another way of looking at the problem is from a point of view that considers how the information is processed in the RLS algorithm. Equation (3-24) can also be expressed as:

$$P^{-1}(kT) = P^{-1}\{(k-1)T\} - (1-\lambda)\, P^{-1}\{(k-1)T\} + v^{-1}(kT)\, \tau(kT)\, \tau(kT)^T \qquad (3\text{-}27)$$

where $P^{-1}(kT)$ is the information matrix. From Eqn (3-27) it can be seen that the first term represents the old information, the second term represents the information taken out, and the third term represents the information that is added by the measurement. Careful examination of Eqn (3-27) shows that data is discounted in all directions but the measurement is bringing information in only one direction (the first two terms of Eqn (3-27) are full rank while the third term is of rank one). Because of this, if persistency of excitation is not present, more

information will be discounted than brought in and eventually $P^{-1}(kT)$ will go to zero thereby causing instabilities in the algorithm.

There are several ways to avoid estimator wind-up. One is obviously making sure that the plant is properly excited before performing the identification. The condition for persistent excitation can be monitored and perturbations may be introduced if the excitation is poor. In cases where perturbations are not convenient, the identification process can be discontinued temporarily. Supervisory loops ((5, 24), Figure 3-2) are often employed to perform these functions. The price paid for this safeguard is the extra logic and data storage required to perform the appropriate checks.

Another possibility of dealing with the changing demands for data discounting is the use of time-variable forgetting factors (16) to adjust the amount of discounting automatically. The use of variable forgetting factors, however, is often heavily dependent on the assumptions imposed on parameter and noise level variations. Typically, the forgetting factor is adjusted in a manner inversely related to the prediction error or an estimate of its variance. The prediction error can be thought of as being composed of two independent components as indicated below:

$$\varepsilon = y(kT) - \phi^T(kT)\,\hat{c}(kT) = \varepsilon_m(kT) + \varepsilon_n(kT) \qquad (3\text{-}28)$$

where $\varepsilon_m(kT)$ is the model error and $\varepsilon_n(kT)$ is the measurement noise. In the least-squares method, each measurement is weighted according to an estimate of its uncertainty (Eqn 3-19), which can be expressed as

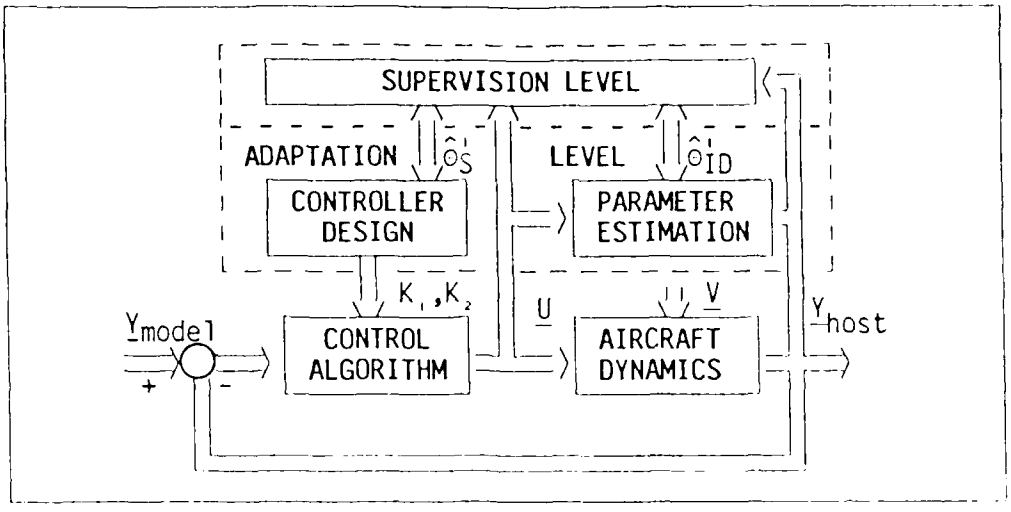

Figure 3-2. Parameter-adaptive Control system with supervision functions. (24)

follows:

$$\sigma^2(kT) = \sigma_m^2(kT) + \sigma_n^2(kT) \qquad (3\text{-}29)$$

where $\sigma^2(kT)$ is the estimate of the prediction error variance at time kT, $\sigma_m^2(kT)$ and $\sigma_n^2(kT)$ are the model error variance and measurement noise variance at time kT respectively. In the case of small and constant noise levels, assuming that the plant is properly excited, any changes in the plant will be reflected in the prediction error and the forgetting factor will be adjusted accordingly for improved convergence to the new parameter values. The problem with this technique is that an increase of the noise level will in most algorithms be interpreted as a variation of the parameters, i.e. an increase in $\sigma_m(kT)$. This action is a serious mistake (19:28) since the algorithm will discount old (and possibly good) information to favor new measurements with poor information content.

In order to avoid these problems, and the required assumptions about how the parameters and noise level vary, the approach taken in this thesis is to use a modified RLS algorithm developed by Hagglund (19). This algorithm automatically discounts old data depending on the amount of incoming information and updates the parameter estimates only in the direction where new information is entering. Section 3.4 discusses this algorithm in more detail.

3.4 Hagglund's Algorithm (19)

To account for time varying parameters and to remedy the weighting problem discussed in the previous section, a new principle of forgetting old data was presented by Hagglund (19) and used in a modified RLS algorithm. This section summarizes the development of Hagglund's algorithm.

As discussed earlier, the purpose of the least-squares estimator is to provide rasonably accurate estimates of the parameter vector $\theta(kT)$. To accomplish this objective, Hagglund approaches the information weighting problem from a different point of view. Typically, the information about the uncertainties in the measurements is rather poor. Thus instead of using assumptions on how the parameters and noise level vary, the information weighting is handled by relating the accuracy of the parameter estimates i.e. to the amount of information available, and the incoming information. Hagglund developed his algorithm adhering to the following principle:

"Discount old data in such a way that a constant desired amount of information is retained, if the parameters are constant (19:70)".

The amount of information is signified by the inverse of the P matrix. The goal of the estimator developed by Hagglund is to weight the incoming data so that the covariance matrix becomes proportional to the identity matrix. The diagonal elements of P(kT) may be interpreted as approximations of the variances of the corresponding parameters. The weights W(kT) in Eqn (3-19) are chosen so that these variances get a desired value. As a result, the amount of the data included in calculating an estimate of the parameter vector is dependent on the information the estimator is receiving. If there is no information coming in nothing will be forgotten. If the incoming information is small the convergence time will be long. However, if the information content in the data is large, old measurements will be discounted quickly so that fast parameter adaptation can occur.

If data is to be discounted according to the new principle, the information discounted must be the same as the information brought in by the new measurements. Recalling from Eqn (3-27), the new information is proportional to $\bar{r}(kT)\,\bar{r}^T(kT)$. It may be said that the new information is coming in the direction of $\bar{r}(kT)$. Thus old information is to be discounted in the same direction. In terms of the information matrix this is expressed as:

$$P^{-1}(kT) = P^{-1}\{(k-1)T\} + v^{-1}(kT)\,\bar{r}(kT)\bar{r}^T(kT) - \alpha(kT)\,\bar{r}(kT)\bar{r}^T(kT) \quad (3\text{-}30a)$$

$$P^{-1}(kT) = P^{-1}\{(k-1)T\} + [\, v^{-1}(kT) - \alpha(kT)\,]\, \bar{r}(kT)\, \bar{r}^{T}(kT) \quad (3\text{-}30b)$$

where $\alpha(kT)$ is a discounting factor. Note that in the updating of Eqn (3-30), information is removed only in the direction that information is added. This is in contrast to the earlier discusson of the least-squares algorithm with exponential discounting in Eqn (3-27) where information was removed in all directions due to the second term being full rank. The information matrix equation (3-30) gives way to the new method of updating the covariance matrix in Hagglund's modified RLS algorithm:

$$P(kT) = P\{(k-1)T\} - \frac{P\{(k-1)T\}\, \bar{r}(kT)\, \bar{r}^{T}(kT)\, P\{(k-1)T\}}{[v^{-1}(kT) - \alpha(kT)]^{-1} + \bar{r}^{T}(kT)\, P\{(k-1)T\}\, \bar{r}(kT)} \quad (3\text{-}31)$$

Since the form of the covariance matrix update has changed, the equation for updating the parameter estimates will also change. Using Eqn (3-31) along with the basic definition of the parameter update equation in the least-squares algorithm, Hagglund derives the following parameter estimate update equation:

$$\hat{\theta}(kT) = \hat{\theta}\{(k-1)T\} + \frac{P\{(k-1)T\}\, \bar{r}(kT)\, \varepsilon(kT)}{v(kT) + \bar{r}^{T}(kT)\, P\{(k-1)T\}\, \bar{r}(kT)\, [1-\alpha(kT)v(kT)]} \quad (3\text{-}32a)$$

$$= \hat{\theta}\{(k-1)T\} + \frac{1}{v(kT)}\, P(kT)\, \bar{r}(kT)\, \varepsilon(kT) \quad (3\text{-}32b)$$

It remains to be shown the choice of an appropriate discounting factor $\alpha(kT)$ in Eqns (3-31) and (3-32a). Equation (3-30) shows that $\alpha(kT)$ must be positive or information would be added instead of removed. Also, if $\alpha(kT)$ is too large the covariance matrix could become non positive definite. These and other considerations establish the need for a set bounds to which the discounting factor must be limited. In deriving a set of bounds on $\alpha(kT)$, Hagglund performed a stability investigation which included showing that a proper choice of $\alpha(kT)$ would ensure that the covariance matrixx remained positive definite. The stability investigation yielded the bounds on $\alpha(kT)$ and were chosen such that

$$0 \leq \alpha(kT) \leq \frac{1}{\bar{r}^T(kT)\ P\{(k-1)T\}\ \bar{r}(kT)} \qquad (3\text{-}33)$$

Furthermore, in order to obtain a diagonal P-matrix of the form $a \cdot I$ where a is the desired variance of the parameter estimates, Hagglund shows that $\alpha(kT)$ must be selected so that

$$\frac{\bar{r}^T(kT)\ P\{(k-1)T\}\ P(kT)\ P\{(k-1)T\}\ \bar{r}(kT)}{\bar{r}^T(kT)\ P\{(k-1)T\}\ P\{(k-1)T\}\ \bar{r}(kT)} = a \qquad (3\text{-}34)$$

Substituting Eqn (3-31) into Eqn (3-34) yield the following desired value of $\alpha(kT)$

$$\alpha_d(kT) = v^{-1}(kT) + \frac{\Delta_d(kT)}{\Delta_d(kT)\ \bar{r}^T(kT)\ P\{(k-1)T\}\ \bar{r}(kT) - 1} \qquad (3\text{-}35)$$

where

$$\delta_d(kT) = \frac{1}{\Upsilon^T(kT)\ P^2\{(k-1)T\}\ \Upsilon(kT)} \left[\frac{\Upsilon^T(kT)\ P^3\{(k-1)T\}\ \Upsilon(kT)}{\Upsilon^T(kT)\ P^2\{(k-1)T\}\ \Upsilon(kT)} - a \right] \quad (3\text{-}36)$$

To gain some insight as to the physical interpretation of the parameter $\delta(kT)$, a substitution of Eqn (3-35) into Eqn (3-31) is made. This results in a covariance matrix update equation of the form

$$P(kT) = P\{(k-1)T\} - \delta(kT)\ P\{(k-1)T\}\ \Upsilon(kT)\ \Upsilon^T(kT)\ P\{(k-1)T\} \quad (3\text{-}37)$$

From this equation, it can be seen that $\delta(kT)$ can be interpreted as a gain term for updating the covariace matrix.

Although application of Eqn (3-35) will result in the desired value of the discounting factor, because of the restrictions given in Eqn (3-33), Eqn (3-35) cannot always be used. Hagglund shows that by incorporating the bounds of $\alpha(kT)$ in Eqn (3-33) in conjunction with Eqn (3-35) the choice of $\alpha(kT)$ becomes

$$\alpha(kT) = \begin{cases} 0 & \text{if} \quad \alpha_d(kT) \leq 0 \\ \alpha_d(kT) & \text{if} \quad 0 < \alpha_d(kT) \leq \frac{1}{\eta(kT)} \\ \frac{1}{\eta(kT)} & \text{if} \quad \frac{1}{\eta(kT)} < \alpha_d(kT) \leq v^{-1}(kT) + \frac{1}{\eta(kT)} \\ 0 & \text{if} \quad \alpha_d > v^{-1}(kT) + \frac{1}{\eta(kT)} \end{cases} \quad (3\text{-}38)$$

where

$$\eta(kT) = \Upsilon^T(kT)\ P\{(k-1)T\}\ \Upsilon(kT) \quad (3\text{-}39)$$

The previous discussion is relevant to the situation where the parameters are constant or change slowly in comparison with the time constants of the plant. The inverse of the covariance matrix is then a good measure of the information content. In the case of abrupt plant parameter changes, $P^{-1}(kT)$ is no longer a good description of the information content in the estimator. It will take some time for the algorithm to reflect the uncertainty of the old parameter estimates by an increase of the covariance matrix. Since the covariance matrix partially determines the gain of the of the estimation algorithm, the low "magnitude" of the P matrix will most likely cause a slow parameter adaptation rate. To deal with this situation, Hagglund developed a "fault" detection procedure to speed up the adaptation in case of abrupt parameter changes.

The problem of how to account for step-like parameter changes can be broken down into two parts. The first of these is how to detect the parameter change (or fault). The second part is, once the parameter change has been detected, what modifications to the estimation algorithm need to be made to correctly account for these changes.

A fault detection procedure is accomplished by forming a test sequence that is sensitive to faults. The fault detection sequence should have properties that are significantly different before and after the fault. Following the development of a test sequence, the sequence is evaluated and decision theory is applied to determine if a fault has occurred.

Although the predominently used test sequence for fault detection is

often the residual sequence, its use can cause erroneous results as indicated in section 3.3 since an increase in the noise level can lead to false alarms. To solve this problem, Hagglund proposed to use the changes in the parameter estimate vector $\hat{\Theta}(kT)$ as the basis for the fault detection sequence.

Hagglund shows that when using the differences between two succesive estimates, $\Delta\hat{\Theta}(kT) = \hat{\Theta}(kT) - \hat{\Theta}\{(k-1)T\}$, as the basis of the fault detection sequence, the probabilities of $\Delta\hat{\Theta}(kT)$ being positive versus negative are approximately the same when the estimated parameters are close to the true values. This assumes that the equation error term in Eqns (3-9), (3-10), and (3-12) has white Gaussian noise characteristics. Representing this mathematically yields

$$P[\ \Delta\hat{\Theta}^T(kT)\ \Delta\hat{\Theta}\{(k-1)T\} > 0\ ] \approx P[\ \Delta\hat{\Theta}^T(kT)\ \Delta\hat{\Theta}\{(k-1)T\} < 0\ ] \quad (3\text{-}40)$$

When a fault has occurred, the above discussion and Eqn (3-40) no longer hold. The estimated parameters will be driven toward the new values and therefore Eqn (3-40) will be replaced by

$$P[\ \Delta\hat{\Theta}^T(kT)\ \Delta\hat{\Theta}\{(k-1)T\} > 0\ ] > P[\ \Delta\hat{\Theta}^T(kT)\ \Delta\hat{\Theta}\{(k-1)T\} < 0\ ] \quad (3\text{-}41)$$

Instead of observing the scalar product $\Delta\hat{\Theta}^T(kT)\ \Delta\hat{\Theta}\{(k-1)T\}$, it is more efficient to observe the scalar product between $\Delta\hat{\Theta}^T(kT)$ and a sum of the latest estimate increments. To simplify the algorithm, Hagglund performs an exponential filtering of the increments of the estimates instead of an ordinary sum. This results in the function $w(kT)$ being

defined as

$$w(kT) = \gamma_1 \, w\{(k-1)T\} + \Delta\hat{\Theta}(kT) \qquad 0 \leqslant \gamma_1 < 1 \qquad (3\text{-}42)$$

where the design parameter γ_1 controls the number of estimate increments that will significantly influence the resulting $w(kT)$. In case of a fault occurrence, $w(kT)$ can be viewed as being an estimate of the direction of the parameter change. This leads to the test sequence as developed by Hagglund, $s(kT)$. The test sequence, $s(kT)$, is defined to be

$$s(kT) = \text{sign}[\, \Delta\hat{\Theta}^T(kT) \, w\{(k-1)T\} \,] \qquad (3\text{-}43)$$

The sign function makes the test sequence insensitive to the noise variance. As was the case earlier, when the parameter estimates are in proximity to their actual values, the function $s(kT)$ has approximately a symmetric two point distribution with mass 0.5 each at +1 and -1. However, with the occurence of a fault, the distribution is no longer symmetric and the mass at +1 is larger. The idea behind the fault detection technique is then to inspect the latest values of $s(kT)$. If $s(kT)$ is +1 an unlikely number of times in a row, a fault is then declared.

To add the most recent values of $s(kT)$, Hagglund introduces the stochastic variable $r(kT)$ defined as

$$r(kT) = \gamma_2 \, r\{(k-1)T\} + (1-\gamma_2) \, s(kT) \qquad 0 \leqslant \gamma_2 < 1 \qquad (3\text{-}44)$$

which produces an exponential smothing of the test sequence $s(kT)$ in order to obtain a simple algorithm. When the parameters are close to their true values, and the equation error term has "white noise" characteristics, $r(kT)$ has a mean value close to zero. When a fault has occurred, a positive mean is expected. A fault is then declared when the value of $r(kT)$ exceeds a certain threshold. The design parameter here γ_2 controls how many $s(kT)$ values will be included in $r(kT)$.

As in the case with most design parameters, there are tradeoffs to be made when selecting the value of γ_2. If a small value of γ_2 is selected, fast fault detection will result at the cost of less security against false alarms. In instances where the signal to noise ratio in the system is poor, speedy fault detection is not feasible. For cases such as this, more information is required for proper decision making. By assigning γ_2 a larger value, more information will be available for the fault detection algorithm to determine the presence of a fault.

As is mentioned earlier, if $r(kT)$ exceeds a certain threshold, say r_0, a fault may be concluded with a confidence determined from the value of the threshold. The threshold r_0 can be computed as a function of γ_2 and the acceptable rate of false alarms, f_f, which may be chosen to suit the particular application in question (19:40). Hagglund performed this calculation and his results are ilustrated in Figure 3-3.

Having found a way of detecting large (and fast) parameter changes, the next step is to determine a suitable way of increasing the gain of the algorithm to speed-up the adaptation rate. To accomplish this, Hagglund chose to add the quantity $\beta(kT)$ times the identity matrix to the covariance matrix $P(kT)$. The covariance update equation

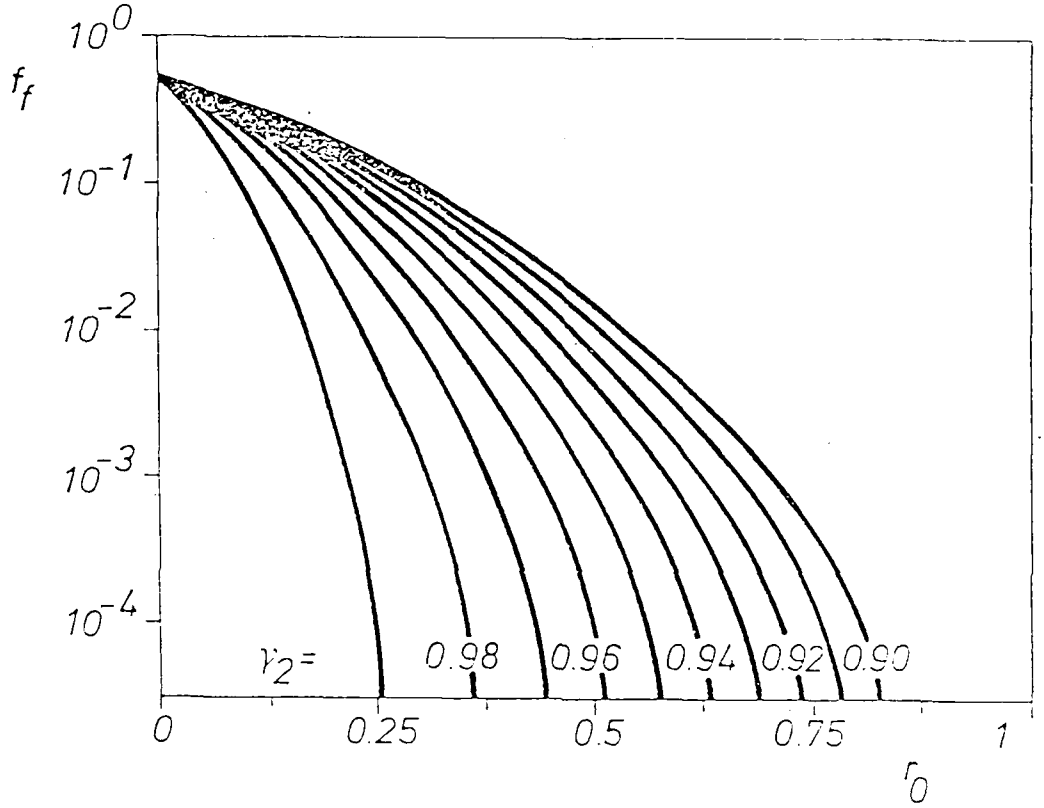

Figure 3-3. The error frequency f_f versus the threshold r_0 (19:41).

becomes

$$P(kT) = P\{(k-1)T\} - \frac{P\{(k-1)T\}\ \bar{\imath}(kT)\ \bar{\imath}^T(kT)\ P\{(k-1)T\}}{[v^{-1}(kT) - \alpha(kT)]^{-1} + \eta(kT)} + \beta(kT)\ I \quad (3\text{-}45)$$

where $\eta(kT)$ is given by Eqn (3-39). The parameter $\beta(kT)$ has the value of zero in all cases except when a fault is detected. Then, a positive value for $\beta(kT)$ will have the desired effect of increasing the covariance. It remains to specify a suitable choice for $\beta(kT)$.

One possibility of choosing $\beta(kT)$ is to let it be a function of the current value of $P(kT)$ and of the significance of the fault, i.e., of the value of $r(kT)$. In deriving the equation for $\beta(kT)$, Hagglund defines the following expression

$$\beta(kT) = \begin{cases} 0 & \text{if } r(kT) < r_0 \\ \dfrac{v(kT)}{\bar{\imath}^T(kT)\ \bar{\imath}(kT)}\ [\ \nu_0(kT) - \nu(kT)\ ] & \text{if } r(kT) \geq r_0 \end{cases} \quad (3\text{-}46)$$

where $\nu(kT)$ was shown to be an eigenvalue of the parameter update equation that could be assigned arbitrarily to control the step length of the algorithm (a small eigenvalue causes bigger steps towards the new parameter values, while an eigenvalue close to one causes smaller steps), ν_0 is the current eigenvalue, defined as

$$\nu_0(kT) = 1 - \frac{\eta(kT)}{v(kT) + [\ 1 - \alpha(kT)\ v(kT)\ ]\ \eta(kT)} \quad (3\text{-}47)$$

and r_0 is the fault detection threshold.

To ensure that the covariance matrix remains positive definte, the eigenvalue $v(kT)$ needs to meet the following condition

$$0 < v(kT) \leq v_0(kT) \tag{3-48}$$

A simple way of accomplishing this is by letting $v(kT)$ be a piecewise linear function of the significance of the fault as depicted in Figure 3-4.

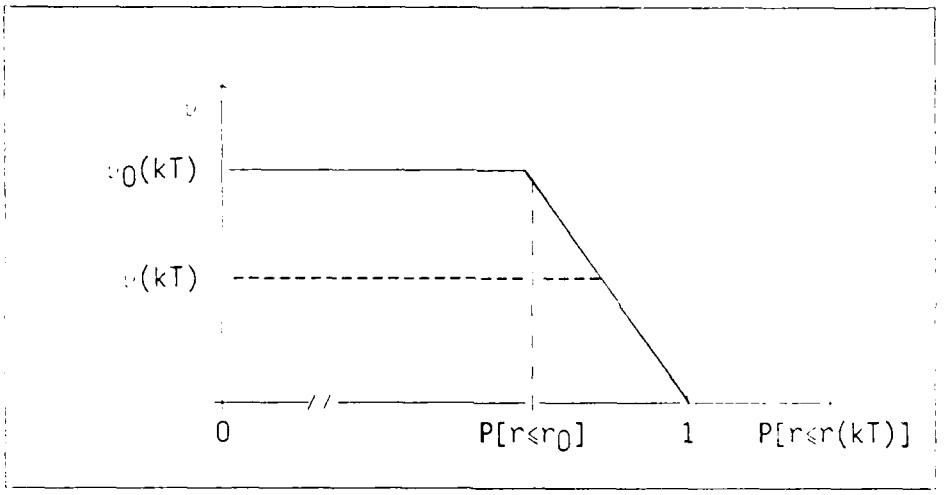

Figure 3-4. Possible choice of the eigenvalue $v(kT)$. (19:52)

The above choice of $v(kT)$ causes Eqn (3-46) to become

$$g(kT) = \begin{cases} 0 & \text{if } r\{(k-1)T\} < r_0 \\ \dfrac{v(kT)\, v_0(kT)\, (r\{(k-1)T\} - r_0)}{\bar{r}^T(kT)\, \bar{r}(kT)\, (1 - r_0)} & \text{if } r\{(k-1)T\} \geq r_0 \end{cases} \tag{3-49}$$

also independent with respect to the others (Appendix C), the estimation problem can be solved by adding the effects of one output at a time by going through the algorithm m times per time step. The procedure is summarized with the following algorithm

At time kT ($k \geq 0$, where 0 is initiation time)
calculate for i=1,...,m (see Eqns (3-9), (3-10) and (3-12))

$$\hat{\Theta}'_i(kT) = \hat{\Theta}'_{i-1}(kT) + \frac{1}{v_i(kT)} P_i(kT)\, \varphi_i(kT)\, \bar{\varepsilon}_i(kT) \qquad (3\text{-}51)$$

where

$\bar{\varepsilon}_i(kT)$ is the estimated prediction error

$v_i(kT)$ is the estimated prediction error variance

$P_i(kT)$ is the estimated parameter covariance matrix

$\varphi_i(kT)$ is the i^{th} column of measurements in $\bar{Y}(kT)$

with initial conditions

$\hat{\Theta}'_0(0)$ initial presumed values of the step-response matrix elements

$v_i(0)$ initial presumed value for prediction error variance for i=1,... m

$P_0(0)$ estimated covariance of the parameter estimates at initiation time

$\varphi_i(0)$ vector of past measurements prior to initiation of identification for i=1,... m

with design parameters

"a" desired variance of the parameter estimates

γ_1, γ_2, r_0 design parameters for a fault detection scheme

γ_3 , τ, r_1 design parameters of the prediction error variance estimator

and recursive relationships (in proper order of occurrence)

$$\hat{\Theta}'_0(kT) = \hat{\Theta}'_m\{(k-1)T\} \tag{3-52}$$

$$\varepsilon_i(kT) = y_i(kT) - v_i^T(kT)\,\hat{\Theta}'_{i-1}(kT) + \Omega_i(kT) \tag{3-53}$$

$$P_0(kT) = P_m\{(k-1)T\} \tag{3-54}$$

$$\eta_i(kT) = v_i^T(kT)\,P_{i-1}(kT)\,v_i(kT) \tag{3-55}$$

$$\mu_i(kT) = v_i^T(kT)\,P^2_{i-1}(kT)\,v_i(kT) \tag{3-56}$$

$$\lambda_i(kT) = v_i^T(kT)\,P^3_{i-1}(kT)\,v_i(kT) \tag{3-57}$$

$$\delta i_d(kT) = \frac{1}{\mu_i(kT)}\left|\frac{\lambda_i(kT)}{\mu_i(kT)} - a\right| \tag{3-58}$$

$$r_0(kT) = r_m\{(k-1)T\} \tag{3-59}$$

$$v_i(kT) = \begin{cases} \gamma_3\, v_i\{(k-1)T\} + (1-\gamma_3)\,\varepsilon^2_i(kT-\tau) & \text{if } r_{i-1}(kT) < r_1 \\ v_i\{(k-1)T\} & \text{if } r_{i-1}(kT) \geq r_1 \end{cases} \tag{3-60}$$

$$\alpha i_d(kT) = v_i^{-1}(kT) + \frac{\delta i_d(kT)}{\delta i_d(kT)\,\eta_i(kT) - 1} \tag{3-61}$$

$$\alpha_i(kT) = \begin{cases} 0 & \text{if } \alpha i_d(kT) \leq 0 \\ \alpha i_d(kT) & \text{if } 0 < \alpha i_d(kT) \leq \dfrac{1}{\eta_i(kT)} \\ \dfrac{1}{\eta_i(kT)} & \text{if } \dfrac{1}{\eta_i(kT)} < \alpha i_d(kT) \leq v_i^{-1}(kT) + \dfrac{1}{\eta_i(kT)} \\ 0 & \text{if } \alpha i_d > v_i^{-1}(kT) + \dfrac{1}{\eta_i(kT)} \end{cases} \tag{3-62}$$

$$v_{0_i}(kT) = 1 - \frac{\eta_i(kT)}{v_i(kT) + [\ 1 - \alpha_i(kT)\ v_i(kT)\ ]\ \eta_i(kT)} \tag{3-63}$$

$$\beta_i(kT) = \begin{cases} 0 & \text{if } r_{i-1}(kT) < r_0 \\ \dfrac{v_i(kT)\ v_{0_i}(kT)\ (r_{i-1}(kT) - R_0)}{v_i^T(kT)\ v_i(kT)\ (1 - R_0)} & \text{if } r_{i-1}(kT) \geq r_0 \end{cases} \tag{3-64}$$

$$P_i(kT) = P_{i-1}(kT) - \frac{P_{i-1}(kT)\ v_i(kT)\ v_i^T(kT)\ P_{i-1}(kT)}{[v_i^{-1}(kT) - \alpha_i(kT)]^{-1} + \eta_i(kT)} + \beta_i(kT)\ I \tag{3-65}$$

(equation (3-51) evaluated here)

$$w_0(kT) = w_m\{(k-1)T\} \tag{3-66}$$

$$w_i(kT) = \gamma_1\ w_{i-1}(kT) + [\ \hat{\theta}'_i(kT) - \hat{\theta}'_{i-1}(kT)\ ] \tag{3-67}$$

$$s_i(kT) = \text{sign}\ [\ (\ \hat{\theta}'_i(kT) - \hat{\theta}'_{i-1}(kT))^T\ w_{i-1}(kT)\ ] \tag{3-68}$$

$$r_i(kT) = \gamma_2\ r_{i-1}(kT) + (1-\gamma_2)\ s_i(kT) \tag{3-69}$$

By incorporating Hagglund's modifications to the recursive least-squares algorithm, it is posible to account for the time variation of plant parameters in a more efficient manner as compared to the standard RLS algorithm. The major advantage of using Hagglund's algorithm is that it solves the problems caused by nonuniform excitation of the plant. This is important since it allows for the identification procedure to take place during general aircraft maneuvers by discounting data depending on the amount of information available. A convenient

feature is also that the previous, ad hoc choices of forgetting factors are replaced by the performance related choices of the desired parameter variances (19:115).

3.5 Summary

Chapter 3 has presented the theory behind the recursive identification scheme that, together with the control law presented in chapter 2, will allow for the development of an adaptive system to compensate for aircraft parameter variations. This is done in order to demonstrate the capability to maintain good model-following performance while conducting in-flight simulations under different flight conditions. Throughout these discussions, many variables have been identified as user defined design quantities. The next chapter will provide the details of the design procedures for determining the appropriate design parameters for both the control law, and the recursive identification algorithm.

IV. Design Process

4.1 Introduction

The previous chapters in this thesis provide some insight into the theory of both the control law and the recursive identification algorithm used in the adaptive system. The intent of this chapter is twofold, namely, to present a detailed description of the procedure and practical aspects considered for selecting the design parameters of the adaptive system, and to provide details of the system's representation and simulation with $MATRIX_X$.

Although deterministic in nature, the control law design techniques developed by Prof. Porter require some amount of trial and error in the development of a particular design. A number of variables are to be defined by the user based on theoretical insight and experience gained throughout the trial and error process. This process must also be applied in adjusting the design parameters of Hagglund's algorithm to optimize the adaptation mechanism's ability to estimate the open-loop aircraft dynamics.

The adaptive system designs presented in this thesis are based on the use of the linearized longitudinal equations of motion of the AFTI/F-16 aircraft at a nominal flight condition of Mach 0.9 at 10,000 ft. of altitude. Also, a model of the aircraft at Mach 0.3, 10,000 ft. is used to test the system's ability to perform under changing conditions.

This chapter begins by presenting a brief description of the

mathematical models used to represent the aircraft and actuator dynamics in section 4.2. Section 4.3 presents the developments that lead into the final control law design. General mathematical considerations, as well as peculiarities of the Porter design method are discussed. Finally, section 4.4 addresses the issue of fine tuning the estimator design variables, and also highlights the various practical signal processing aspects required for its implementation.

4.2 Aircraft Model

The airplane dynamics used in this study are represented by a set of first order matrix diferential equations in the state space form of equations (2-1) and (2-9). These state space equations are obtained from the forces and moments acting upon the aircraft, and are expressed using the body axis system centered at the aircraft's center of gravity (Figure 4-1). A detailed derivation of the longitudinal state perturbation equations used in this thesis is presented in Reference 7.

Equation (4-1) shows the longitudinal state space model of the AFTI/F-16 in terms of the primed dimensionalized stability deri...

$$\begin{bmatrix} \dot{\theta} \\ \dot{u} \\ \dot{\alpha} \\ \dot{q} \end{bmatrix} = \begin{bmatrix} 0 & 0 & 0 & 1 \\ X'_{\theta} & X'_{u} & X'_{\alpha} & X'_{q} \\ Z'_{\theta} & Z'_{u} & Z'_{\alpha} & Z'_{q} \\ M'_{\theta} & M'_{u} & M'_{\alpha} & M'_{q} \end{bmatrix}$$

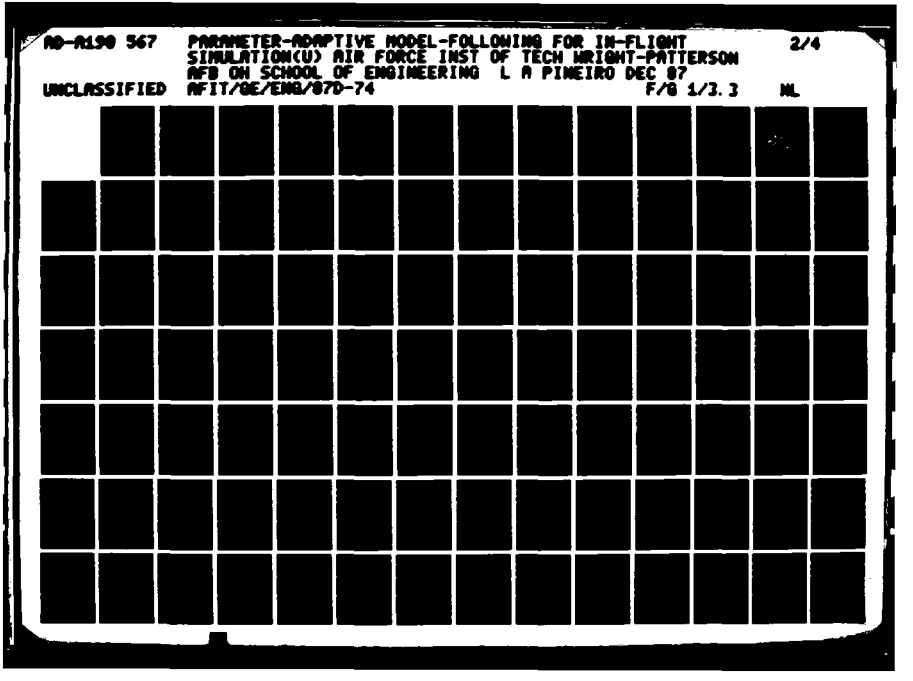
AD-A190 567 PARAMETER-ADAPTIVE MODEL-FOLLOWING FOR IN-FLIGHT SIMULATION(U) AIR FORCE INST OF TECH WRIGHT-PATTERSON AFB OH SCHOOL OF ENGINEERING L A PINEIRO DEC 87 2/4
UNCLASSIFIED AFIT/GE/ENG/87D-74 F/G 1/3.3 NL

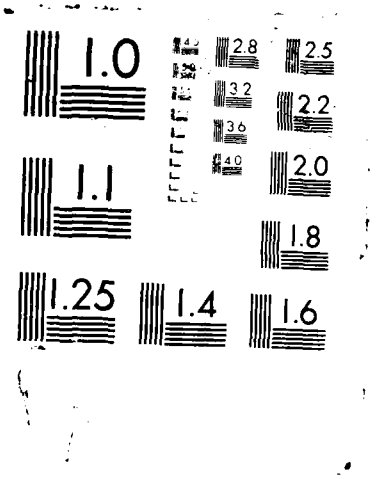
1.0
1.1
1.25
2.8
3.2
3.6
4.0
2.5
2.2
2.0
1.8
1.4
1.6

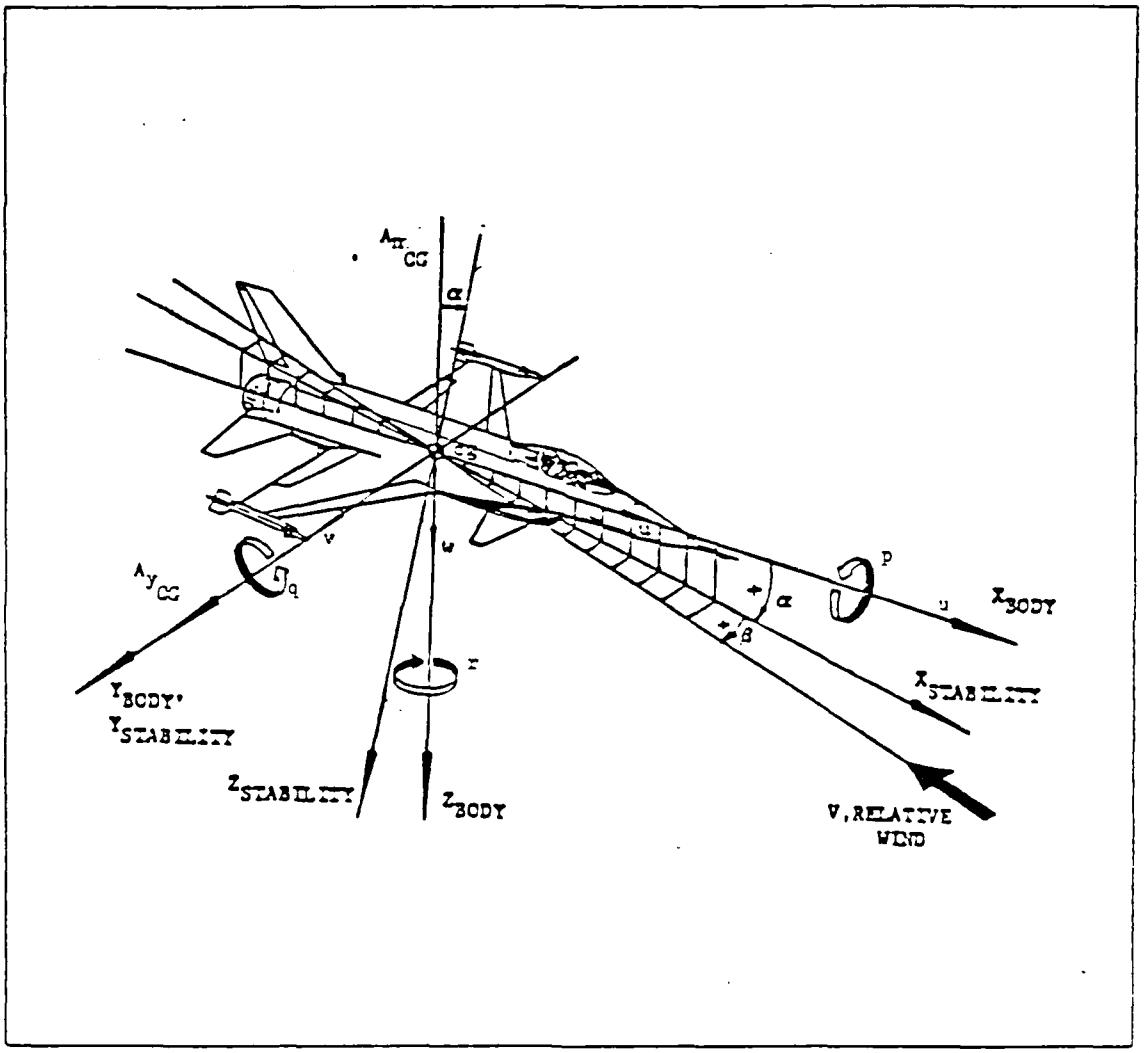

Figure 4-1. Aircraft axis system.

where

θ is the pitch angle

u is the forward velocity

α is the angle of attack

q is the pitch rate

δ_e is the elevator deflection

δ_f is the flaperon deflection

The equations used to calculate the coefficients in Eqn (4-1) are also found in Reference 7. In this case, a Flight Dynamics Laboratory aerodynamic data package for the AFTI/F-16 was used to obtain the coeficients in Eqn (4-1) by trimming the aircraft at the previously named flight conditions. The relevant data for these models is presented in appendix A.

The next step is simply to define the output vector of the quantites of interest. In this case, the desired outputs are flight path angle and pitch rate. The flight path angle is defined as

$$\gamma = \theta - \alpha \tag{4-2}$$

This leads to the following output equation

$$\begin{bmatrix} \gamma \\ q \end{bmatrix} = \begin{bmatrix} 1 & 0 & -1 & 0 \\ 0 & 0 & 0 & 1 \end{bmatrix} \begin{bmatrix} \theta \\ u \\ \alpha \\ q \end{bmatrix} \tag{4-3}$$

These equations, representing the aircraft dynamics, are implemented by means of the computer aided design package $MATRIX_X$ with its simulation facility SYSTEM-BUILD (23). This is ilustrated in Figure 4-2 thru 4-4. Figure 4-2 shows the elements of the block "A/C" wich depicts the overall aircraft model with a representation directly derived from the state space equations. The different set of dynamics associated with the two flight conditons of interest are implemented by means of gain scheduler functions (Figures 4-3 - 4-4) which change the elements of the A and B matrices in the model of Figure 4-2. The elements in the C matrix remain constant throughout the simulation.

Figure 4-2 also shows the addition of actuator dynamics into the aircraft simulation. These include nonlinearities such as surface position and rate limits. Consideration of their effects is very important, especially in the case were the control system is to provide artificial stability to the aircraft as it is the situation here.

The actuator model used in this simulation is derived from the VISTA design requirements that call for faster actuator dynamics than those found in the regular F-16 aircraft. For purposes of these simulations a simple first order model will be used. The actuator model for both the elevator and flaperon is of the form

$$\frac{\delta}{\delta_{cmd}} = \frac{44}{(s + 44)} \tag{4-4a}$$

or equivalently

$$\dot{\delta} = -44\ \delta + 44\ \delta_{cmd} \tag{4-4b}$$

Equation (4-4) is implemented for both actuators with the models shown in Figures 4-5 and 4-6. Figure 4-5 shows the overall actuator model as

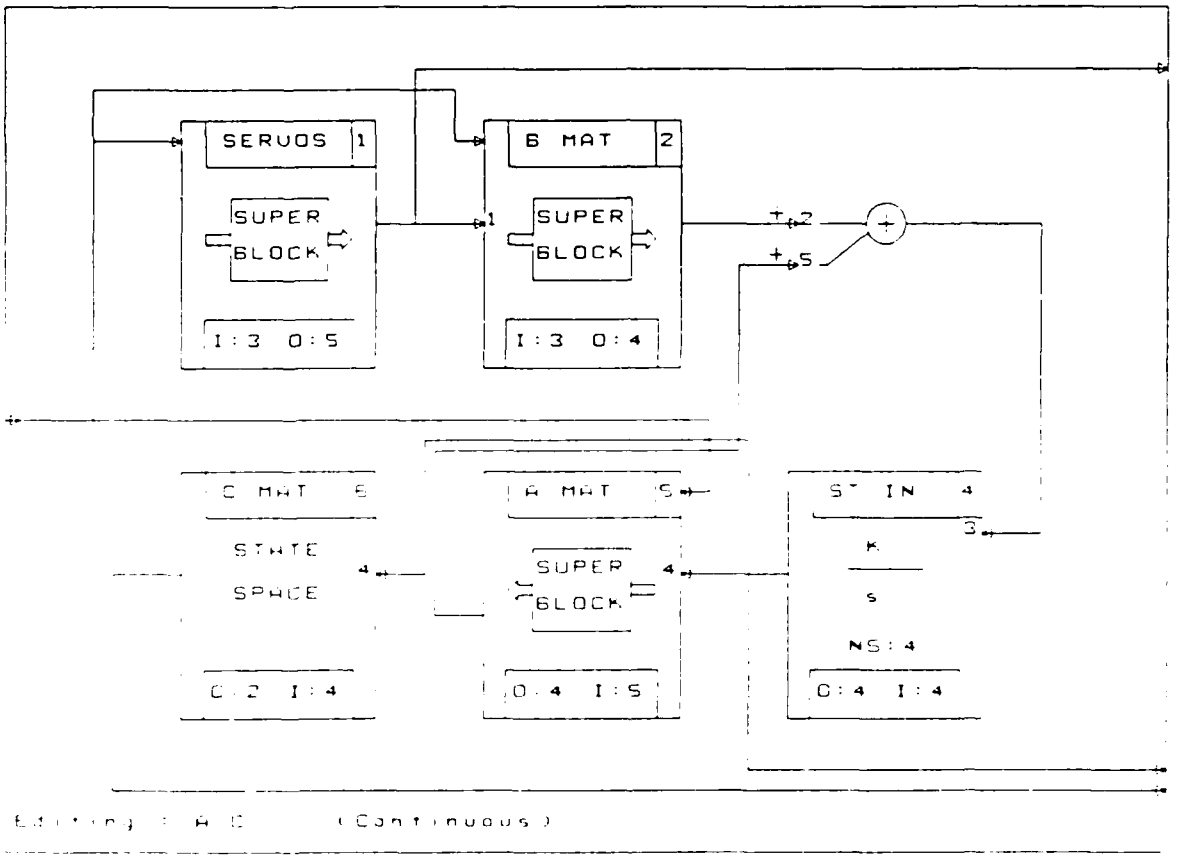

Figure 4-2. Aircraft Dynamics Representation.

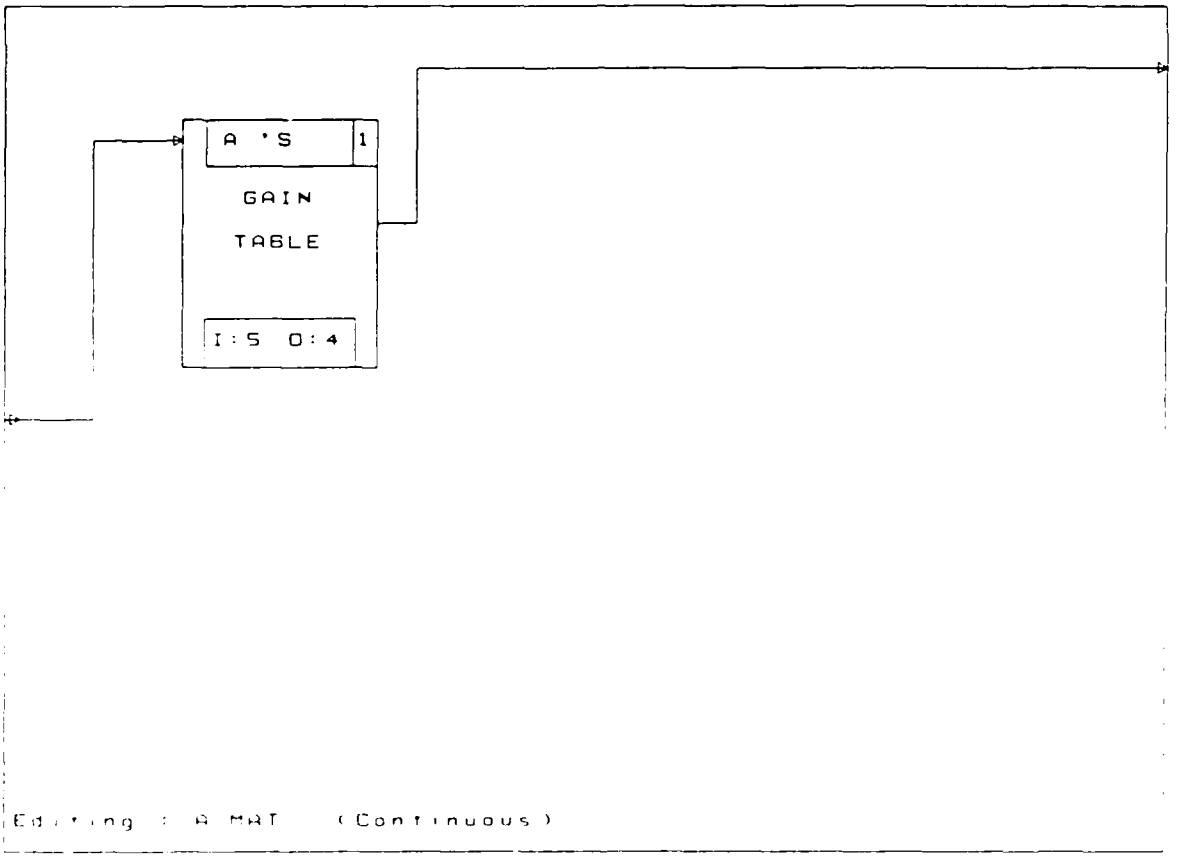

Figure 4-3. Gain Scheduler Function for the Aircraft's A Matrix.

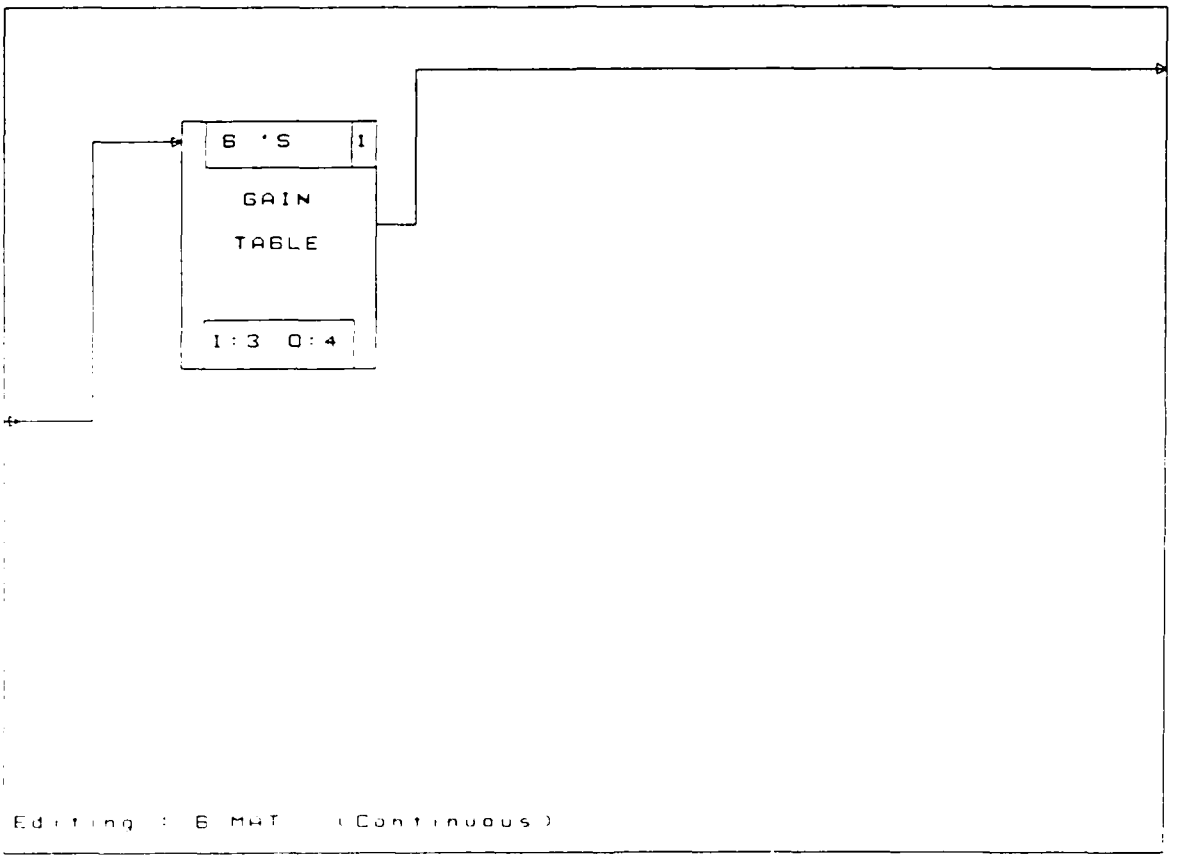

Figure 4-4. Gain Scheduler Function for the Aircraft's B Matrix.

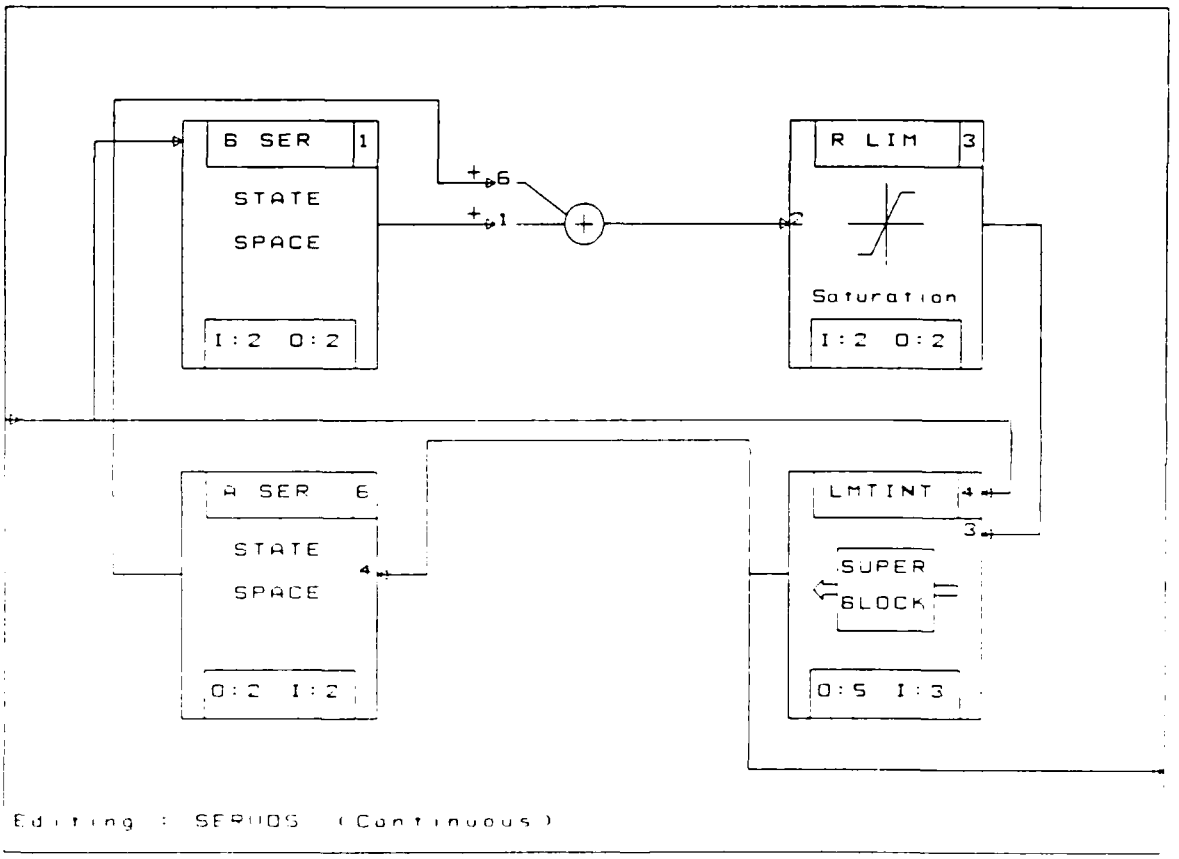

Figure 4-5. Actuator Model Representation.

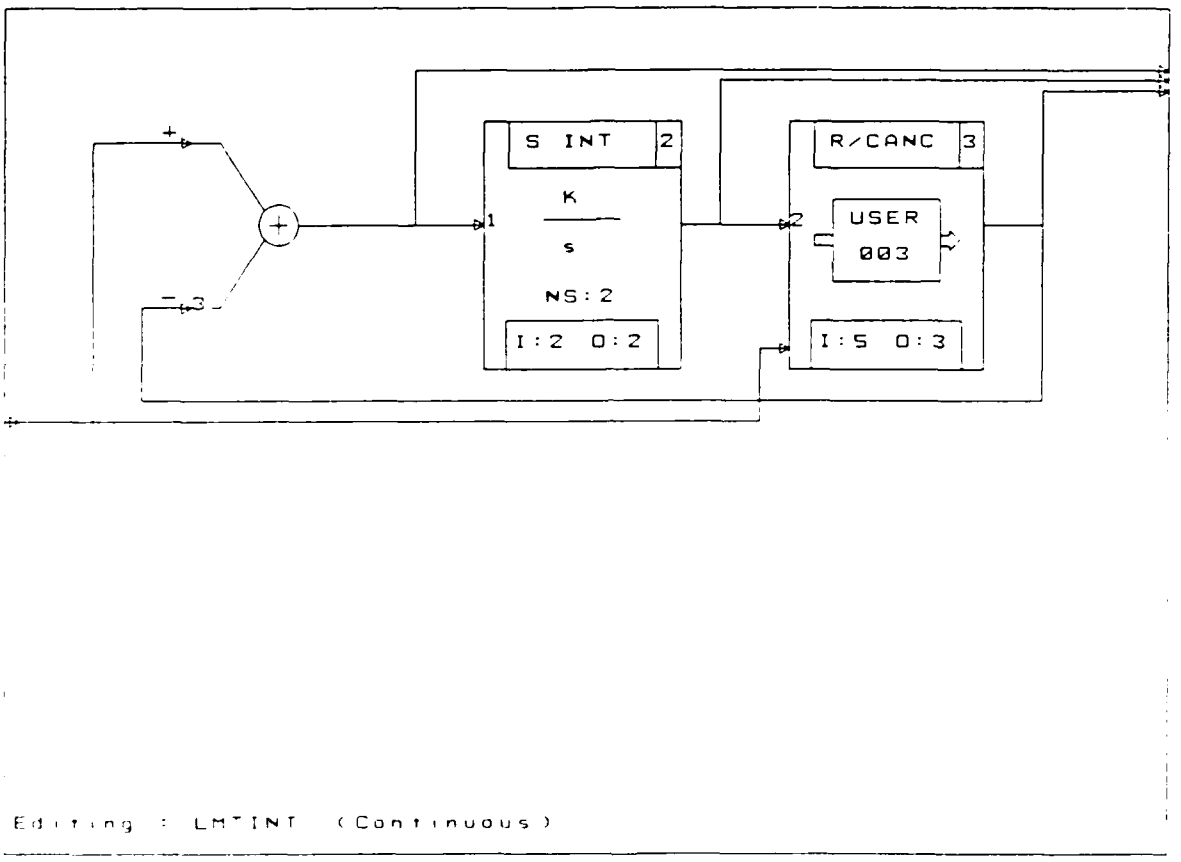

Figure 4-6. Limited Integrator Funtion Representation.

derived from Eqn (4-4b), with the addition of the rate and position limiting functions.

The control surface rate is limited simply by placing a limiter function after the rate of Eqn (4-4b) is calculated. This is implemented after the summing junction in Figure 4-5. The implementation of the control surface position limiting function is slightly more involved. It would be erroneous to simply place a limiter after the position of the surface is calculated from the integration of the surface rate, since this would imply that the calculated surface rate of motion would not be zero when the surface is stuck at a limit. Instead, a limited integrator function is implemented to calculate the control surface position from the calculated surface rate. This is ilustrated in Figure 4-6. The rate canceler in the limiter integrator (block labeled R/CANC) monitors the calculated surface position and compares it to the surface's position limits. If the surface deflection is at a limit, the rate canceler function negates the commanded rate at the summing junction location. This causes the desired effects of zeroing the surface rate and stoping the surface position calculation at its current point until the commanded surface rate changes direction. While the surface deflections are within the normal range, the rate canceler simply outputs zero, thus letting the incoming surface rate be integrated to obtain the surface position. The control surface position and rate limits used in this study are given in Table 4-1.

The position limits are relative from the trim position of the surfaces. Since the simulation is based on perturbation equation of motion at different flight conditions, these limits are scheduled

Table 4-1

Control Surface Position and Rate Limits

Surface	Flt. Condition	Position Limit (deg)	Rate Limit (deg/sec)
Elevator	Nominal	+ 27.37/ - 22.63	90
"	Off Nominal	+ 27.06/ - 22.94	"
Flaperon	Nominal	+ 22.0 / - 21.0	78
"	Off nominal	+ 7.54/ - 35.46	"

according to which model is being used at any given time. The absolute limits are ± 25 deg. for the elevator and + 20 deg. / - 23 deg. for the flaperon. The direction of positive surface deflection is indicated in Figure 4-7.

Finally, consideration to imperfect measurements is given in the design by providing the capability to inject measurement noise into the simulation. This is ilustrated in Figure 4-8, which shows the details of the sensor block. A simple model for zero-mean, white, Gaussian noise is used to corrupt the individual measurements independently. The specific noise levels used are provided in the next chapter. Figure 4-8 also shows the capability of including sensor dynamics in the simulation. The sensor dynamics implementation in this case is limited to simple low-pass anti-aliasing filters with corner frequency of 40 Hz. The reason for this is that, at the time of this study, no specific information was available on the sensors to be used in the design of the variable stability system for VISTA.

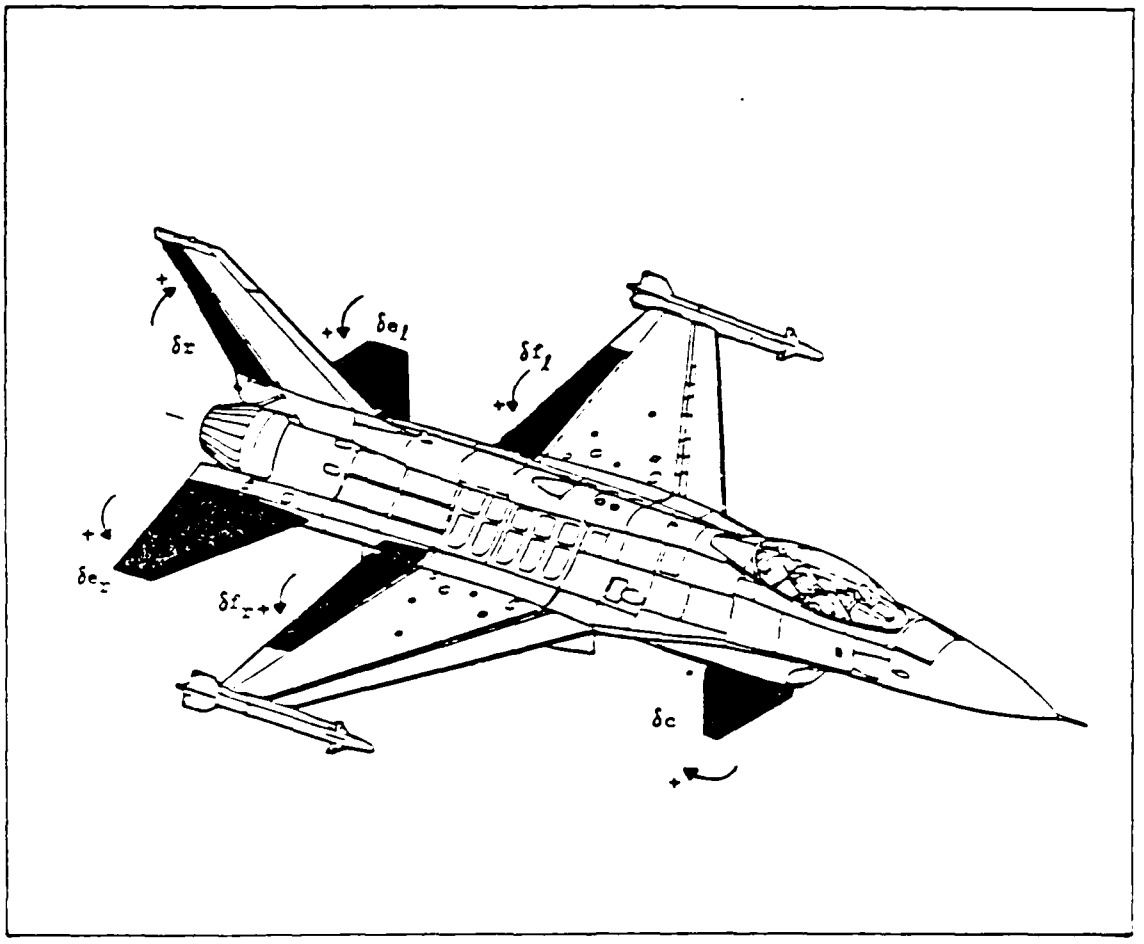

Figure 4-7. Definition of Positive Control Surface Deflections.

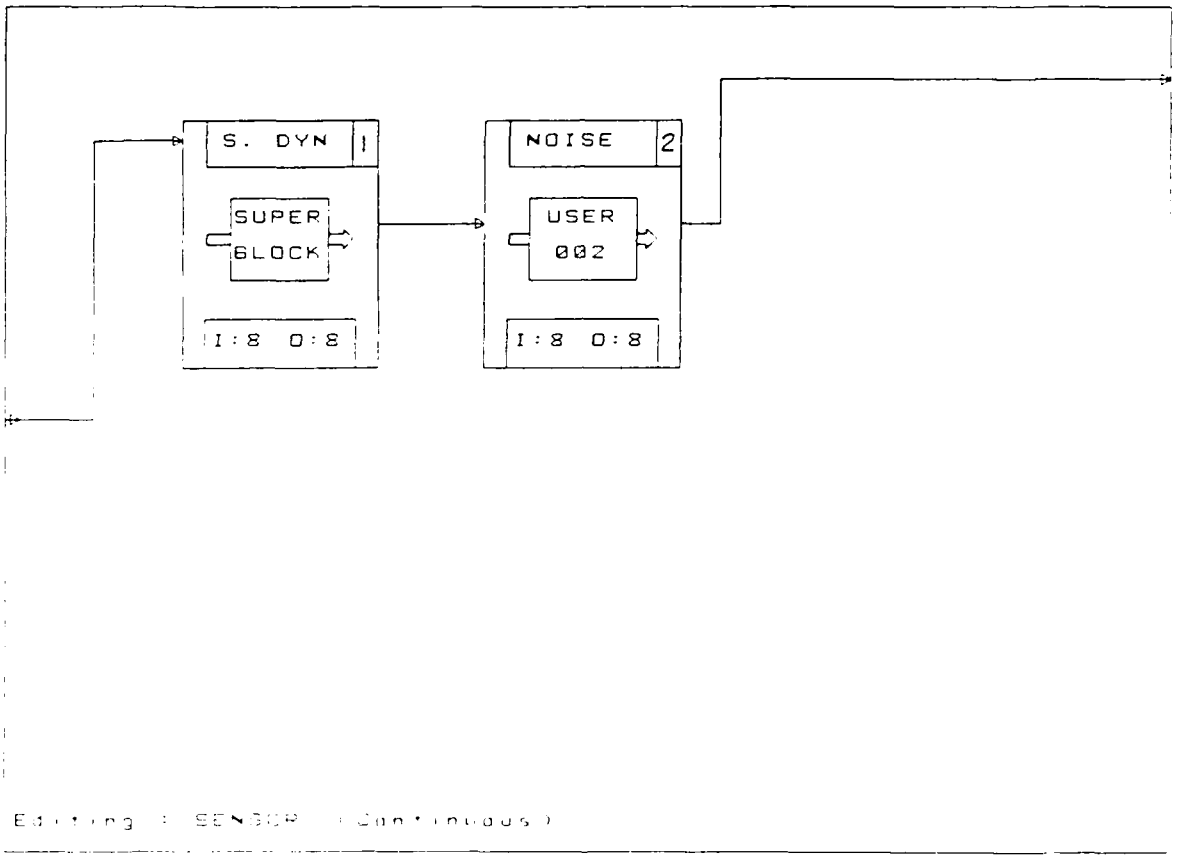

Figure 4-8. Sensor Measurement Noise Representation.

4.3 Control Law Design

4.3.1 Mathematical Background. Before a particular control law design is developed it is necessary to make sure that the system for which it is intended satisfies a number of requirements. Of fundamental importance is for the plant to be completely controllable and observable. Controllability implies that the inputs can affect all the modes (poles) of the system, thus making it possible to alter these modes in order to effectively modify the system's characteristics. For a linear time-invariant system described by Eqn (2-1) controllability can be checked by evaluating the rank of the controllability matrix (14,40), denoted M_C, given by

$$M_C = [\ B \mid AB \mid A^2B \mid \ldots \mid A^{n-1}B\ ] \qquad (4\text{-}5)$$

where n is the number of states. If the rank of M_C is equal to n, then the system is completely controllable. If M_C is rank defective the system is deemed uncontrollable signifying that some of the modes cannot be affected by the input to the plant. In this case the rank defect of M_C (i.e., n minus the actual rank of M_C) tells us how many modes are uncontrolable.

Observability implies that the outputs of the plant are affected by every mode, and that every state affect the outputs of the plant (40). This property is particularly important since control is to be provided by output feedback. Although not all the states are to be measured, their influence on the outputs is necessary if proper control of the modes is to be achieved. In addition, observability becomes necessity

in this particular case where the dynamics of the plant are to be identified from input-output data for the purpose of applying adaptive control. Lack of observability would imply that the plant could not be properly characterized solely from input-output data. This would lead to an erroneous plant representation and, in turn, an incorrect control strategy. For the linear time-invariant system represented by Eqns (2-1) and (2-9) the property of observability can be checked by evaluating the rank of the observability matrix M_O (14,40), defined as

$$M_O = [\ C^T \mid A^TC^T \mid (A^T)^2C^T \mid \ldots \mid (A^T)^{n-1}C^T\ ] \qquad (4\text{-}6)$$

Analogously to the controllability check, if the rank of M_O is equal to n then the plant is deemed fully observable. If this is not the case, then the rank defect of M_O indicates the number of unobservable modes.

Controllability and observability are checked for the two sets of dynamics used in this thesis (Appendix A). This is done with the aid of the matrix manipulation and control design functions of the $MATRIX_X$ package. Both models satisfy the full controllability and observability conditions.

Another important consideration in the Porter method is that of the location of transmission zeros. The transmission zeros of the plant, defined as zeros of the equivalent transfer function representation that block particular modes from the input, are regions to which some of the slow roots of the closed loop system migrate as the gain approaches infinity. Output feedback does not alter the location of transmission

zeros, therefore it is desired that these zeros be stable in order to insure system stability at high values of gain. This however does not guarantee stability for lower values of gain for which the system roots may pass through unstable regions before approaching the transmission zero locations. It is therefore imperative that the system's roots be checked throughout the design stages to verify the stable location of the closed-loop roots. This task is easily accomplished with the analysis tools provided by $MATRIX_X$.

Of particular interest is the existance of a transmission zero at the origin. This condition results from the inclusion of the pitch rate in the output vector. The presence of a transmission zero at the origin suggest that the system is unstable and uncontrollable (35) because of the location of a closed-loop system root at the transmission zero location. An analysis of this situation is required at this point. As pointed out by Barfield (7:83-85) the transmission zero at the origin results from the assumptions made in forming the equations of motion for the aircraft in which the following relationship between the pitch rate and pitch angle is established

$$q = \dot{\theta} \tag{4-7}$$

If q is to be commanded with step functions, θ would ramp to infinity due to the integration caused by the pole located at the transmission zero location. Thus some of the system's responses are unbounded for bounded inputs. For any practical maneuver, q commands resemble pulses, more than steps, or perhaps some other shape applied for a finite amount

of time that produces a bounded pitch angle response. This is precisely what is expected given the relationship of Eqn (125).

A by-product resulting from the existance of the transmission zero at the origin is that the introduction of integral action in the control law produces what is termed a "functionally uncontrollable" system (35). The vector integrator that is part of the control law introduces additional dynamics in the control loop. As part of the design procedure, it is necessary to check for controllability of the augmented system composed of the control law and plant dynamics (which may include the actuators and sensors). A simple check for this is performed by satisfying the following rank test (38)

$$\text{rank} \begin{vmatrix} B & A \\ 0 & -C \end{vmatrix} = n + m \qquad (4\text{-}8)$$

Executing this test for the aircraft models of this thesis results in a rank deficiency of one for both models in question. Again, additional discussion is required at this time. A rank deficiency of one implies that only one closed-loop pole is uncontrollable. An analysis of the behavior of the closed-loop poles of the system (Appendix D) reveals that the uncontrollable mode corresponds to one of the poles at the origin introduced by the vector integrator of the control law. This uncontrollable closed-loop pole at the origin accounts for the integration that takes place due to Eqn (4-7). The fact that the location of this root cannot be changed merely reflects the case that the definition given in Eqn (4-7) must prevail in the resulting pitch

angle response. The other roots of the system are controllable and their asymptotic behavior follows the theory presented in chapter 2. The condition of functional uncontrollability is not considered an adverse indication in this design but rather a reflection of the assumptions made in defining the dynamics of the problem. The system is then deemed conditonally stable for the particular design in question, and thus considered satisfactory for purposes of this study.

4.3.2 Design Variables. The key elements of the proportional plus integral control law of Eqn (2-46) are the proportional gain matrix $\bar{K}_1$ and the integral gain matrix $\bar{K}_2$. Once the step-response matrix of the aircraft model is known for a particular flight condition and sampling time, the gain matrices are calculated according to Eqns (2-47) and (2-48) using the following design variables:

Σ = the diagonal weighting matrix, diag{ σ , σ_2 }

γ = the ratio of integral to proportional control

The values of σ , σ_2, and γ are chosen so that several objectives are satisfied; the first of which is to stabilize the aircraft. After this is accomplished the controller is tailored to produce the desired tracking characteristics. The selection of these design parameters in this thesis is based on the use of an aircraft model trimmed at Mach 0.9 and 10,000 ft. altitude, with a sampling time of 0.01 sec. for the control law. The value chosen for the sampling time is considered sufficiently short as to be possible to observe all relevant modes of the open-loop plant, and is within the capability of the state-of-the-art in flight control computers.

The Porter design technique is based primarily on the assumption of linear plant models, and the availability of sufficient control authority. The limitations imposed by control surface deflection and rate limits make the system nonlinear. This situation imposes additional constraints in the design task. The problem then becomes the formulation of a control law that provides for sufficiently fast responses, with an acceptable level of tracking error, and while staying within control surface deflection and rate limits. A trial and error procedure is used to achieve this purpose.

Initial guidance in the trial and error process can be gained by considering the asymptotic characteristics of the closed-loop system. Recalling from the discussion in chapter 2, as the sampling frequncy is increased the closed-loop tranfer function matrix (Eqn (2-42)) approaches the diagonal form

$$\Gamma(z) = \text{diag}\left[\frac{\sigma_1}{z - 1 + \sigma_1}, \frac{\sigma_2}{z - 1 + \sigma_2}\right] \qquad (4\text{-}9)$$

which contains only the fast roots of the system. This relationship provides the insight as to how the system exhibits increasingly tight and decoupled control with increasing gain. It is obvious then that by proper selection of the elements of the Σ weighting matrix the transient responses can be independently adjusted, and thus the speed at which the outputs follow their corresponding command signal from the model aircraft. The level of error in the responses can then be adjusted by the selection of the ratio of proportional to integral control (.). This ratio also controls some of the slow roots of the

system. Although not present in the asymptotic transfer function, at finite values of gain these slow roots become observable and thereby are present in the outputs.

The control law representation in $MATRIX_X$ is given in Figure 4-9. Its implementation follows directly from Eqn (2-46) with the exception of the block labeled "INTLIM" that stands for integration limiter. The intent of this function is to stop the integration of the error signals if any control surface is commanded to a position limit. The integration of the error signals continue once the affected surface(s) leave the maximun deflection position. This action can improve the closed-loop system response signicantly (see Appendix D) in a manner analogous to that discussed in the implementation of the actuator models.

All of the elements of the $MATRIX_X$ implemetation discussed so far are now collected in the closed-loop simulation diagram of Figure 4-10. The block labeled ADAPT2 implements the recursive identification algorithm and is discussed in section 4.4. The simulation setup of Figure 4-10 permits a trial and error evaluation of different combinations of weighting matrix elements and proportional to integral control ratios. At each design iteration, and prior to any simulation, the poles of the closed-loop system are checked as a first means of assesing the the stability of the design. If the particular selection of design parameters produces a stable location for the closed-loop poles, then a time response analysis is conducted via simulation. This is necessary since tne close-loop pole location analysis can only be done for the linear representation of the system. The nonlinear effects can be better acounted for in simulations.

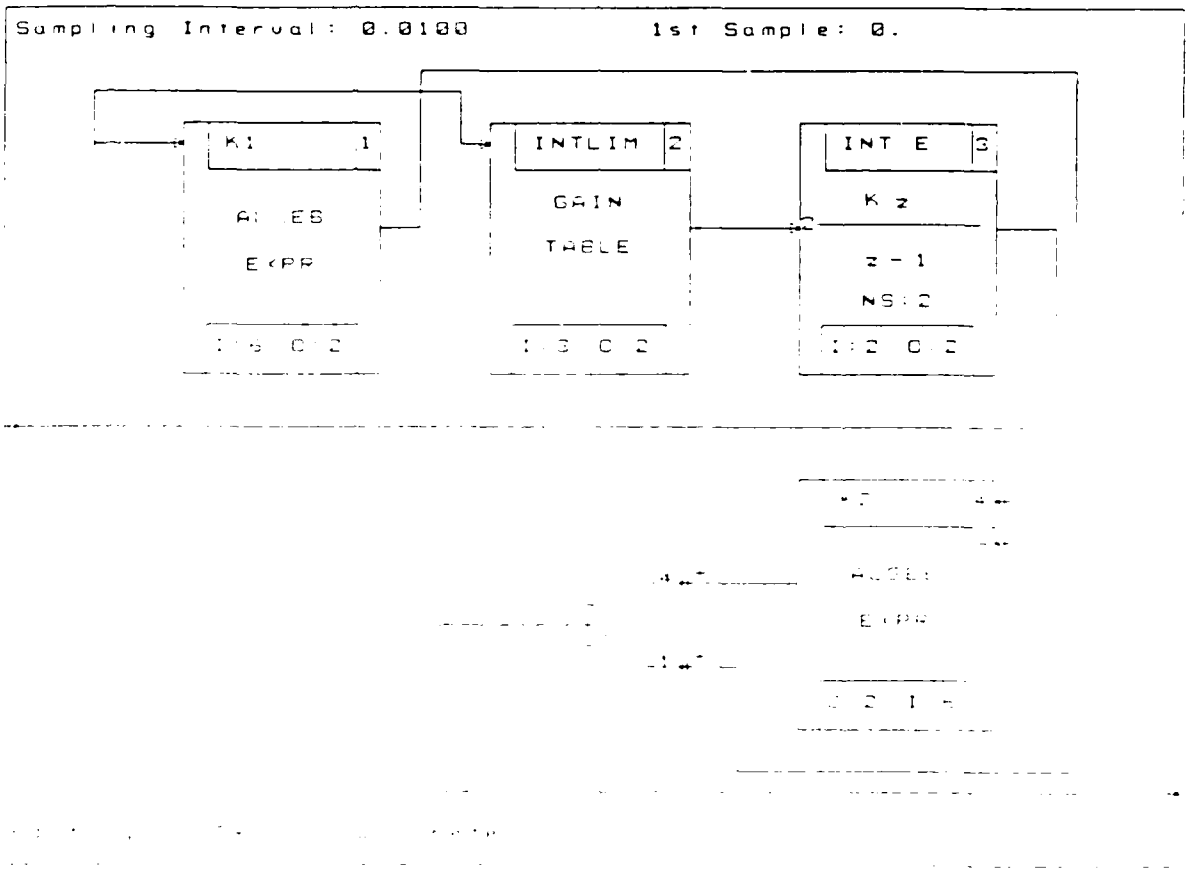

Figure 4-9. Control law representation.

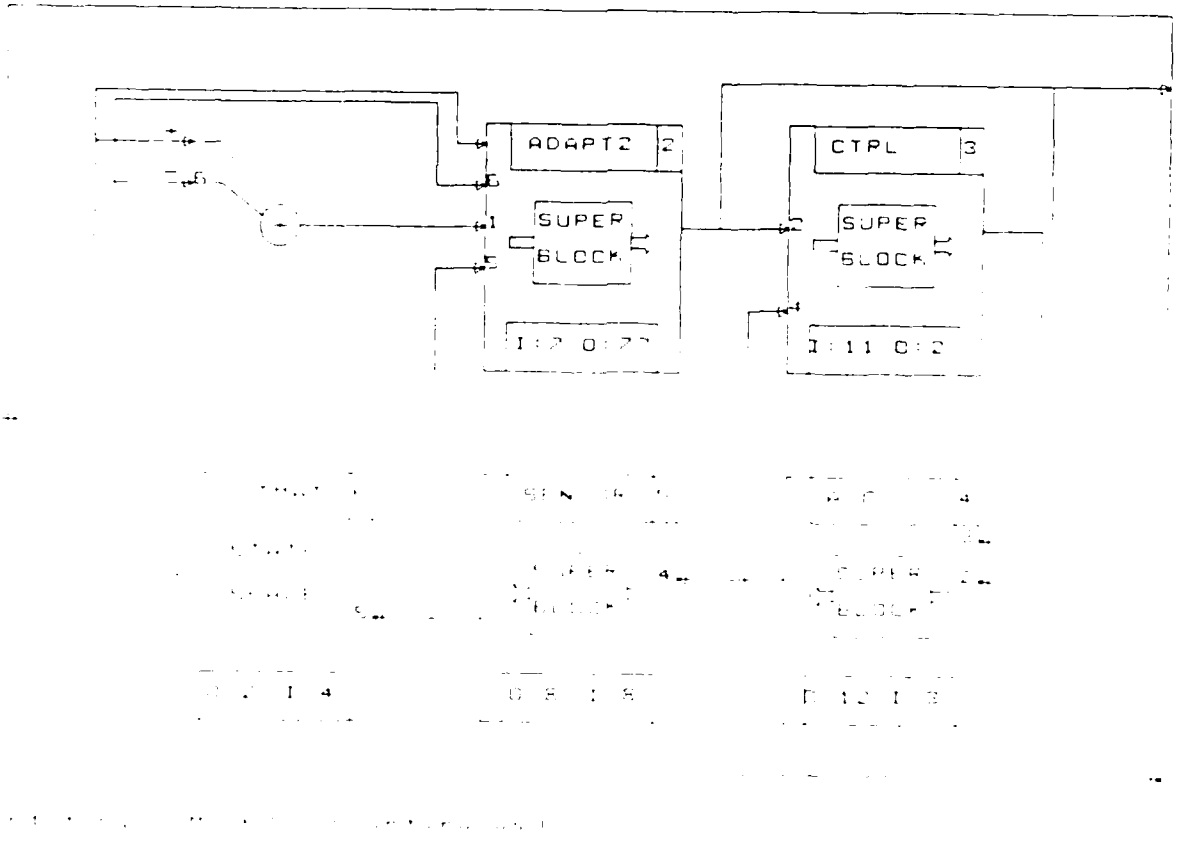

Figure 4-10. Closed-loop system representation.

4.3.3 Command Maneuver. In the case of a model-following control law, the command inputs are typically a set of time histories coming from a model of the simulated vehicle that is being tested by the evaluation pilot. These model responses have to be modified by a number of transformations that account for differences in geometry, attitude, and speed between the model and host aircraft (Figure 4-11). To simplify the design procedure, this thesis addresses the case in which the host aircraft is following a model of itself at an identical flight condition throughout a particular maneuver. This has the effect of making the aforementioned transformation equal to identity. This action is practically motivated since, in the case of the actual flight test program of the VISTA it will provide a highly controlled experiment to evaluate and validate the model of the host vehicle. The model of the host vehicle will be required for ground simulation efforts and variable stability system control law development.

The flight path angle and pitch rate time histories used in this thesis were obtained from a real-time simulation of the AFTI/F-16, conducted at the Flight Dynamics Laboratory's Control Synthesis Branch. These time histories are shown in Figures 4-12 and 4-13.

4.3.4 Design Simulations. A number of preliminary design trials are accomplished using MATRIX$_x$ and its simulation tool SYSTEM-BUILD. Variations of the elements of the L weighting matrix and are performed until the reponses of the plant follow closely the model commands. Values for the elements of L were selected from a range of 0.1 to 0.5 for , and 0.4 to 0.8 for . The proportional to integral ratio ( ) was varied from 0.6 to 1.2.

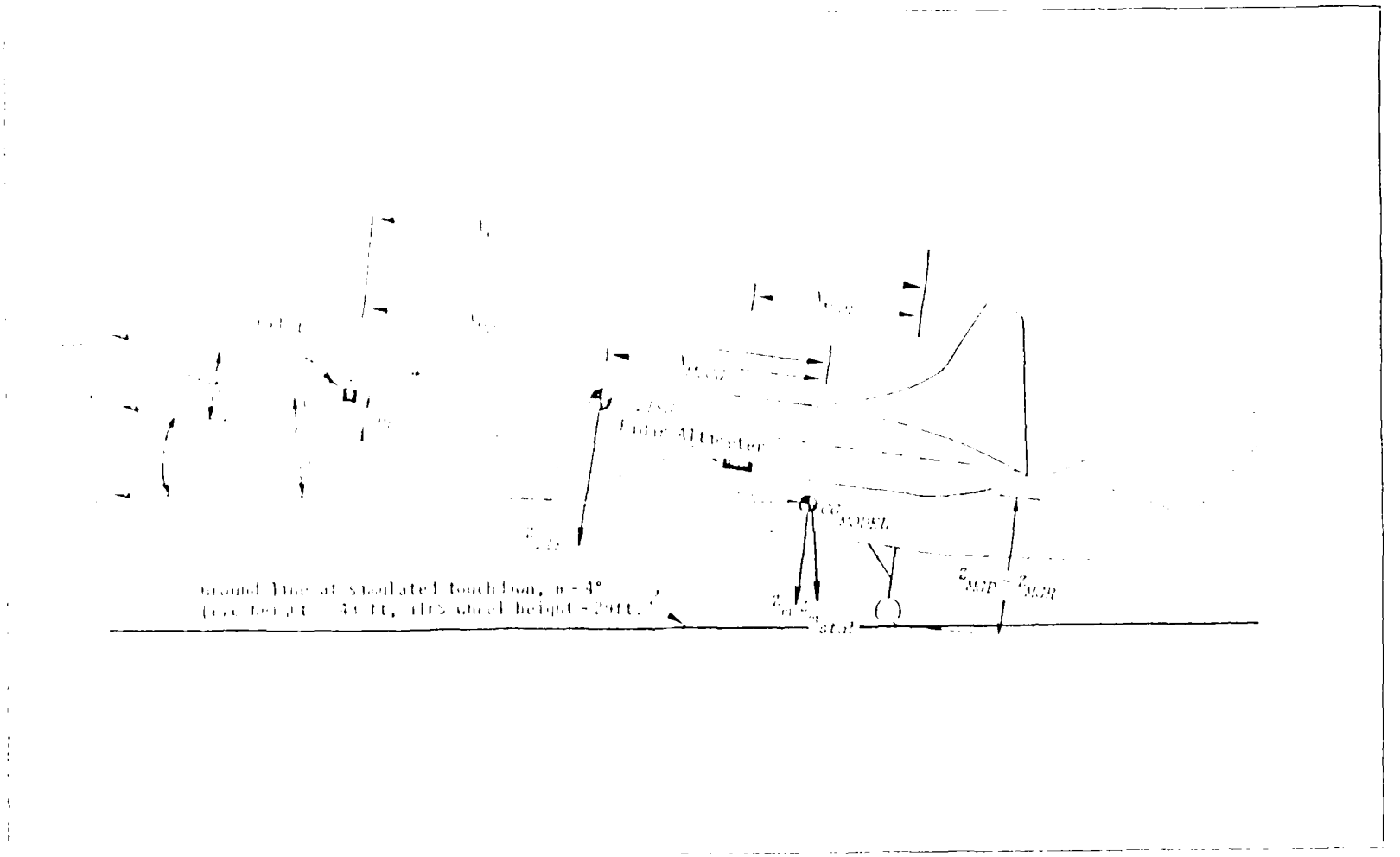

Figure 4-11. Model-Following Simulation Geometry

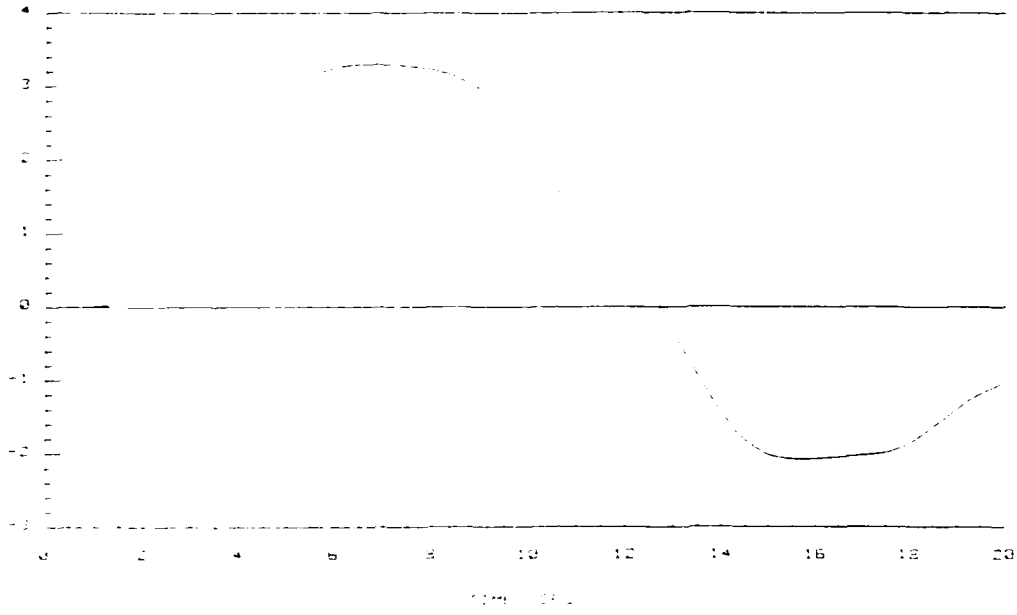

Figure 4-12. Flight Path Command Maneuver (deg).

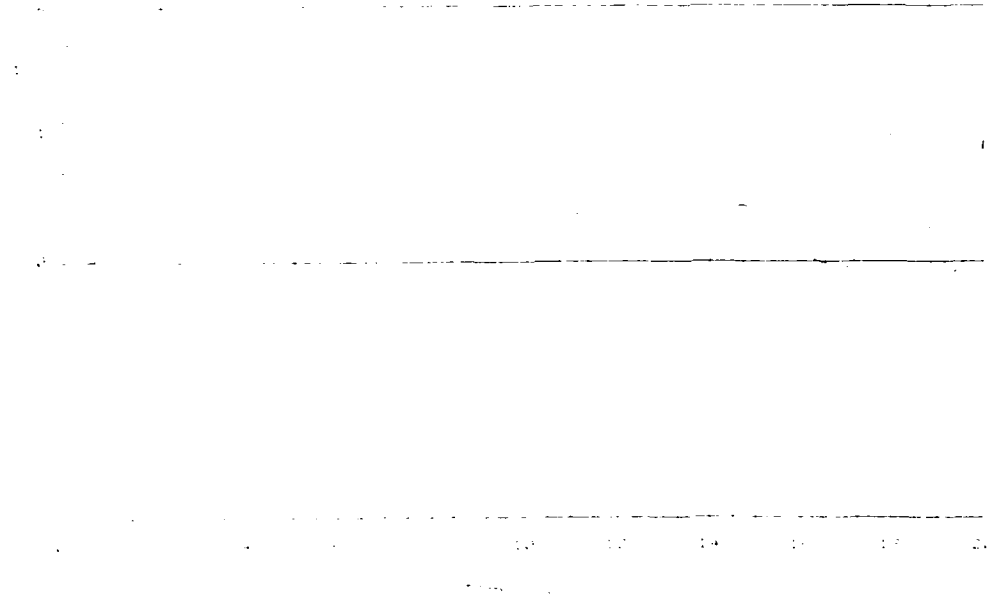

Figure 4-13. Pitch rate command maneuver (deg/sec).

Figures 4-14 thru 4-69 show a representative sample of the design simulations conducted.

To assess the tracking performance of the system, a model following performance index is calculated for each of the commanded quantities. It is desired that the average response error absolute value of each output quantity should not exceed the average absolute value of ten percent of its corresponding reference signal. This is expressed as follows

$$\frac{1}{t}\int_{.01}^{t_f} \left| y_m(i) - y_h(i) \right| dt \leq \frac{1}{t}\int_{.01}^{t_f} \left| .1(y_m(i)) \right| dt \qquad (4\text{-}10)$$

where the subscript m indicates a model output, the subscript h indicates a host airplane output, t_f the ending time of the maneuver, and the index i pertaints to the i^{th} element of the output vector. In addition to a model-following tracking criteria, the control surface deflections are checked for possible reaching of position and/or rate limits.

Based on the results of these simulations a final controller design is chosen that satisfies the desired performance specifications without putting serious demands upon the actuator deflections and rates for the specific maneuver used. The selected controller design parameters are given in Table 4-2.

Table 4-2

Final Control Law Design Parameters

$\Sigma =$	$\begin{vmatrix} 0.3 & 0.0 \\ 0.0 & 0.7 \end{vmatrix}$	$\rho = 0.8$

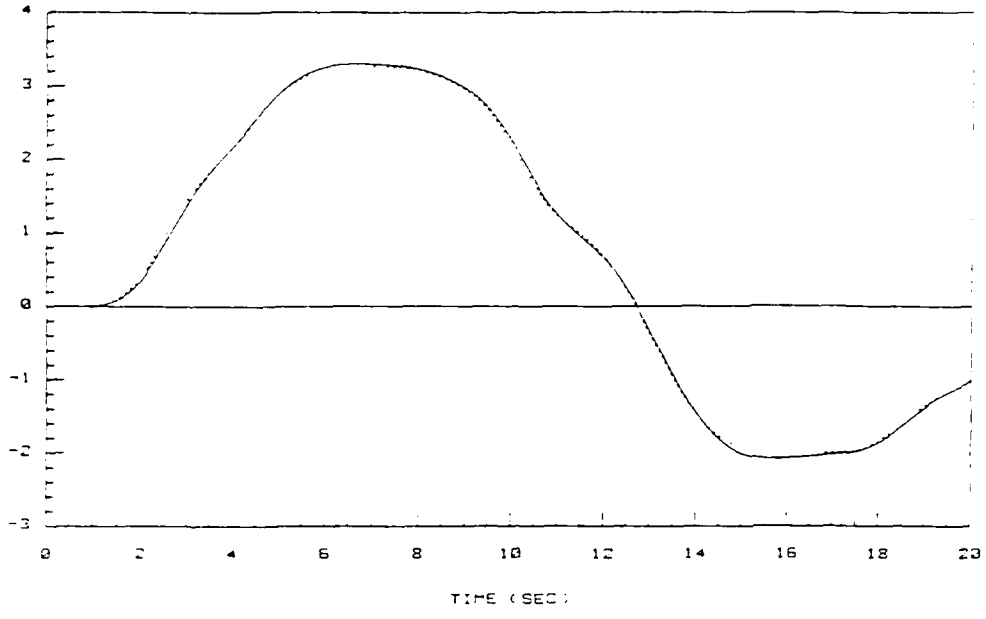

Figure 4-14. Flight path angle command and response (deg).
Σ = diag{ 0.1, 0.7 }, ρ = 0.8

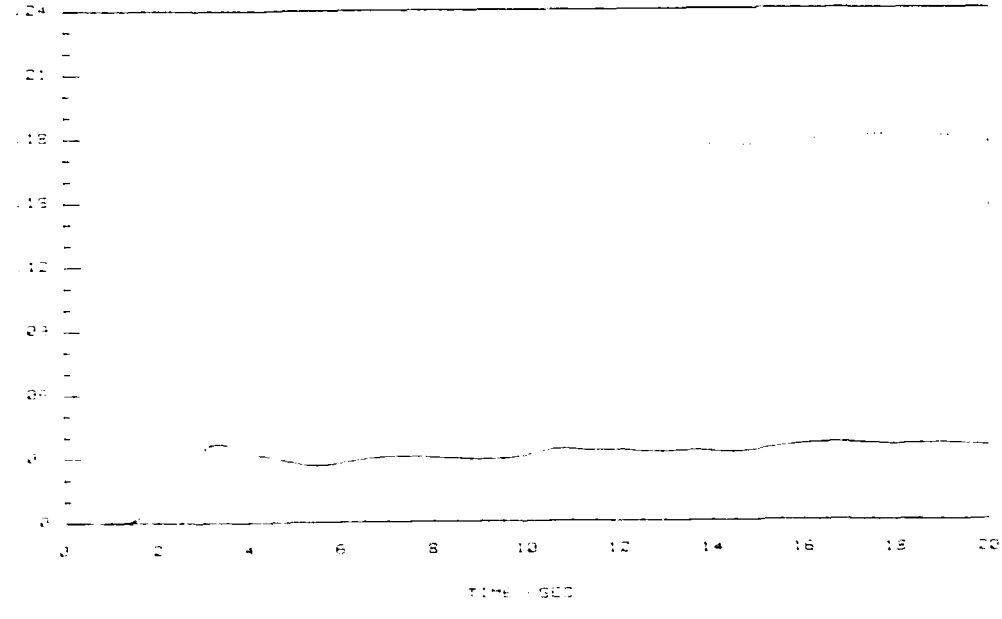

Figure 4-15. Flight path angle tracking performance index (deg).
Σ = diag{ 0.1, 0.7 }, ρ = 0.8

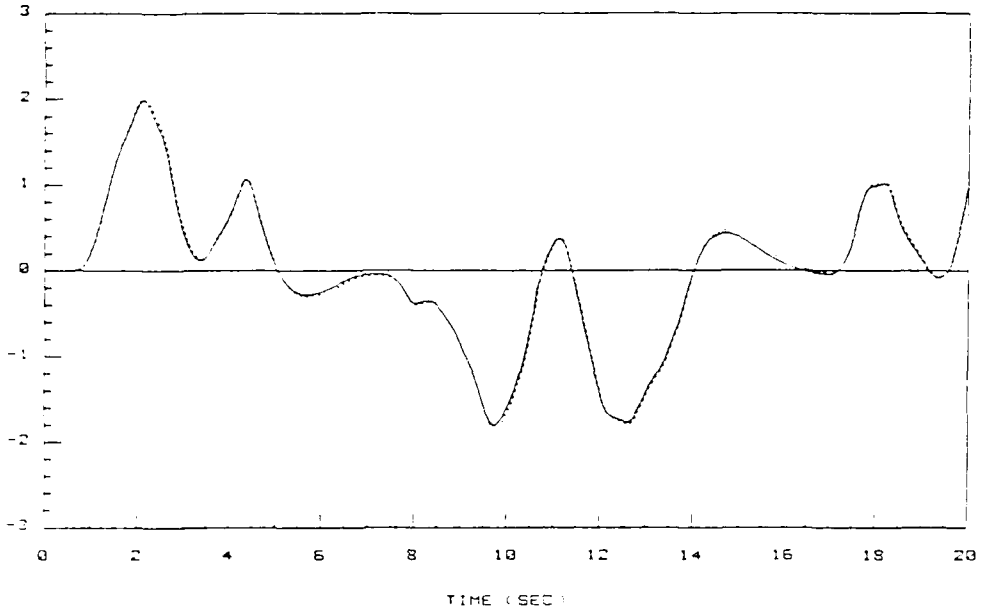

Figure 4-16. Pitch rate command and response (deg/sec).
Σ = diag{ 0.1, 0.7 }, ρ = 0.8

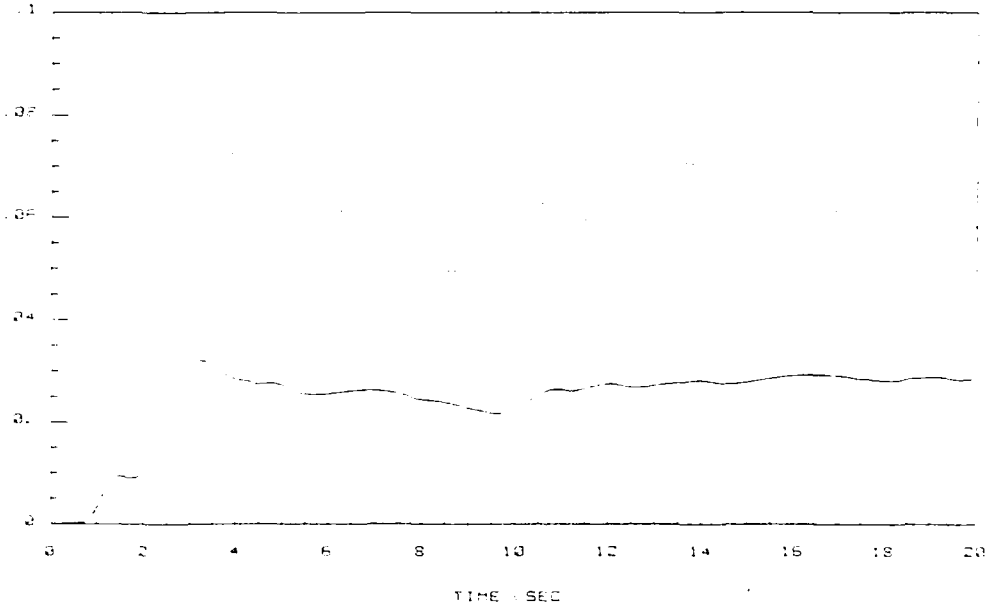

Figure 4-17. Pitch rate tracking performance index (deg/sec).
Σ = diag{ 0.1, 0.7 }, ρ = 0.8

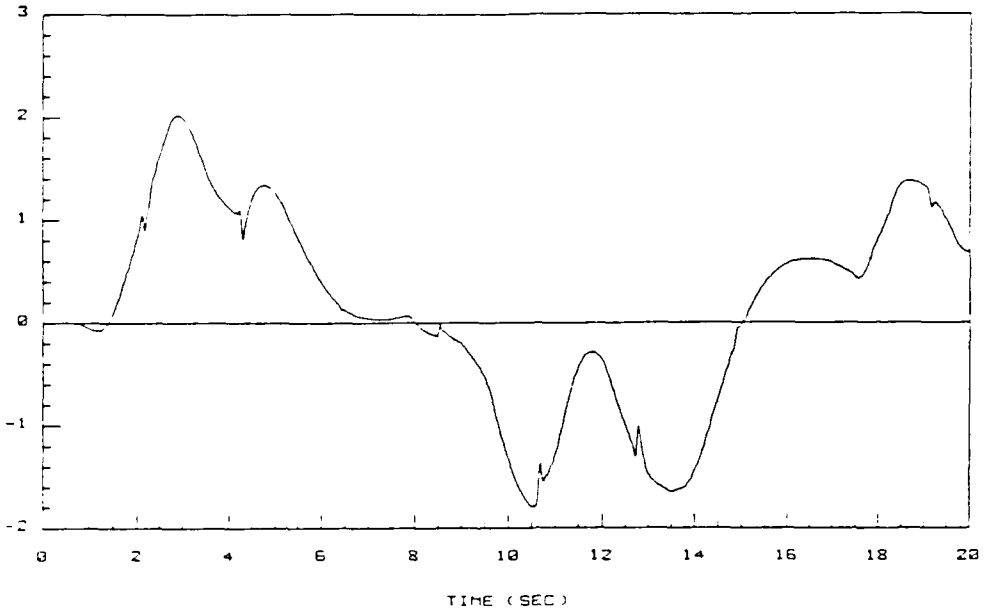

Figure 4-18. Elevator deflection (deg).
Σ = diag{ 0.1, 0.7 }, ρ = 0.8

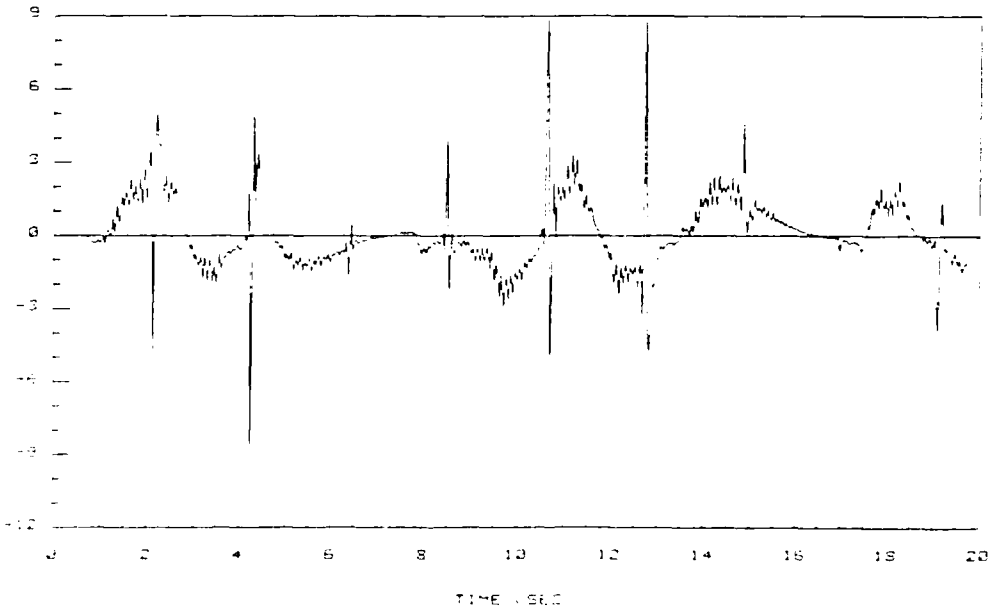

Figure 4-19. Elevator deflection rate (deg/sec).
Σ = diag{ 0.1, 0.7 }, ρ = 0.8

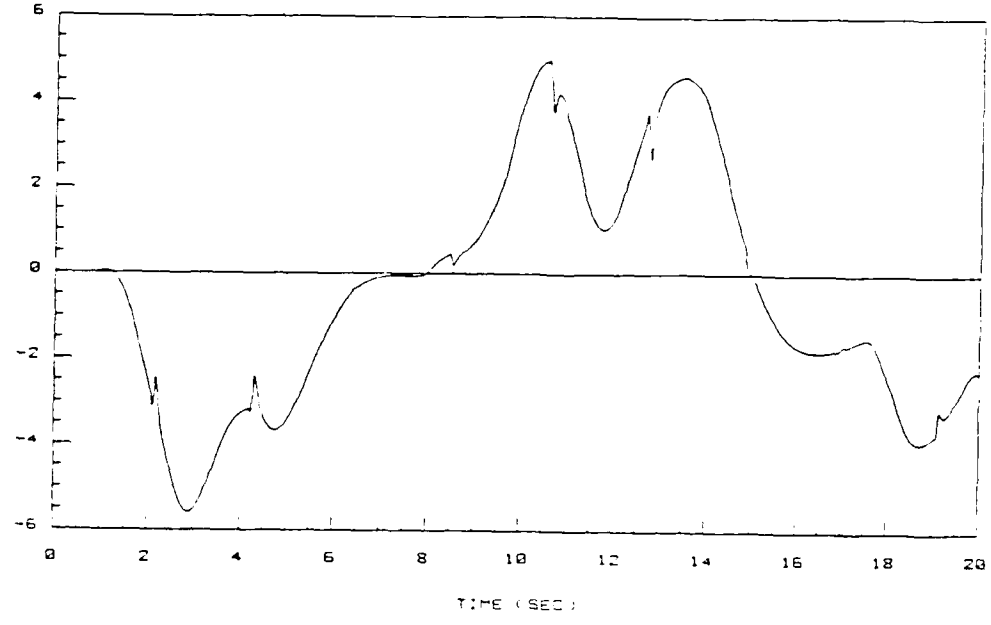

Figure 4-20. Flaperon deflection (deg).
Σ = diag{ 0.1, 0.7 }, ρ = 0.8

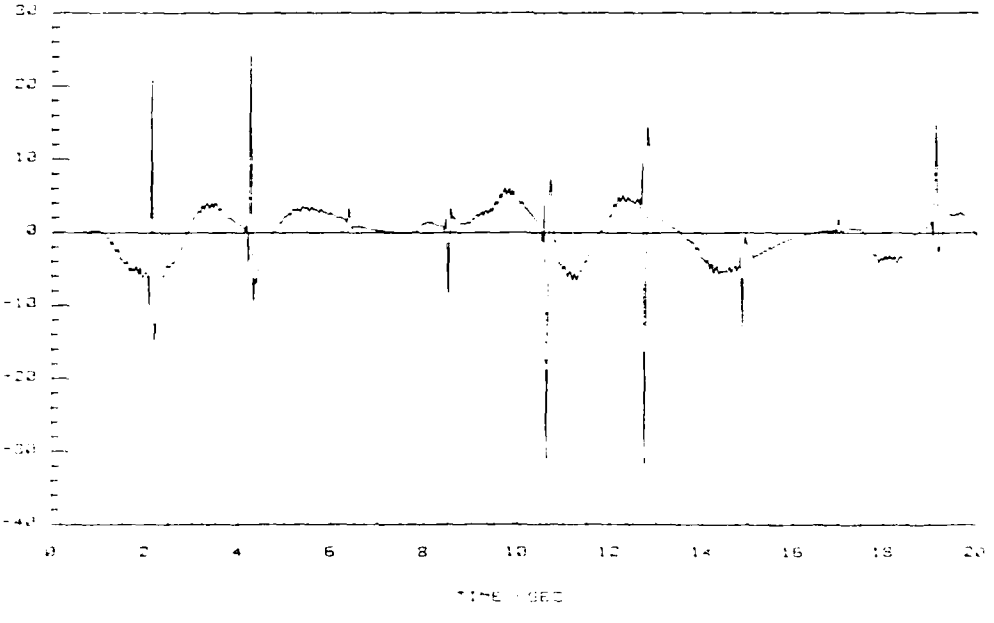

Figure 4-21. Flaperon deflection rate (deg/sec).
Σ = diag{ 0.1, 0.7 }, ρ = 0.8

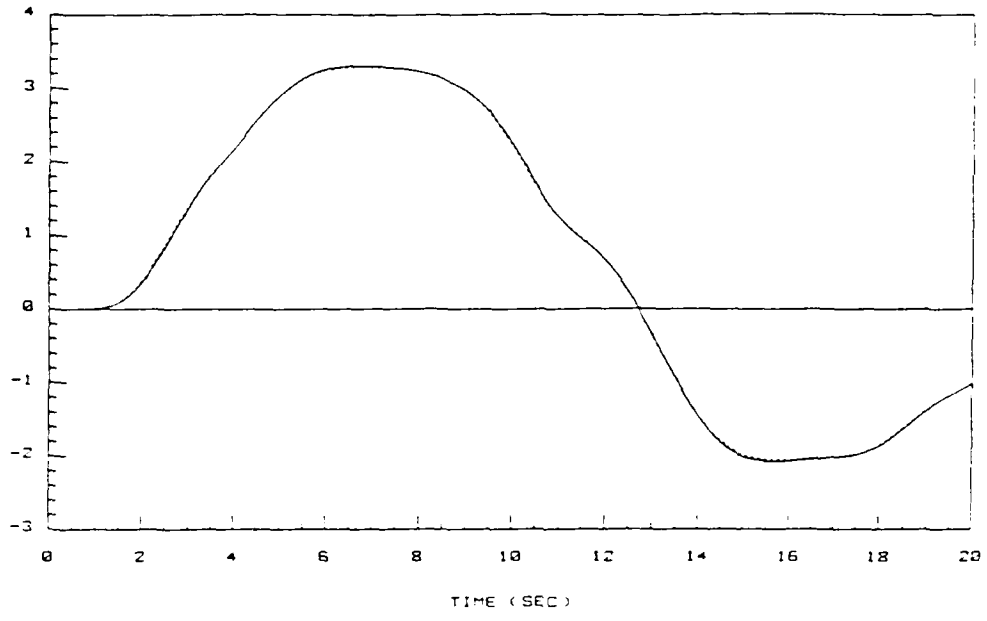

Figure 4-22. Flight path angle command and response (deg).
Σ = diag{ 0.3, 0.7 }, ρ = 0.8

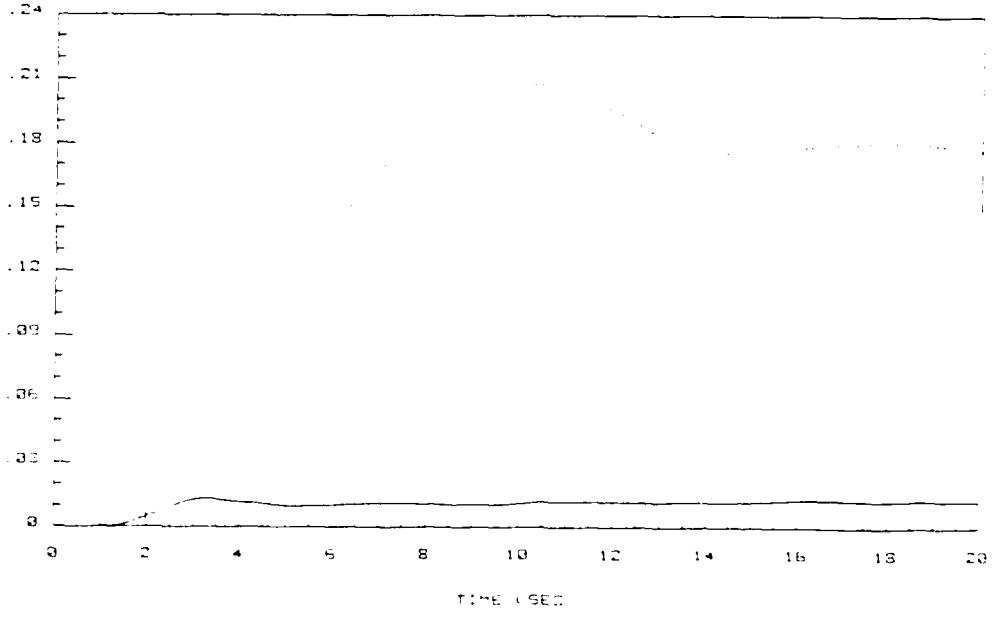

Figure 4-23. Flight path angle tracking performance index (deg).
Σ = diag{ 0.3, 0.7 }, ρ = 0.8

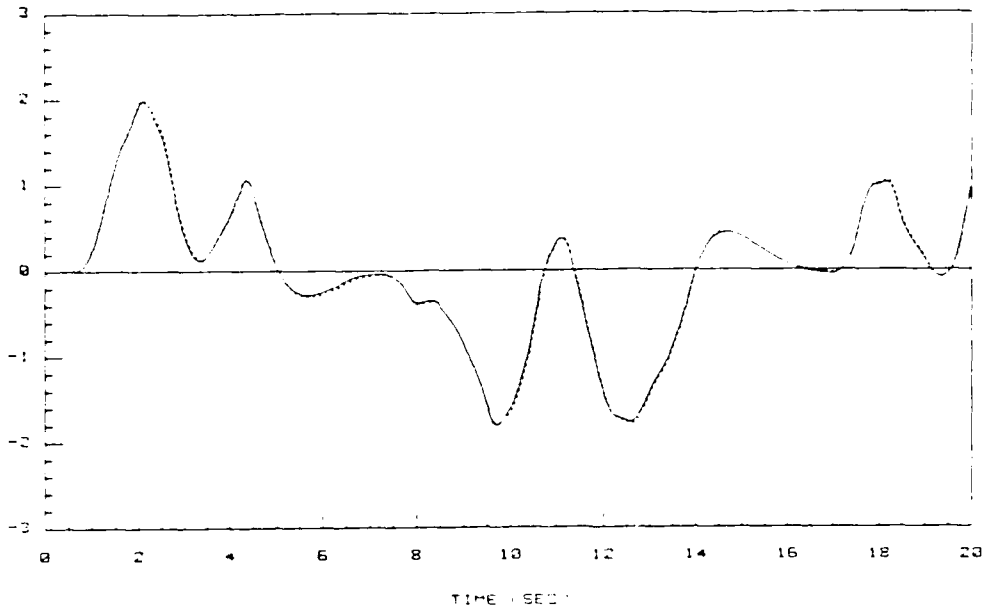

Figure 4-24. Pitch rate command and response (deg/sec).
Σ = diag{ 0.3, 0.7 }, λ = 0.8

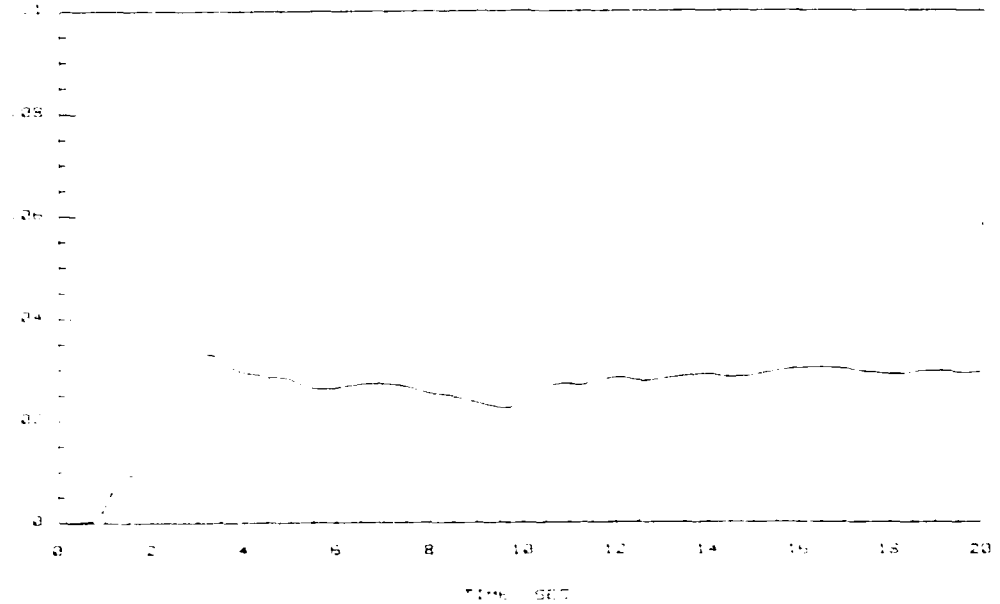

Figure 4-25. Pitch rate tracking performance index (deg/sec).
Σ = diag{ 0.3, 0.7 }, λ = 0.8

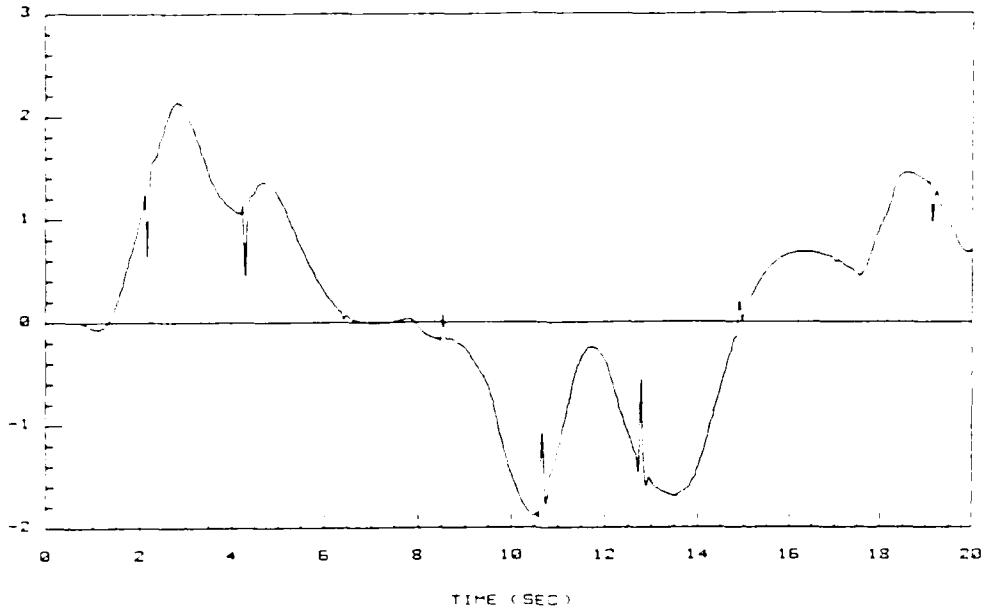

Figure 4-26. Elevator deflection (deg).
Σ = diag{ 0.3, 0.7 }, ρ = 0.8

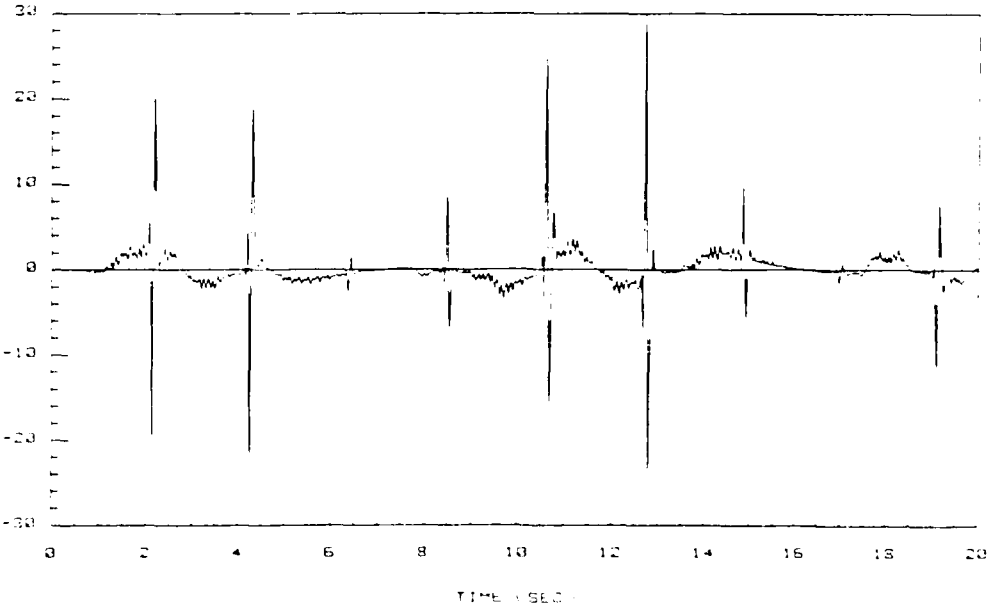

Figure 4-27. Elevator deflection rate (deg/sec).
Σ = diag{ 0.3, 0.7 }, ρ = 0.8

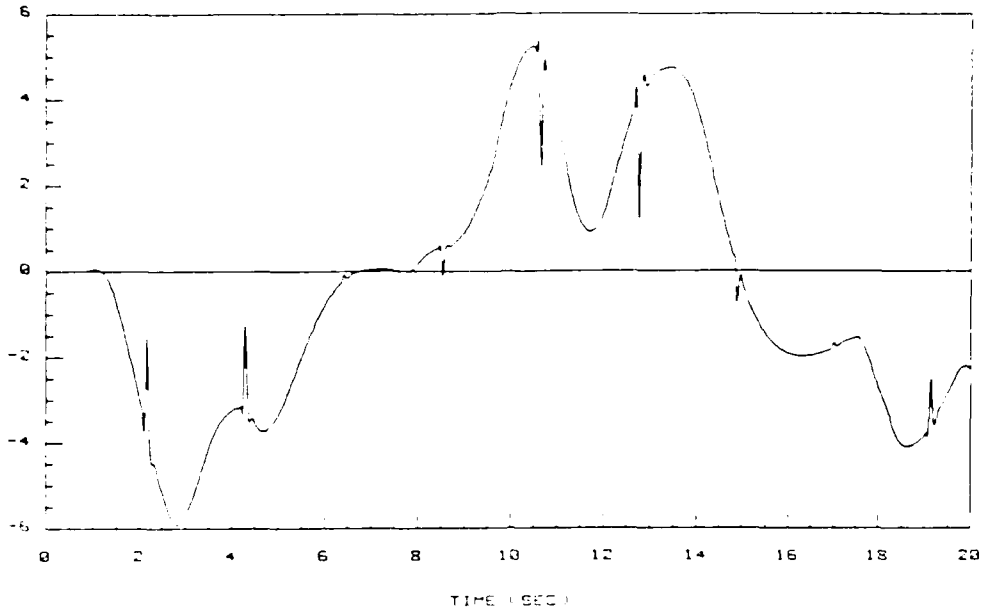

Figure 4-28. Flaperon deflection (deg).
Σ = diag{ 0.3, 0.7 }, ρ = 0.8

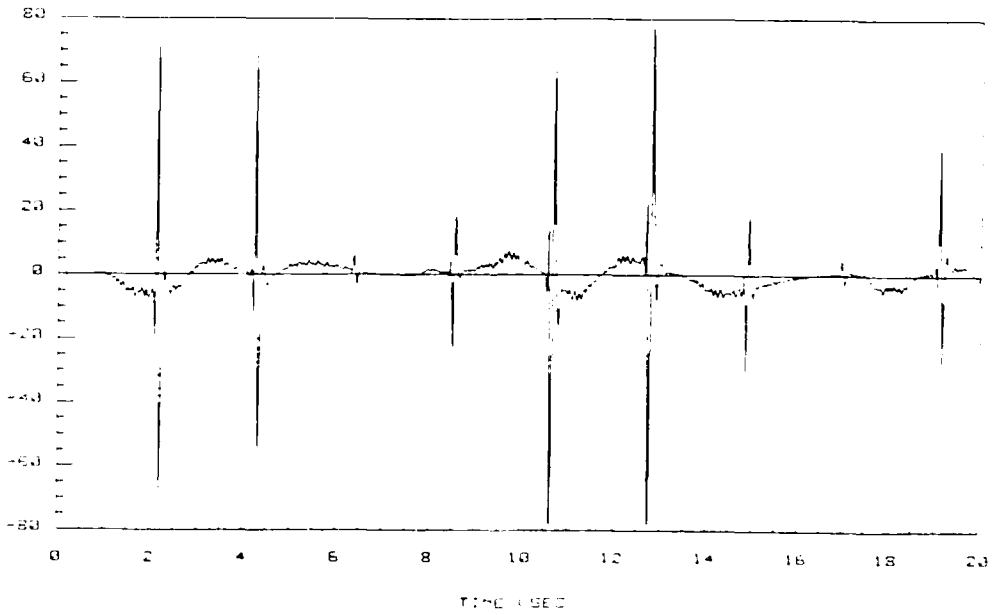

Figure 4-29. Flaperon deflection rate (deg/sec).
Σ = diag{ 0.3, 0.7 }, ρ = 0.8

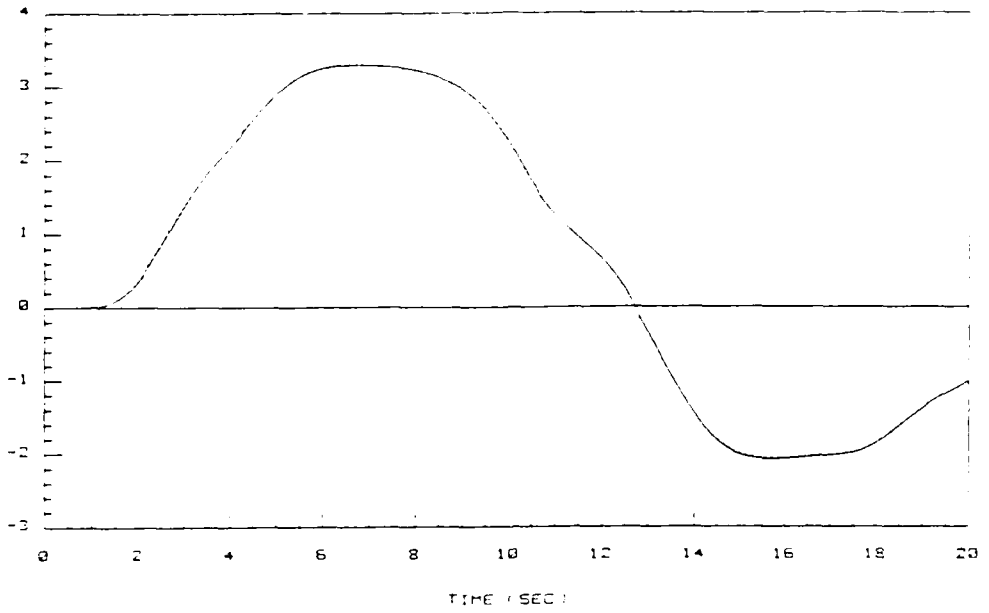

Figure 4-30. Flight path angle command and response (deg).
Σ = diag{ 0.5, 0.7 }, ρ = 0.8

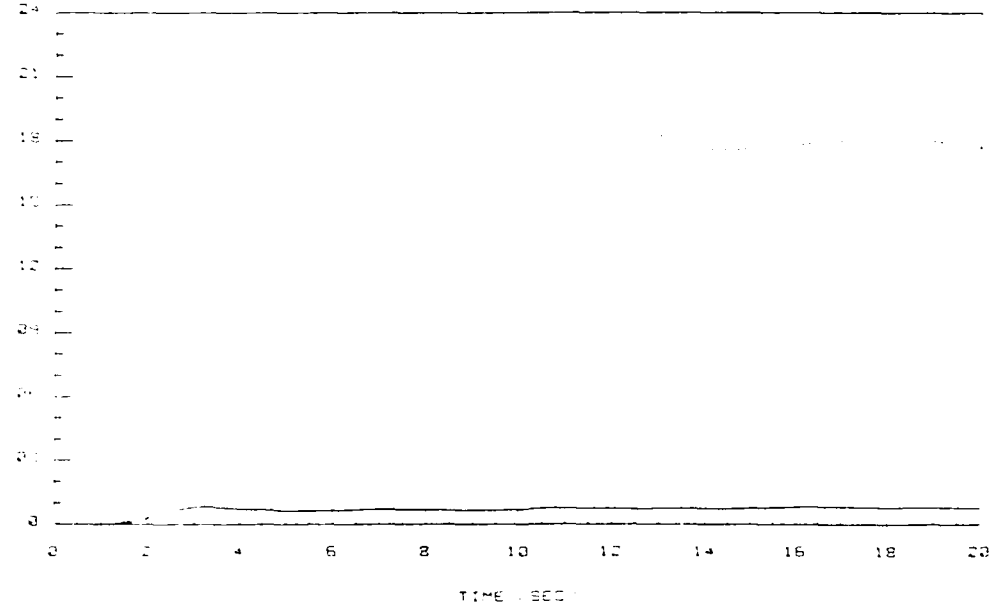

Figure 4-31. Flight path angle tracking performance index (deg).
Σ = diag{ 0.5, 0.7 }, ρ = 0.8

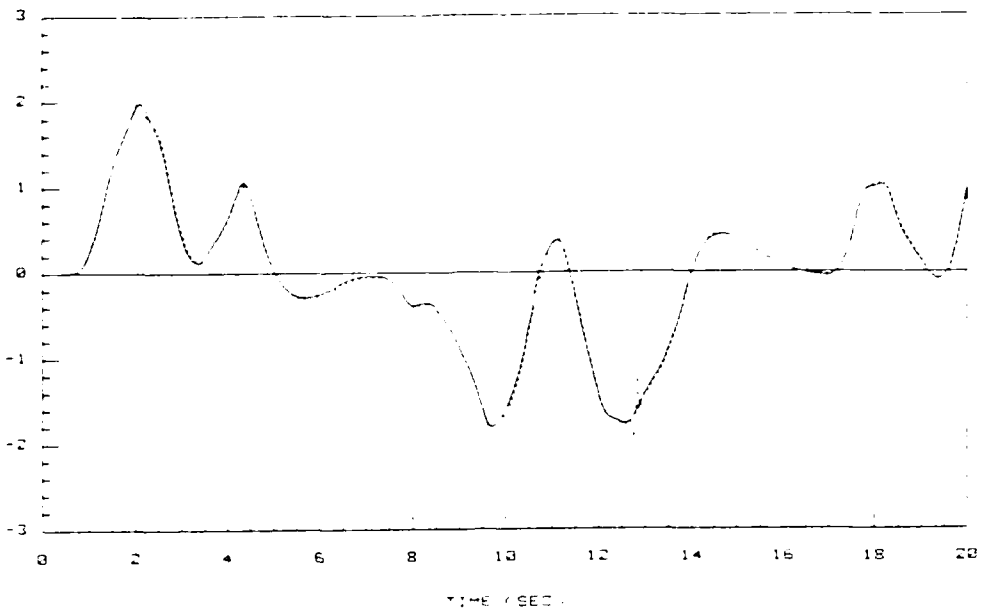

Figure 4-32. Pitch rate command and response (deg/sec).
Σ = diag{ 0.5, 0.7 }, ρ = 0.8

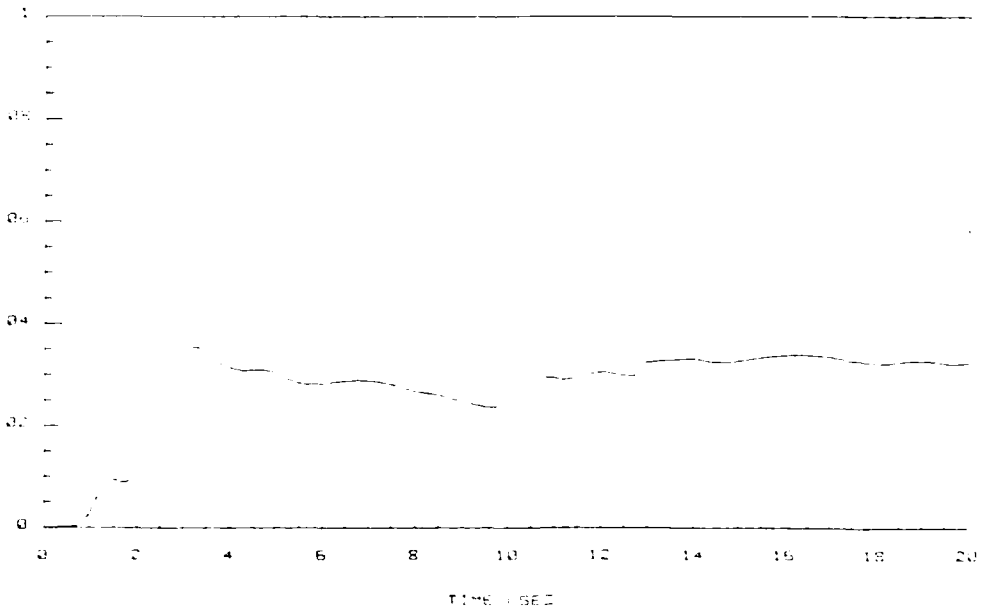

Figure 4-33. Pitch rate tracking performance index (deg/sec).
Σ = diag{ 0.5, 0.7 }, ρ = 0.8

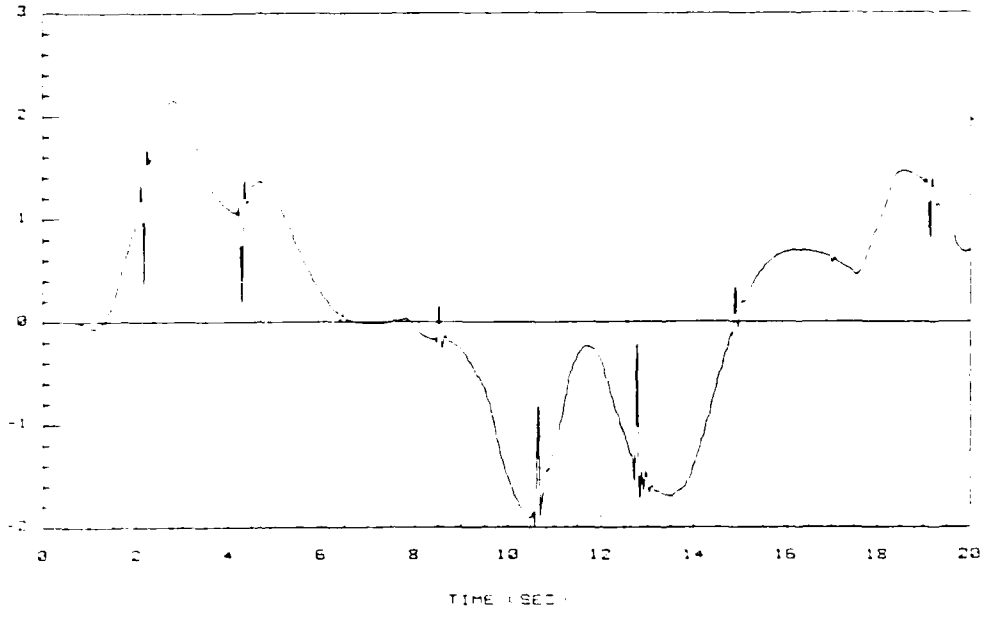

Figure 4-34. Elevator deflection (deg).
Σ = diag{ 0.5, 0.7 }, ρ = 0.8

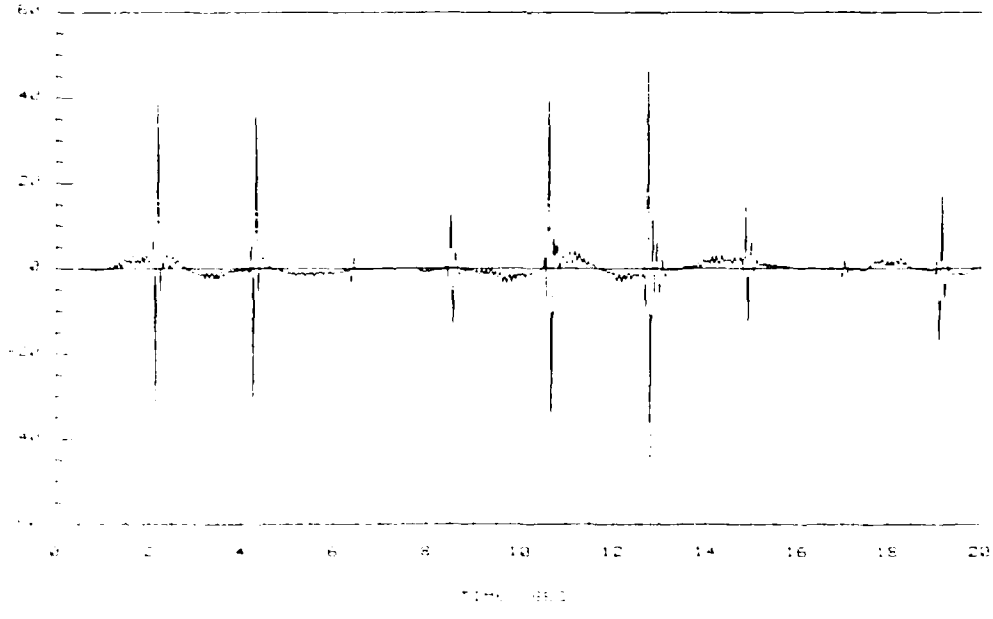

Figure 4-35. Elevator deflection rate (deg/sec).
Σ = diag{ 0.5, 0.7 }, ρ = 0.8

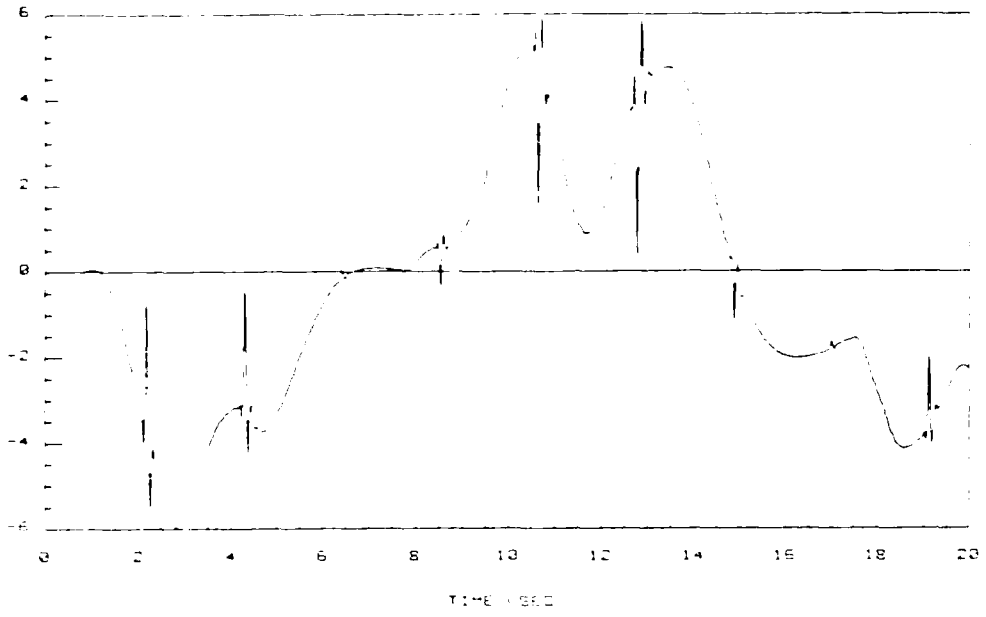

Figure 4-36. Flaperon deflection (deg).
Σ = diag{ 0.5, 0.7 }, . = 0.8

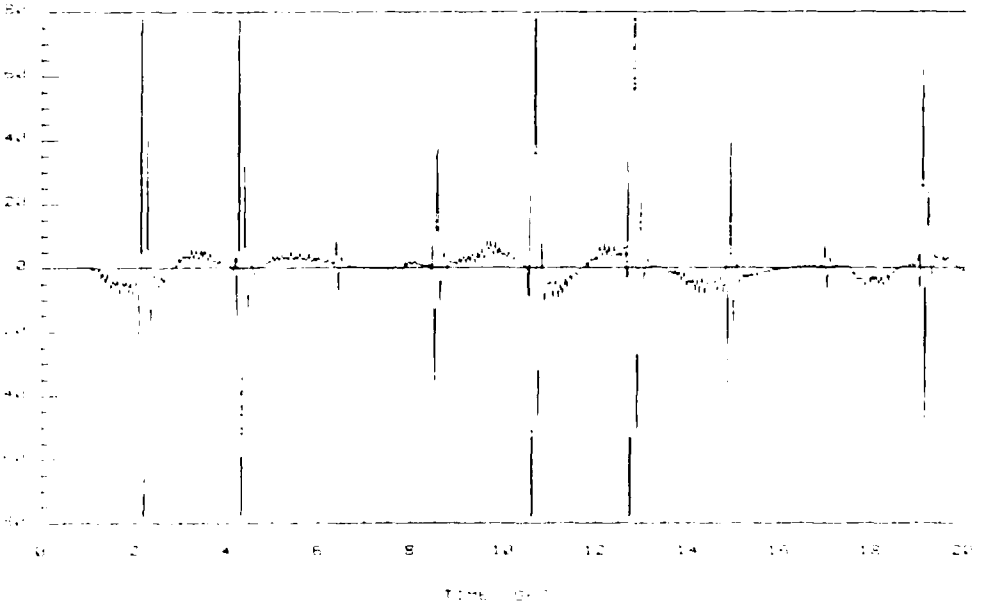

Figure 4-37. Flaperon deflection rate (deg/sec).
Σ = diag{ 0.5, 0.7 }, = 0.8

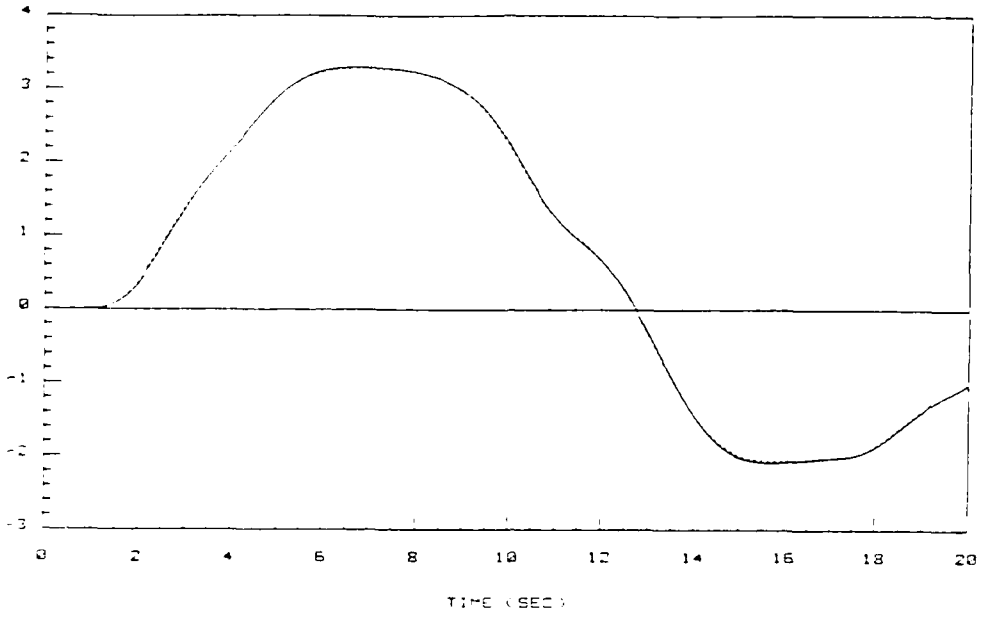

Figure 4-38. Flight path angle command and response (deg).
Σ = diag{ 0.3, 0.5 }, ρ = 0.8

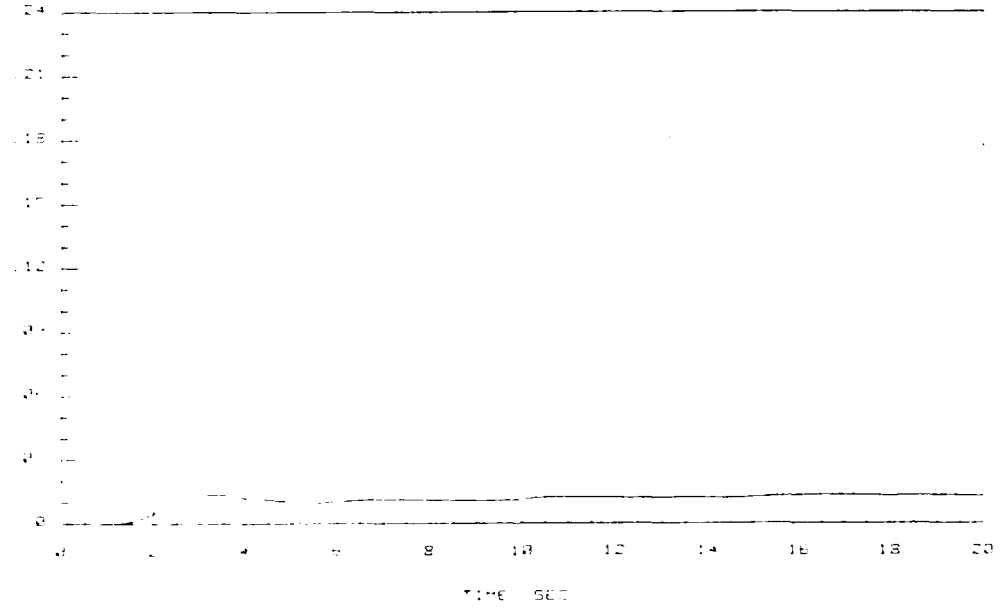

Figure 4-39. Flight path angle tracking performance index (deg).
Σ = diag{ 0.3, 0.5 }, ρ = 0.8

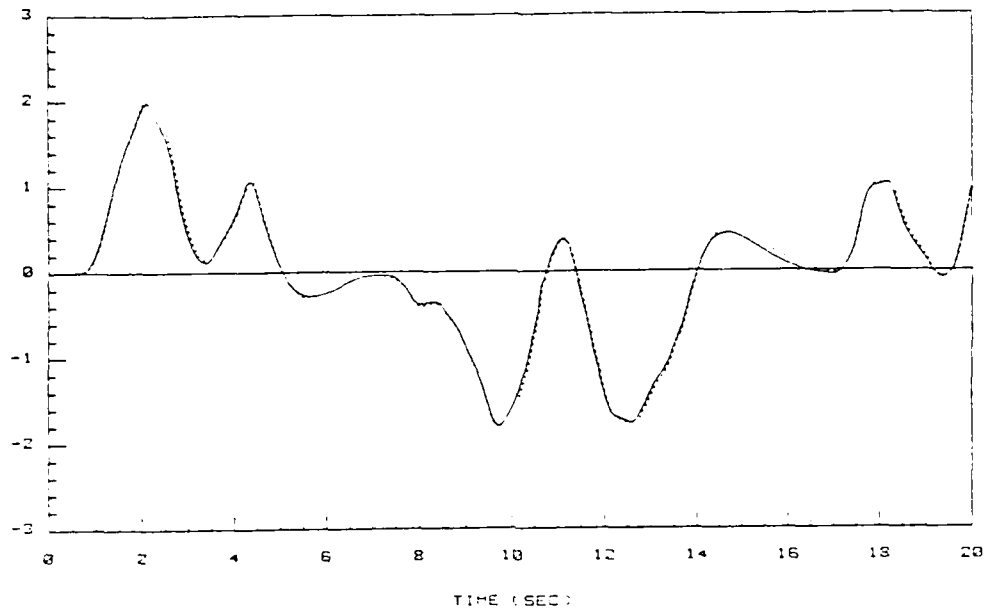

Figure 4-40. Pitch rate command and response (deg/sec).
Σ = diag{ 0.3, 0.5 }, ρ = 0.8

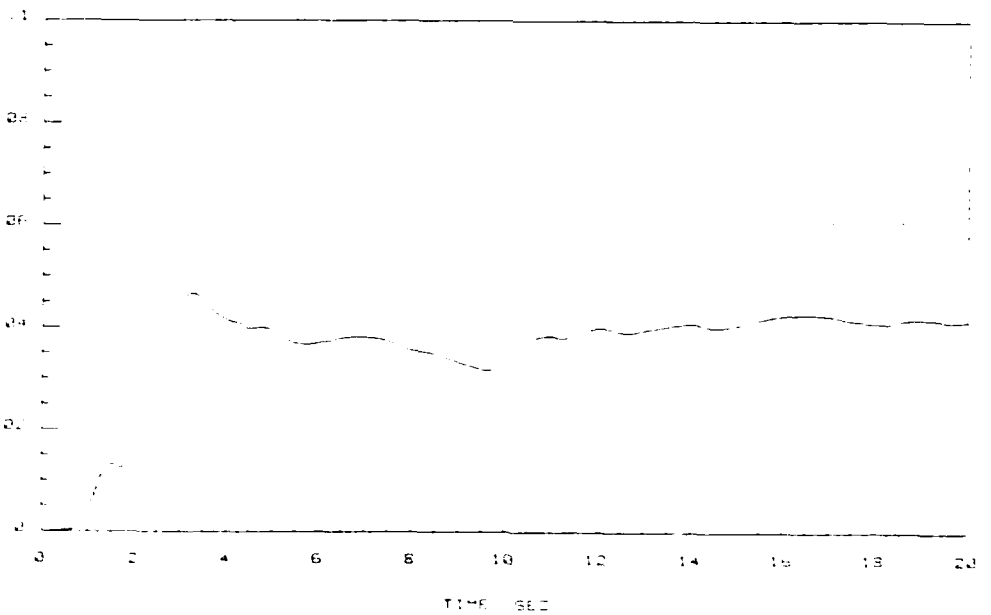

Figure 4-41. Pitch rate tracking performance index (deg/sec).
Σ = diag{ 0.3, 0.5 }, ρ = 0.8

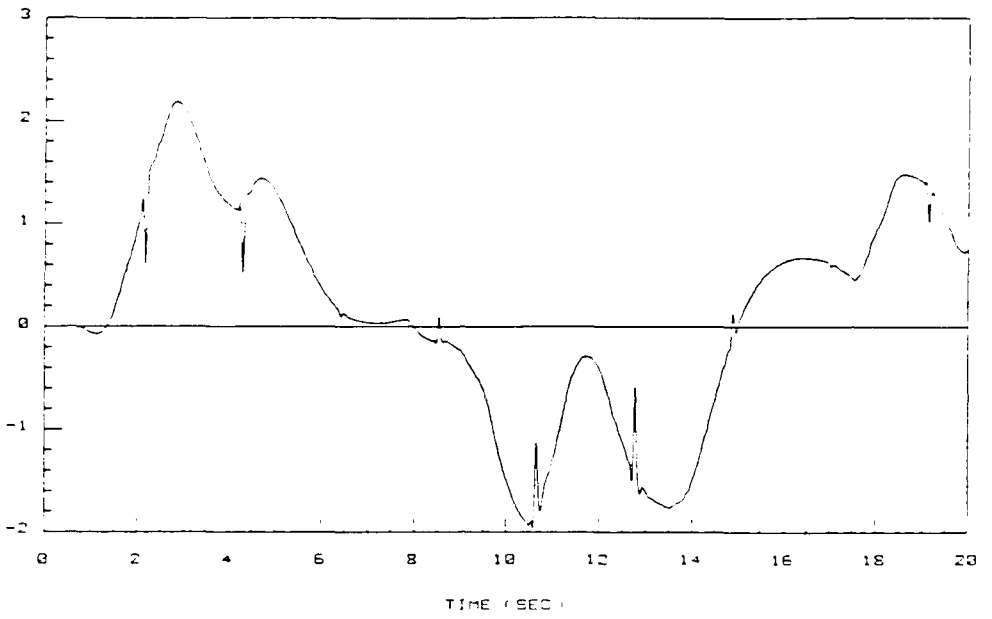

Figure 4-42. Elevator deflection (deg).
Σ = diag{ 0.3, 0.5 }, ρ = 0.8

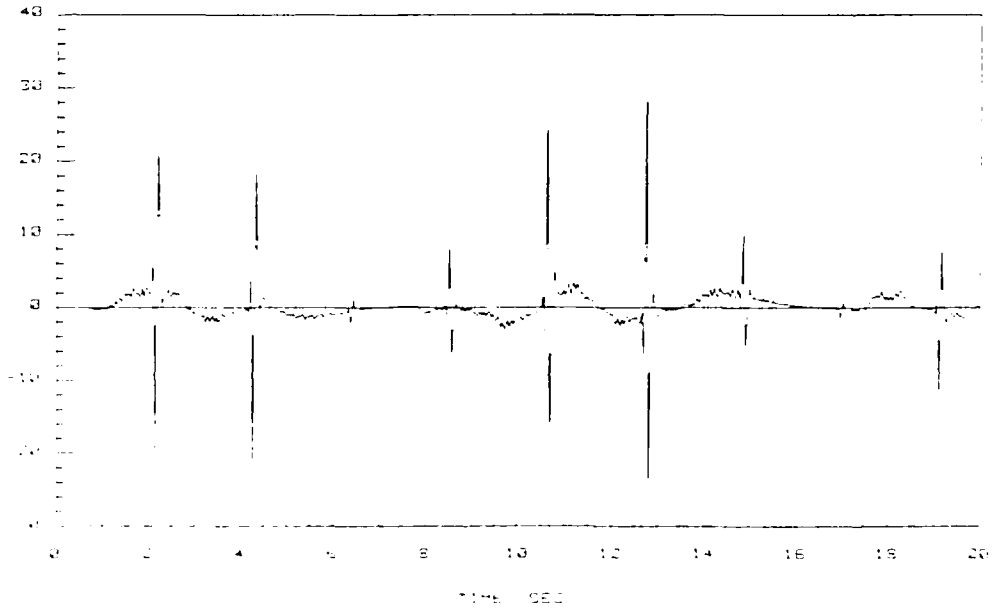

Figure 4-43. Elevator deflection rate (deg/sec).
Σ = diag{ 0.3, 0.5 }, ρ = 0.8

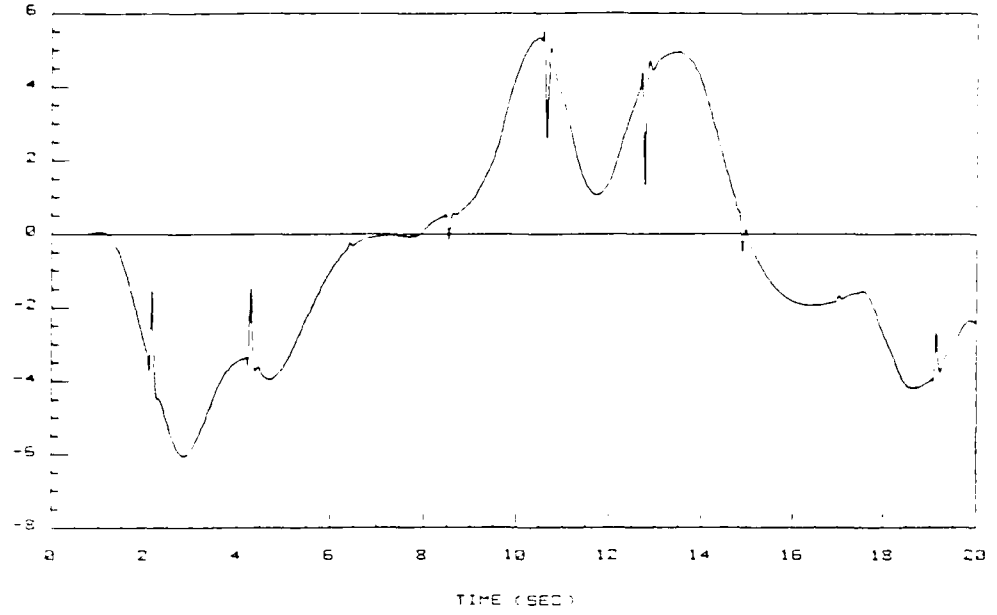

Figure 4-44. Flaperon deflection (deg).
Σ = diag{ 0.3, 0.5 }, ρ = 0.8

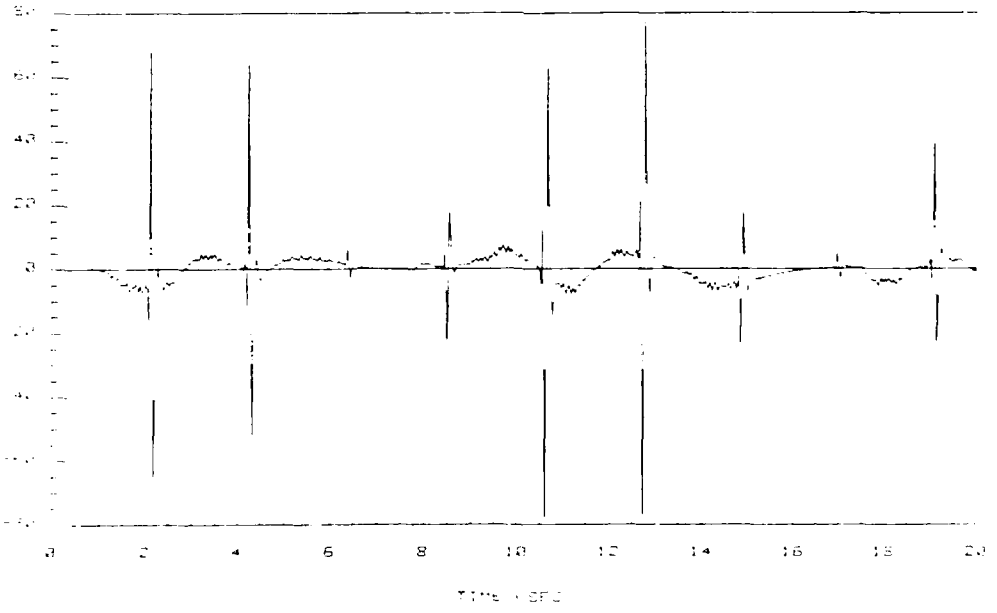

Figure 4-45. Flaperon deflection rate (deg/sec).
Σ = diag{ 0.3, 0.5 }, ρ = 0.8

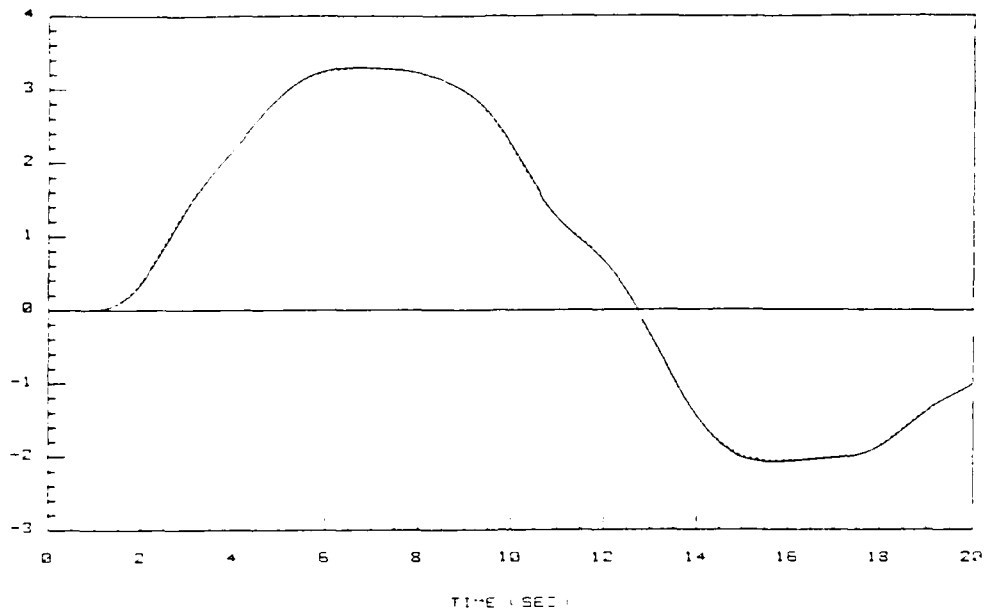

Figure 4-46. Flight path angle command and response (deg).
Σ = diag{ 0.3, 0.8 }, ρ = 0.8

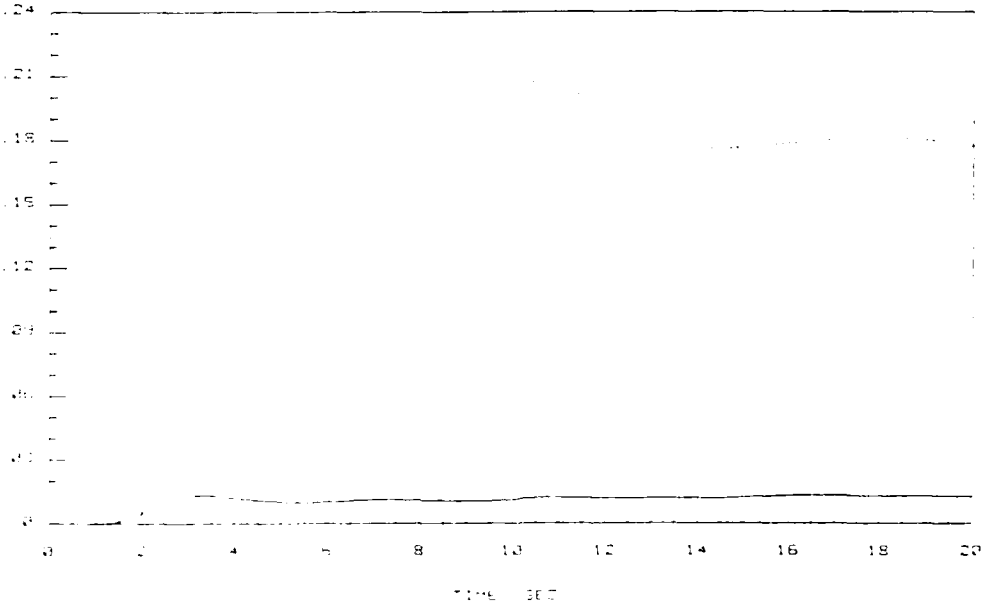

Figure 4-47. Flight path angle tracking performance index (deg).
Σ = diag{ 0.3, 0.8 }, ρ = 0.8

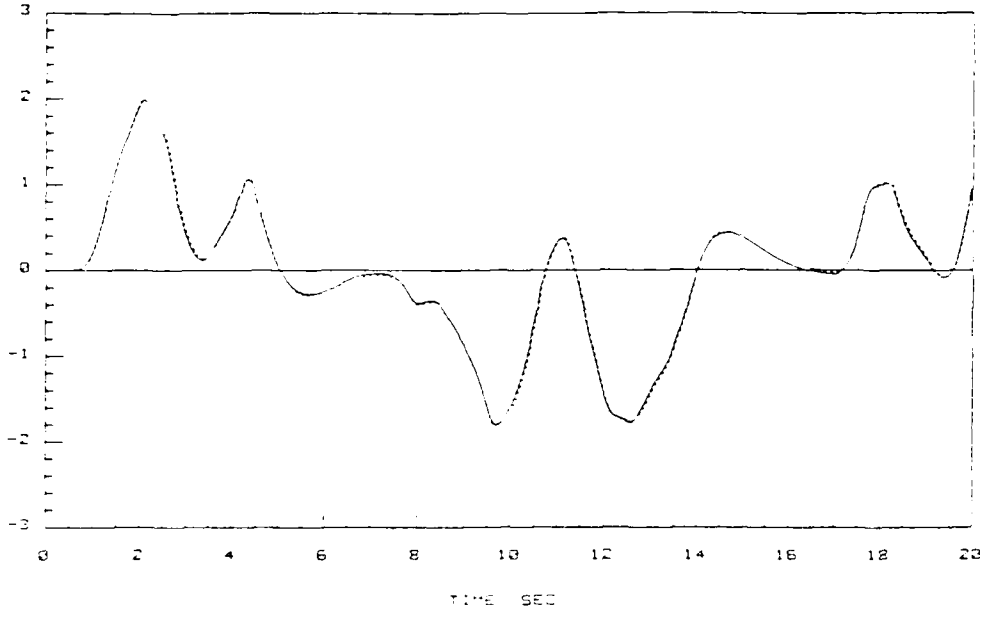

Figure 4-48. Pitch rate command and response (deg/sec).
Σ = diag{ 0.3, 0.8 }, γ = 0.8

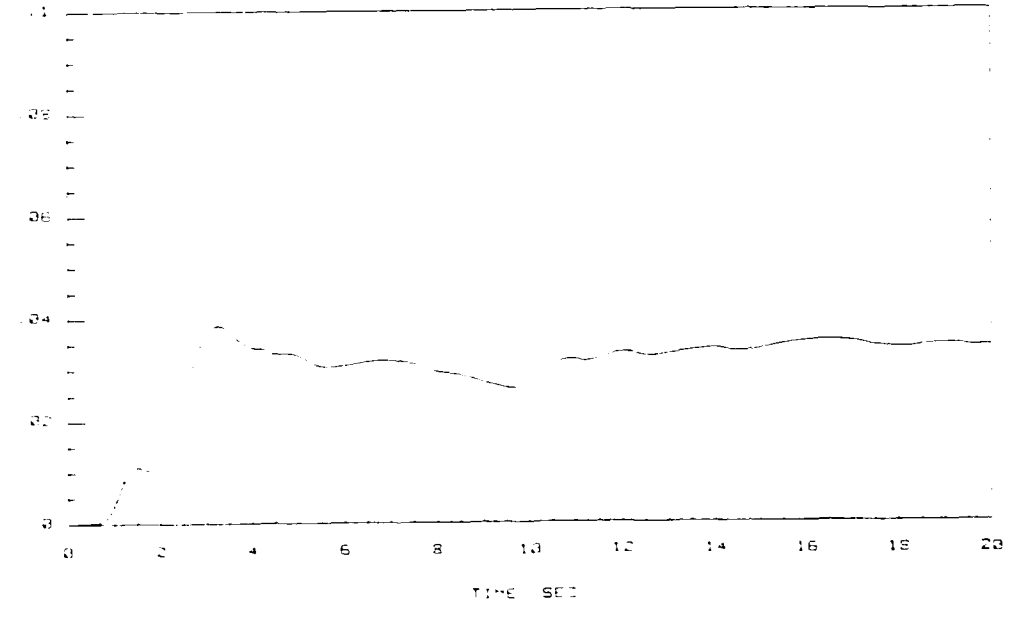

Figure 4-49. Pitch rate tracking performance index (deg/sec).
Σ = diag{ 0.3, 0.8 }, γ = 0.8

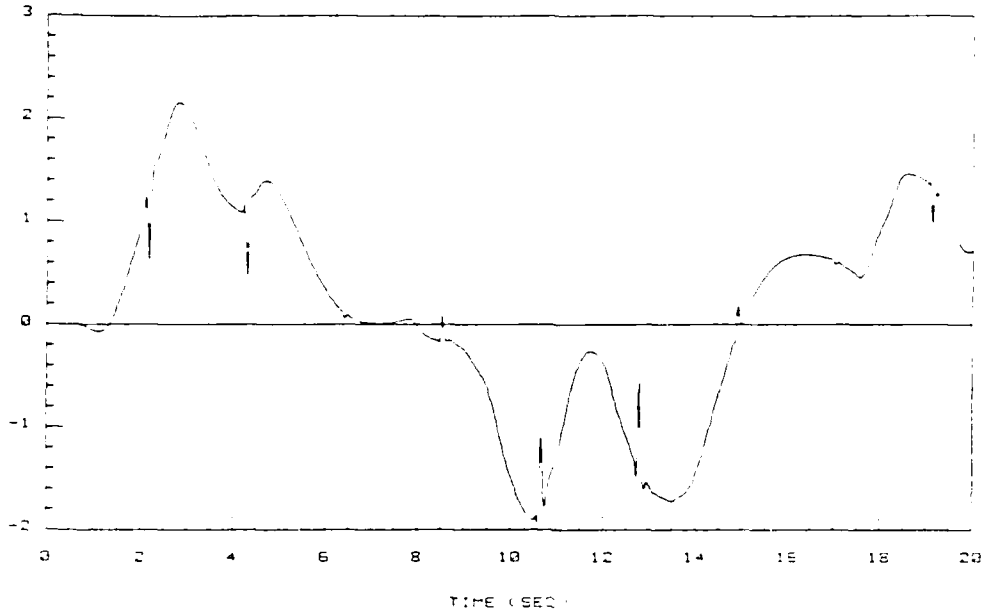

Figure 4-50. Elevator deflection (deg).
Σ = diag{ 0.3, 0.8 }, ρ = 0.8

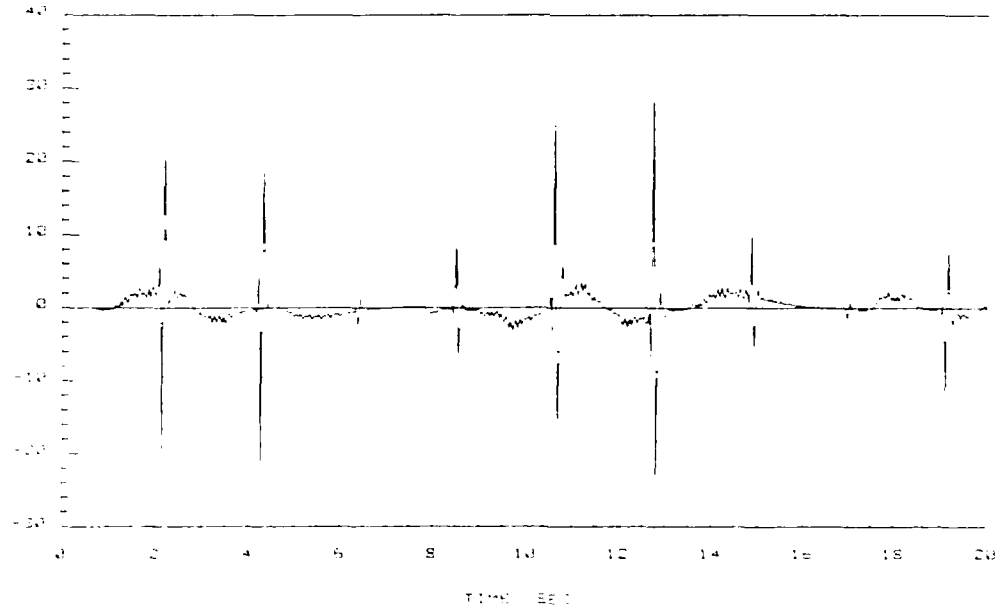

Figure 4-51. Elevator deflection rate (deg/sec).
Σ = diag{ 0.3, 0.8 }, ρ = 0.8

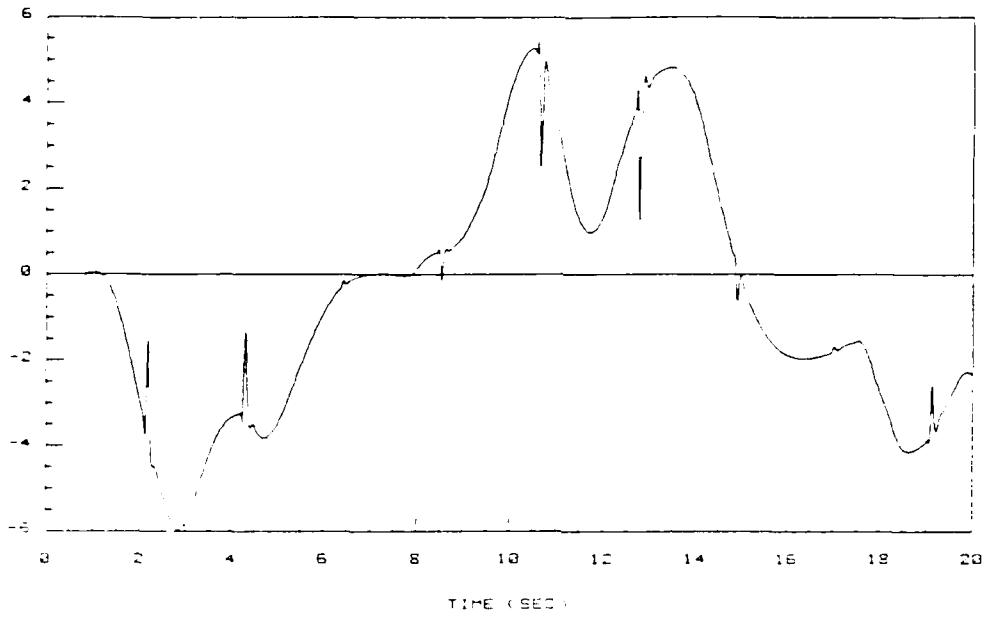

Figure 4-52. Flaperon deflection (deg).
Σ = diag{ 0.3, 0.8 }, ρ = 0.8

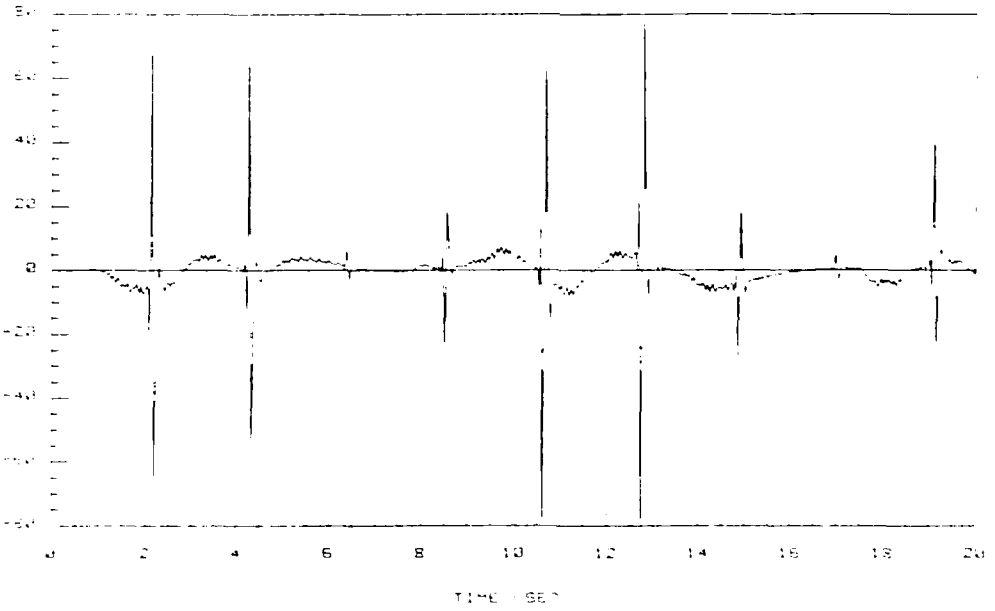

Figure 4-53. Flaperon deflection rate (deg/sec).
Σ = diag{ 0.3, 0.8 }, ρ = 0.8

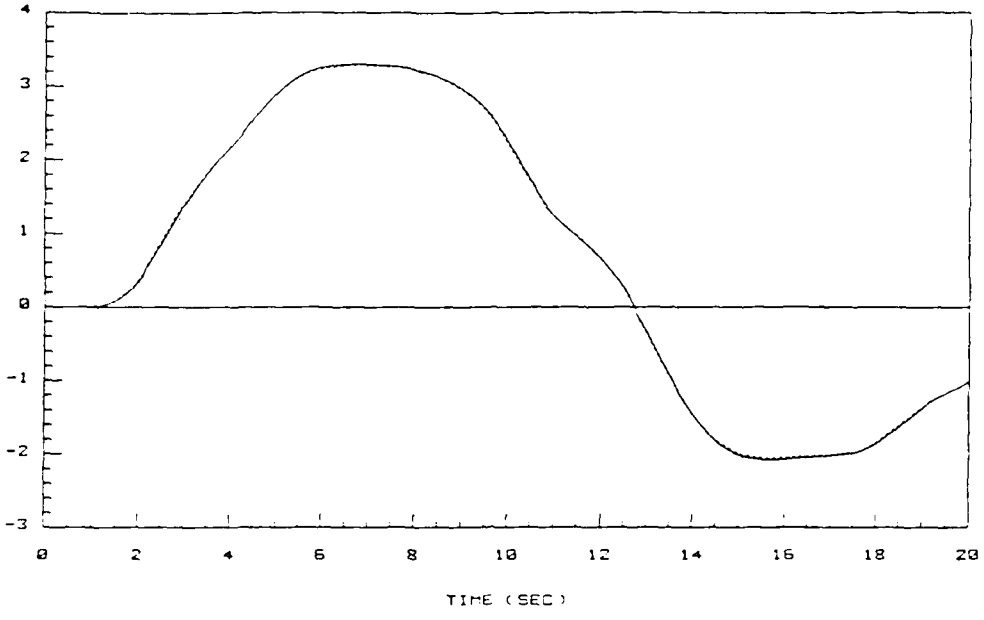

Figure 4-54. Flight path angle command and response (deg).
Σ = diag{ 0.3, 0.7 }, ρ = 0.6

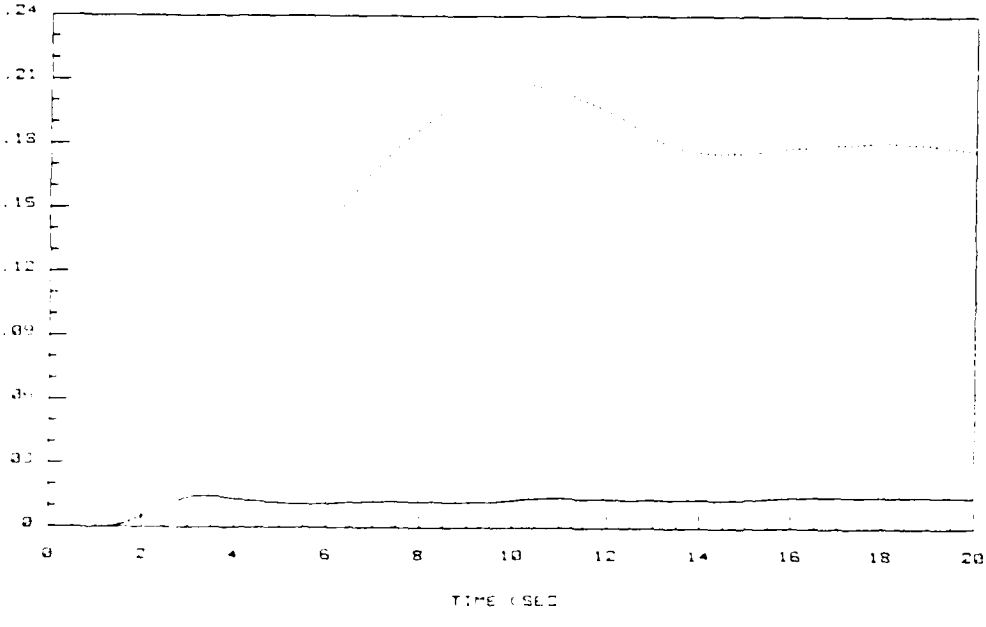

Figure 4-55. Flight path angle tracking performance index (deg).
Σ = diag{ 0.3, 0.7 }, ρ = 0.6

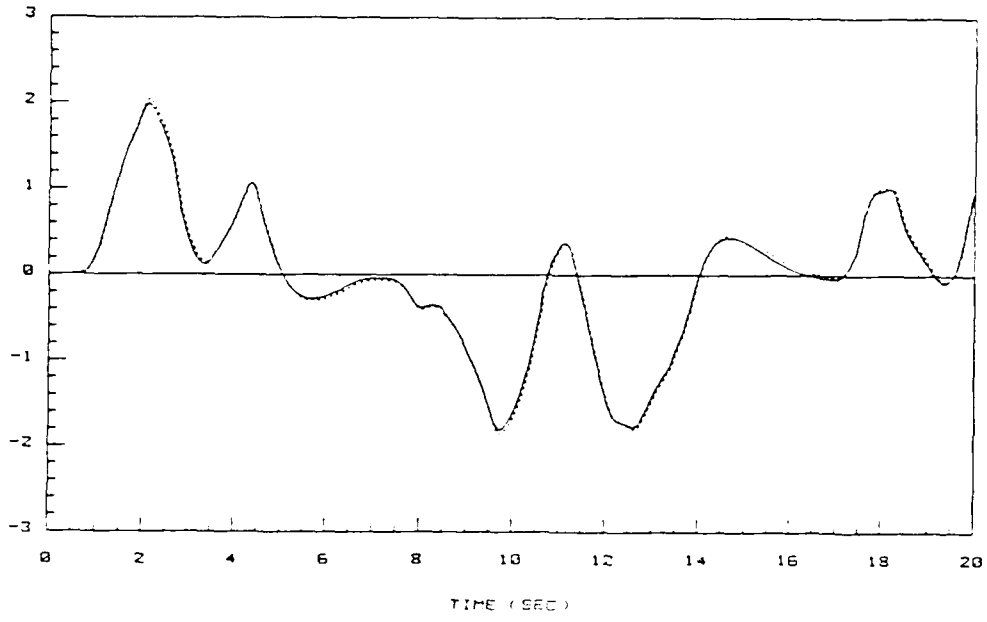

Figure 4-56. Pitch rate command and response (deg/sec).
Σ = diag{ 0.3, 0.7 }, γ = 0.6

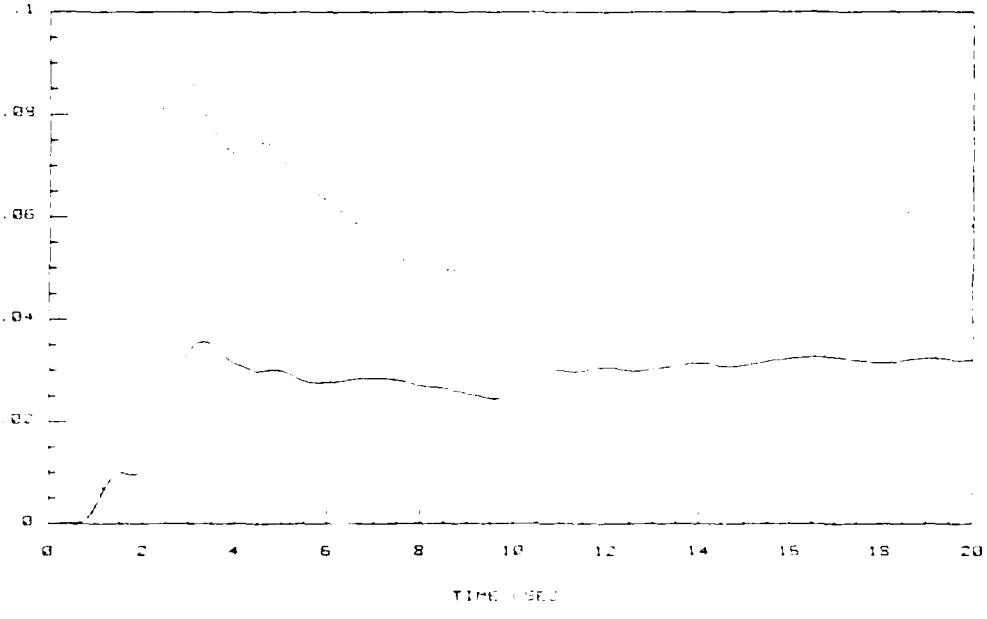

Figure 4-57. Pitch rate tracking performance index (deg/sec).
Σ = diag{ 0.3, 0.7 }, γ = 0.6

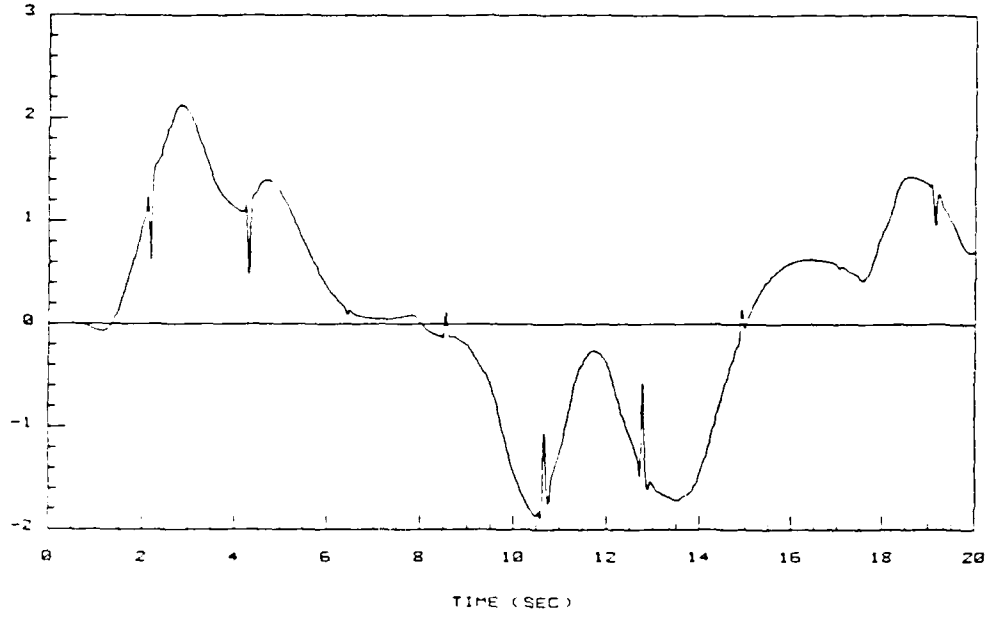

Figure 4-58. Elevator deflection (deg).
Σ = diag{ 0.3, 0.7 }, ρ = 0.6

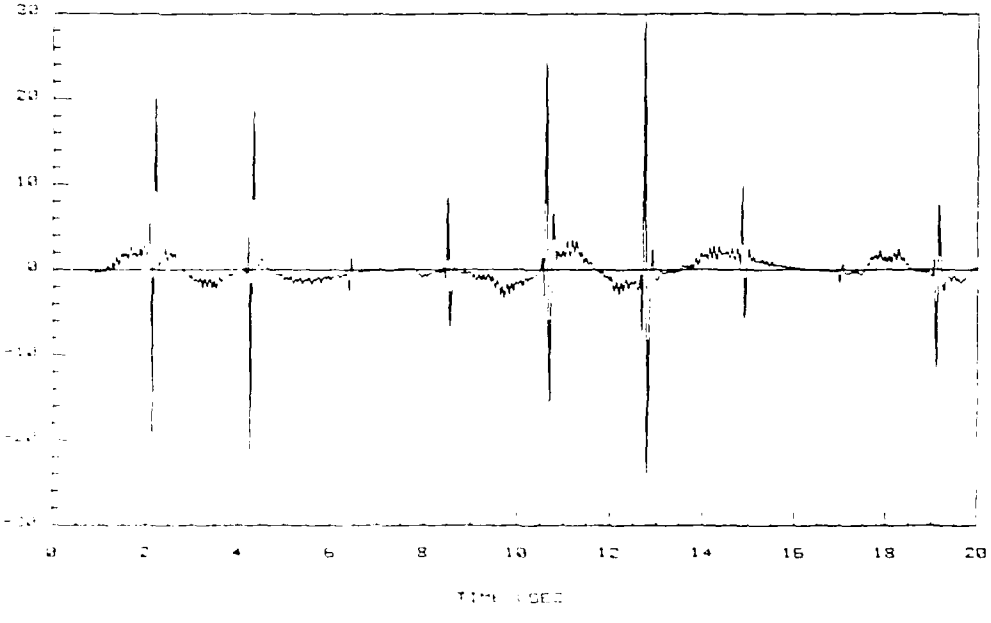

Figure 4-59. Elevator deflection rate (deg/sec).
Σ = diag{ 0.3, 0.7 }, ρ = 0.6

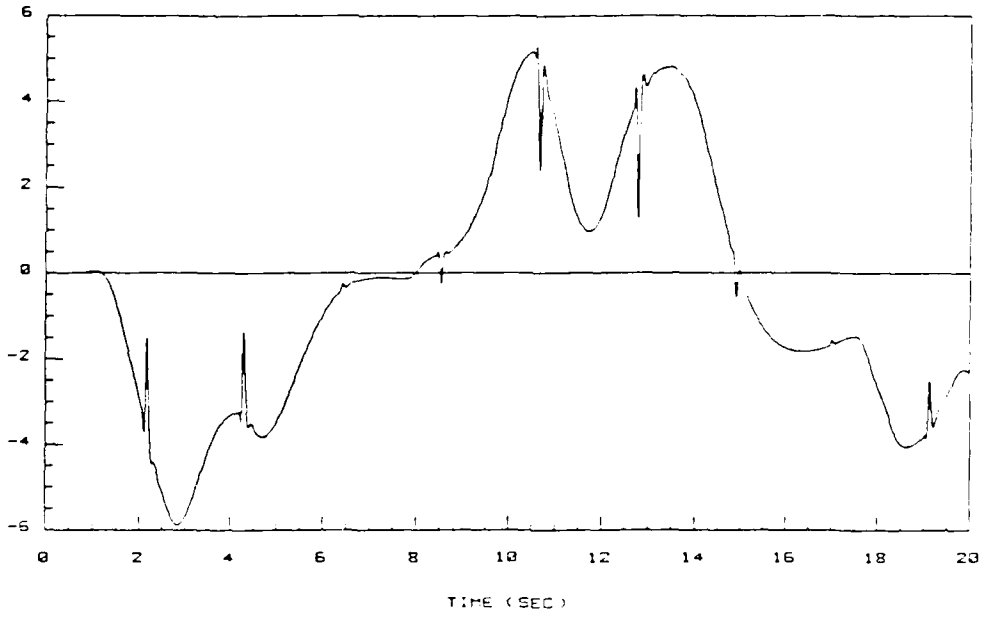

Figure 4-60. Flaperon deflection (deg).
Σ = diag{ 0.3, 0.7 }, ρ = 0.6

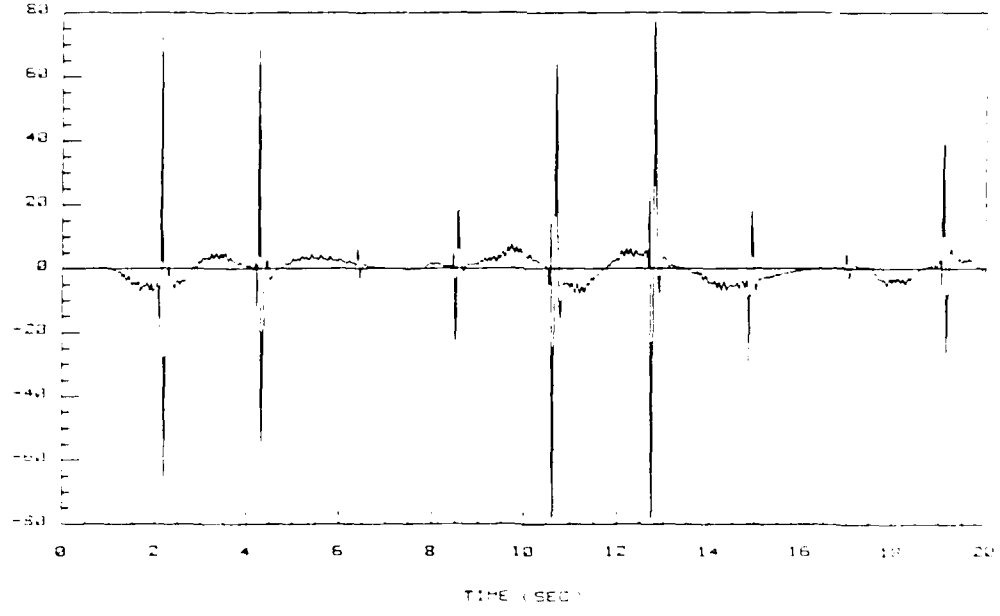

Figure 4-61. Flaperon deflection rate (deg/sec).
Σ = diag{ 0.3, 0.7 }, ρ = 0.6

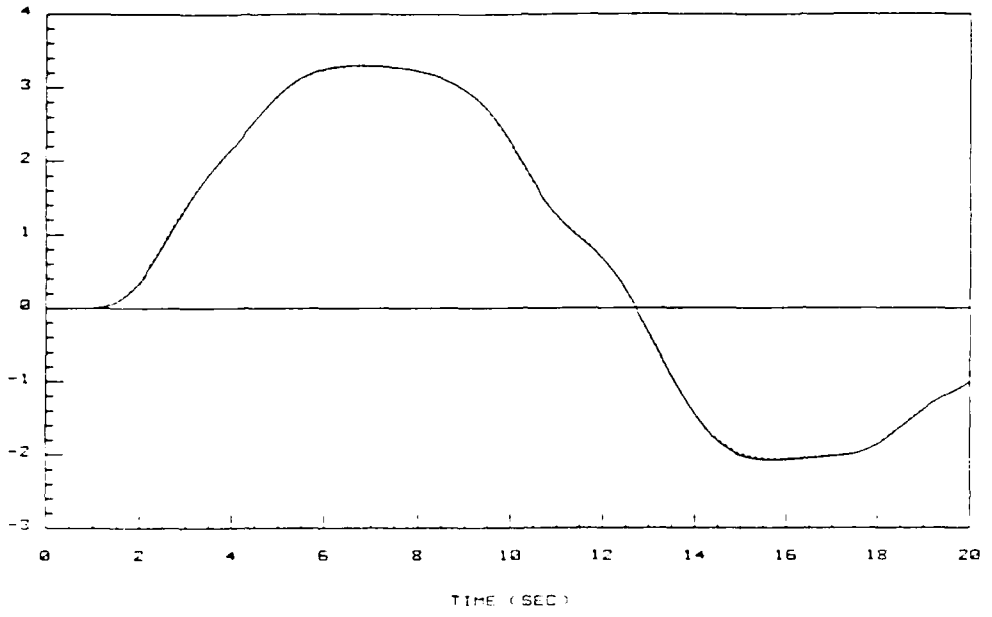

Figure 4-62. Flight path angle command and response (deg).
Σ = diag{ 0.3, 0.7 }, ρ = 1.0

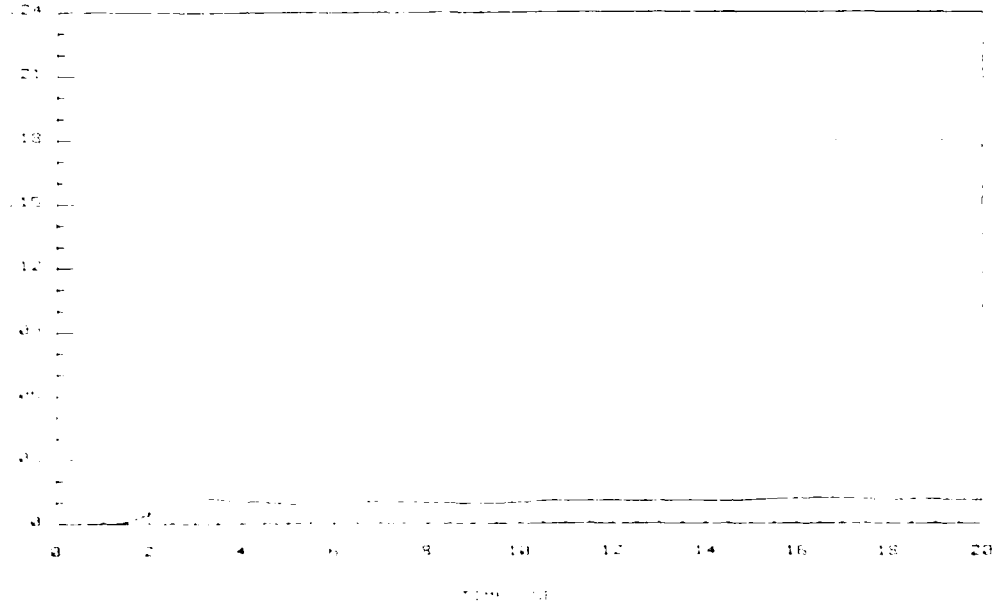

Figure 4-63. Flight path angle tracking performance index (deg).
Σ = diag{ 0.3, 0.7 }, ρ = 1.0

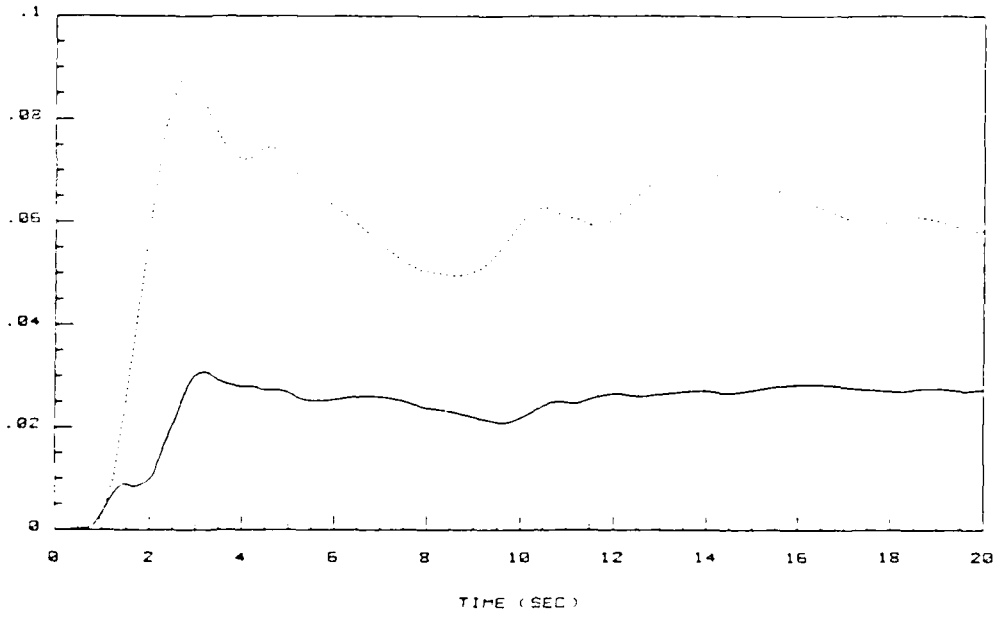

Figure 4-64. Pitch rate command and response (deg/sec).
Σ = diag{ 0.3, 0.7 }, ρ = 1.0

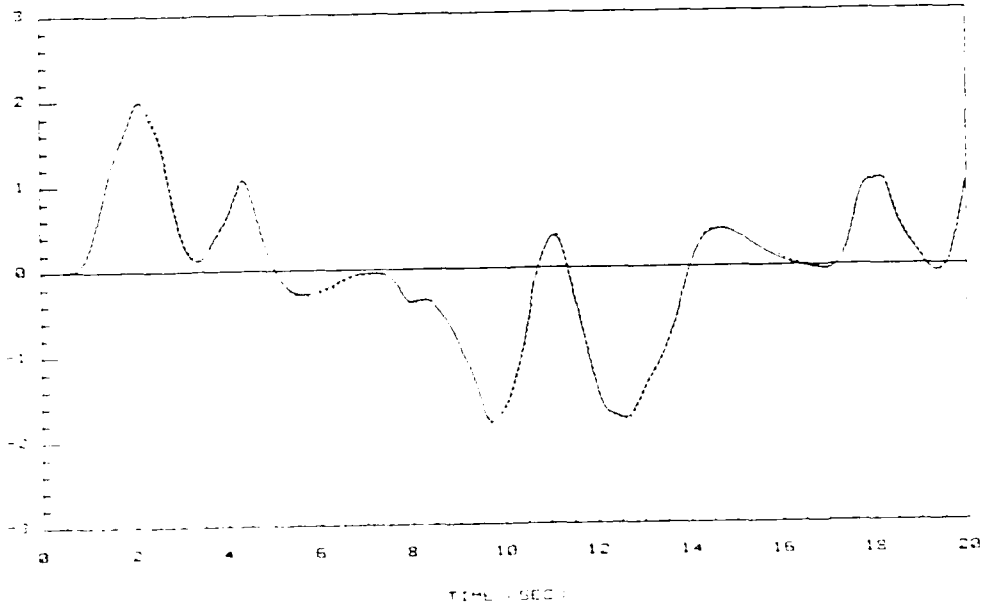

Figure 4-65. Pitch rate tracking performance index (deg/sec).
Σ = diag{ 0.3, 0.7 }, ρ = 1.0

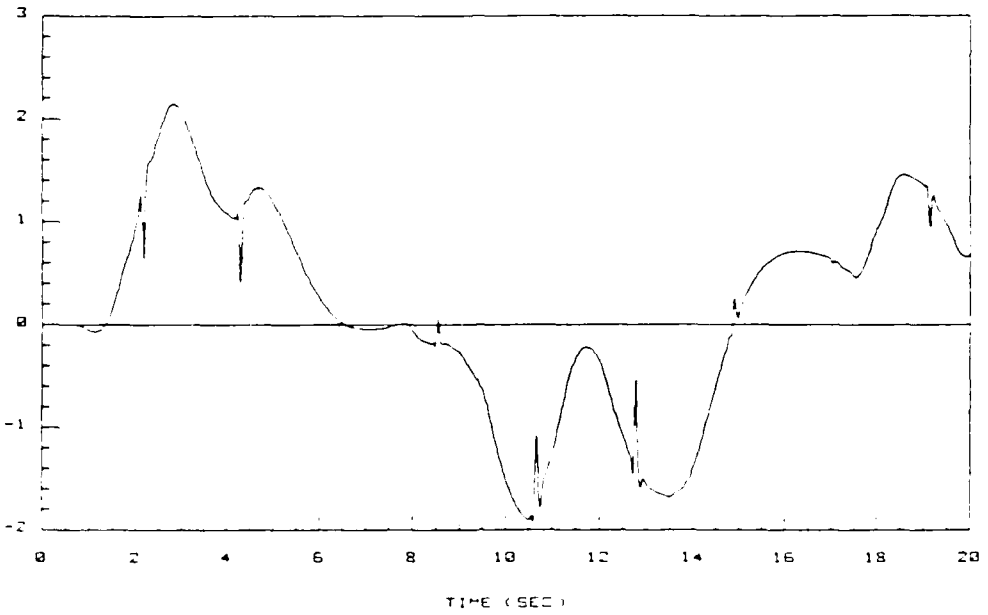

Figure 4-66. Elevator deflection (deg).
Σ = diag{ 0.3, 0.7 }, ρ = 1.0

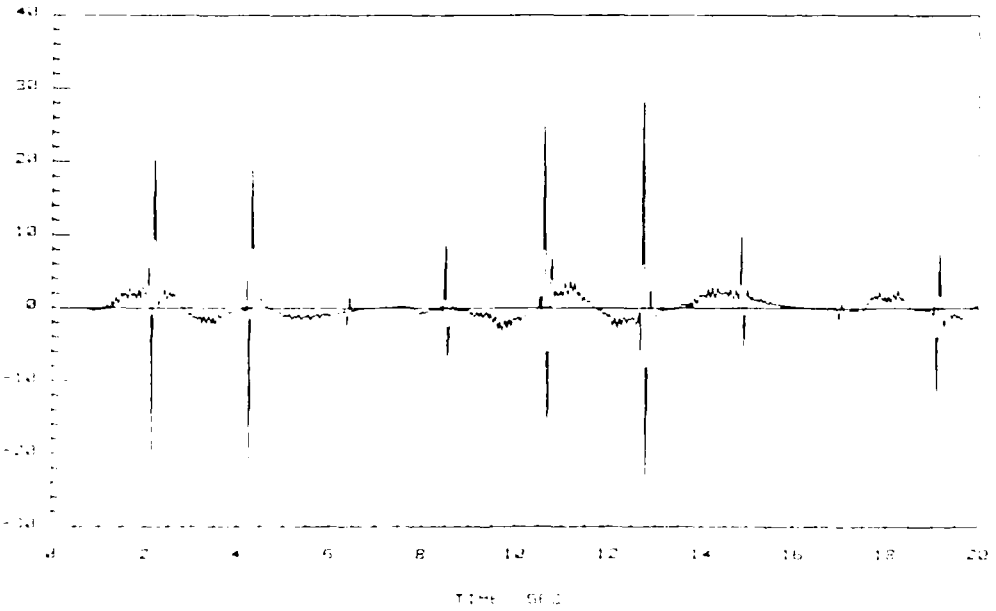

Figure 4-67. Elevator deflection rate (deg/sec).
Σ = diag{ 0.3, 0.7 }, ρ = 1.0

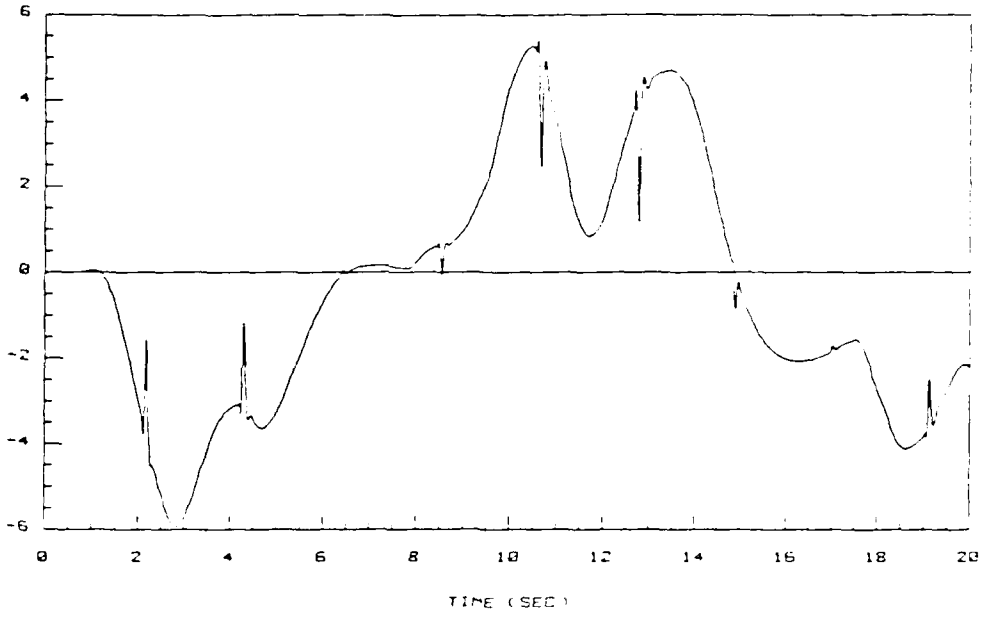

Figure 4-68. Flaperon deflection (deg).
Σ = diag{ 0.3, 0.7 }, γ = 1.0

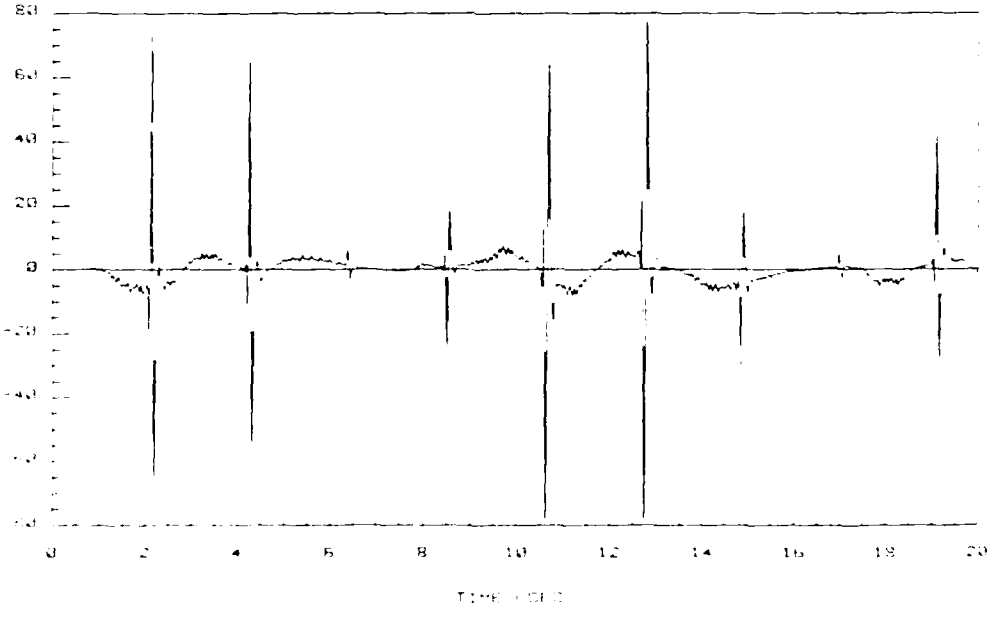

Figure 4-69. Flaperon deflection rate (deg/sec).
Σ = diag{ 0.3, 0.7 }, γ = 1.0

4.3.5 Parameter Variation and Sensor Noise. To assess the capability of the resulting fixed gain control law design in the presence of plant uncertainty, the controller resulting from the design parameters of Table 4-2 is subjected to step changes in the plant dynamics by using a model of the AFTI/F-16 trimmed at a flight condition of mach 0.3 and 10,000 ft. MSL. This is to represent either uncertainty on the knowledge of the stability derivatives of the aircraft, or simply a change of flight condition of the host aircraft during a flight. In addition, several simulations are conducted with the inclusion of various levels of sensor measurement noise. This is done either independently, or jointly with plant step changes in order to determine their effect on simulation fidelity. Results of these tests are documented in chapter 5.

4.4 Parameter Identifier Design

4.4.1 Design Variables. Although seemingly complex, the recursive identification algorithm proposed by Hagglund has relatively few design variables. Their specification is mostly based on experience gained by trial and error and a few analytical relationships as it is shown next. Recalling from chapter 3, these design parameters are

"a"	desired variance of the parameter estimates
γ_1, γ_2, r_0	design parameters for a fault detection scheme
γ_3 , γ_4, r_1	design parameters of the prediction error variance estimator

The next paragraphs will address briefly the different aspects involved

in their final selection.

4.4.2 Parameter Estimate Variance. The first of the design parameters to be considered is the desired variance of the parameter estimates ("a" in Eq (3-58)). Simply stated, this design parameter correspond to a specification of how precise we wish the parameter estimates to be. The selection of "a" is conceptually a simpler choice compared to the selection of the forgetting factor in the standard RLS algorihtm, since it is not based on any assunptions of the rate of change of plant parameters.

Typical considerations for the selection of "a" are the relative magnitudes of the parameters to be estimated and the noise level in the input-output data used in the algorithm. It may be argued that these considerations are themselves subject of speculation by the designer in the case of unknown plants, however, this issue is not considered a critical one due to a peculiar property of the algorihtm used. Given a particular level of plant excitation and signal to noise ratio, the algorithm does its best to converge to the specified parameter variance by adjusting its time horizon for convergence. Stability analysis conducted by Hagglund indicate however that if the signal to noise ratio happens to be larger than the one assumed, the P matrix will not converge to $a \cdot I$, but it will be actually smaller (19:81). This is hardly any problem since the algorithm will then provide a higher accuracy for the estimates than the one specified. A few design iterations can easily reveal a suitable choice for "a". The particular value selected for this investigation is 5.0 E-5.

4.4.3 Fault Detector Design. The next design step is the selection of suitable parameters for the fault detection algorithm. Its design begins with the selection of the integrator gain γ_1 in Eqns (3-42) and (3-67). The value of γ_1 controls the number of most recent parameter updates that affect the estimation of the average direction in which the parameter vector is updated. It is desired for γ_1 to be relatively high (close to 1) so that a sufficient number of samples are included in the estimate of the update direction, but not so high that it would delay the detection of direction change due to plant parameter changes. After conducting various simulations, the value of $\gamma_1 = 0.85$ was found to give satisfactory results for the particular case considered here.

The selection of γ_2 in Eqns (3-44) and (3-69) is based on the same rationale used in selecting γ_1. Hagglund indicates (19:39) that a value of $\gamma_2 = 0.95$ corresponds to the inclusion of approximately 20 of the most recent values of s(kT) in determining the stochastic variable r(kT). This is considered satisfactory for this study since it only introduces a detection delay between 20 and 30 samples.

The remaining design variable, the threshold r_0, is assigned a value that depends on the value chosen for γ_2, and what is considered an acceptable rate of false alarms for the particular design in question. If a small value is selected for the threshold it is possible to detect faults quickly, but the false alarm rate will be high. The chart produced by Hagglund, ilustrated in Figure 3-3, shows the compromise on false alarm rate versus the value of the threshold r_0, for various values of γ_2. For this study it is considered that an

expected false alarm rate of one in one thousand samples is satisfactory, given the length of the design simulations. Using Figure 3-3, and the values chosen for γ_2 and f_f, a value of $r_0 = 0.5$ is selected.

4.4.4 Noise variance estimator design. The design of the noise variance estimator is composed of the selection of the residual weighting coeficient γ_3, the time delay compensation parameter τ, and the threshold r_1 in Eqns (3-50) and (3-60). Initially, Eqn (3-50) is evaluated independently in several design simulations with a Gaussian white noise source of known variance. These simulations are used to determine a suitable value for γ_3 that produces results as close as posible to the known variance of the noise generator. This is done with τ set to zero. A value of $\gamma_3 = 0.95$ is found to produce satisfactory results.

The time delay compensation parameter τ is easily adjusted, recalling that the selection γ_2 previously mentioned caused a detection delay of approximately 20 to 30 samples. The parameter τ is therefore assigned a value of 20. Finally, it remains to assign a value for the threshold r_1. This is done on a trial an error basis by repeated simulation with the entire algorithm, and noticing how the fluctuations in the parameter estimates affect the signal $r(kT)$. The threshold r_1 is usually chosen smaller than r_0 since it is desired to exclude the effects of parameter estimate transients on the residuals used to estimate the noise variance. These transients are typical in this type of estimation algorithms, but are not necessarily the result of plant parameter changes. The threshold $r_1 = 0.2$ is used in this

study.

This concludes the dicussion on the selection of the primary design variables of the identification algorithm. Several practical considerations however, make necessary the use of additional signal processing techniques to complete the implementation of the identification algorithm. Section 4.4.5 discusses this topic.

4.4.5 Practical Signal Processing Considerations. In order to implement (and in some instances improve the performance of) the identification algorithm, it is necesary to use a series of additional filters to ensure that the signals used in the identification and the control law design process are well conditioned for such purposes. For example, the estimation algorithm is designed to use perturbations of the plant's input-output signals, however, the sensors typically provide data on "absolute" measurements. In other words, the measurements U(kT) and Y(kT) are composed of nominal values $U_o(kT)$ and $Y_o(kT)$, and perturbation signals $u(kT)$ and $y(kT)$. This can be expressed as

$$U(kT) = U_o(kT) + u(kT) \tag{4-11}$$

$$Y(kT) = Y_o(kT) + y(kT) \tag{4-12}$$

In the case of the output signal, the nominal value $Y_o(kT)$ may be assumed as the commanded quantity. Then Eqn (4-12) may be used to obtain the perturbations. Unfotunately, the procedure for obtaining $U_o(kT)$ would involve inverting the model of the plant which is of course what we are trying to determine. It is highly desirable to use a

technique that does not requires knowledge of the nominal measurements. Assuming that any changes in the nominal values (caused by the maneuvers of the aircraft) are slow compared to the sampling period, so that they remain relatively constant between any two consecutive sampling instants, the perturbations may be approximated using the differences

$$U(kT) - U\{(k-1)T\} \approx u(kT) - u\{(k-1)T\} \approx \Delta u(kT) \qquad (4\text{-}13)$$

$$Y(kT) - Y\{(k-1)T\} \approx y(kT) - y\{(k-1)T\} \approx \Delta y(kT) \qquad (4\text{-}14)$$

These differences essentially produce a high-pass filtering effect on the measured quantities, thus removing their nominal components. Instead of $u(kT)$ and $y(kT)$, the signals $\Delta u(kT)$ and $\Delta y(kT)$ are used for the parameter estimation (25).

Another consideration in the conditioning of input-output data, especially in the case of a tracking control law, is the effect that changes in the command signal have on the parameter estimates. Because of the high-pass filtering effect of Eqns (4-13) and (4-14), abrupt changes in the command signals to the closed-loop system produce spikes in the input-output differences $\Delta u(kT)$ and $\Delta y(kT)$. These spikes are reflected in the residuals that are used to update the parameter and noise variance estimates by virtue of Eqns (3-51), (3-53), and (3-60); thus producing spikes in the parameter estimates themselves. This effect is highly undesirable, however, a reduction of the parameter variations can be achieved by filtering both the input and output differences with identical low pass filter algorithms. Various forms of low pass algorithms may be used for this purpose. The one selected for

this application is of the form

$$\Delta_f(kT) = (1 - \varepsilon)\ \Delta_f\{(k-1)T\} + \varepsilon\ \Delta(kT) \qquad (4\text{-}15)$$

where

$\Delta(kT)$ = input(output) difference signal

$\Delta_f(kT)$ = filtered input(output) difference signal

ε = filter constant

The filter constants must be identical in order to preserve the input-output relationship that defines the plant. The value of ε is selected again by trial and error as a tradeoff between the desire to attenuate noise spikes in the input-output data, and the need to maintain sufficient excitation in the input-output perturbation signals. The value of $\varepsilon = 0.2$ represents an acceptable compromise for this study.

To deal directly with the problem of noise spikes, and/or abrupt variations of the parameter estimates in general, the estimates themselves are filtered before they are used for any control law calculation. The form of the low pass filter chosen for this function is a discretized version of a simple first order analog filter given by

$$\frac{\quad}{s + \quad} \qquad (4\text{-}16)$$

The discretization is accomplished by using the Tustin transformation (22) given by

$$s = \frac{2}{T}\ \frac{z - 1}{z + 1} \qquad (4\text{-}17)$$

where s is the Laplace operator, T is the sampling period and z is the discrete Z transform operator. This results in the following filter algorithm

$$\hat{\Theta}_f(kT) = c_1 \hat{\Theta}_f\{(k-1)T\} + c_2 [\hat{\Theta}(kT) + \hat{\Theta}\{(k-1)T\}] \qquad (4\text{-}18)$$

with

$$c_1 = \frac{2 - \alpha T}{2 + \alpha T} \qquad (4\text{-}19)$$

$$c_2 = \frac{\alpha T}{2 + \alpha T} \qquad (4\text{-}20)$$

where $\hat{\Theta}_f(kT)$ is the filtered parameter estimate.

Although this low-pass filtering helps, often the transients are of such magnitude that the filter may "charge-up" to a very large offset as compared to the magnitude of the correct parameter estimate. In that case it may take the filter a long time to return to the nominal estimate depending on the value chosen for α, even though the estimator itself may return quickly to the correct value. This situation can cause a slower rate of adaptation than desired. A very simple way of solving the problem is to implement a rate limiter at the input of the parameter filter to restrict the magnitude of the fluctuations in the incoming estimates. Because the relative magnitude of the individual parameters may vary significantly, the rate limit is not set to an absolute quantity, but rather expressed as a percentage variation from

the last input received to the parameter estimate filter. The final version of the parameter estimate filter is then given by the following algorithm

For each element $\hat{\Theta}^i$ of the parameter vector $\hat{\Theta}$, iterate thru

$$\text{IF} \quad \left| \hat{\Theta}^i\{(k-1)T\} \right| > \Lambda \quad \text{THEN} \tag{4-21a}$$

$$\Delta\hat{\Theta}^i_{RL}(kT) = \left| \hat{\Theta}^i\{(k-1)T\} \right| \frac{\Xi}{100} \tag{4-21b}$$

$$\hat{\Theta}^i_{RL}(kT) = \hat{\Theta}^i_{RL}\{(k-1)T\} + \ldots$$

$$\text{MAX}\left[-\Delta\hat{\Theta}^i_{RL}(kT) , \text{MIN}\left[(\hat{\Theta}^i(kT) - \hat{\Theta}^i_{RL}\{(k-1)T\}) , \Delta\hat{\Theta}^i_{RL}(kT) \right] \right] \tag{4-21c}$$

ELSE

$$\hat{\Theta}^i_{RL}(kT) = \hat{\Theta}^i(kT) \tag{4-21d}$$

ENDIF

$$\hat{\Theta}^i_f(kT) = c_1 \hat{\Theta}^i_f\{(k-1)T\} + c_2 [\hat{\Theta}^i_{RL}(kT) + \hat{\Theta}^i_{RL}\{(k-1)T\}] \tag{4-21e}$$

where

Λ is a very small number ($\approx$ 1e-6)

$\Delta\hat{\Theta}^i_{RL}(kT)$ is a rate limited parameter estimate increment

Ξ is the allowable percentage of the last input to form the rate limit

$\hat{\Theta}^i_{RL}(kT)$ is a rate limited parameter estimate

and $\hat{\theta}^i_f(kT)$, ε_1 , ε_2 are defined as before. The magnitude test in the begining IF statement is necessary in case the parameter estimate passes through zero. If this test were not included, because the maximun and minimun limits in Eqn (4-21c) are dependent on the magnitude of the last incoming estimate, the filter would "lock on" to a value of zero. Therefore, when the estimates are within a very small band around zero the limiter is bypassed and the estimates are fed directly into the low-pass filter as Eqn (4-21d) indicates.

The filter pole location α and the input rate limiter percentage value Ξ are both design parameters and are adjusted by trial and error. The values of $\alpha = 2.25$ and $\Xi = 25$ are used throughout the study. The filtering procedure just discussed helps in preventing transients to be passed on to the calculation of the control law in Eqns (2-47) and (2-48) and therefore improves the performance of the adaptive control system.

Another way of improving the the performance of the estimation algorithm in the presence of noise is by proper scaling of the parameter vector $\hat{\Theta}$ and measurement matrix Υ. Although not formally a signal filtering technique, the scaling of these variables helps to increase the dynamic range of the identification procedure in regards to noise level effects. When the standard deviation of the noise level is roughly the same order of magnitude of some of the elements in the parameter vector, the estimates of those parameters may suffer from large transients and biases that may lead to close-loop instability. This is specially true for parameters that are very close to zero, for example, elements of the step-response matrix corresponding to a model

of an aircraft at a flight condition characterized by low dynamic pressure and low control surface effectiveness. If an estimate of a particular element of $H(T)$ goes to zero or oscilates substantially around that region because of noise or poor input-output excitation, the control law gains become undefined or vary wildly because of the inverse relationship between $H(T)$ and the control law gains. This situation may then lead to instability if proper precations are not taken.

The scaling of $\hat{\Theta}$ and $\bar{r}$ may be used to help reduce the effects of transients, and it can be carried out in various ways. The method used here comes from Eqns (3-9) and (3-11). If one considers the response of the dicrete system given by Eq (3-9) at $t = T$,with zero initial conditions and input $u(0)$, we have

$$y(T) = B_1\, u(0) + \epsilon(T) \tag{4-22a}$$

$$\simeq TCB\, u(0) + \epsilon(T) \tag{4-22b}$$

Eqn (4-22) can also be expressed as

$$y(T) \simeq \left[\frac{1}{T} TCB \right] T\, u(0) + \epsilon(T) \tag{4-23}$$

which suggest that by multiplying the elements in $\hat{\Theta}$ by the sampling frequency (f = scale factor), and the measurement matrix $\bar{r}$ by the sampling time, the magnitude of the parameters can be scaled away from the noise level while maintaining the same input-output relationship. Other scale factors may be applied, however consideration must be given

always to avoid making the magnitude of the elements of measurement matrix too small. The scaling procedure makes it possible for the algorithm to provide better performance in environments with increased sensor noise by reducing the effect of parameter estimate transients in the closed-loop response of the system.

The case in which the estimates go to, or pass through zero momentarily are handled by evaluating the step-response matrix before it is used in the control law calculations. Parameter estimates resulting in a singular step-response matrix are discarded and the control law gains are not updated until new estimates are obtained which result in an invertible H(T).

As it was mentioned in section 4.3.2, all of the elements composing the identification algorithm and control law design equations are implemented in $MATRIX_X$ in the block labeled "ADAPT2" (Figure 4-10). A more detailed look of which is shown in Figure 4-70. The delay blocks labeled "DEL U" and "DEL Y" generate delayed samples of the input and output signals used in forming the measurement matrix T. The block labeled "ADAPT" is a FORTRAN subroutine that implements the estimation, filtering algorithms and safety checks just described, and the block labeled "P INDX" implements the calculation of the model-following criteria given by Eqn (4-10) as shown in Figure 4-71.

To consolidate the discussion on the design of the recursive identification algorithm, a list summarizing the values of the design paremeters used for the estimation, and the signal conditioning filters, is provided in Table 4-3. Chapter 5 will summarize the results obtained comparing the performance of both, fixed gain, and adaptive controllers

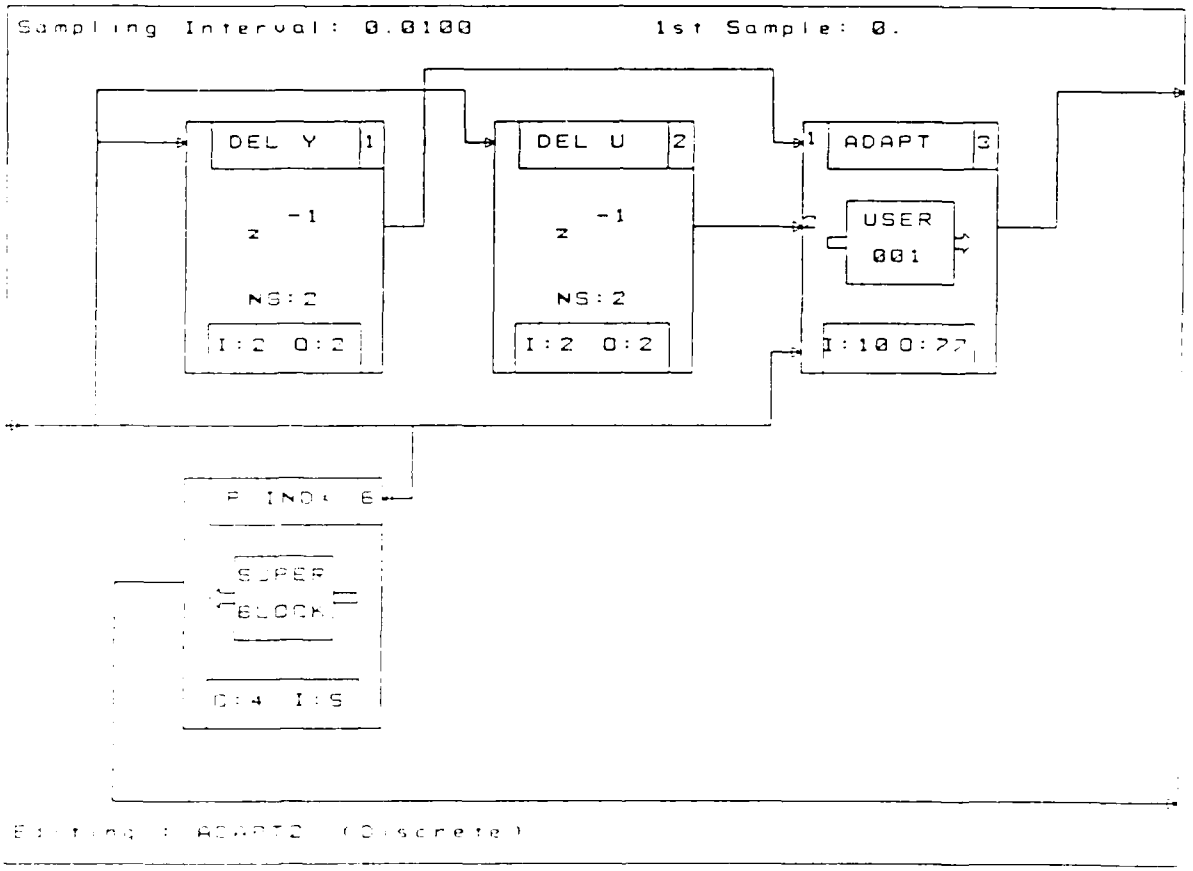

Figure 4-70. Identification Algorithm implementation in MATRIX$_X$.

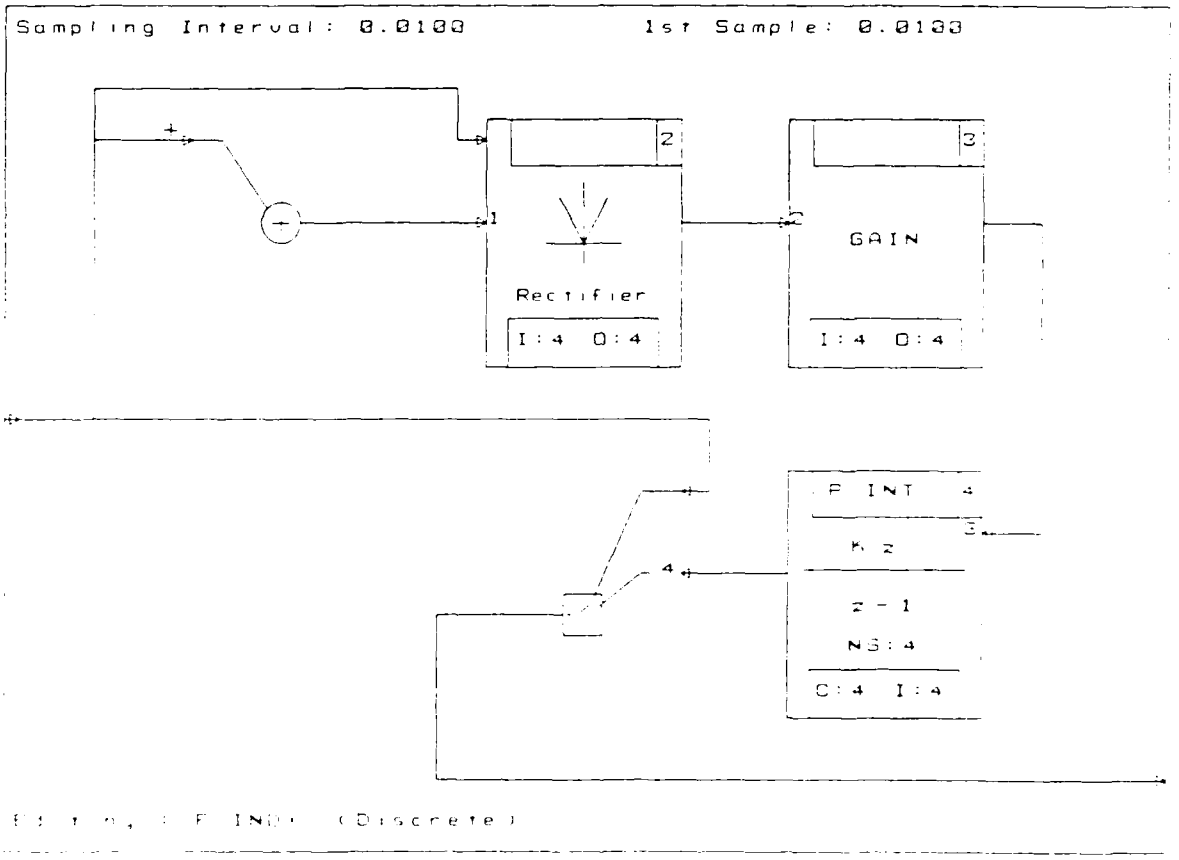

Figure 4-71. Performance Index Calculation.

Table 4-3

Final Estimation Algorithm Design Parameters

Parameter Estimation Algorithm	Input/Output Perturbation Filter
a = 5.0E-5	ε = 0.2
Fault Detector	**Parameter Estimate Filter**
γ_1 = 0.85	α = 2.25
γ_2 = 0.95	Ξ = 25 %
r_0 = 0.5	
Noise variance estimator	
γ_3 = 0.95	
τ = 20	
r_1 = 0.2	

under conditions of plant parameter changes and sensor noise.

V. Results

5.1 Introduction

This chapter presents the simulation responses obtained by applying the design procedures described in chapter 4 of this thesis to an AFTI/F-16 aircraft model used as representative of the VISTA/F-16 dynamics.

The main objective of this study is to determine the effectiveness of a parameter-adaptive control system in maintaining model-following fidelity for an in-flight simulator under changing conditions. This is accomplished by properly adjusting the control law based on information derived from input-output data measurements that reflect the current characteristics of the host vehicle.

This chapter is divided into two main sections corresponding to the evaluations performed on a fixed gain, and a parameter-adaptive control system. Each section in turn includes responses detailing the individual system's behavior under conditions of plant parameter changes and sensor noise. This is done to establish a comparative base upon which the virtues and deficiencies of each approach can be pointed out.

5.2 Fixed Gain Controller Responses

5.2.1 Plant Parameter change. To assess the effect of either plant parameter uncertainties or changes in the model following tracking performance, a fixed gain control law based on the design parameters of Table 4-2 is tested. The input commands of Figures 4-12 and 4-13 are

used. At six seconds into the simulation the plant dynamics are changed from a model at Mach 0.9 to one at Mach 0.3 (both at 10,000 ft.), to obtain information on the robustness properties of the control law. The simulation responses are shown in Figures 5-1 thru 5-8.

Figure 5-1 shows both, the flight path command input (solid line) superimposed on the host aircraft response (dashed line). It is obvious from this plot that the control law offers sufficient robustness to maintain the level of tracking for this command input. This is also exemplified in Figure 5-2, which shows the model-following criteria as calculated from Eqn (4-10). The solid line represents the average error absolute value response, and the dashed line represents the average absolute value response of ten percent of the reference signal. The error response is clearly below the performance limit specification.

In the case of the pitch rate response, the situation changes drastically as shown in Figures 5-3 and 5-4. These Figures follow the same notation as Figures 5-1 and 5-2, as well as all the remaining aircraft and performance index plots in this thesis. Although the response of Figure 5-3 demonstrates the ability of this particular control law design technique to provide satisfactory control in the presence of plant parameter uncertainty, the magnitude of the change in plant dynamics is sufficient to violate the model-following performance criterion, as depicted in Figure 5-4. Figures 5-5 and 5-6 show the host aircraft's elevator deflection, and elevator deflection rate. Those corresponding to the flaperon deflection and deflection rate are shown in Figures 5-7 and 5-8. All of these control surface responses are well within bounds, and considered acceptable.

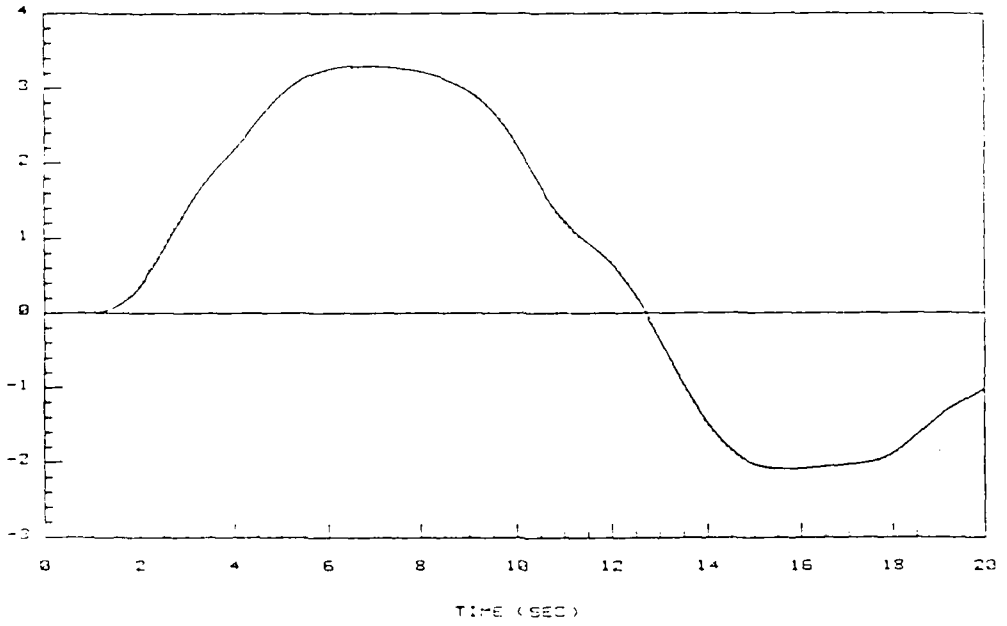

Figure 5-1. Flight path angle command and response (deg). Fixed gain control law. Plant parameter change.

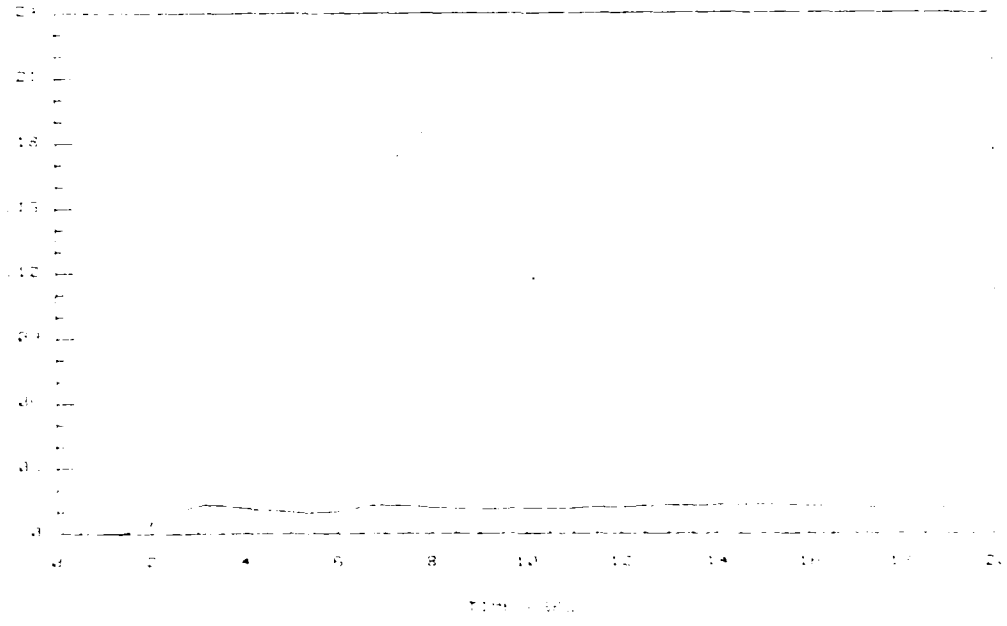

Figure 5-2. Flight path angle tracking performance index (deg). Fixed gain control law. Plant parameter change.

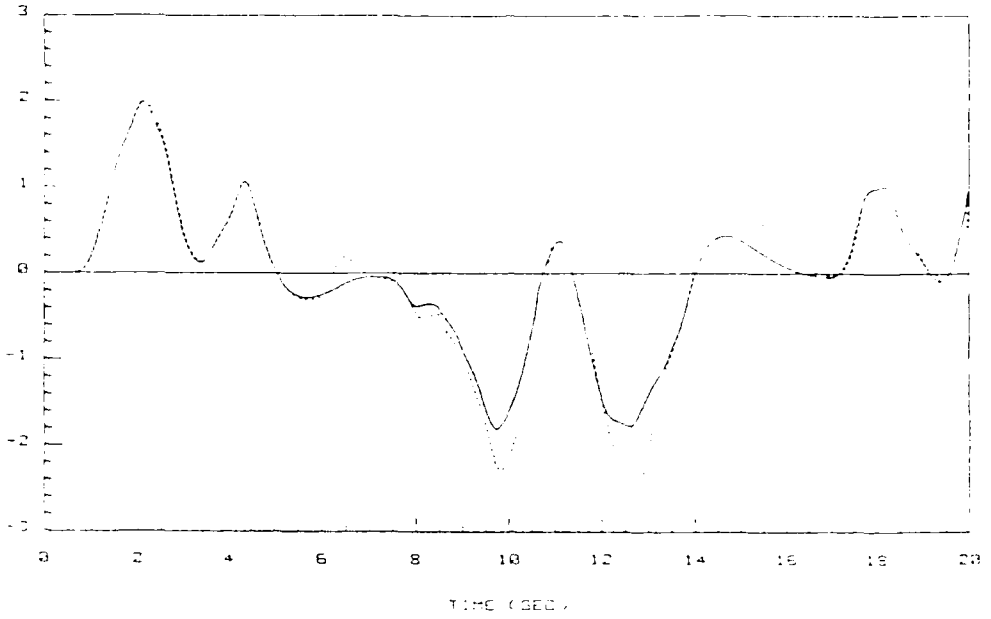

Figure 5-3. Pitch rate command and response (deg/sec).
Fixed gain control law. Plant parameter change.

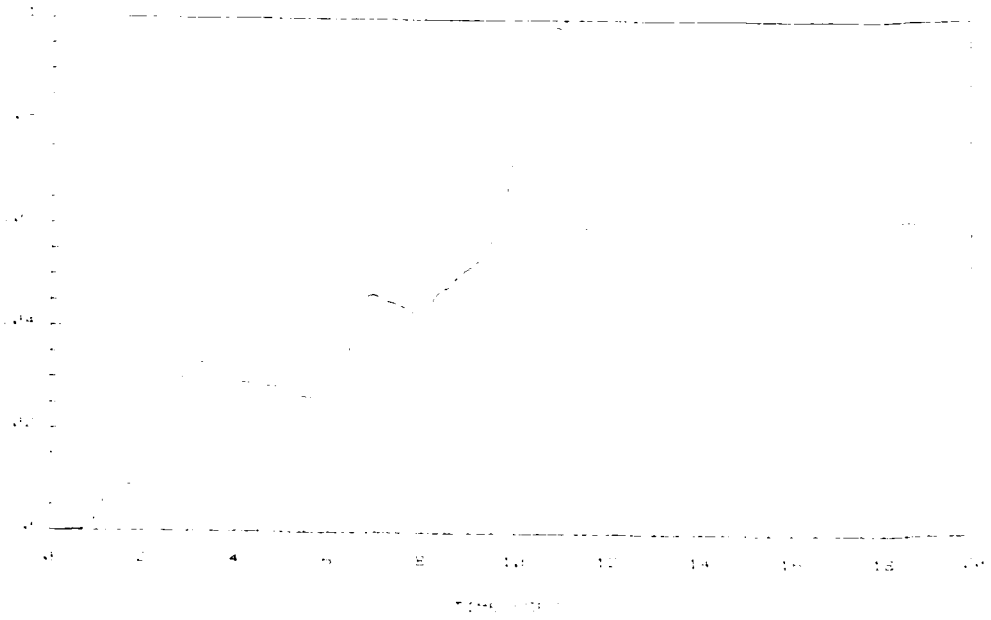

Figure 5-4. Pitch rate tracking performance index (deg/sec).
Fixed gain control law. Plant parameter change.

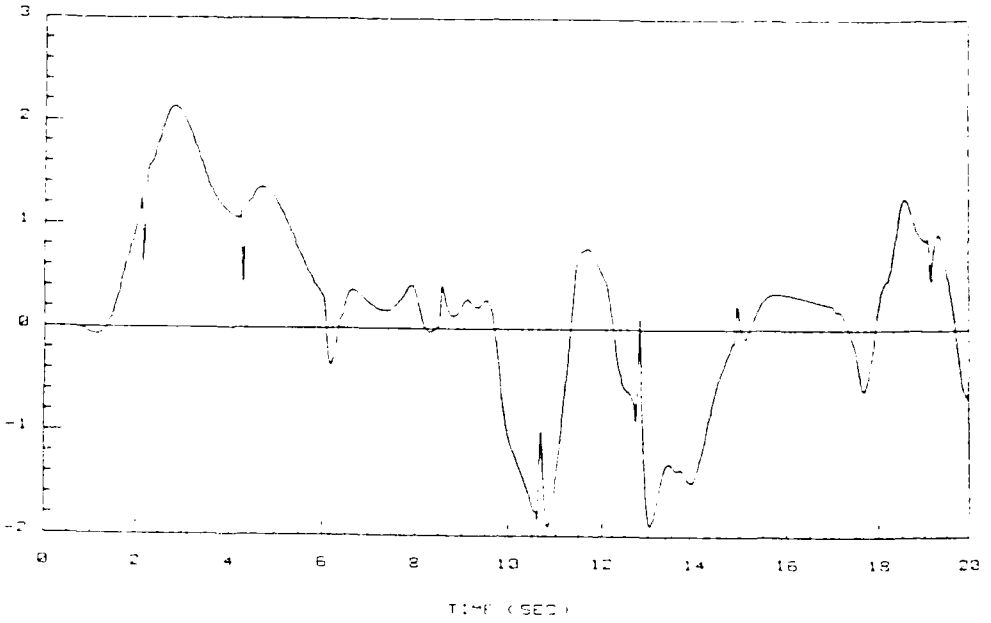

Figure 5-5. Elevator deflection (deg).
Fixed gain control law. Plant parameter change.

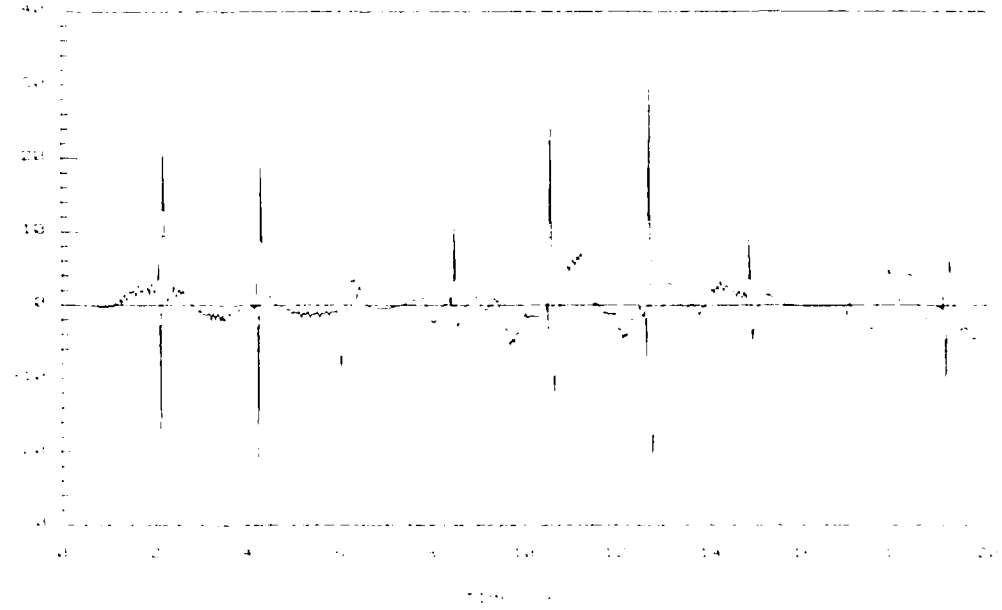

Figure 5-6. Elevator deflection rate (deg/sec).
Fixed gain control law. Plant parameter change.

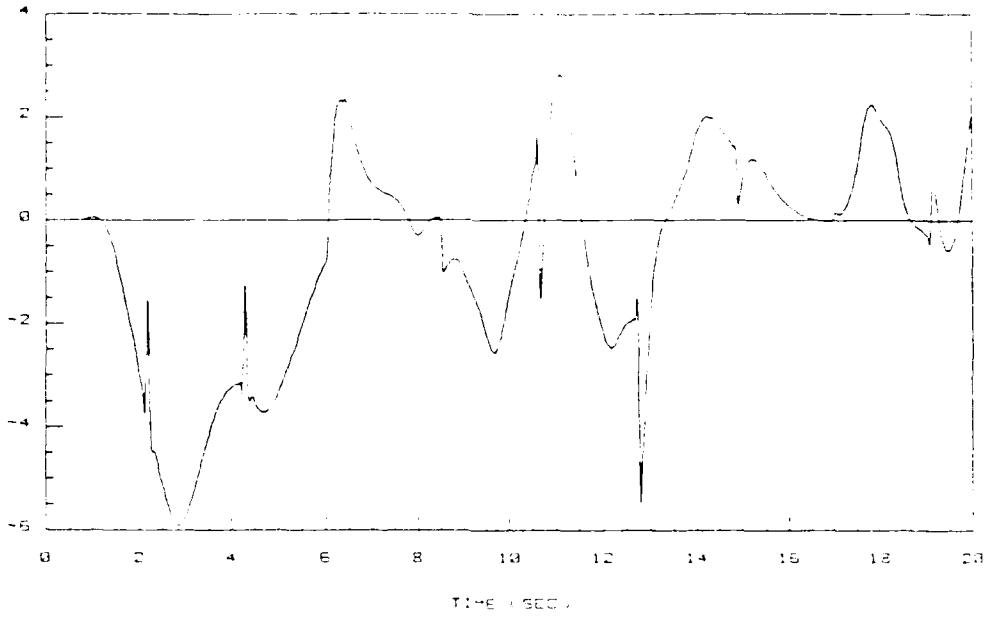

Figure 5-7. Flaperon deflection (deg).
Fixed gain control law. Plant parameter change.

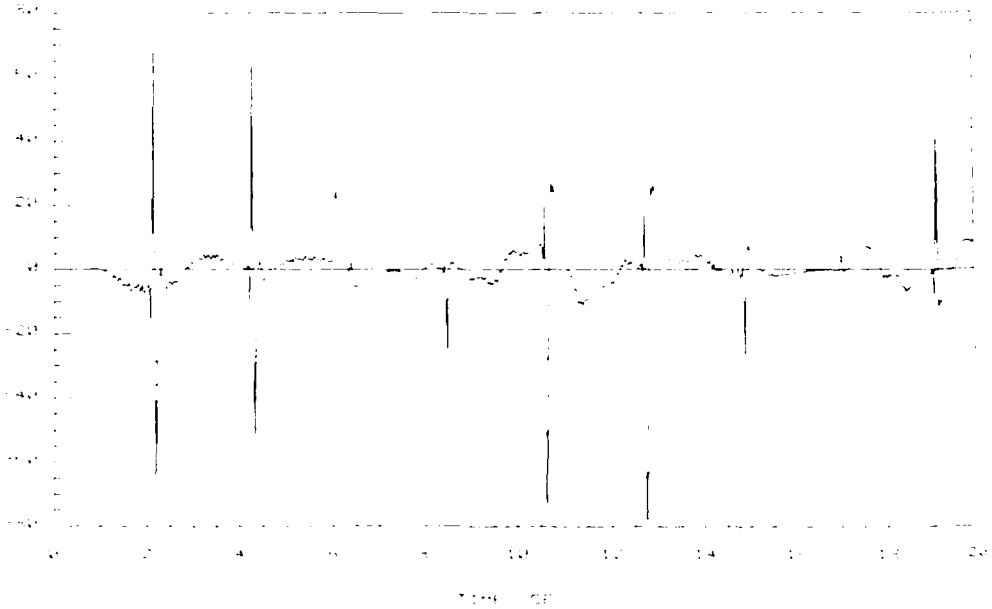

Figure 5-8. Flaperon deflection rate (deg/sec).
Fixed gain control law. Plant parameter change.

5.2.2 Plant Parameter Change and Sensor Noise. In addition to robustness to plant parameter changes, it is important to demonstrate the influence of sensor measurement noise in the closed-loop system response. Each plant output measurement is corrupted by zero-mean, white gaussian noise added to the simulation by the "noise" block location in Figure 4-8. Figures 5-9 thru 5-16, and 5-17 thru 5-24 show two representative samples of the fixed gain system responses to noise levels with standard deviations of 0.0573 deg (deg/sec for pitch rate), and 0.314 deg (deg/sec for pitch rate) respectively.

The most noticeable effect of sensor measurement noise is that of increased control surface deflection and deflection rate activity, particularly the latter. The effect on tracking performance, however, is hardly noticeable.

Although the control surface rates shown in these Figures are below the specified limits, the sustained level of effort required from the actuators indicated by these Figures may represent a severe demand on the aircraft's hydraulic system. These results merely reiterate the need for high quality sensors, in combination perhaps, with complementary filter functions to achieve low noise level specifications. This is particularly appropriate in cases where high gain control laws like the ones used in this thesis are applied. The need for low sensor noise levels will become more evident when the input-output measurements are used to update the control law gains as in the case of the parameter adaptive control law which is presented next.

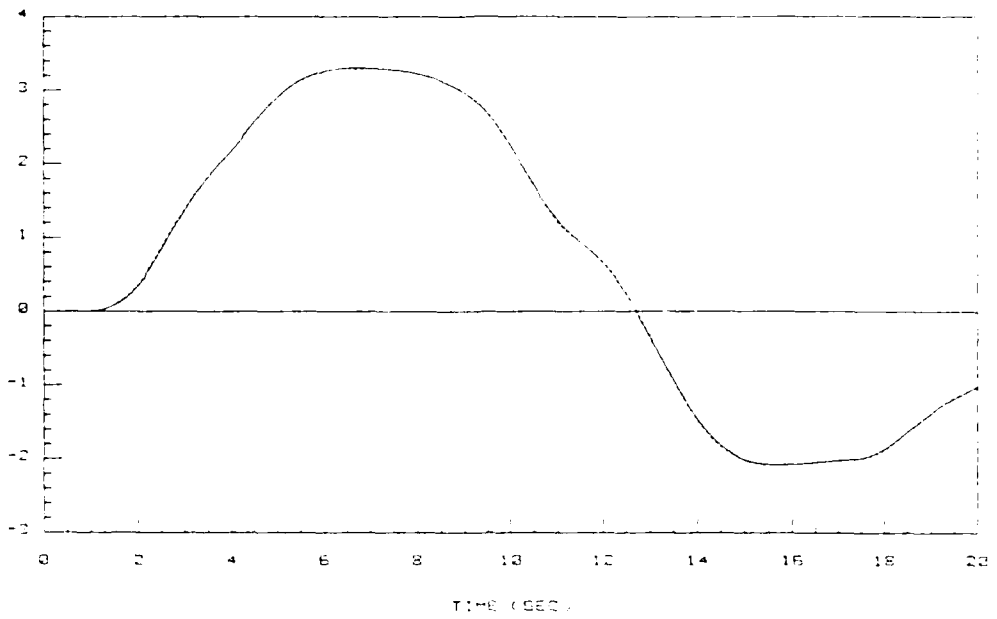

Figure 5-9. Flight path angle command and response (deg).
Fixed gain control law. Plant parameter change and sensor noise.
(std. dev. = 0.0573 deg)

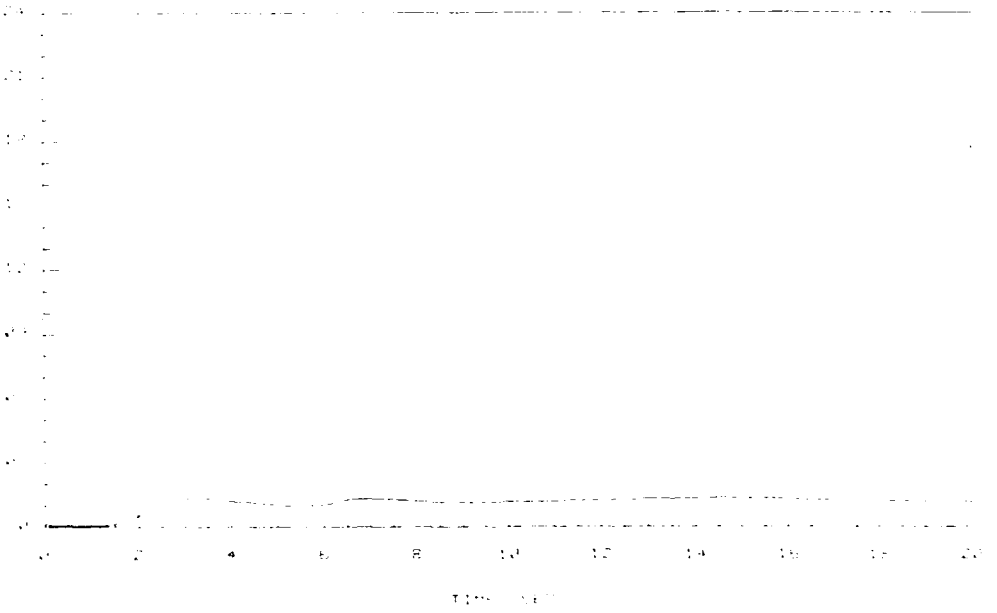

Figure 5-10. Flight path angle tracking performance index (deg).
Fixed gain control law. Plant parameter change and sensor noise.
(std. dev. = 0.0573 deg)

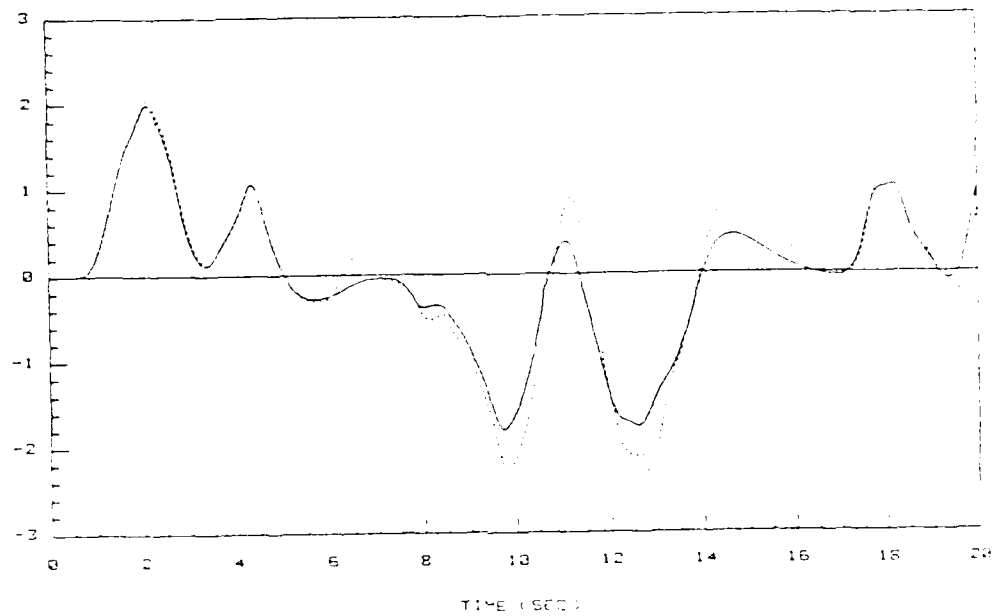

Figure 5-11. Pitch rate command and response (deg/sec).
Fixed gain control law. Plant parameter change and sensor noise.
(std. dev. = 0.0573 deg/sec)

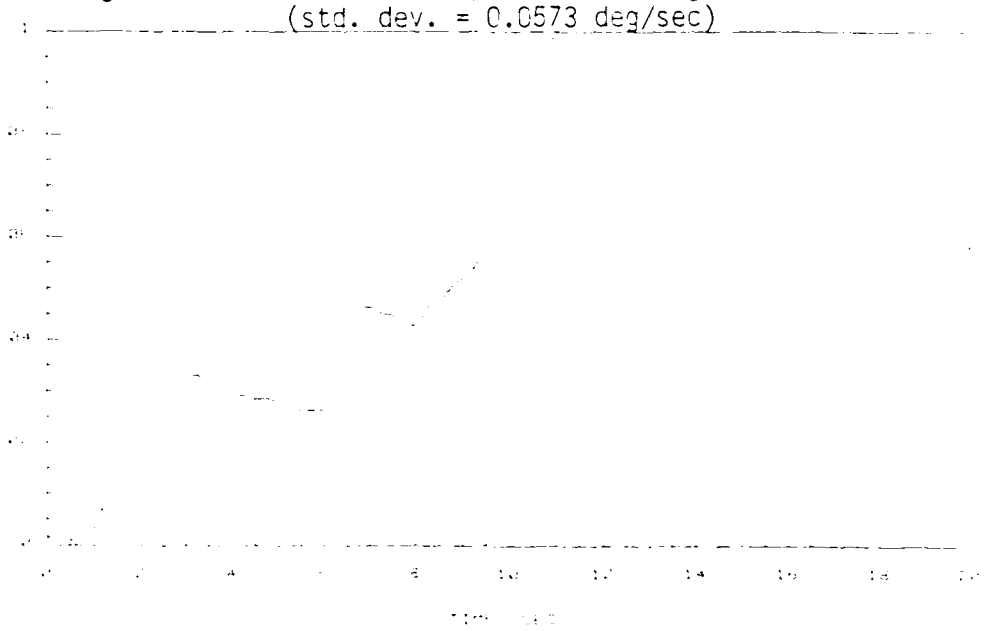

Figure 5-12. Pitch rate tracking performance index (deg/sec).
Fixed gain control law. Plant parameter change and sensor noise.
(std. dev. = 0.0573 deg/sec)

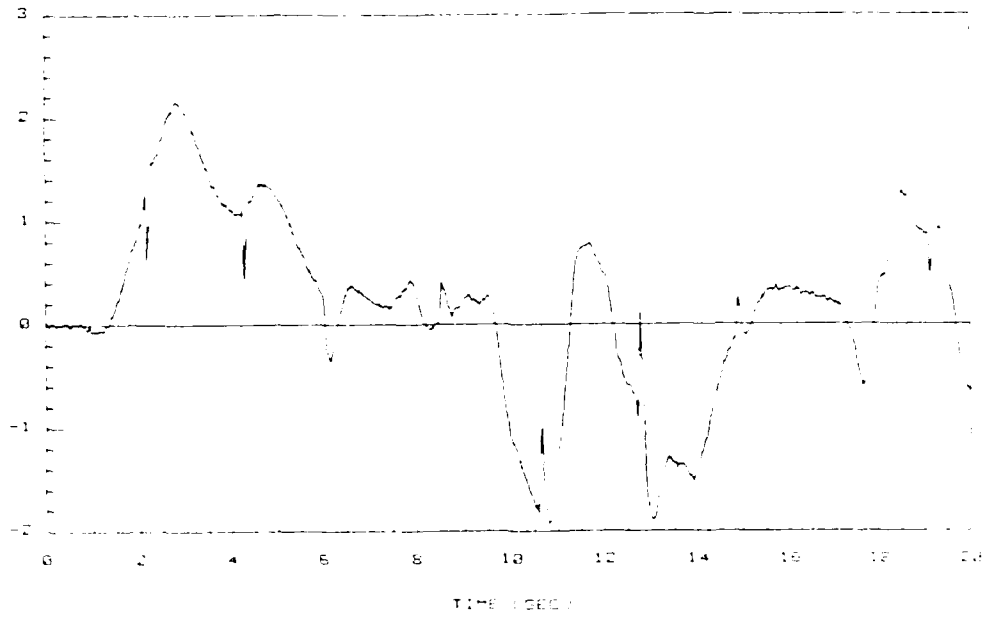

Figure 5-13. Elevator deflection (deg).
Fixed gain control law. Plant parameter change and sensor noise.
(std. dev. = 0.0573 deg (deg/sec))

Figure 5-14. Elevator deflection rate (deg/sec).
Fixed gain control law. Plant parameter change and sensor noise.
(std. dev. = 0.0573 deg (deg/sec))

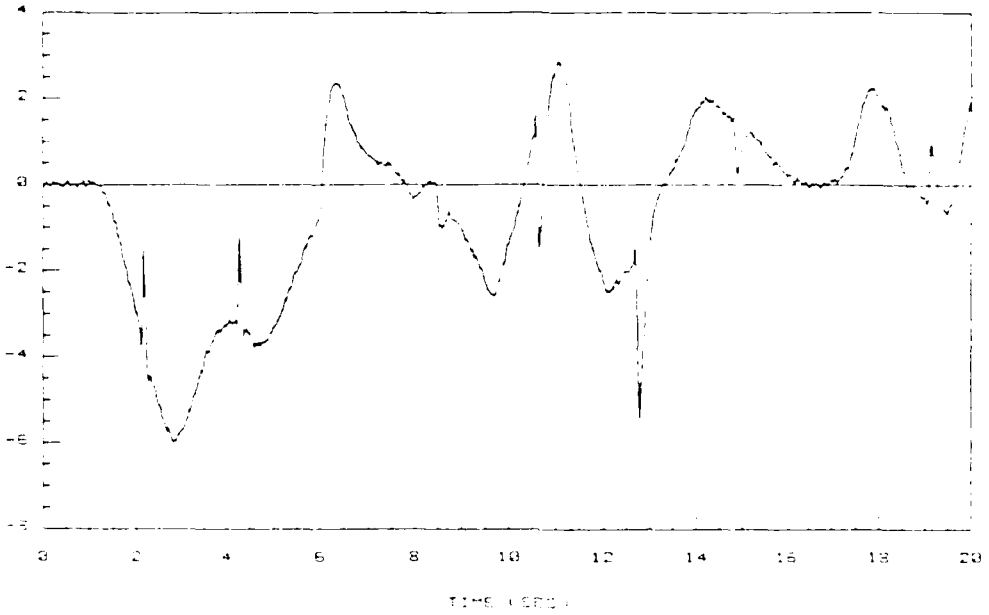

Figure 5-15. Flaperon deflection (deg).
Fixed gain control law. Plant parameter change and sensor noise.
(std. dev. = 0.0573 deg (deg/sec))

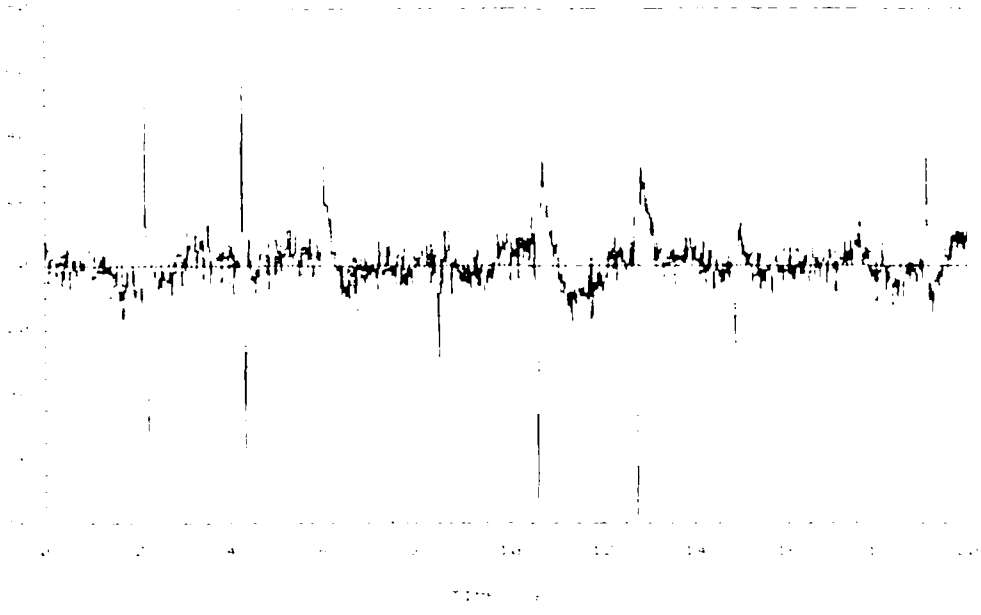

Figure 5-16. Flaperon deflection rate (deg/sec).
Fixed gain control law. Plant parameter change and sensor noise.
(std. dev. = 0.0573 deg (deg/sec))

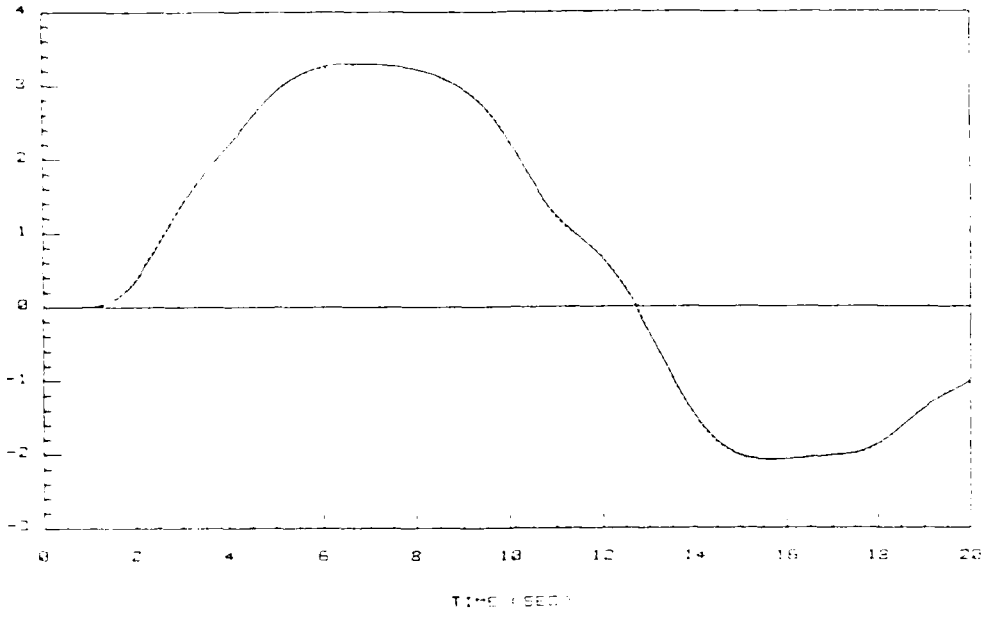

Figure 5-17. Flight path angle command and response (deg). Fixed gain control law. Plant parameter change and sensor noise. (std. dev. = 0.314 deg)

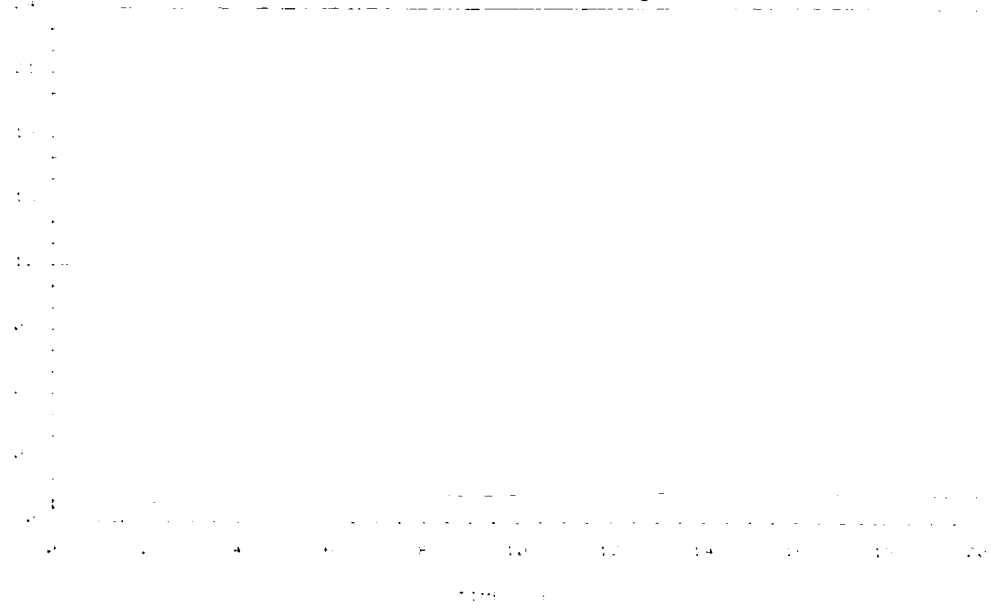

Figure 5-18. Flight path angle tracking performance index (deg). Fixed gain control law. Plant parameter change and sensor noise. (std. dev. = 0.314 deg)

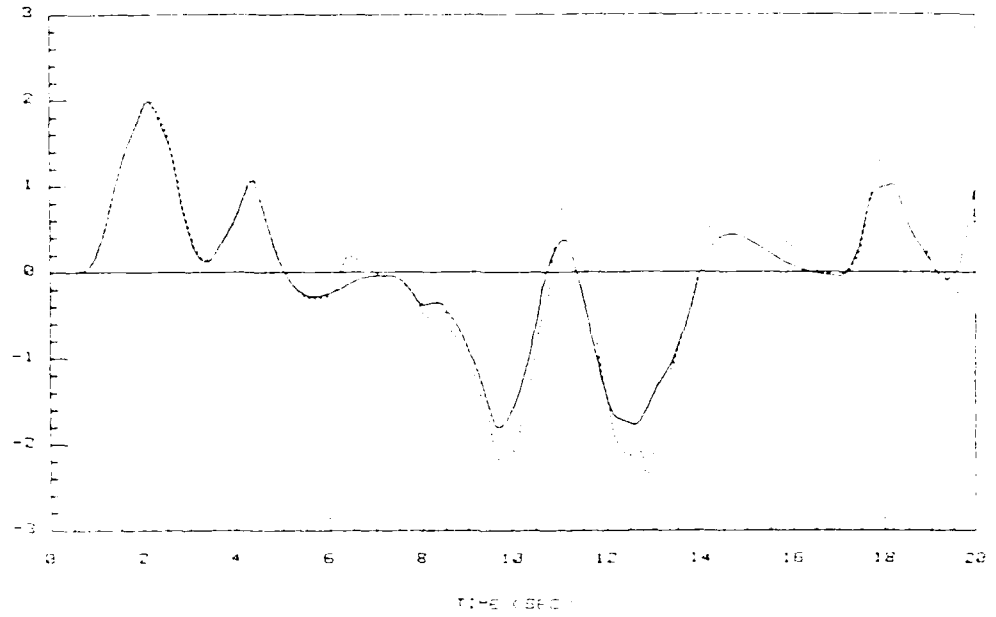

Figure 5-19. Pitch rate command and response (deg/sec).
Fixed gain control law. Plant parameter change and sensor noise.
(std. dev. = 0.314 deg/sec)

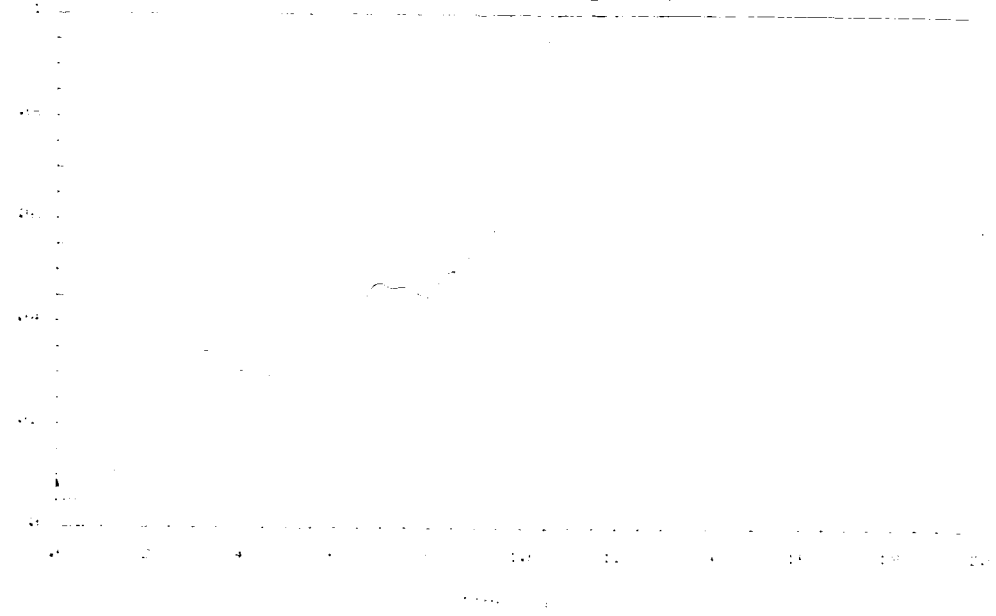

Figure 5-20. Pitch rate tracking performance index (deg sec).
Fixed gain control law. Plant parameter change and sensor noise.
(std. dev. = 0.314 deg/sec)

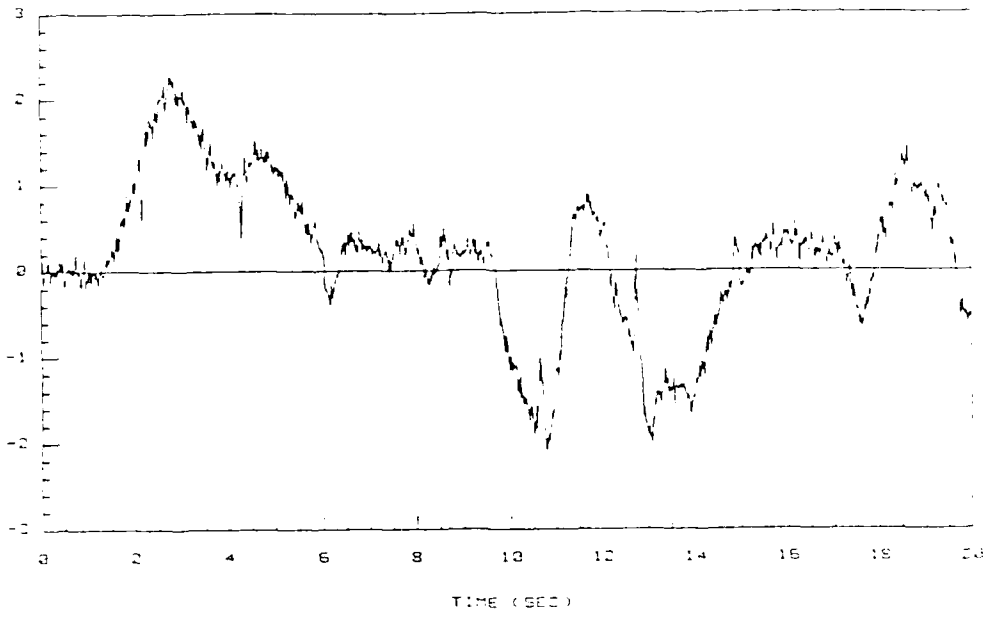

Figure 5-21. Elevator deflection (deg).
Fixed gain control law. Plant parameter change and sensor noise.
(std. dev. = 0.314 deg (deg/sec))

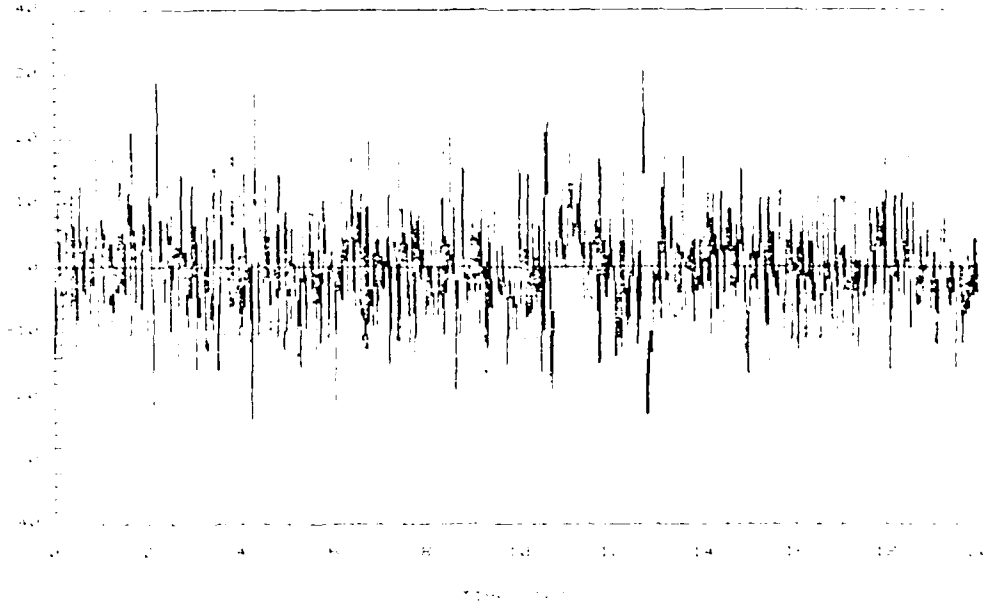

Figure 5-22. Elevator deflection rate (deg/sec).
Fixed gain control law. Plant parameter change and sensor noise.
(std. dev. = 0.314 deg (deg/sec))

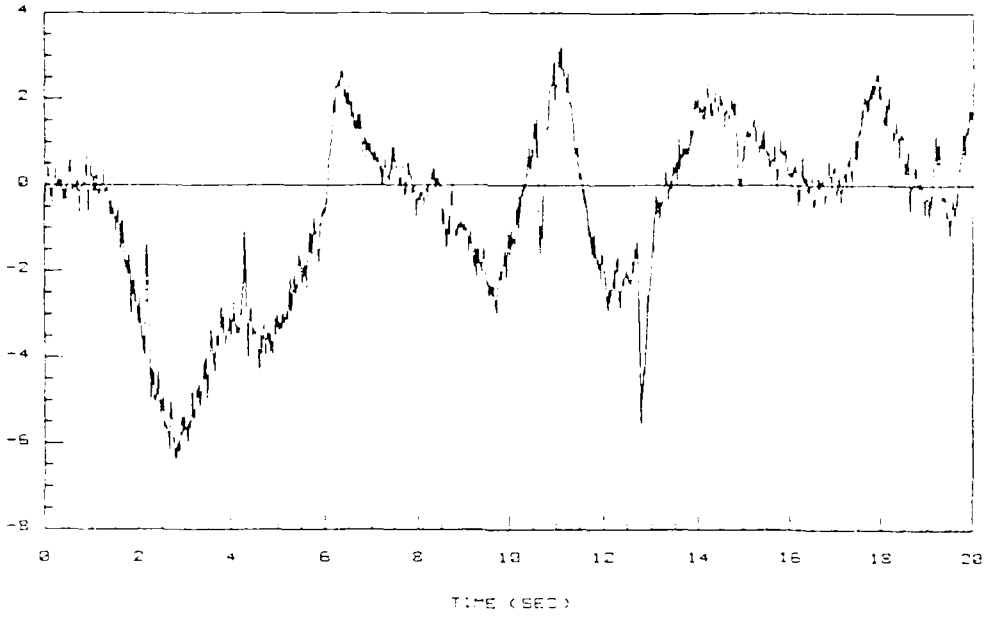

Figure 5-23. Flaperon deflection (deg).
Fixed gain control law. Plant parameter change and sensor noise.
(std. dev. = 0.314 deg (deg/sec))

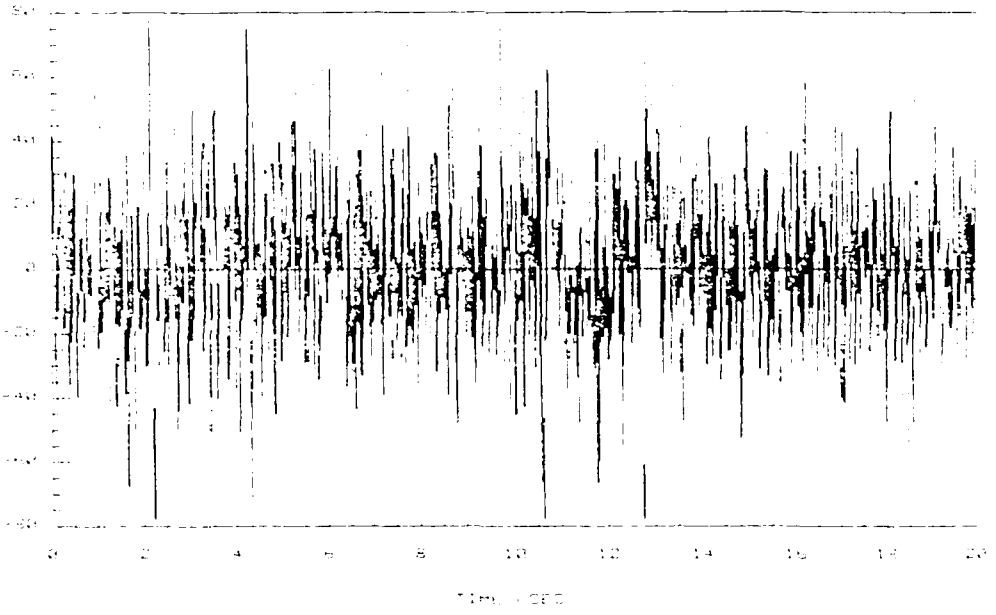

Figure 5-24. Flaperon deflection rate (deg/sec).
Fixed gain control law. Plant parameter change and sensor noise.
(std. dev. = 0.314 deg (deg/sec))

5.3 Parameter-Adaptive Controller

5.3.1 Fixed Plant Dynamics. To become familiar with the characteristics of the parameter-adaptive system under various conditions, its performance is tested in several stages. The adaptation mechanism is first tested with simulations in which the dynamics of the aircraft model (at MACH = 0.9 , 10,000 ft.) are kept constant. The purpose of this test is simply to verify the capability of the identification algorithm to track the parameters of a known model. Initial testing is done without scaling the difference equation model (see section 4.4.5). The identification algorithm is initialized in all simulations with the parameter vector obtained from the transfer matrix of the indicated model (see appendix A). The covariance matrix is set to $a \cdot I$, and the prediction error variance is set to 1×10^{-10} deg^2 (deg^2/sec^2). The adaptation mechanism is not switched on until two seconds into the simulation to allow time for the measurement matrix to fill up with past input-output data and for the prediction error variance calculation (Eqn 3-60) to stabilize.

Figures 5-25 thru 5-32 show the aircraft responses in this simulation. As expected, these do not show variation in tracking performance from those of the nominal design case of Figures 4-22 thru 4-29. The only noticeable difference is a slight increase in control surface deflection rates. This is attributed to the transients that occur in the filtered parameter estimates that are used to update the control law gains. Figure 5-33 shows the fault detector test signal r(kT). Although the signal shows several significant peaks, it remains at all times below the selected threshold of $r_0 = 0.5$, thus indicating

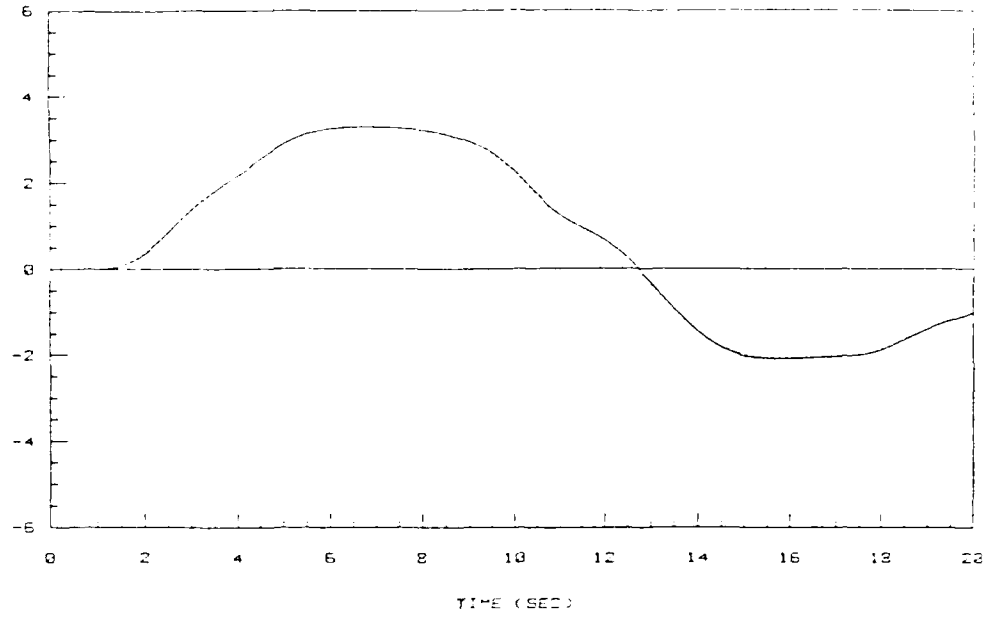

Figure 5-25. Flight path angle command and response (deg). Adaptive control law. No plant parameter change.

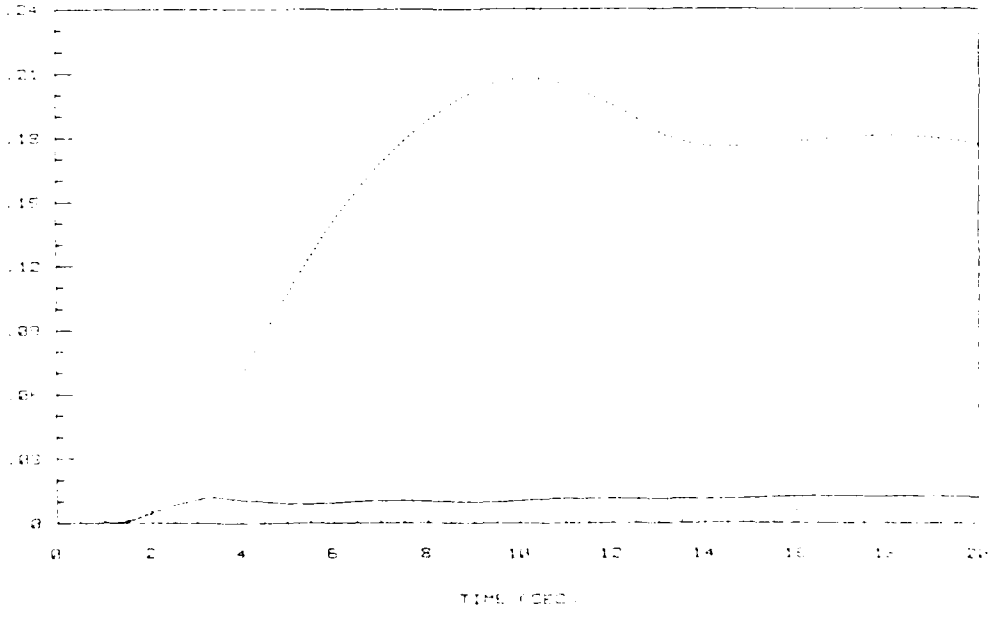

Figure 5-26. Flight path angle tracking performance index (deg). Adaptive control law. No plant parameter change.

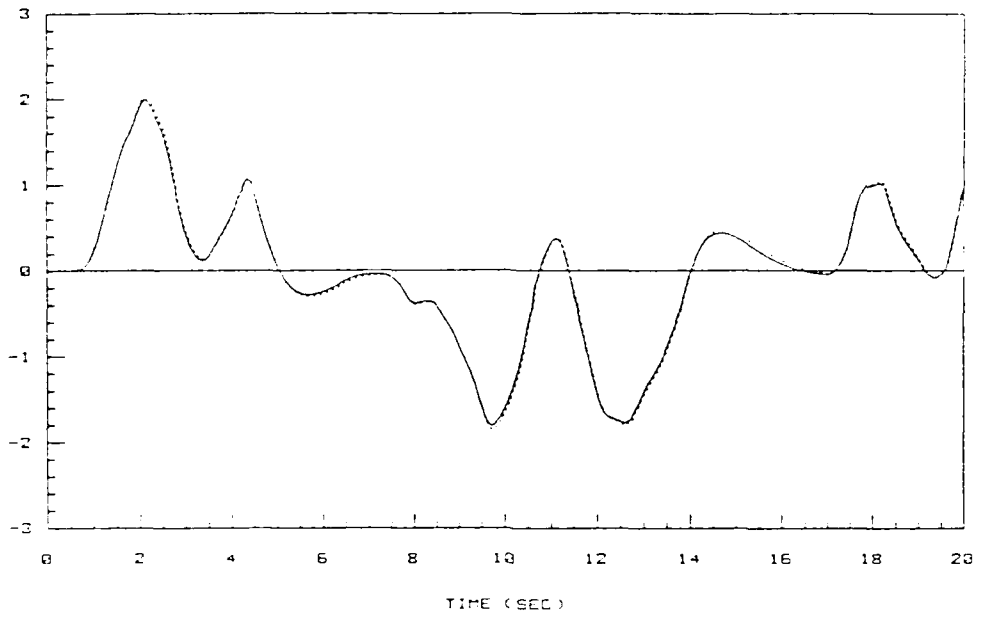

Figure 5-27. Pitch rate command and response (deg/sec). Adaptive control law. No plant parameter change.

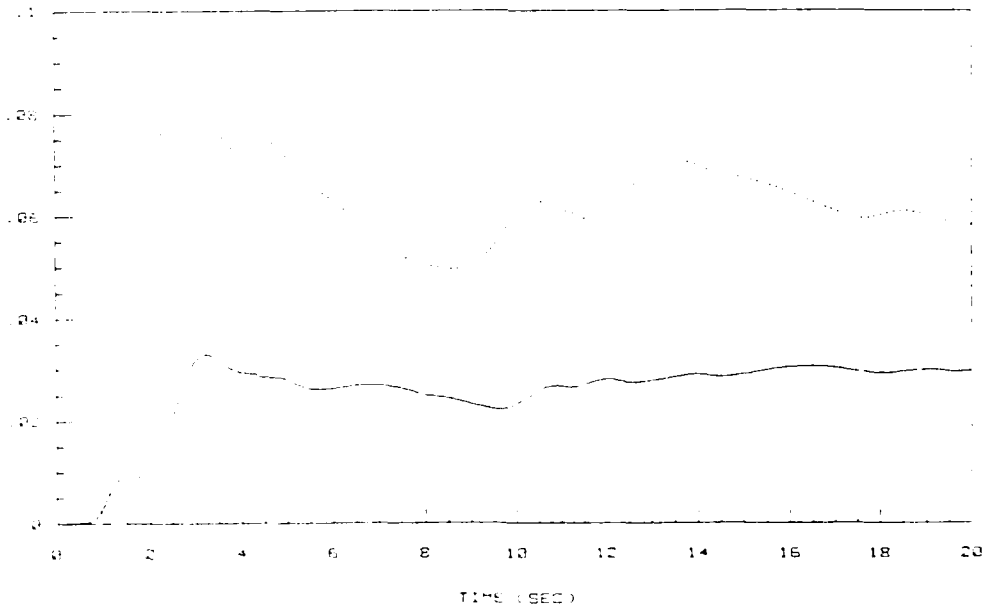

Figure 5-28. Pitch rate tracking performance index (deg/sec). Adaptive control law. No plant parameter change.

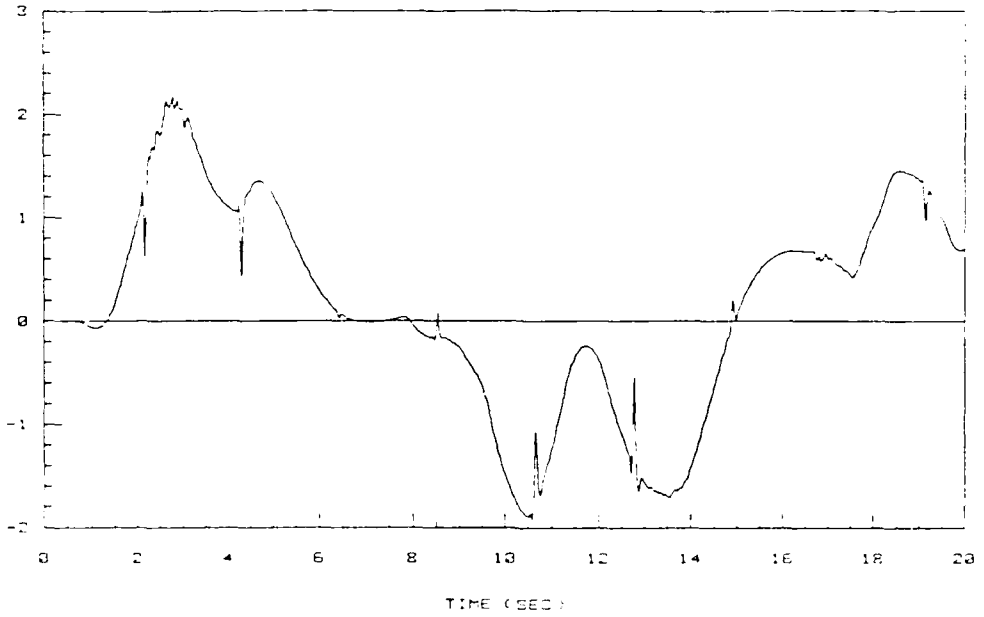

Figure 5-29. Elevator deflection (deg).
Adaptive control law. No plant parameter change.

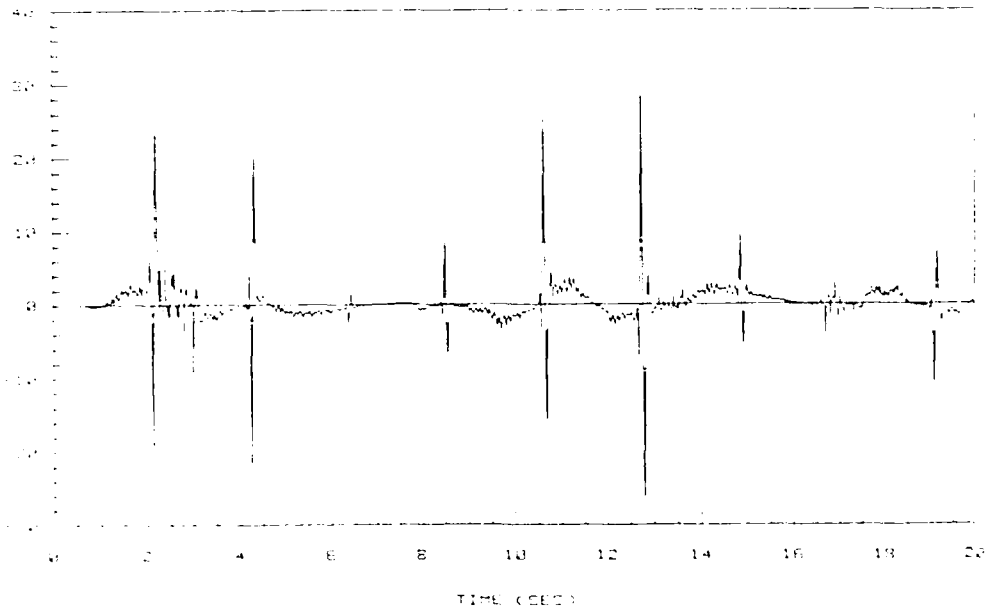

Figure 5-30. Elevator deflection rate (deg/sec).
Adaptive control law. No plant parameter change.

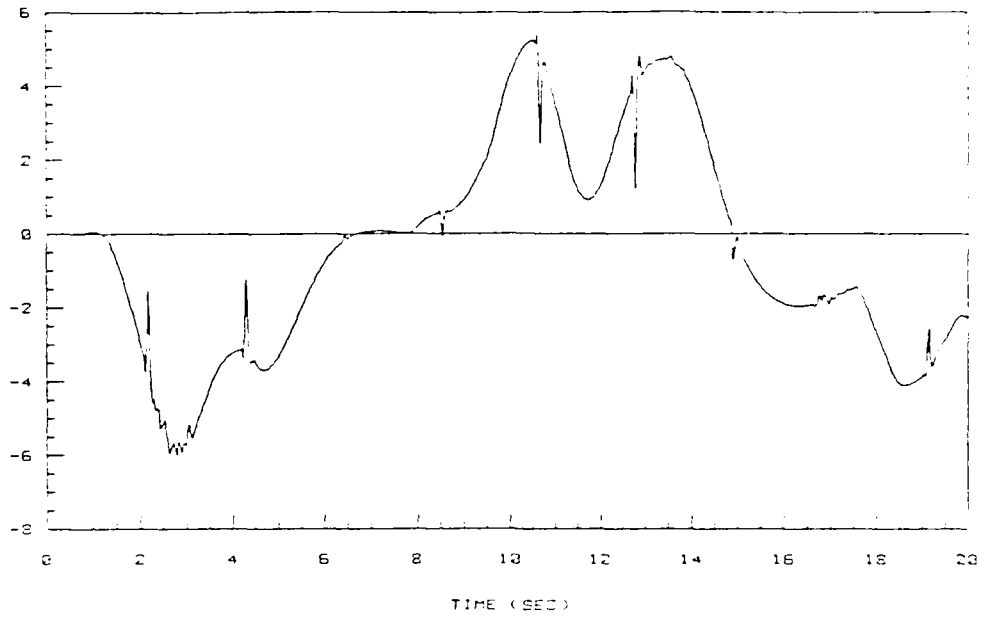

Figure 5-31. Flaperon deflection (deg).
Adaptive control law. No plant parameter change.

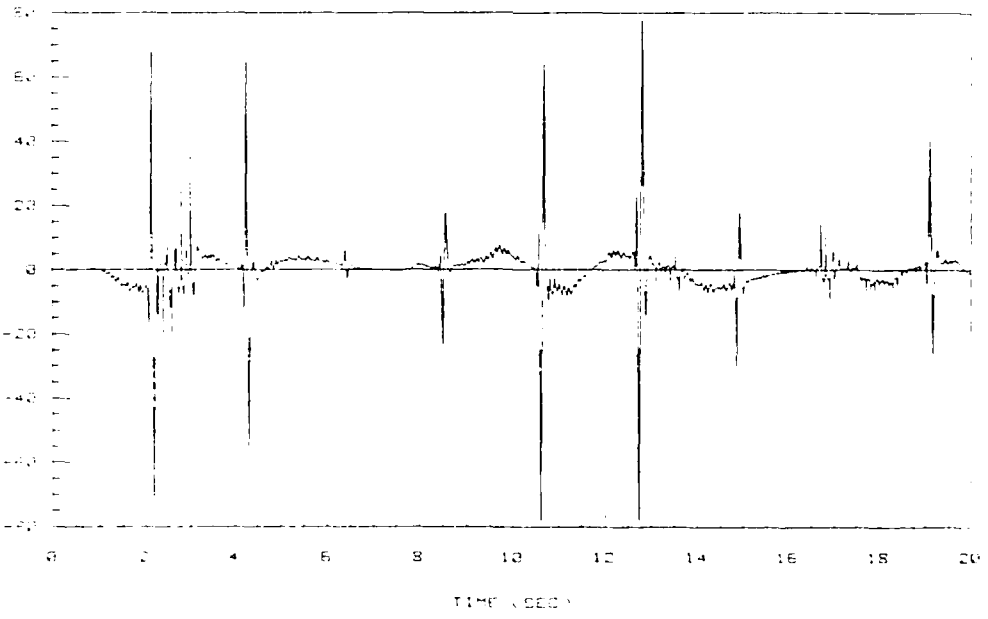

Figure 5-32. Flaperon deflection rate (deg/sec).
Adaptive control law. No plant parameter change.

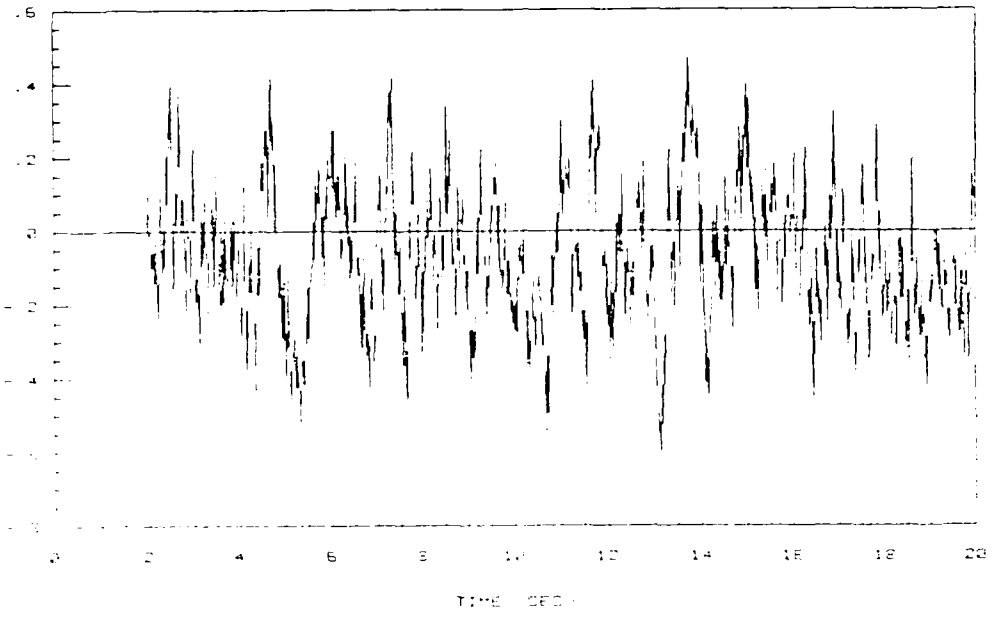

Figure 5-33. Fault detector test signal.

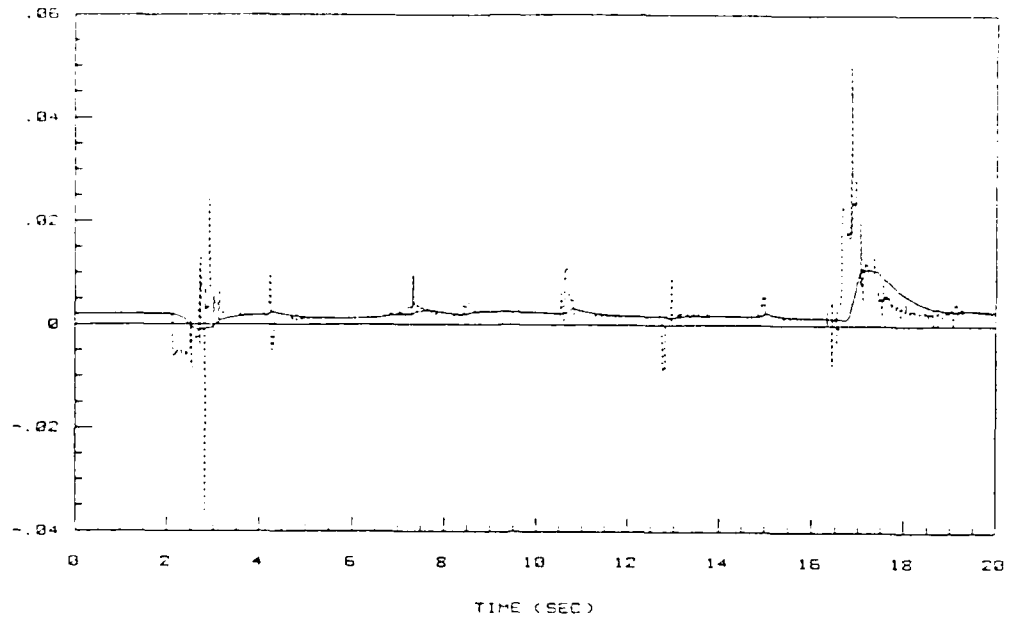

Figure 5-34. Estimate of step-response matrix element $h_{11}(kT)$.

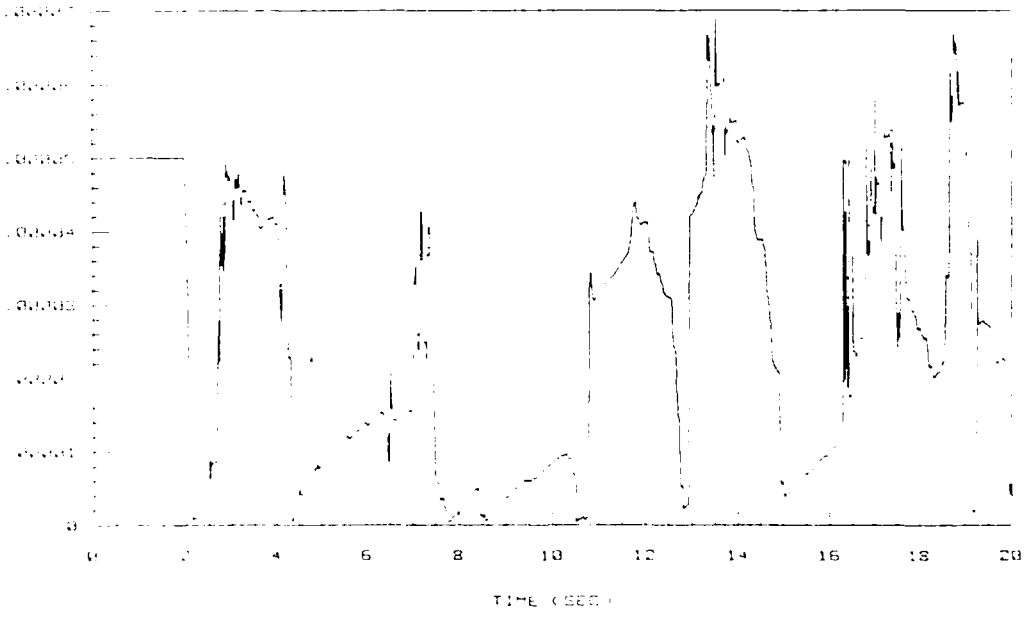

Figure 5-35. Covariance matrix element $p_{11}(kT)$.

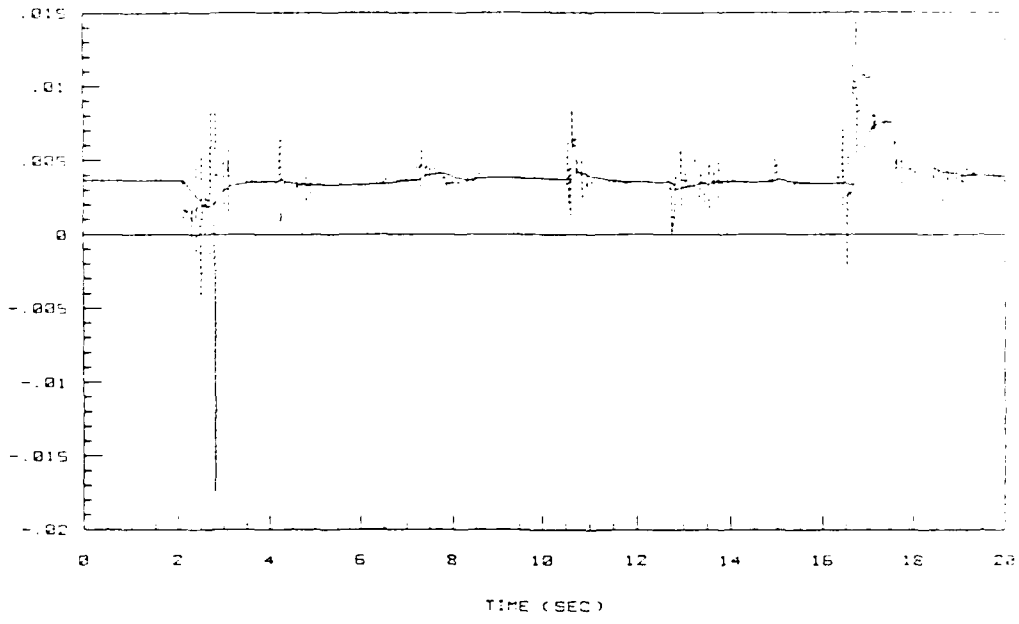

Figure 5-36. Estimate of step-response matrix element $h_{12}(kT)$.

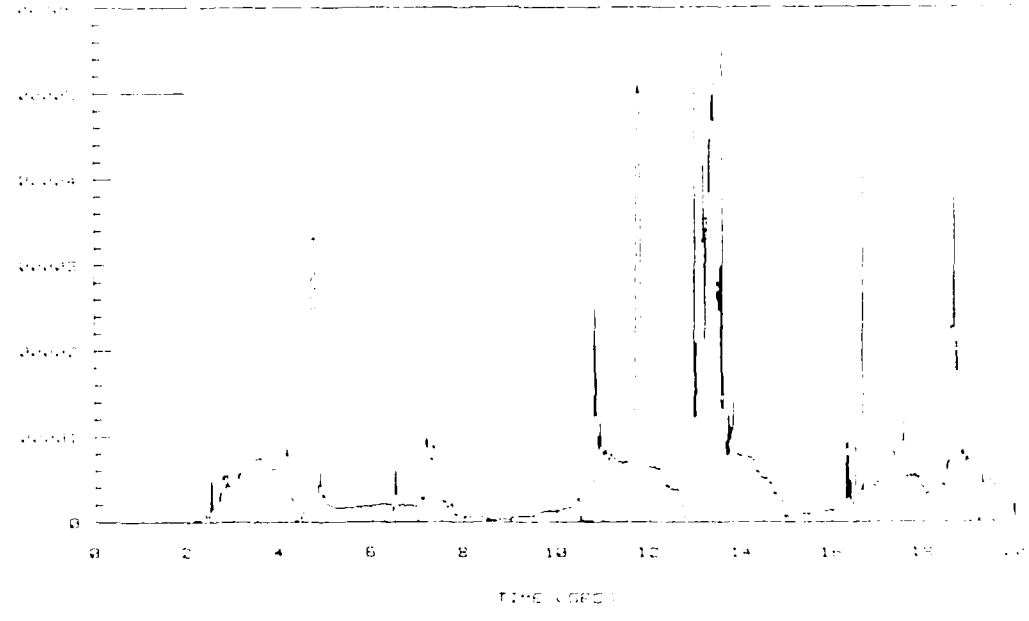

Figure 5-37. Covariance matrix element $p_{22}(kT)$.

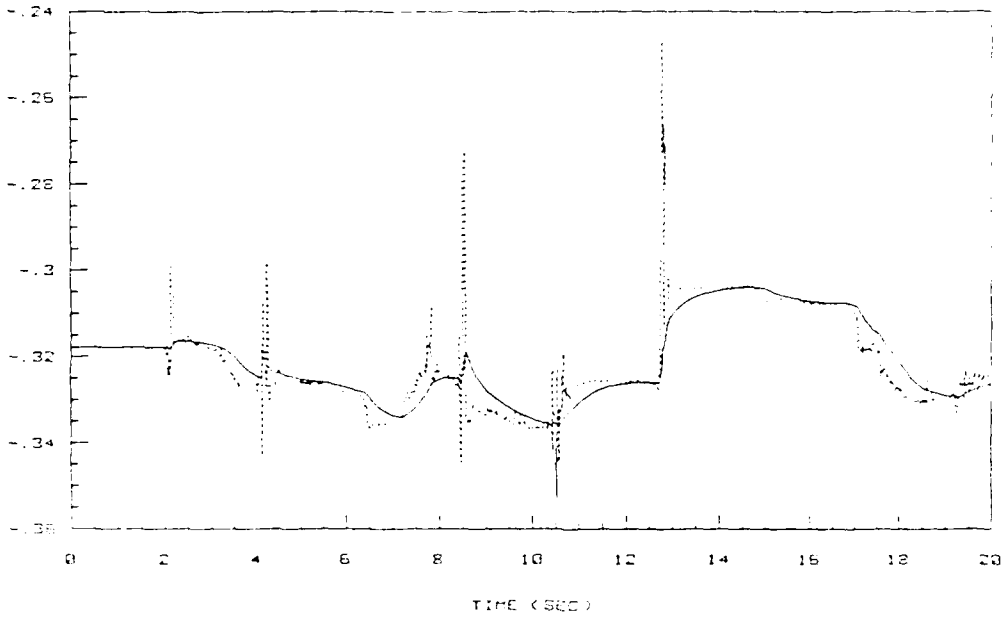

Figure 5-38. Estimate of step-response matrix element $h_{21}(kT)$.

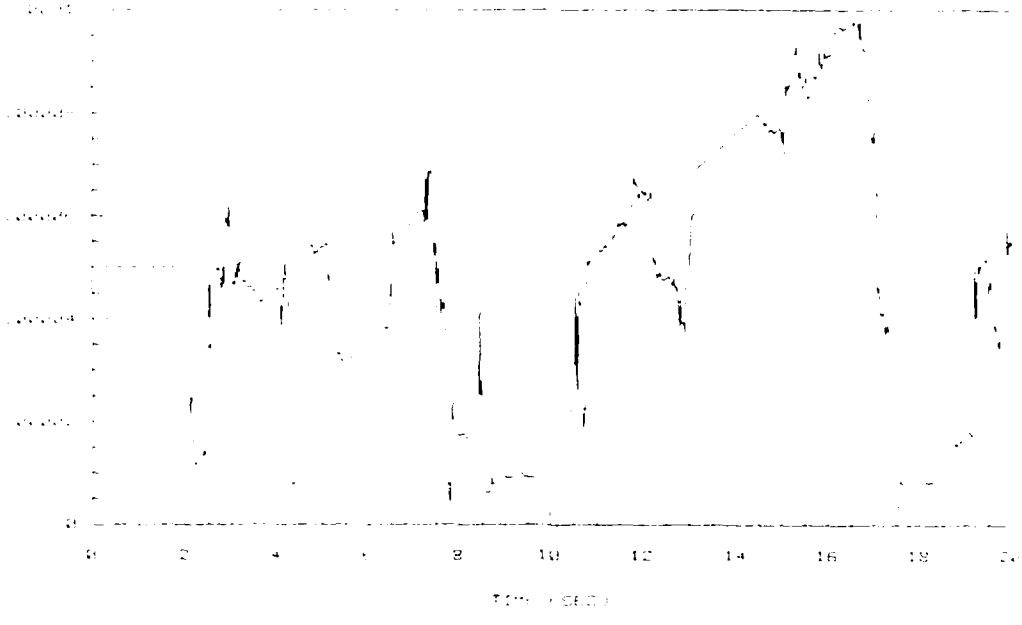

Figure 5-39. Covariance matrix element $p_{33}(kT)$.

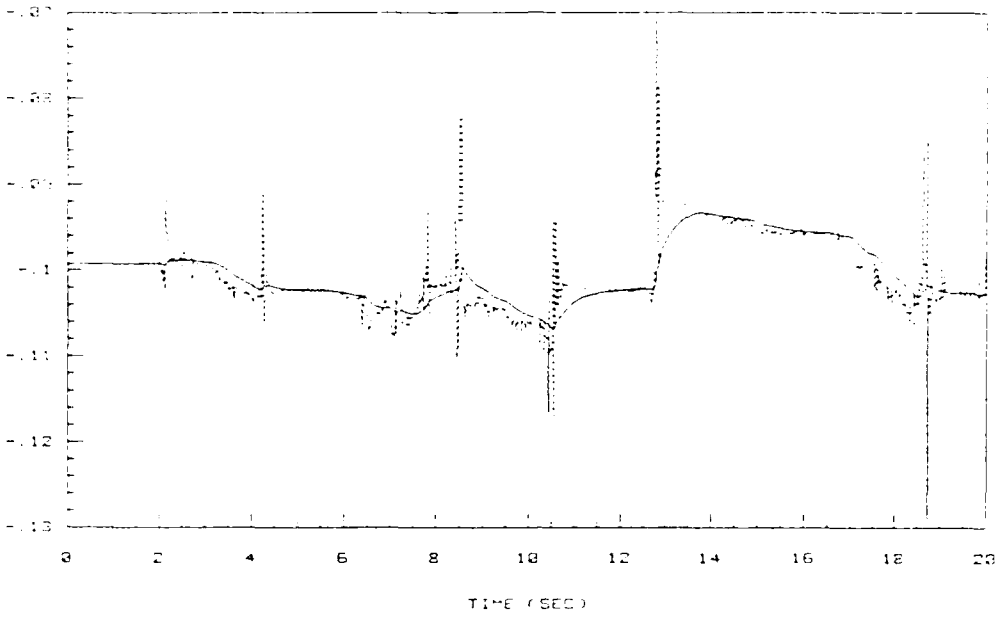

Figure 5-40. Estimate of step-response matrix element $h_{22}(kT)$.

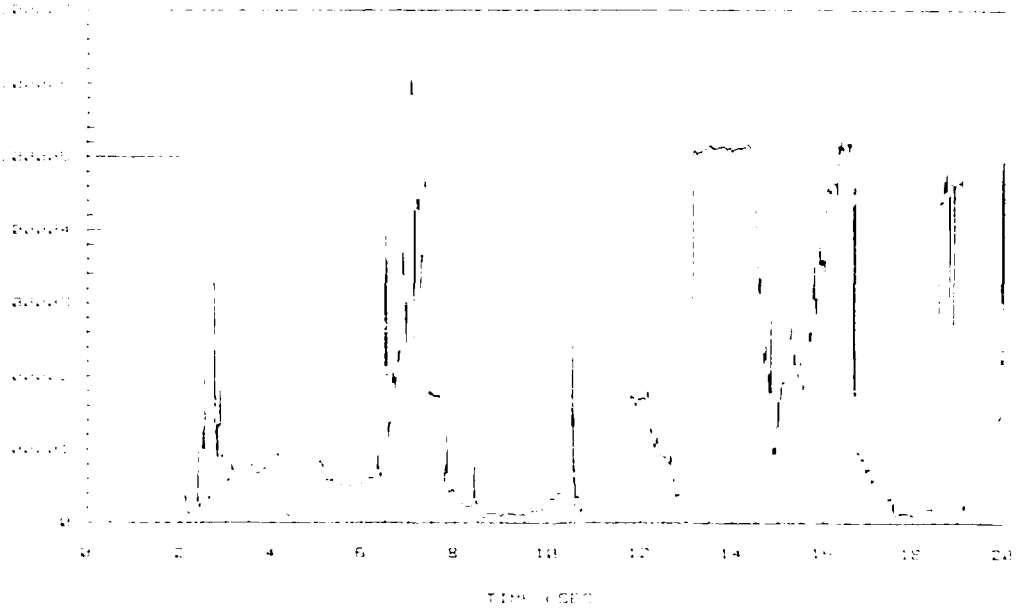

Figure 5-41. Covariance matrix element $p_{44}(kT)$.

that no abrupt plant parameter changes are reported. This is also expexted since no change in aircraft dynamics has taken place. Figures 5-34 thru 5-41 show the estimates of the elements of the step-response matrix, both filtered (solid lines) and unfiltered (dashed lines), and the corresponding diagonal elements of the parameter covariance matrix. Although these plots show the estimates undergoing several transients, their average values remain close to the actual parameters. The variations in the magnitude of the filtered estimates are considered tolerable given the robustness properties of the control law.

The periods in which the estimates show the greater deviations are usually associated with the instances where the control surface deflection rates undergo spikes. These spikes are due to abrupt changes in magnitude and/or direction in the command signals. Here in particular those of the pitch rate command. When the estimation algorithm detects the higher level of excitation to the plant, it quickly discounts old data to keep up with possible changes in the plant dynamics. However, the sudden removal of that excitation (surface deflection rate spike ends) causes the algorithm to slow down (or stop) momentarily its discounting of old information to match whatever information content the current input-output data might bring. This also represents a slow down in adaptation rate. This action may happen at a moment in which the current estimates are far away from the true parameters due to the algorithm's search in different directions of the parameter space trying to minimize the least-squares cost function. That being the case, it may take some time for the algorithm to acquire enough information for it to provide more accurate estimates again.

5.3.2 Fixed Plant Dynamics and Sensor Noise. The previous simulation setup is used here again, this time to assess the effects of sensor measurement noise in the identification procedure. Because of the relatively small magnitude of some of the elements of the step-response matrix, the noise level that can be tolerated (without any additional safety net type features) is significantly smaller than that of the fixed gain system. Figures 5-42 thru 5-58 show the results obtained with a noise standard deviation of 0.00181 deg (deg/sec).

The aircraft's responses in this case are almost identical to those in the previous simulation with the adaptation mechanism, but with still higher control surface deflection rates due to the corrupted measurements and transients in the parameter estimates discussed earlier. Despite this, no degradation of tracking performance occurs. In contrast to the tracking performance, the responses of the identification algorithm are significantly different from the previous ones. The fault detector signal, for example, is shifted in mean value from zero to -0.5. The reason for this behavior is that the fault detector algorithm is derived under the assumption of an equation error term with "white" noise characteristics around the nominal parameter estimates. The introduction of the input-output perturbation filter given by Eqn (4-15) has the side effect of reducing the noise spectrum, thus producing data corrupted by "colored" noise instead. It is a well known fact that "colored" noise produces biases in the parameter estimates, and it is those biases which are being reflected in the mean of the fault detector signal. It is important to note however, that the property of the test signal as an indicator of abrupt plant parameter

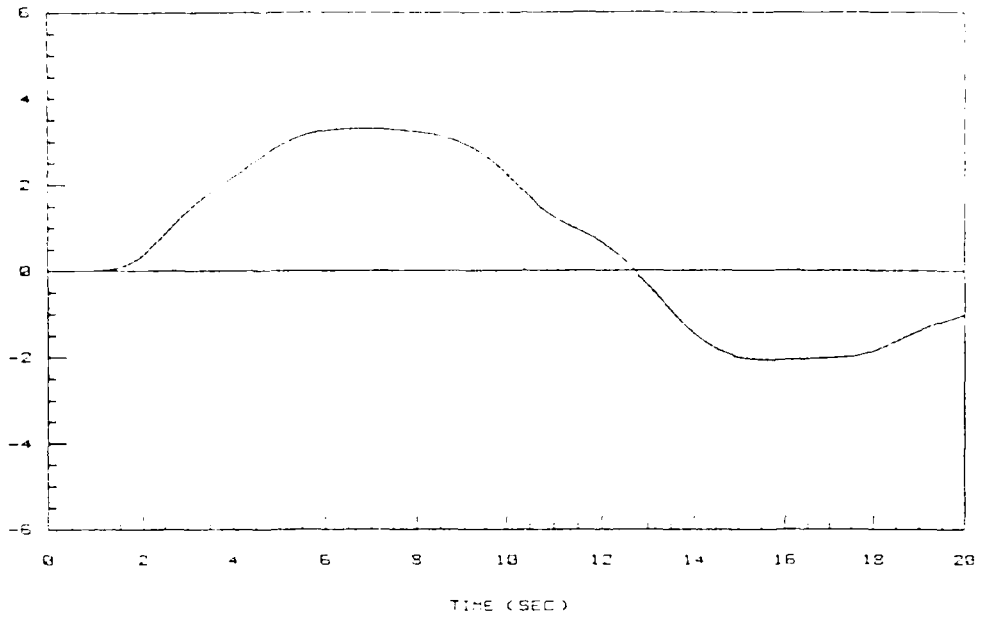

Figure 5-42. Flight path angle command and response (deg). Adaptive control law. No plant parameter change and sensor noise. (std. dev. = 0.00181 deg).

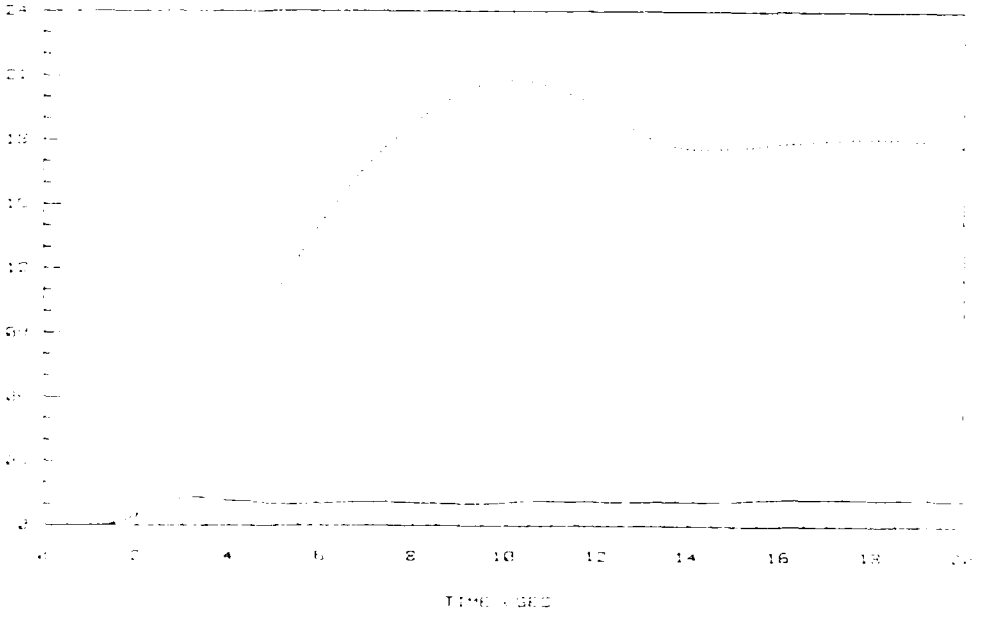

Figure 5-43. Flight path angle tracking performance in[illegible]. Adaptive control law. No plant parameter change and [illegible]. (std. dev. = 0.00181 deg).

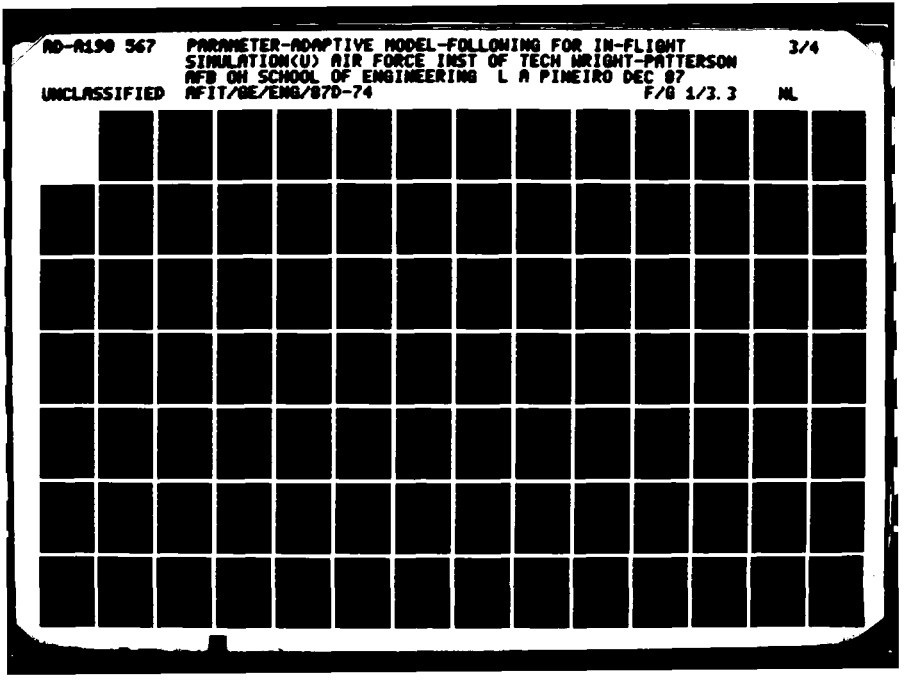
AD-A190 567 PARAMETER-ADAPTIVE MODEL-FOLLOWING FOR IN-FLIGHT SIMULATION(U) AIR FORCE INST OF TECH WRIGHT-PATTERSON AFB OH SCHOOL OF ENGINEERING L A PINEIRO DEC 87
3/4
UNCLASSIFIED AFIT/GE/ENG/87D-74
F/G 1/3.3
NL

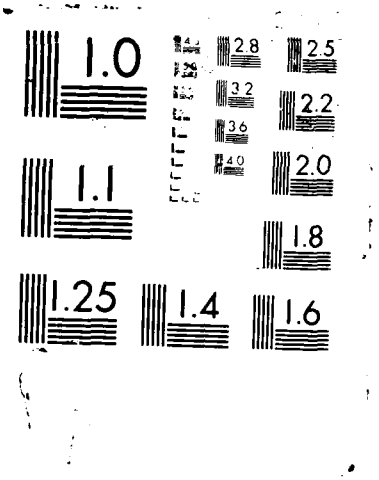
1.0
1.1
1.25
1.4
1.6
1.8
2.0
2.2
2.5
2.8
3.2
3.6
4.0

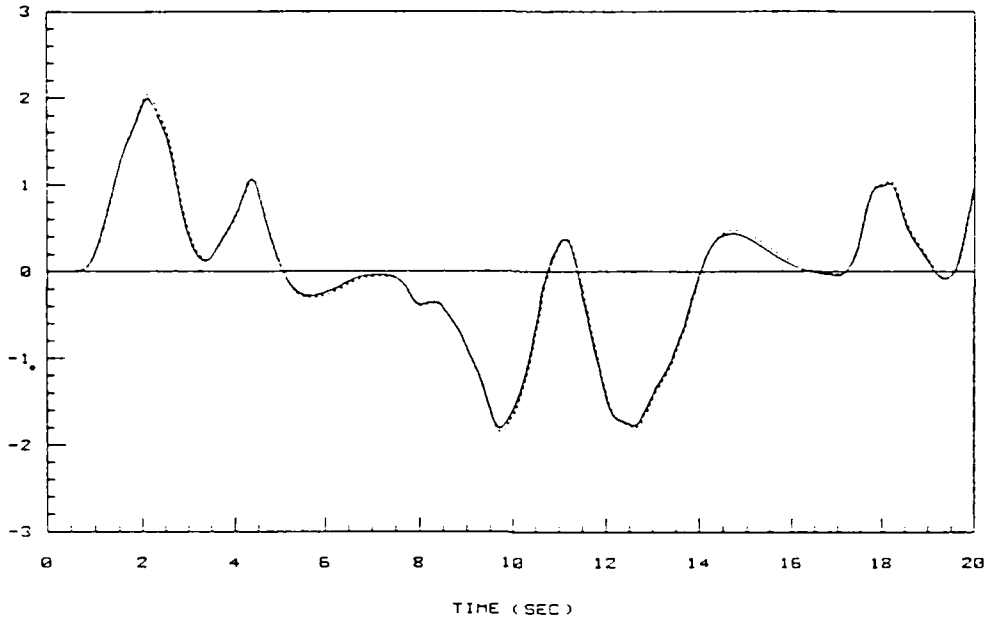

Figure 5-44. Pitch rate command and response (deg/sec).
Adaptive control law. No plant parameter change and sensor noise.
(std. dev. = 0.00181 deg/sec).

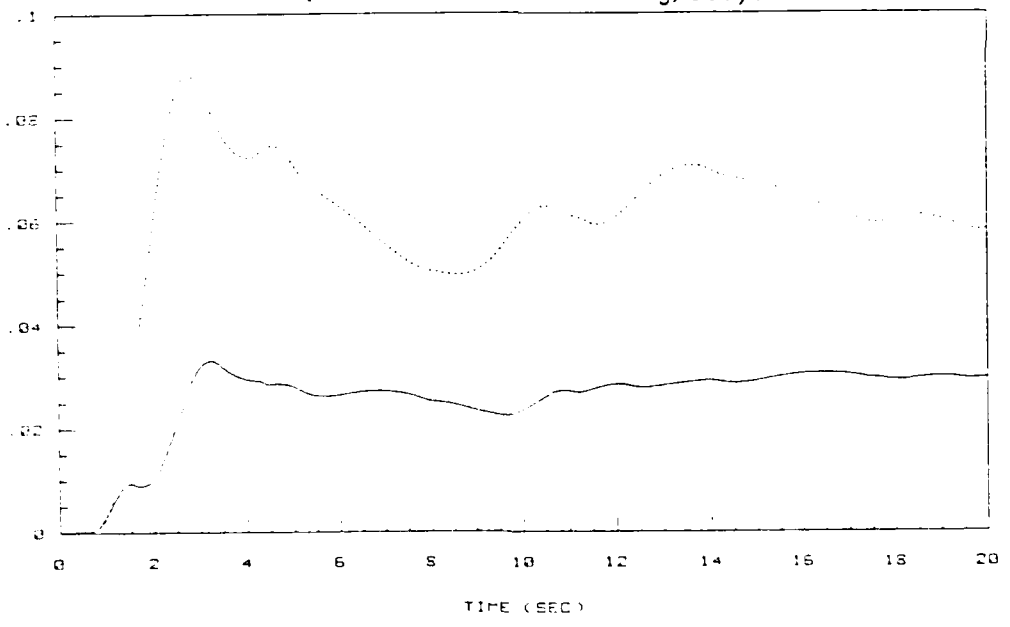

Figure 5-45. Pitch rate tracking performance index (deg/sec).
Adaptive control law. No plant parameter change and sensor noise.
(std. dev. = 0.00181 deg/sec).

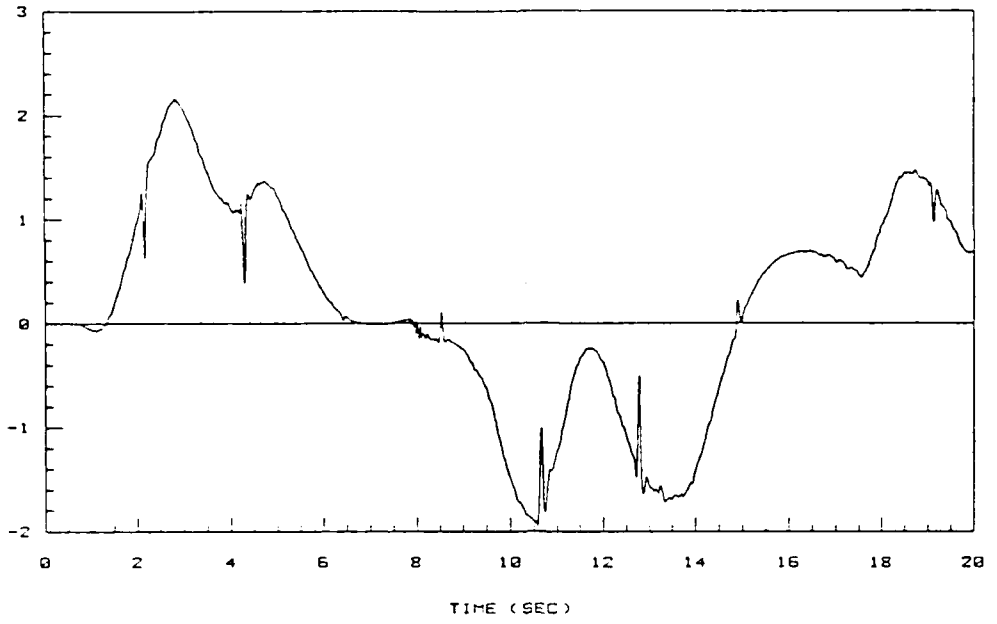

Figure 5-46. Elevator deflection (deg).
Adaptive control law. No plant parameter change and sensor noise.
(std. dev. = 0.00181 deg (deg/sec)).

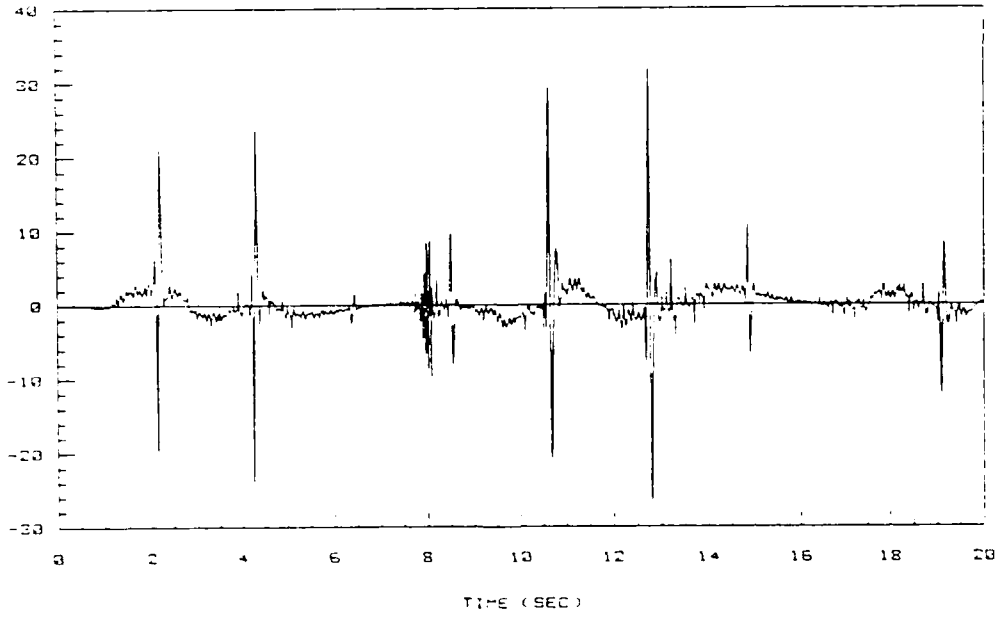

Figure 5-47. Elevator deflection rate (deg/sec).
Adaptive control law. No plant parameter change and sensor noise.
(std. dev. = 0.00181 deg (deg/sec))

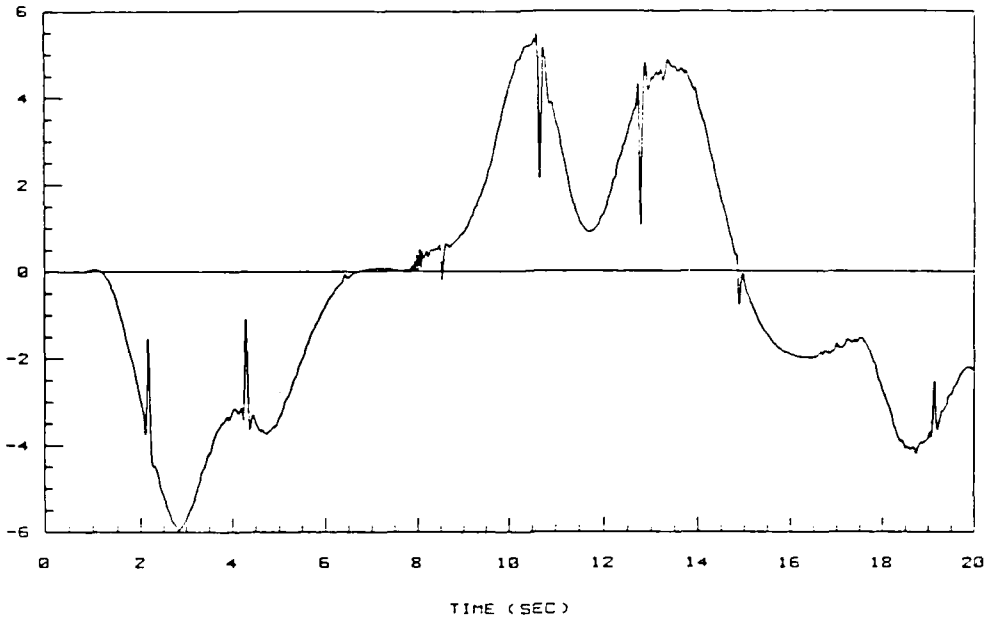

Figure 5-48. Flaperon deflection (deg).
Adaptive control law. No plant parameter change and sensor noise.
(std. dev. = 0.00181 deg (deg/sec)).

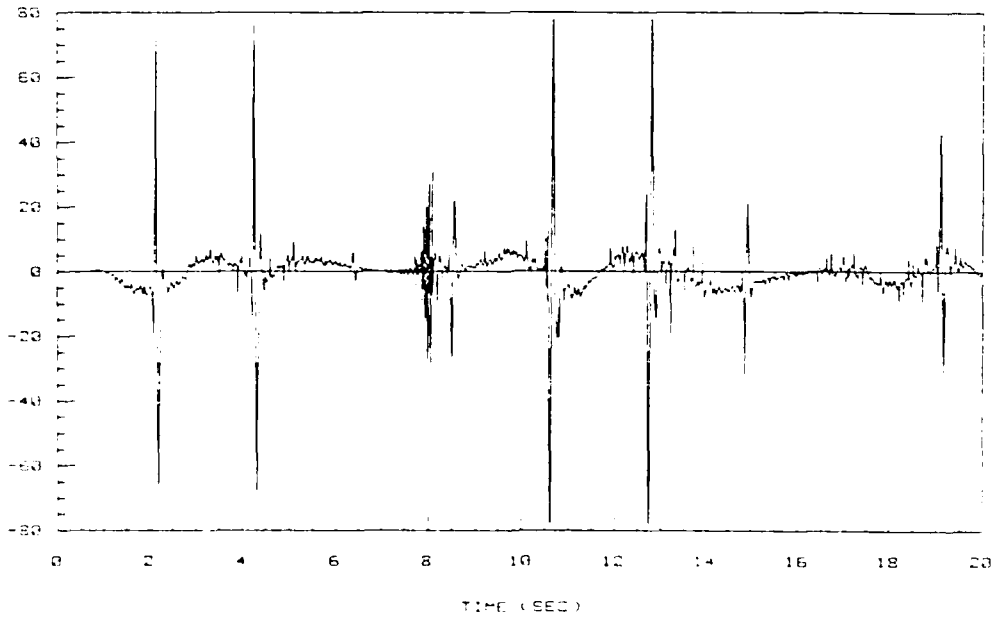

Figure 5-49. Flaperon deflection rate (deg/sec).
Adaptive control law. No plant parameter change and sensor noise.
(std. dev. = 0.00181 deg (deg/sec)).

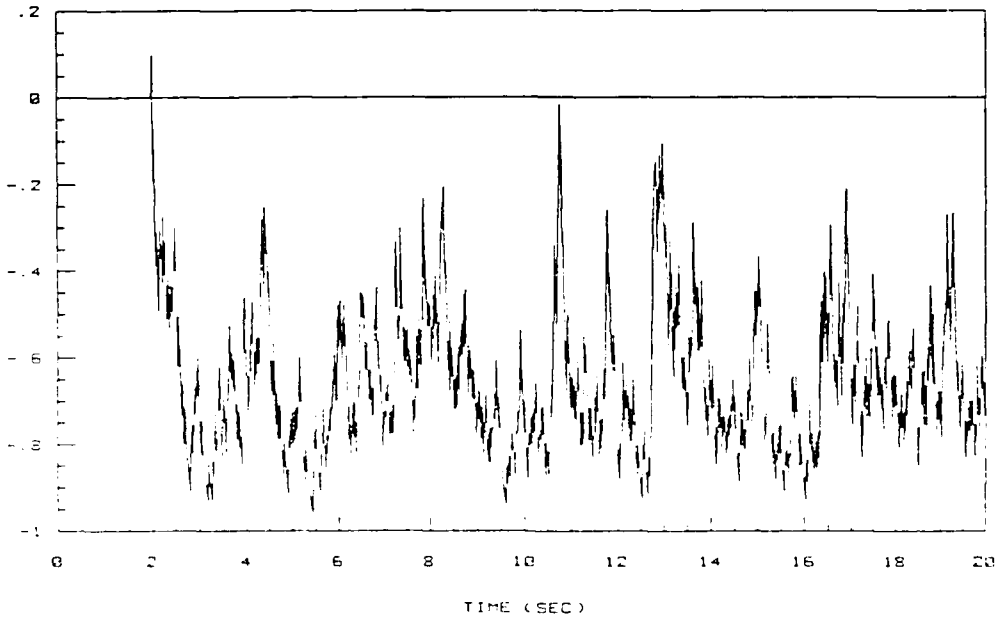

Figure 5-50. Fault detector test signal with sensor noise. (std. dev. = 0.00181 deg (deg/sec)).

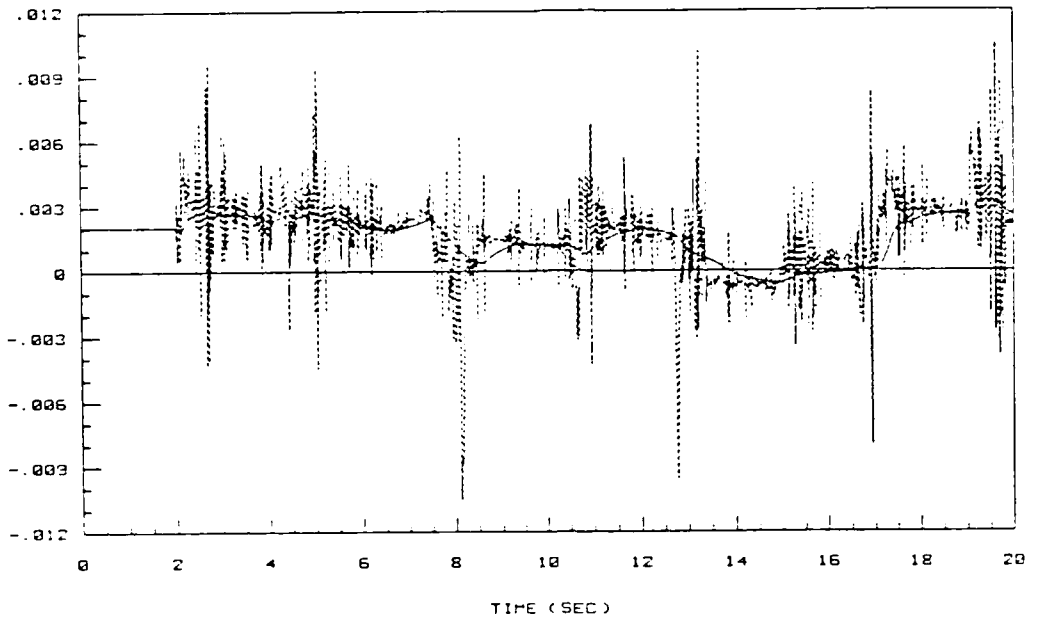

Figure 5-51. Estimate of step-response matrix element $h_{11}(kT)$ with sensor noise. (std. dev. = 0.00181 deg (deg/sec)).

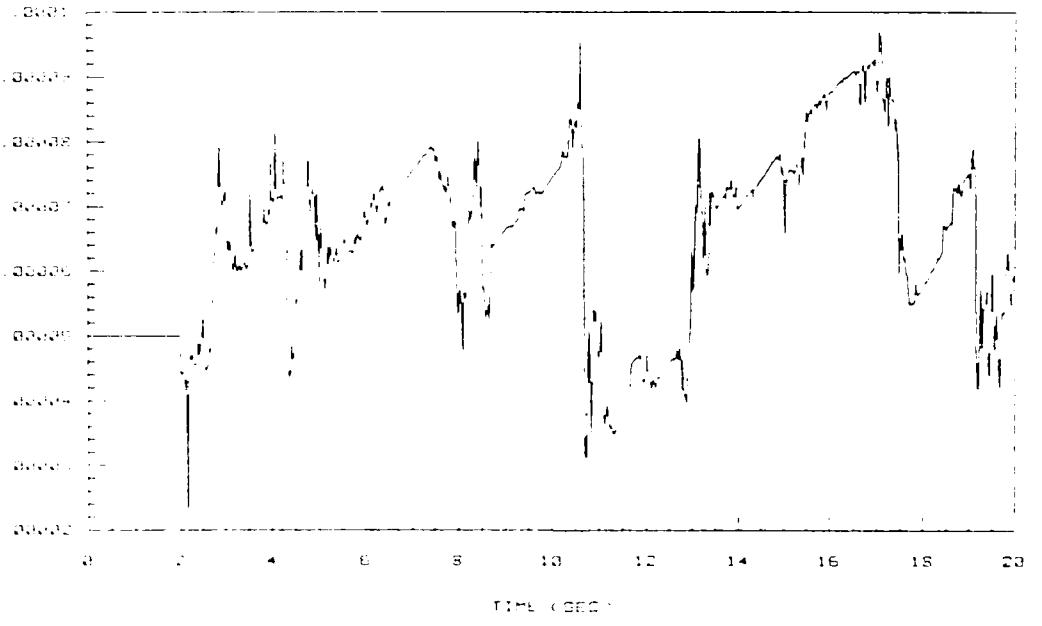

Figure 5-52. Covariance matrix element $p_{11}(kT)$ with sensor noise. (std. dev. = 0.00181 deg (deg/sec)).

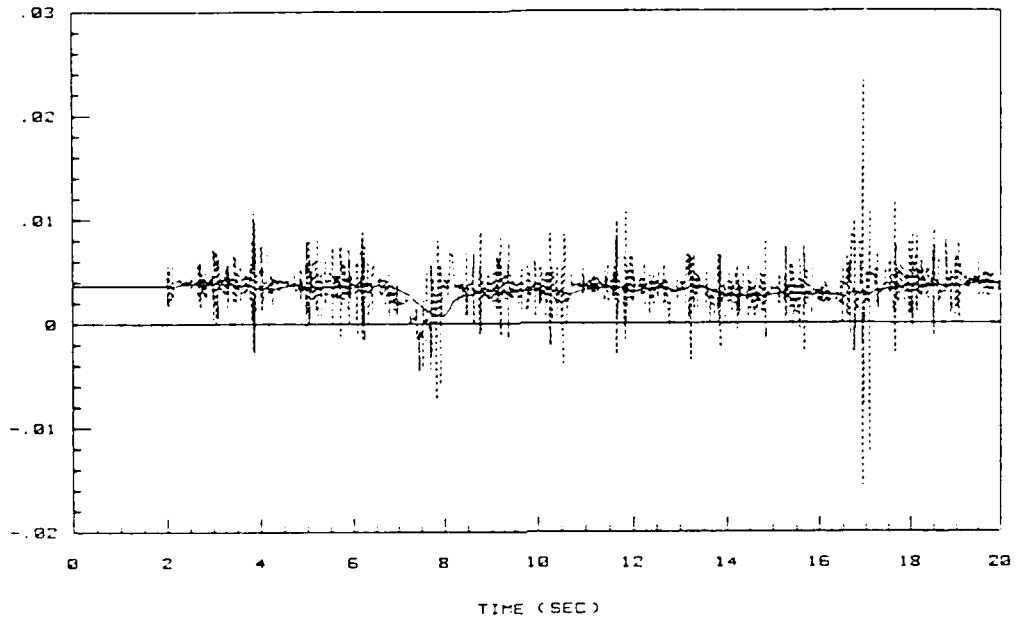

Figure 5-53. Estimate of step-response matrix element $h_{12}(kT)$ with sensor noise. (std. dev. = 0.00181 deg (deg/sec)).

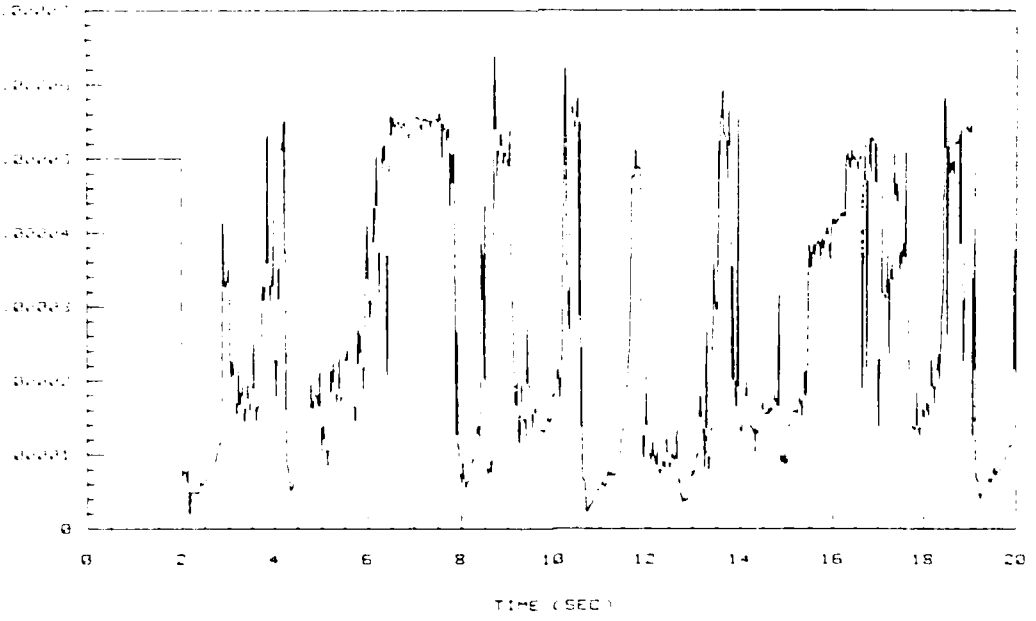

Figure 5-54. Covariance matrix element $p_{22}(kT)$ with sensor noise. (std. dev. = 0.00181 deg (deg/sec)).

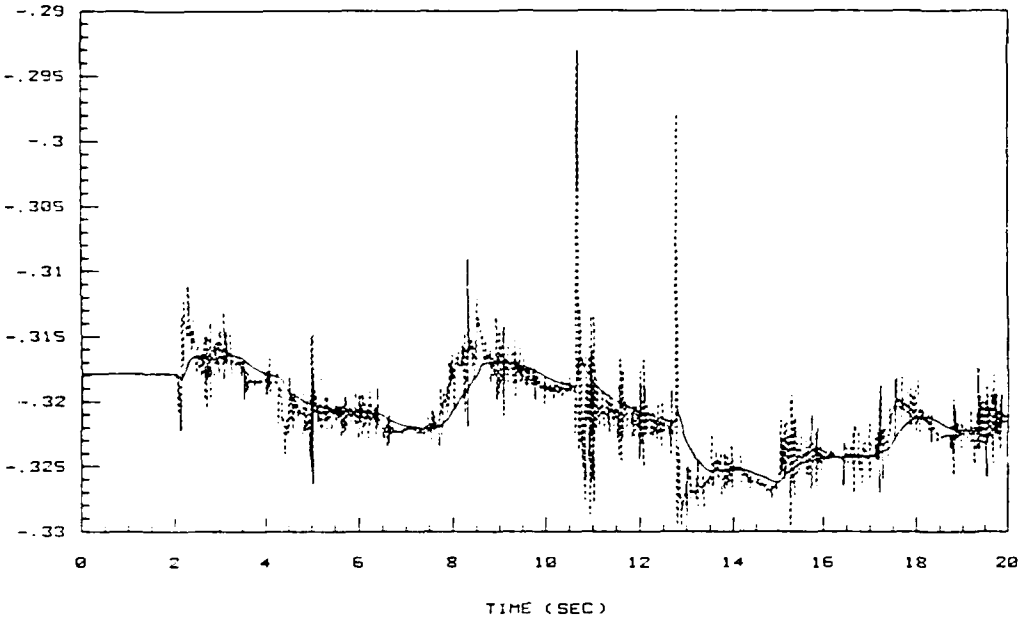

Figure 5-55. Estimate of step-response matrix element $h_{21}(kT)$ with sensor noise. (std. dev. = 0.00181 deg (deg/sec)).

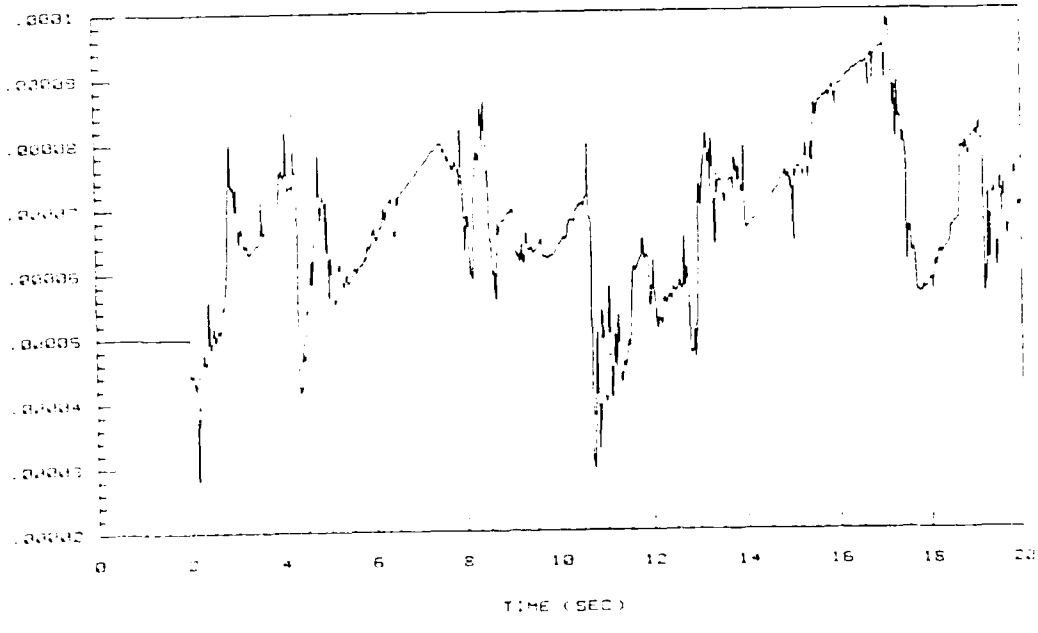

Figure 5-56. Covariance matrix element $p_{33}(kT)$ with sensor noise. (std. dev. = 0.00181 deg (deg/sec)).

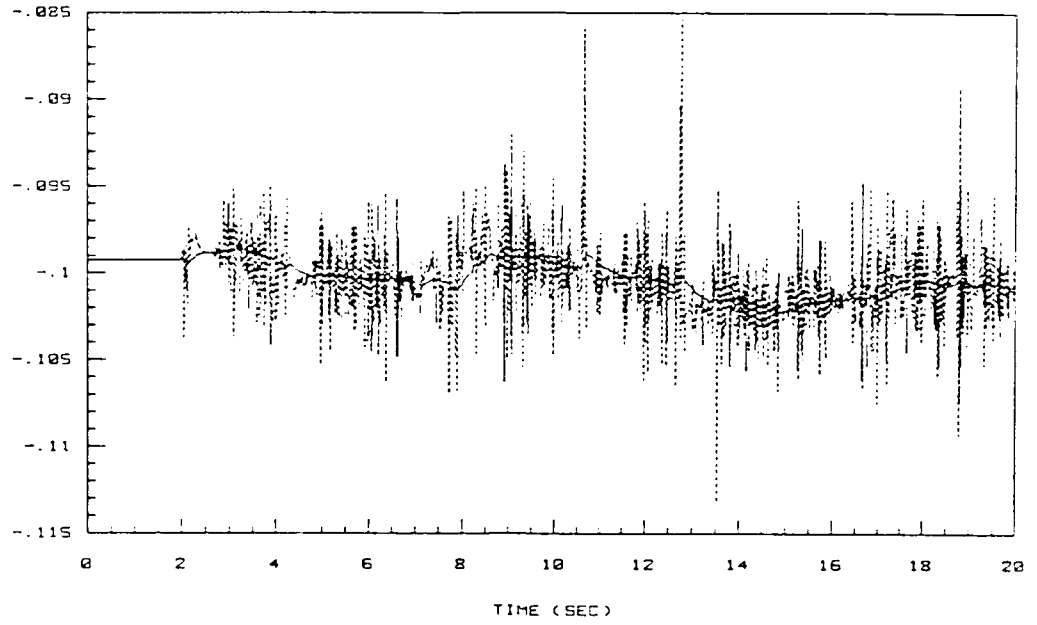

Figure 5-57. Estimate of step-response matrix element $h_{22}(kT)$ with sensor noise. (std. dev. = 0.00181 deg (deg/sec)).

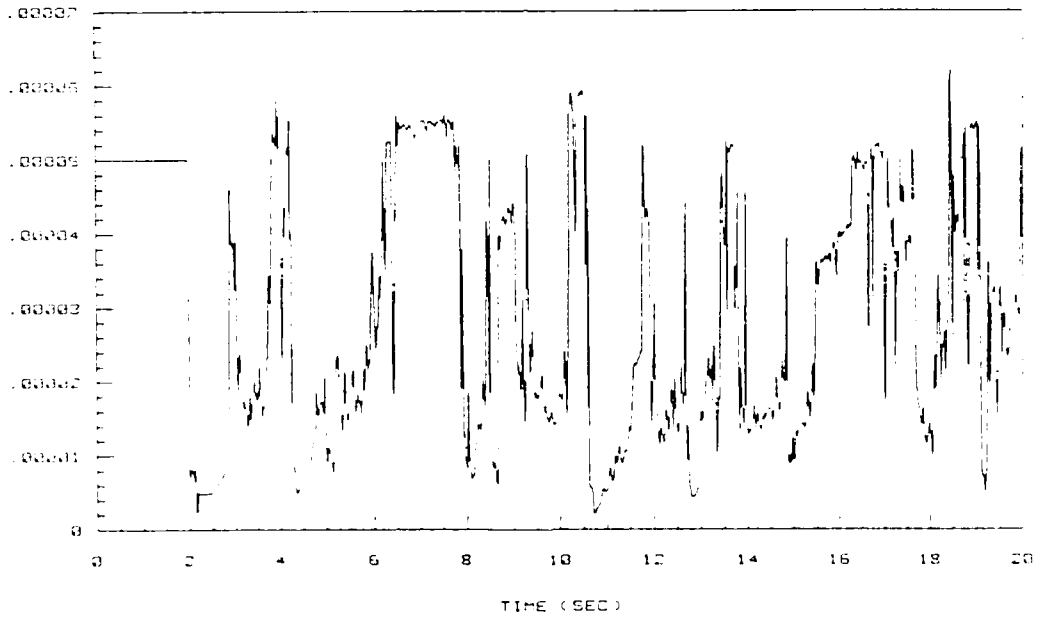

Figure 5-58. Covariance matrix element $p_{44}(kT)$ with sensor noise. (std. dev. = 0.00181 deg (deg/sec)).

changes remains unchanged. The shift in the mean value of r(kT) is easily compensated for by simply adjusting the threshold levels of r_0 and r_1 to account for the new mean signal value of -0.5. This action takes place a few samples after the algorithm is started, to allow for initalization transients to fade out.

The parameter estimates in this simulation show considerable noise jitter superimposed onto them with a corresponding increase in their uncertainty as signified by the plots of their respective covariance matrix diagonal elements. The fluctuations of these estimates around their nominal values however, are significantly smaller than those of the simulation without noise. The reason for this is the additional excitation that the plant is receiving from the control surfaces, which helps the identification process. This additional control surface activity is the result of the control law trying to maintain tracking performance despite the fluctuations of the measured variables due to sensor noise.

5.3.3 Plant Parameter Change. The next step in the testing of the parameter-adaptive system is to assess its capability to track the changes in plant parameters and consequently maintain the tracking performance at a specified level. This is accomplished by running the simulation and specifying a change in the plant dynamics model to occur at six seconds into the simulation. The new set of dynamics corresponds to those of the AFTI/F-16 at a flight condition of mach 0.9 at 10,000 ft. MSL (Appendix A). The simulation responses are shown in Figures 5-59 thru 5-75. When identification of the step-response matrix elements takes place, the tracking performance improves dramatically as

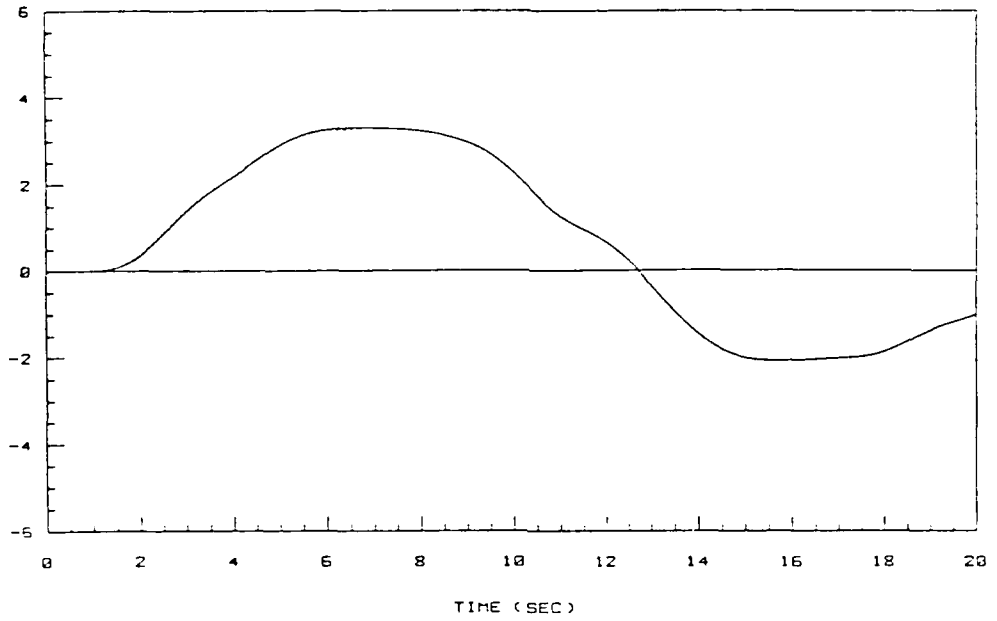

Figure 5-59. Flight path angle command and response (deg). Adaptive control law. Plant parameter change.

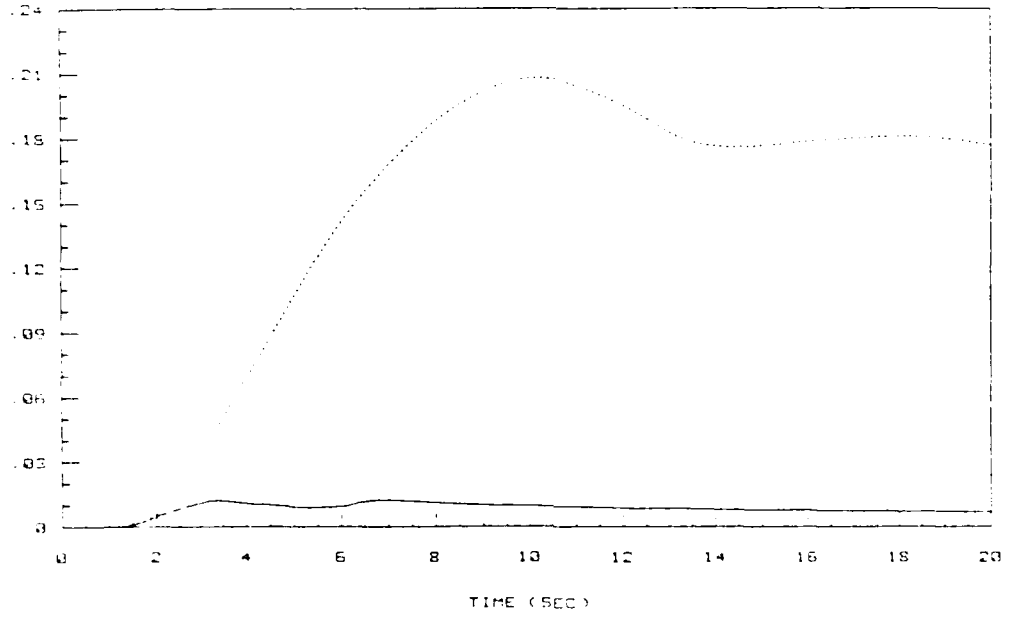

Figure 5-60. Flight path angle tracking performance index (deg). Adaptive control law. Plant parameter change.

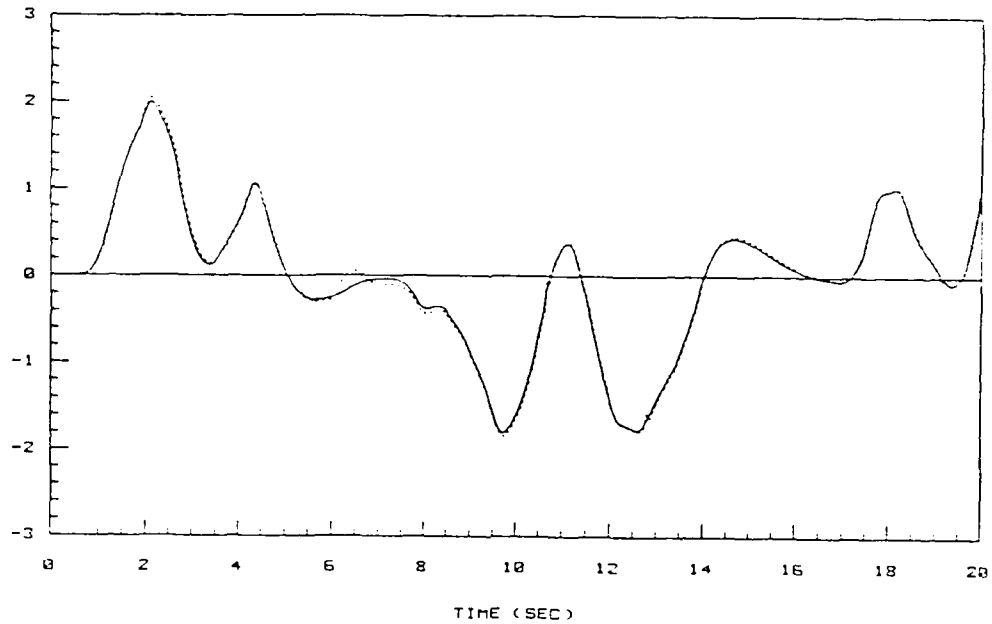

Figure 5-61. Pitch rate command and response (deg/sec). Adaptive control law. Plant parameter change.

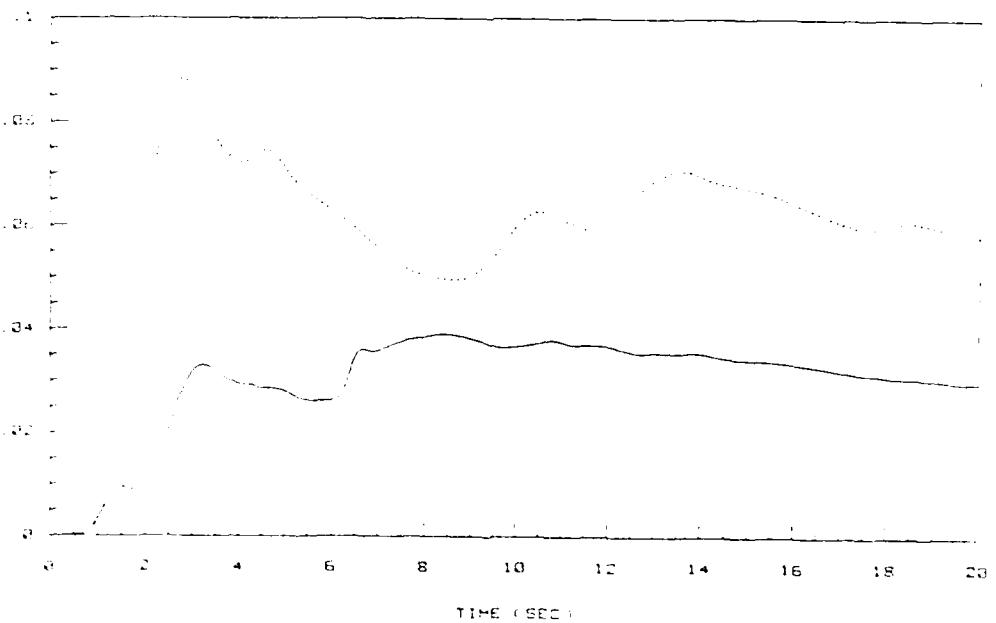

Figure 5-62. Pitch rate tracking performance index (deg/sec). Adaptive control law. Plant parameter change.

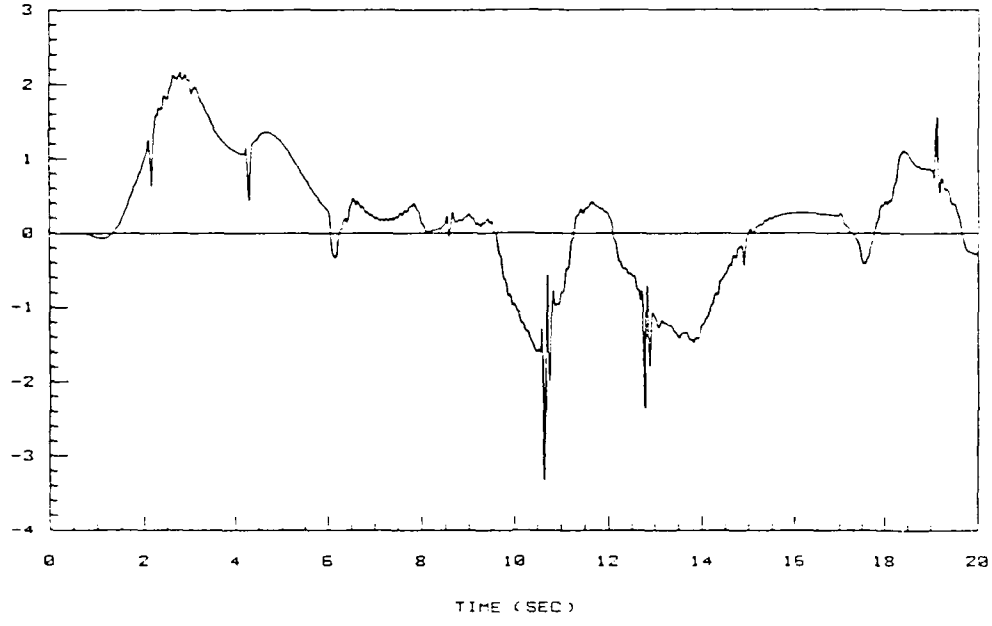

Figure 5-63. Elevator deflection (deg).
Adaptive control law. Plant parameter change.

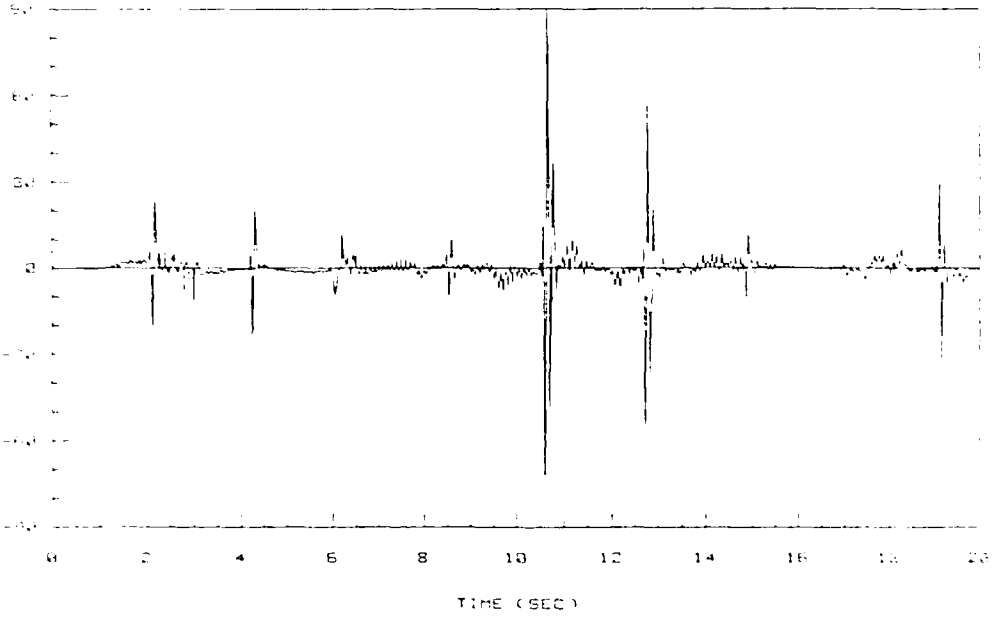

Figure 5-64. Elevator deflection rate (deg/sec).
Adaptive control law. Plant parameter change.

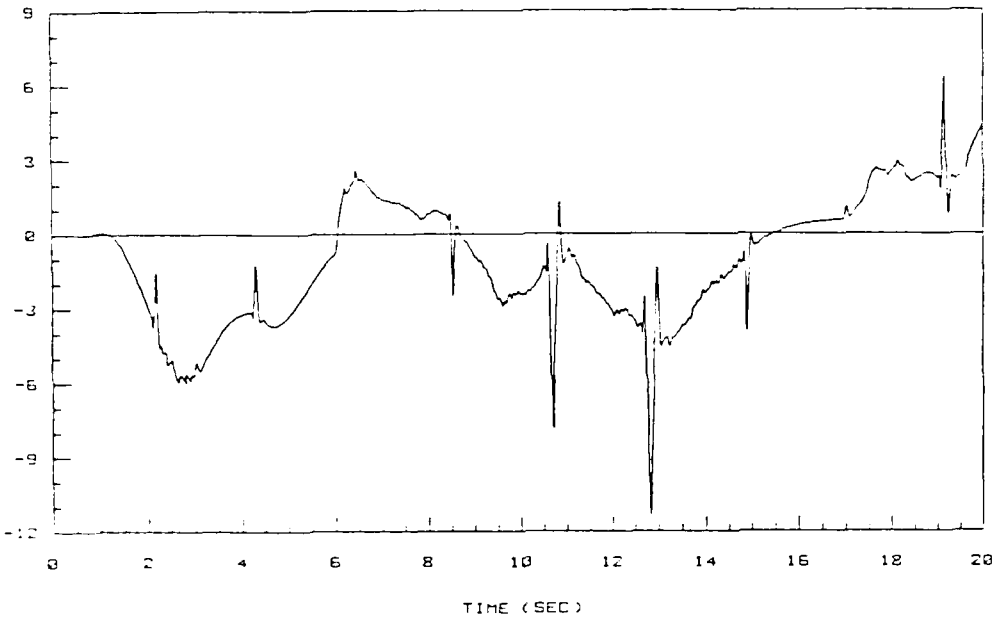

Figure 5-65. Flaperon deflection (deg).
Adaptive control law. Plant parameter change.

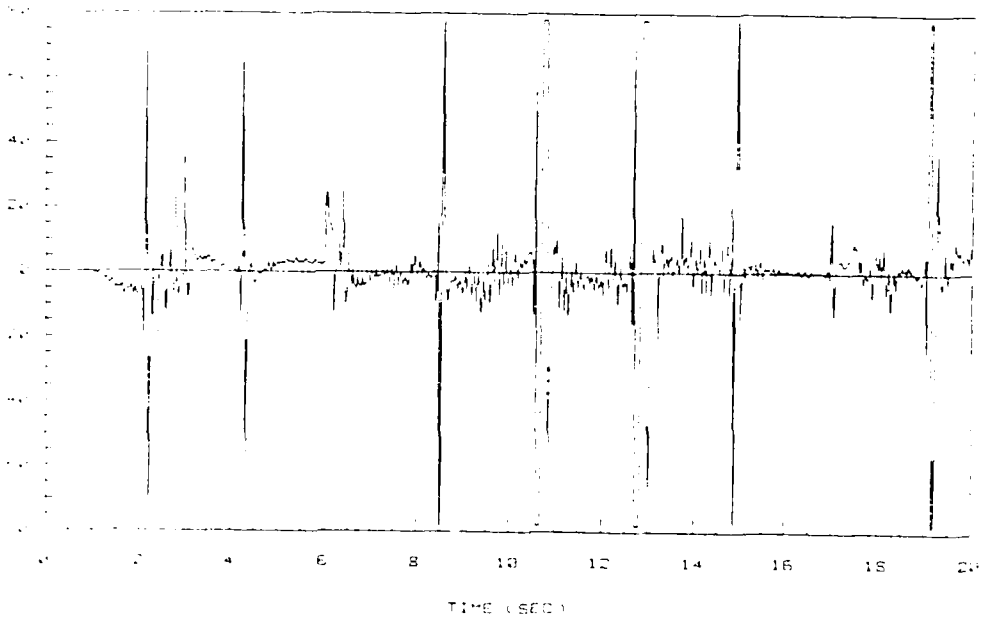

Figure 5-66. Flaperon deflection rate (deg/sec).
Adaptive control law. Plant parameter change.

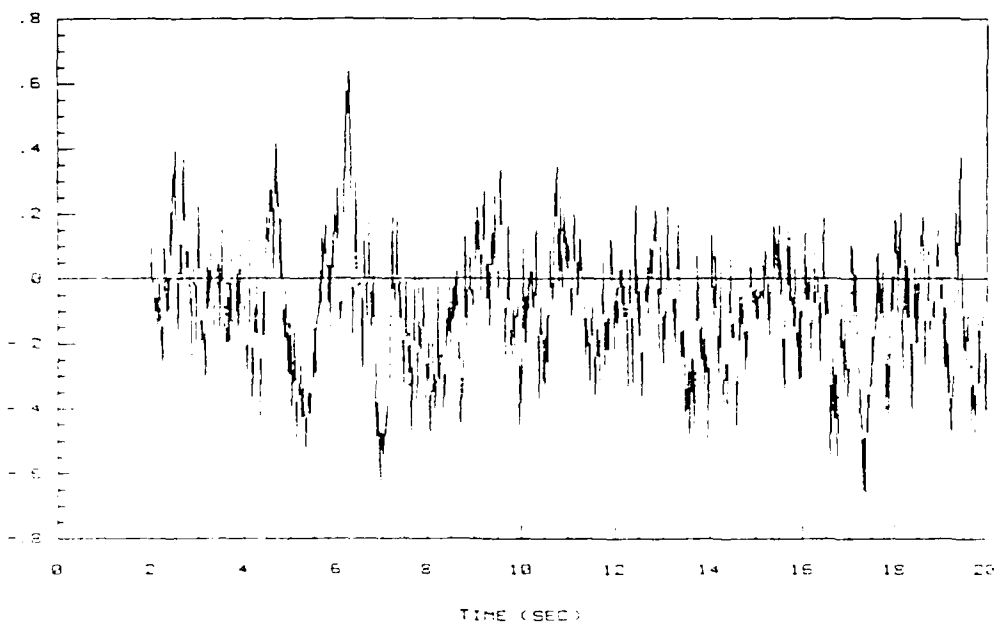

Figure 5-67. Fault detector test signal.
Plant parameter change.

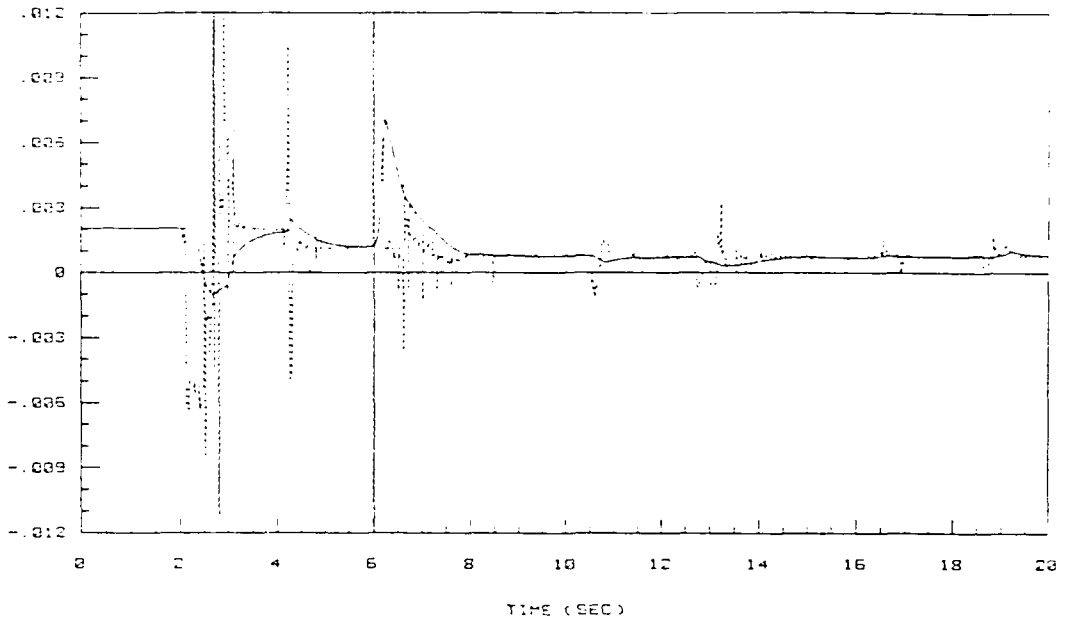

Figure 5-68. Estimate of step-response matrix element $h_{11}(kT)$.
Plant parameter change.

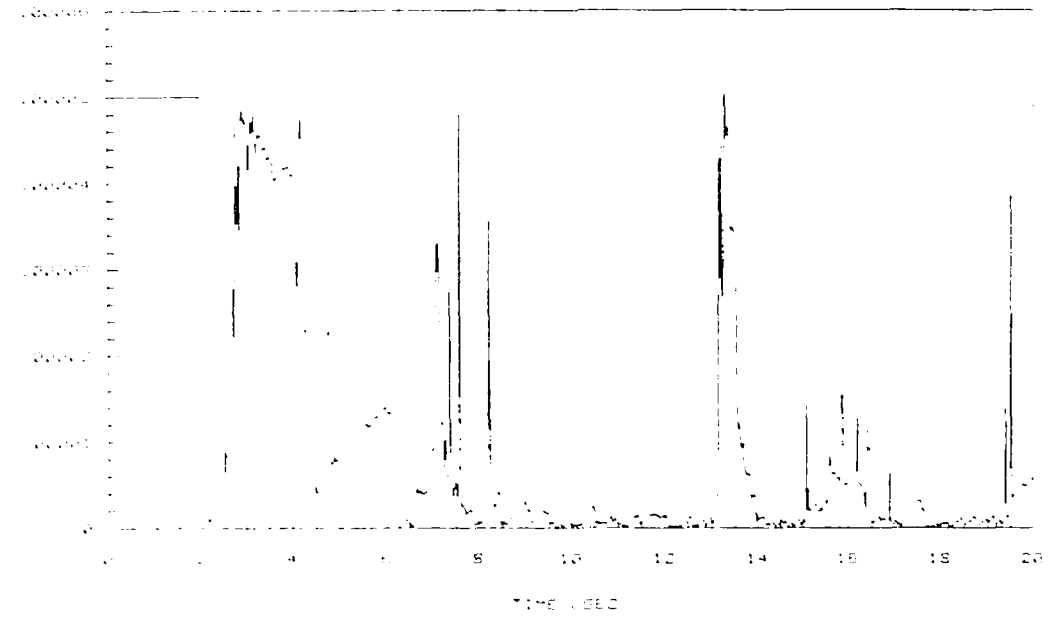

Figure 5-69. Covariance matrix element $p_{11}(kT)$.
Plant parameter change.

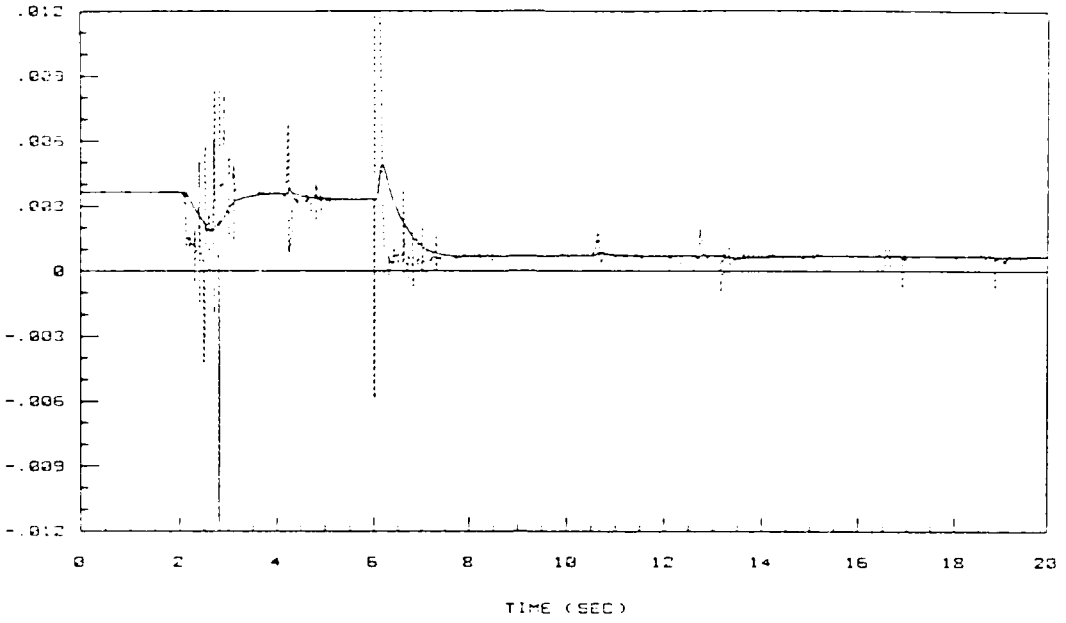

Figure 5-70. Estimate of step-response matrix element $h_{12}(kT)$. Plant parameter chnage.

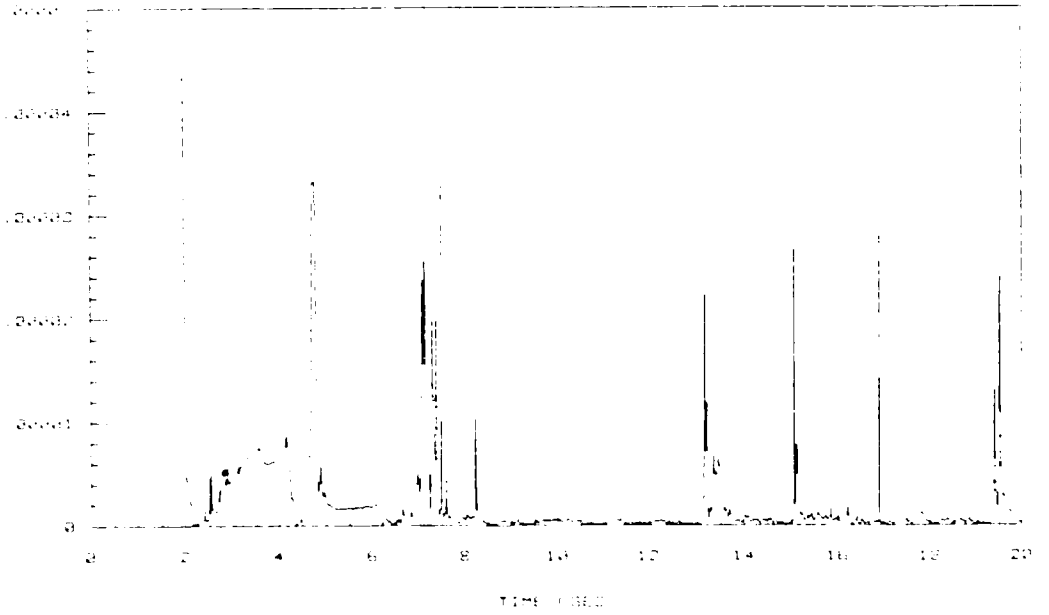

Figure 5-71. Covariance matrix element $p_{22}(kT)$. Plant parameter change.

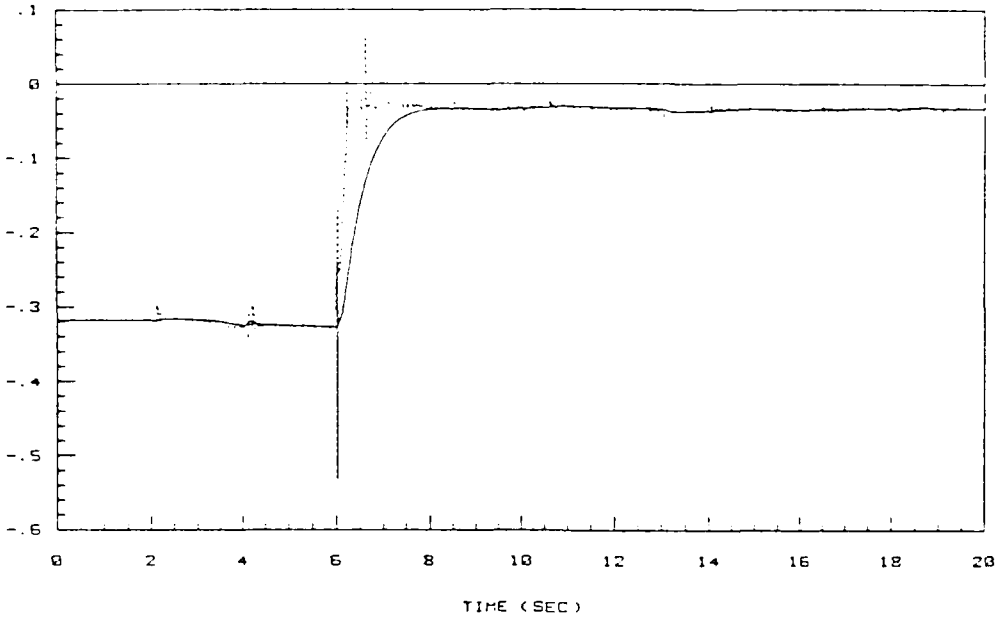

Figure 5-72. Estimate of step-response matrix element $h_{21}(kT)$. Plant parameter chnage.

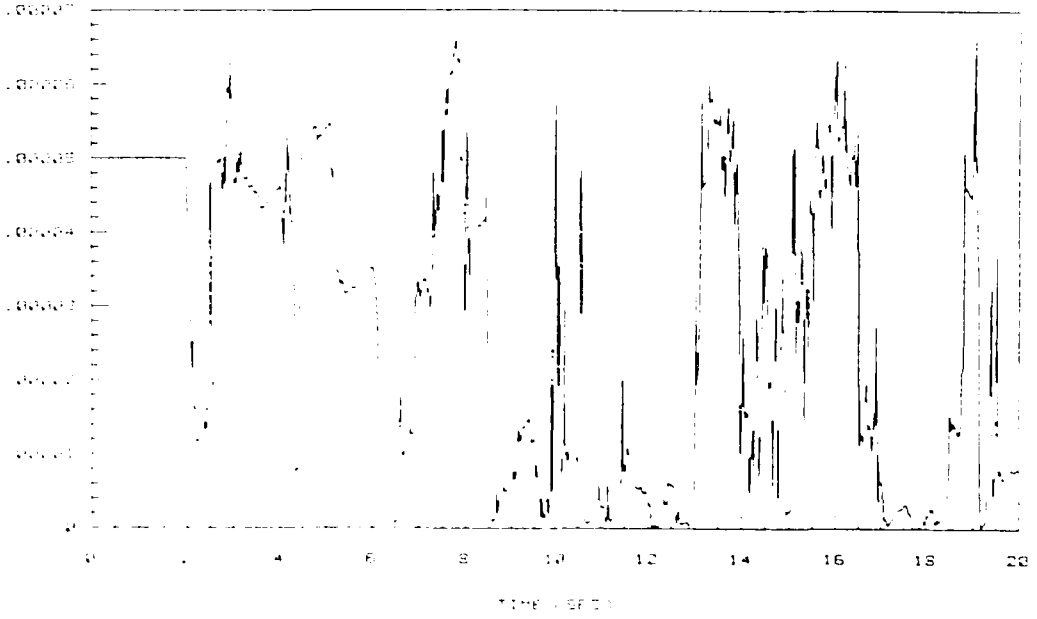

Figure 5-73. Covariance matrix element $p_{33}(kT)$. Plant parameter change.

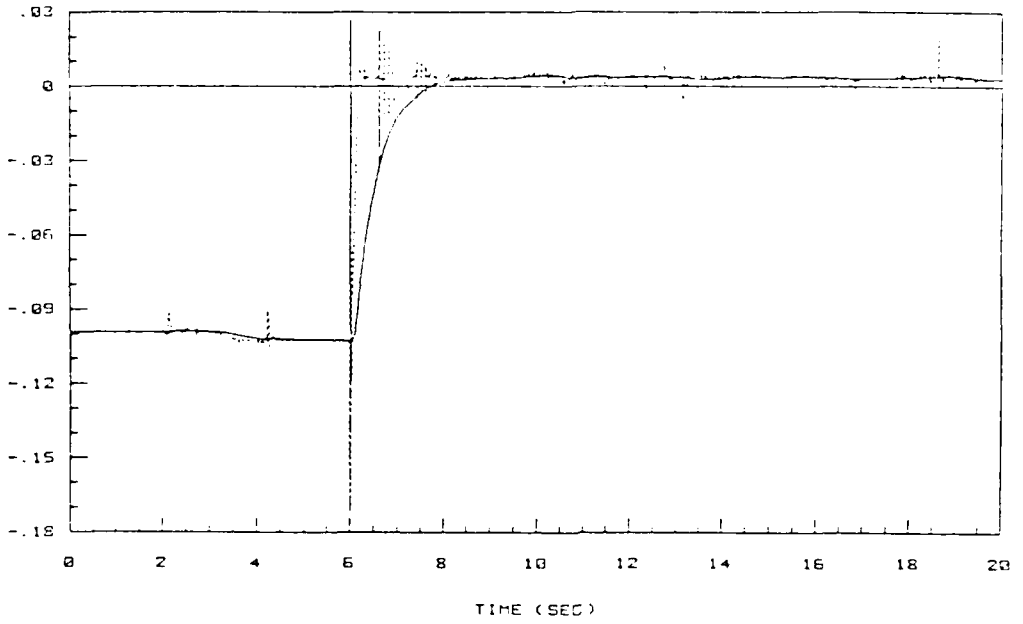

Figure 5-74. Estimate of step-response matrix element $h_{22}(kT)$. Plant parameter change.

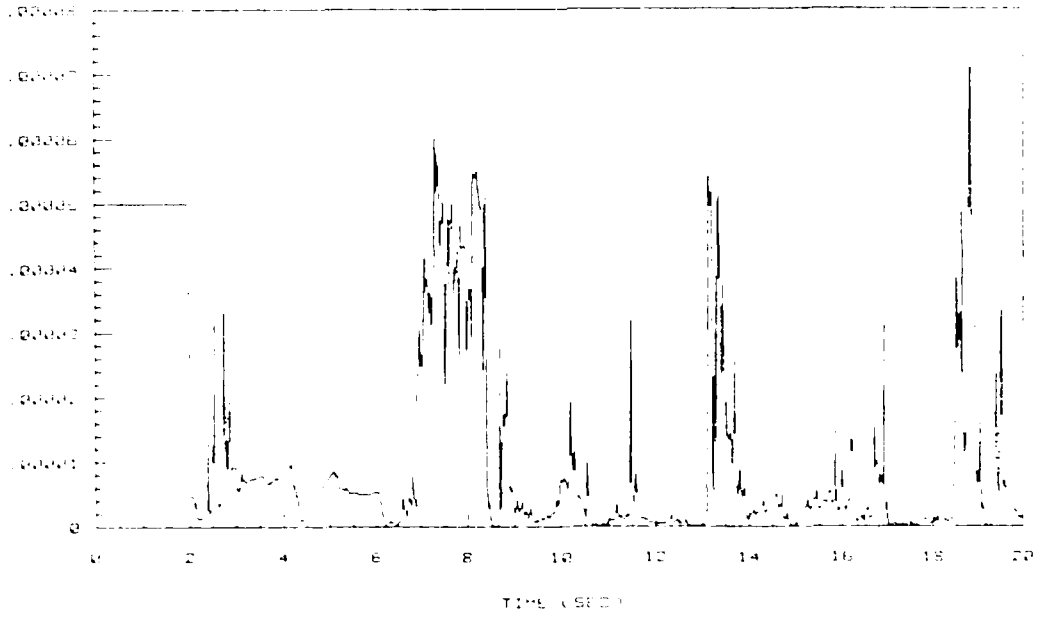

Figure 5-75. Covariance matrix element $p_{44}(kT)$. Plant parameter change.

shown in Figures 5-61 and 5-62 for the pitch rate response. This is in comparison to the performance of the fixed gain system in Figures 5-3 and 5-4.

Another noticeable characteristic in these aircraft's reponses is the encountering of flaperon deflection rate limits. This is attributed to the change in direction of the pitch rate command at those particular instants, in combination with fluctuations suffered by the parameter estimates at the new flight condition. The new set of plant dynamics is characterized by a step-response matrix with significantly smaller elements than the previous one. Fluctuations in these small numbers are bound to produce large variations in the control law gain matrices, and therefore larger deflection rates. The encountering of flaperon rate limits however, is not considered a severe problem in this simulation since the instances in which the flaperon is rate limited are very short, therefore not affecting significnatly the stability of the system.

The performance of the identification algorithm is considered very good. The fault detection algorithm in this simulation clearly indicates the abrupt change in the plant dynamics as shown in Figure 5-67 by the peak of $r(kT)$ exceeding the threshold $r_0 = 0.5$. The abrupt change in the plant's step-response matrix elements, together with the identification of the new parameters and parameter variances is shown in Figures 5-68 thru 5-75.

5.3.4 Plant Parameter Change and Sensor Noise. To present a worst case scenario to the adaptation mechanism, the simulation with abrupt plant parameter changes is now executed with the addition of

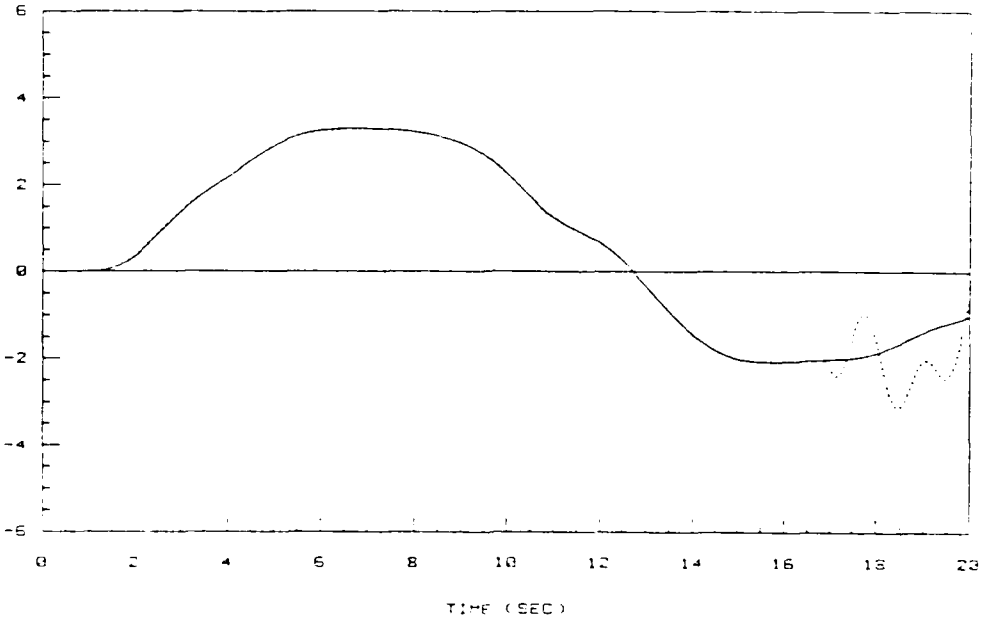

Figure 5-76. Flight path angle command and response (deg). Adaptive control law. Plant parameter change and sensor noise. (std. dev. = 0.00181 deg).

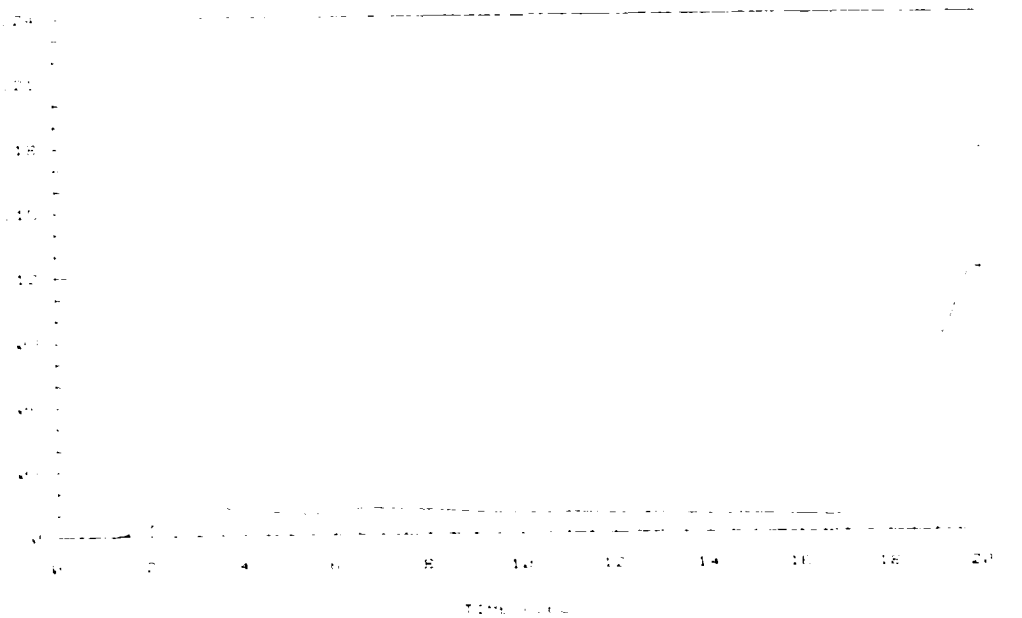

Figure 5-77. Flight path angle tracking performance index (deg). Adaptive control law. Plant parameter change and sensor noise. (std. dev. = 0.00181 deg).

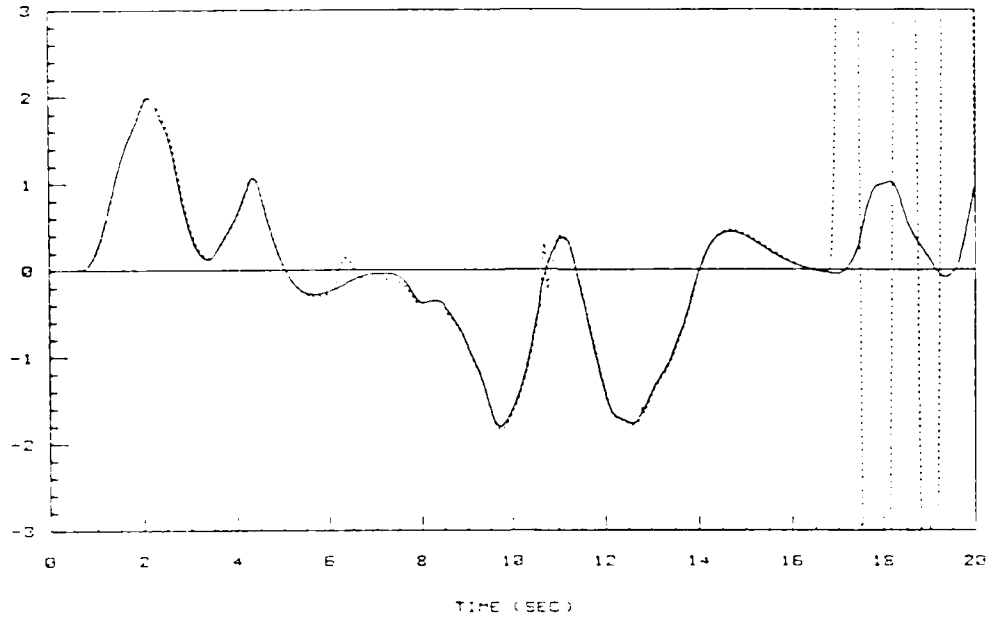

Figure 5-78. Pitch rate command and response (deg/sec). Adaptive control law. Plant parameter change and sensor noise. (std. dev. = 0.00181 deg/sec).

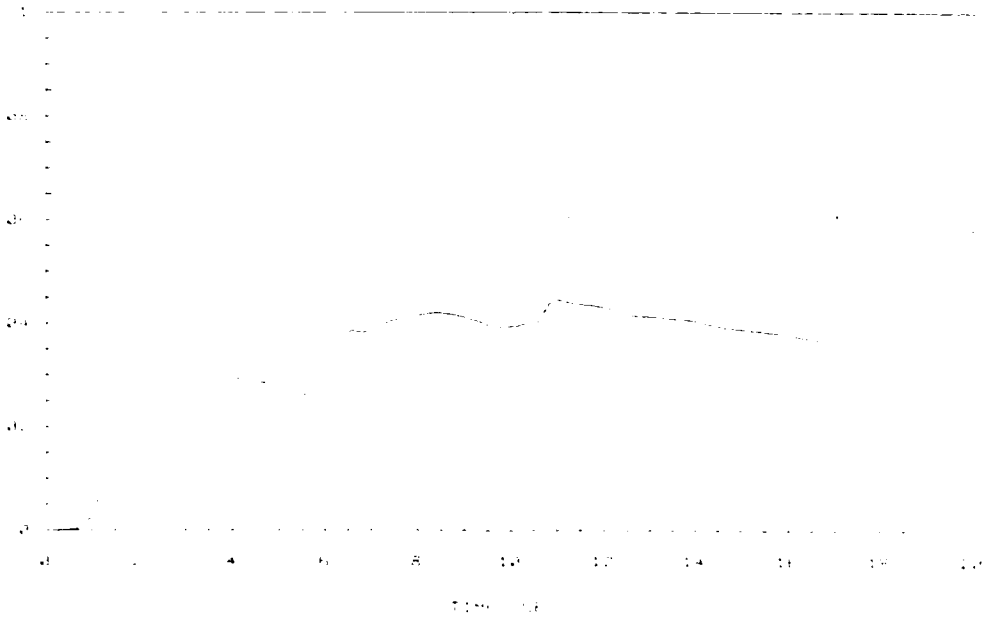

Figure 5-79. Pitch rate tracking performance index (deg/sec). Adaptive control law. Plant parameter change and sensor noise. (std. dev. = 0.00181 deg/sec).

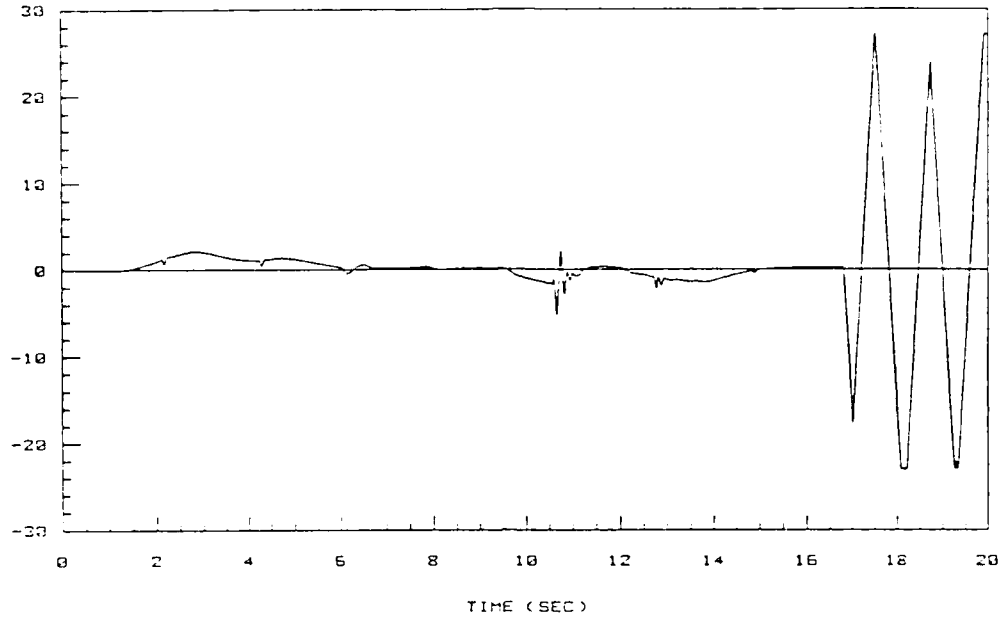

Figure 5-80. Elevator deflection (deg).
Adaptive control law. Plant parameter change and sensor noise.
(std. dev. = 0.00181 deg (deg/sec)).

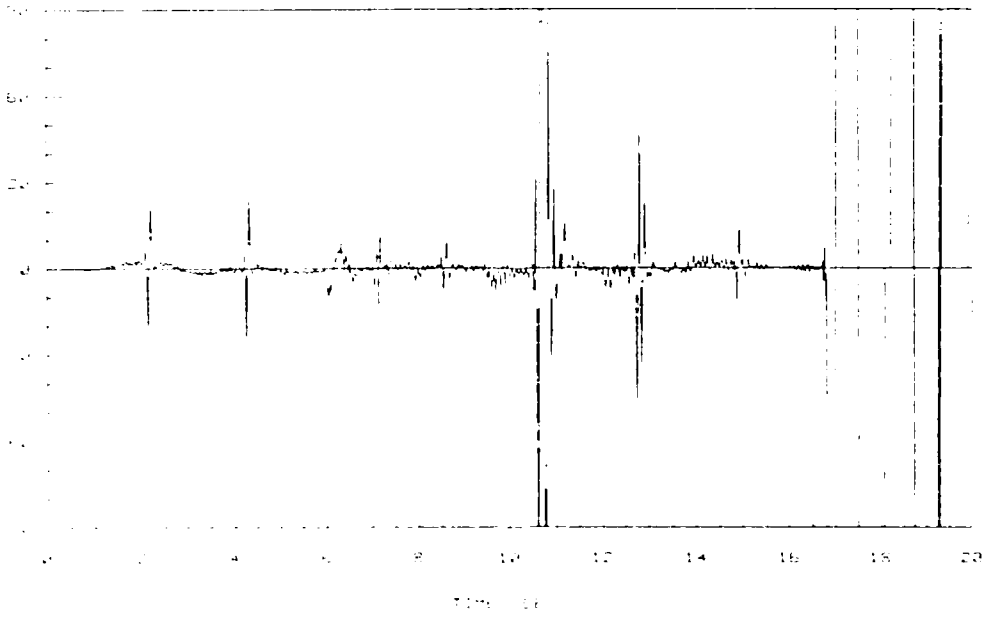

Figure 5-81. Elevator deflection rate (deg/sec).
Adaptive control law. Plant parameter change and sensor noise.
(std. dev. = 0.00181 deg (deg/sec)).

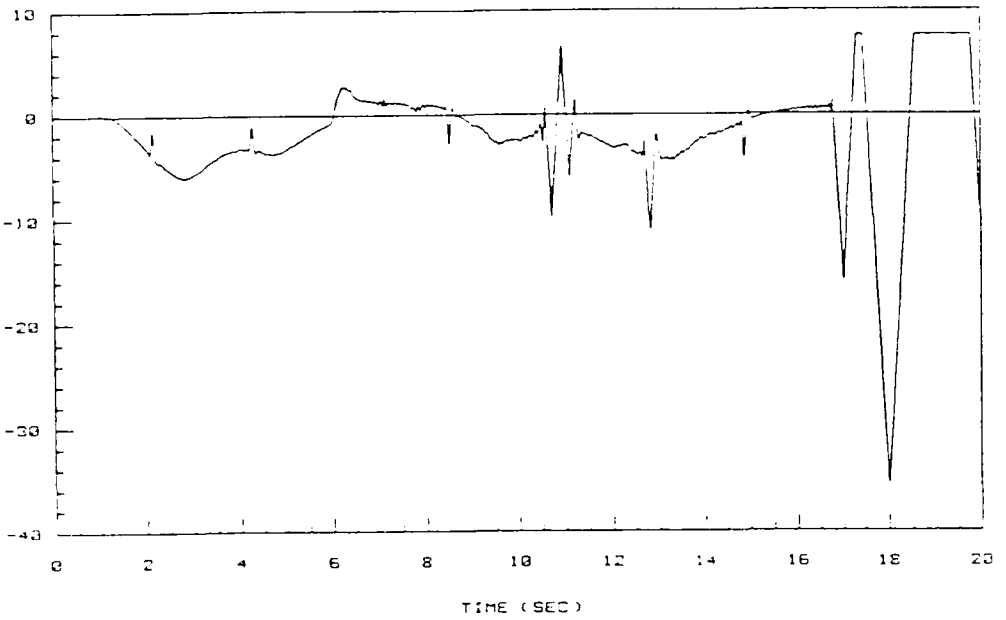

Figure 5-82. Flaperon deflection (deg).
Adaptive control law. Plant parameter change and sensor noise.
(std. dev. = 0.00181 deg (deg/sec)).

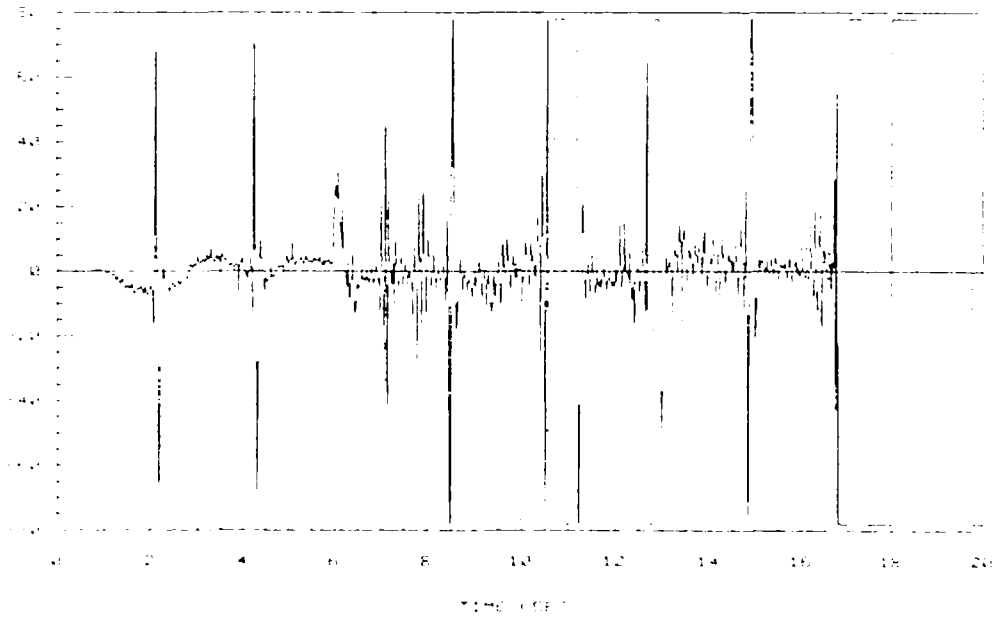

Figure 5-83. Flaperon deflection rate (deg/sec).
Adaptive control law. Plant parameter change and sensor noise.
(std. dev. = 0.00181 deg (deg/sec)).

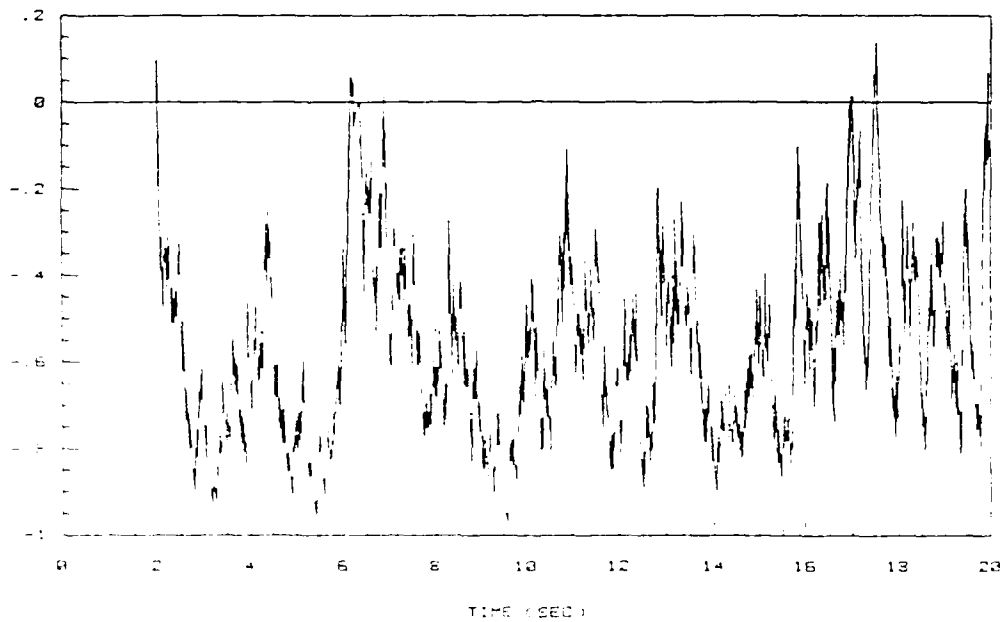

Figure 5-84. Fault detector test signal with plant parameter change and sensor noise. (std. dev. = 0.00181 deg (deg/sec)).

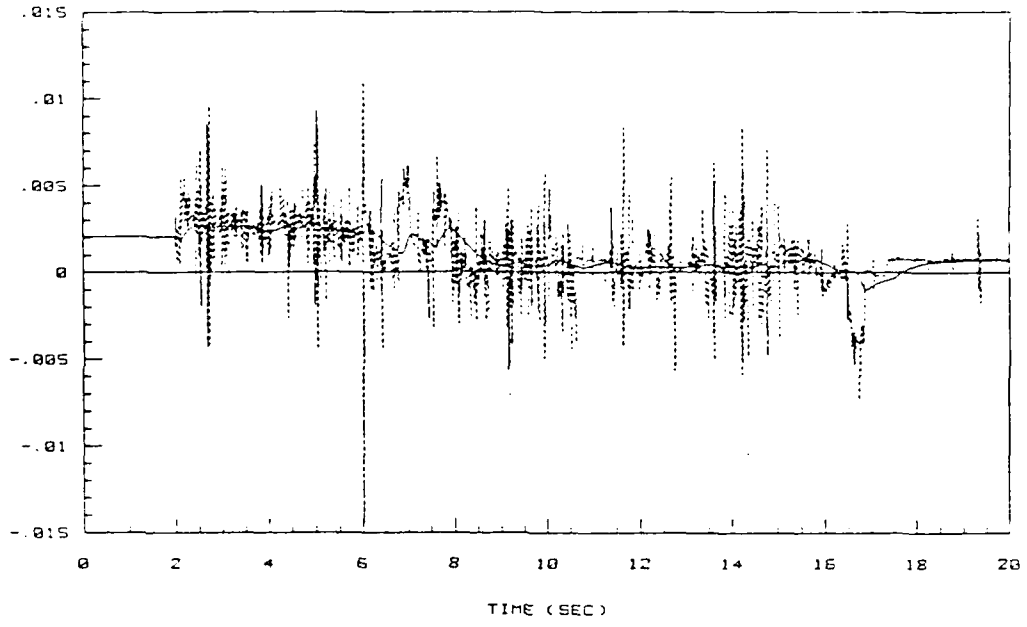

Figure 5-85. Estimate of step-response matrix element $h_{11}(kT)$ with sensor noise. (std. dev. = 0.00181 deg (deg/sec)).

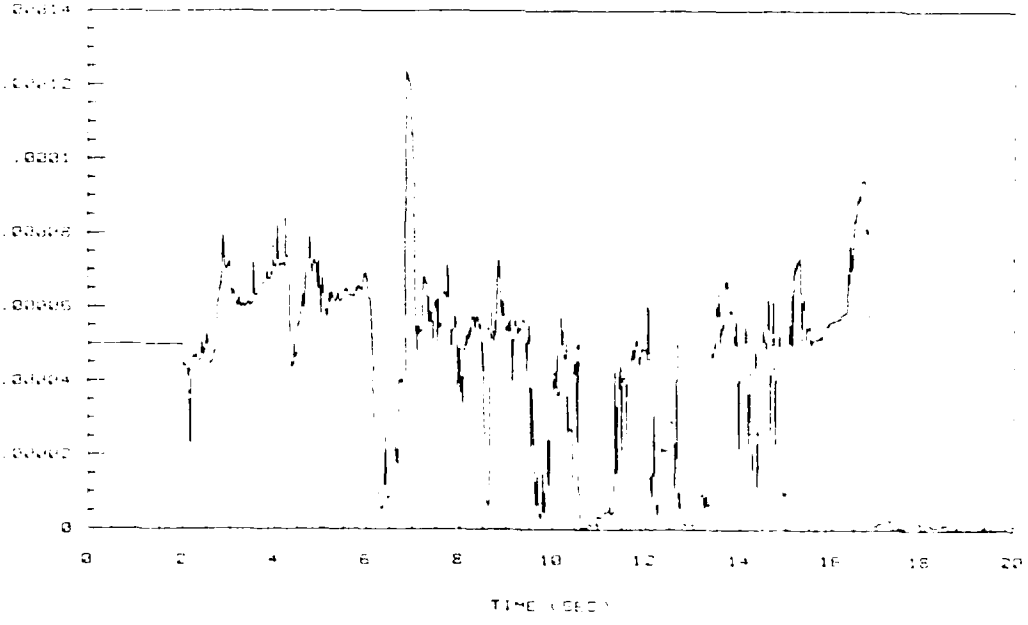

Figure 5-86. Covariance matrix element $p_{11}(kT)$ with sensor noise. (std. dev. = 0.00181 deg (deg/sec)).

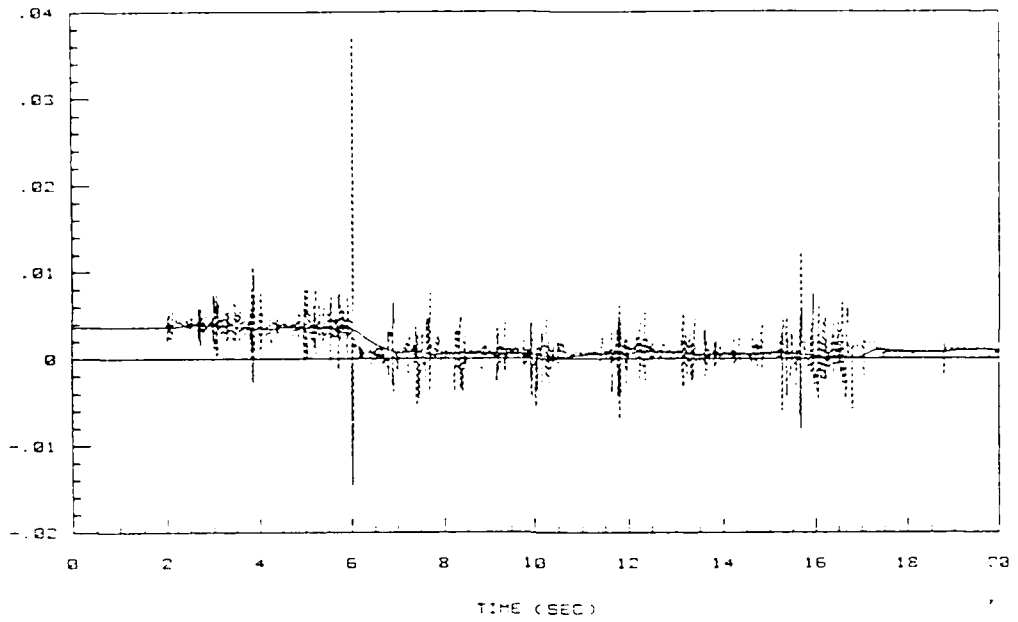

Figure 5-87. Estimate of step-response matrix element $h_{12}(kT)$ with sensor noise. (std. dev. = 0.00181 deg (deg/sec)).

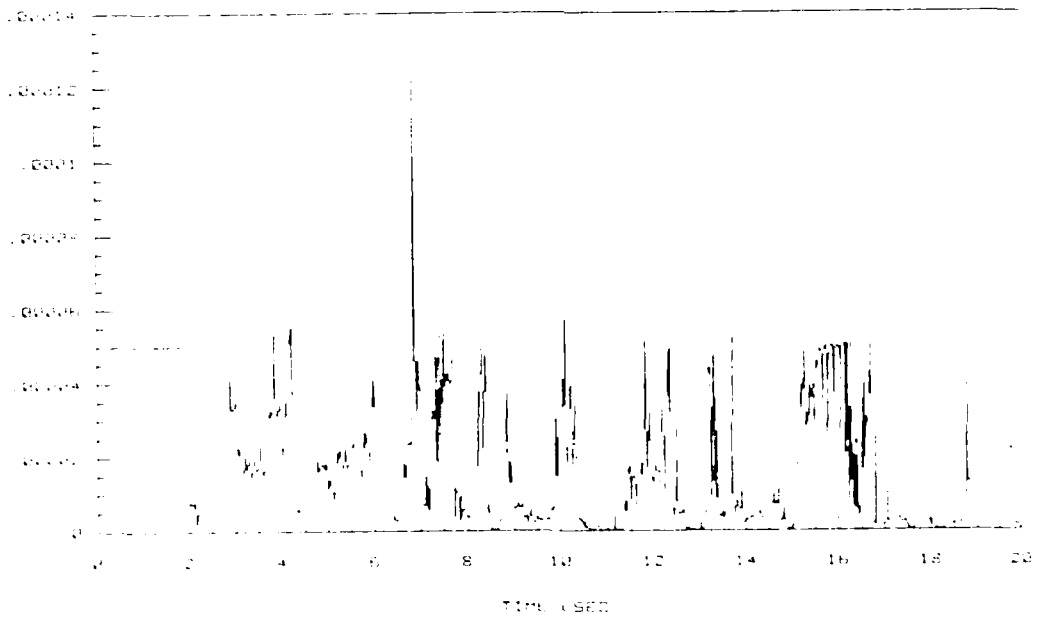

Figure 5-88. Covariance matrix element $p_{22}(kT)$ with sensor noise. (std. dev. = 0.00181 deg (deg/sec)).

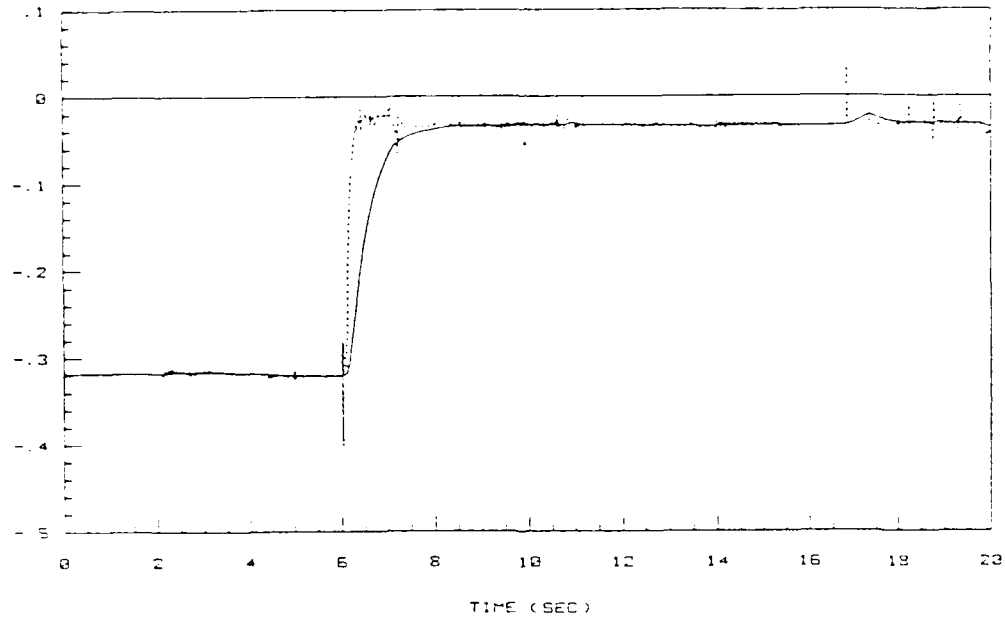

Figure 5-89. Estimate of step-response matrix element $h_{21}(kT)$ with sensor noise. (std. dev. = 0.00181 deg (deg/sec)).

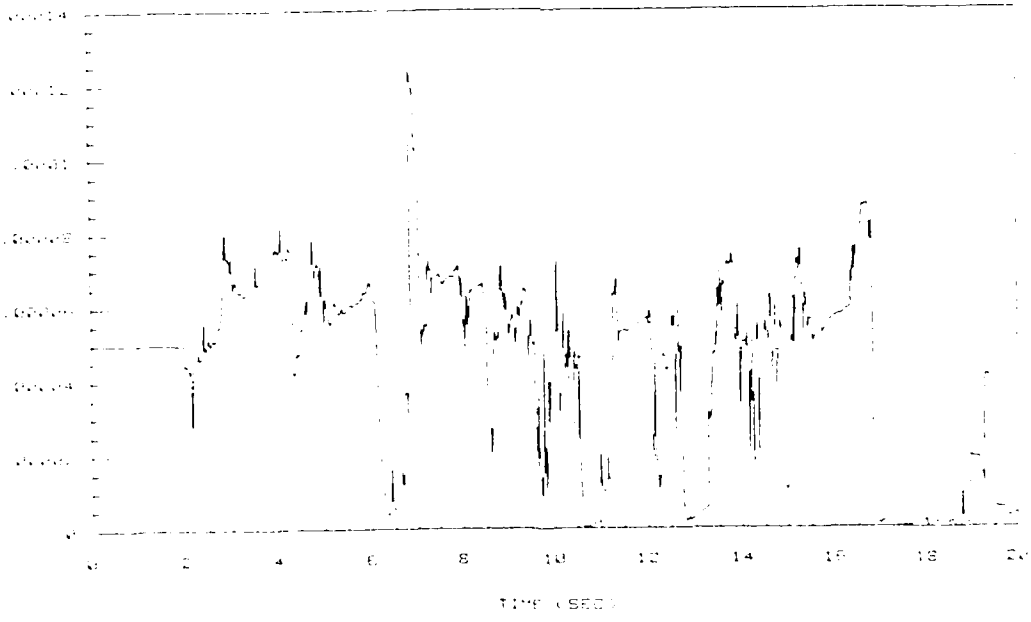

Figure 5-90. Covariance matrix element $p_{33}(kT)$ with sensor noise. (std. dev. = 0.00181 deg (deg/sec)).

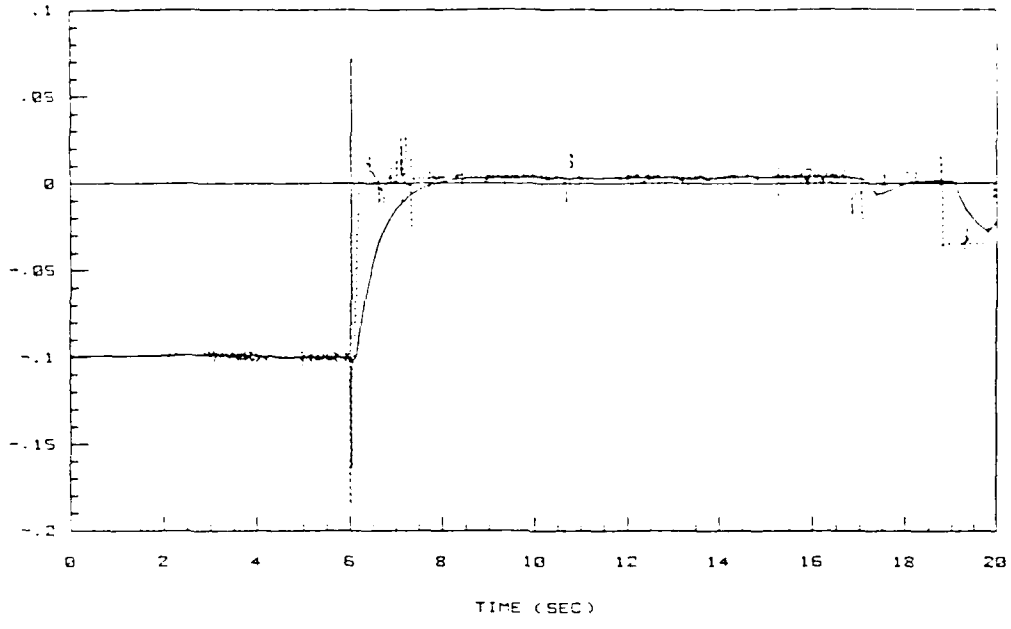

Figure 5-91. Estimate of step-response matrix element $h_{22}(kT)$ with sensor noise. (std. dev. = 0.00181 deg (deg/sec)).

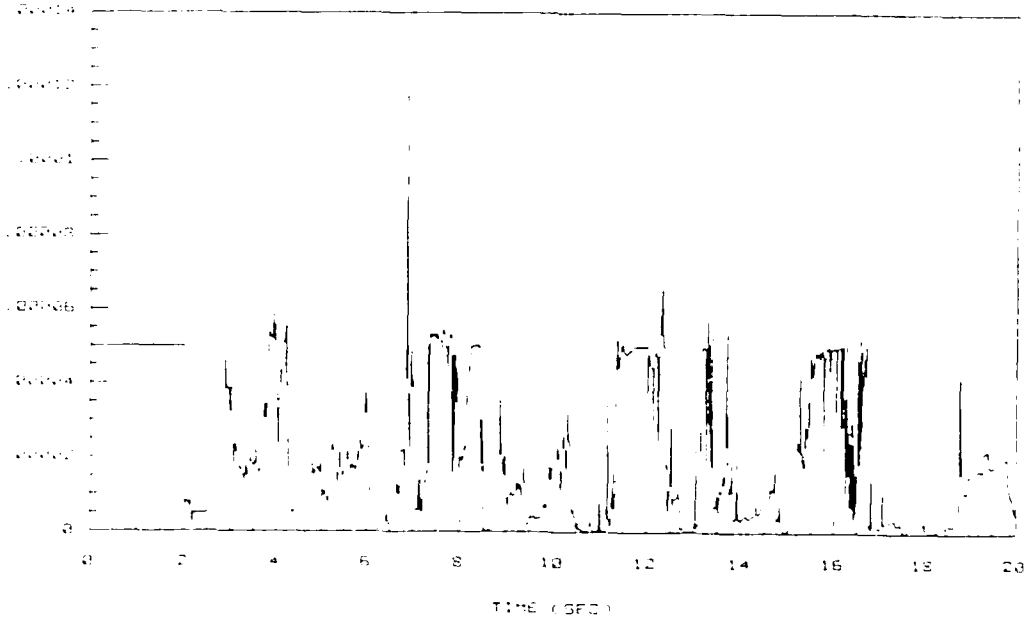

Figure 5-92. Covariance matrix element $p_{22}(kT)$ with sensor noise. (std. dev. = 0.00181 deg (deg/sec)).

sensor measurement noise. The system's performance in this simulation is very similar to that of the previous one until the last few seconds, where the closed-loop system develops an instability in the aircraft's responses. The instability is the result of control surface rate limiting. This condition is caused in turn by noise induced fluctuations in the filtered parameter estimates, at a time when these estimates are extremely close to the zero axis. As it was mentioned earlier, the situation just described causes large changes in the control law gains which are responsible for driving the control surfaces to their motion rate limits.

To alleviate this problem the simulation is then executed with scaled parameter vector and measurement matrix as described in section 4.4.5. The results are ilustrated in Figures 5-93 thru 5-109. The responses of the closed-loop system are stable and tracking performance is maintained as desired. The performance of the identification algorithm is clearly better when scaled variables are used. The fault detector test signal in Figure 5-101 shows a prominent peak shortly after the time of the plant dynamics change, indicating unmistakably the occurence of the fault. The parameter estimates themselves exhibit a significantly smoother behavior (Figures 5-102, 5-104, 5-106, and 5-108), thus the filtered estimates are virtually free of oscillations or fluctuations around the zero axis. This behavior accounts for the improved performance of the closed-loop system responses over the ones shown using the unscaled algorithm, for the level of noise used.

The scaled version of the algorithm is again tested, this time with a higher noise level of standard deviation of 0.00573 deg (deg/sec).

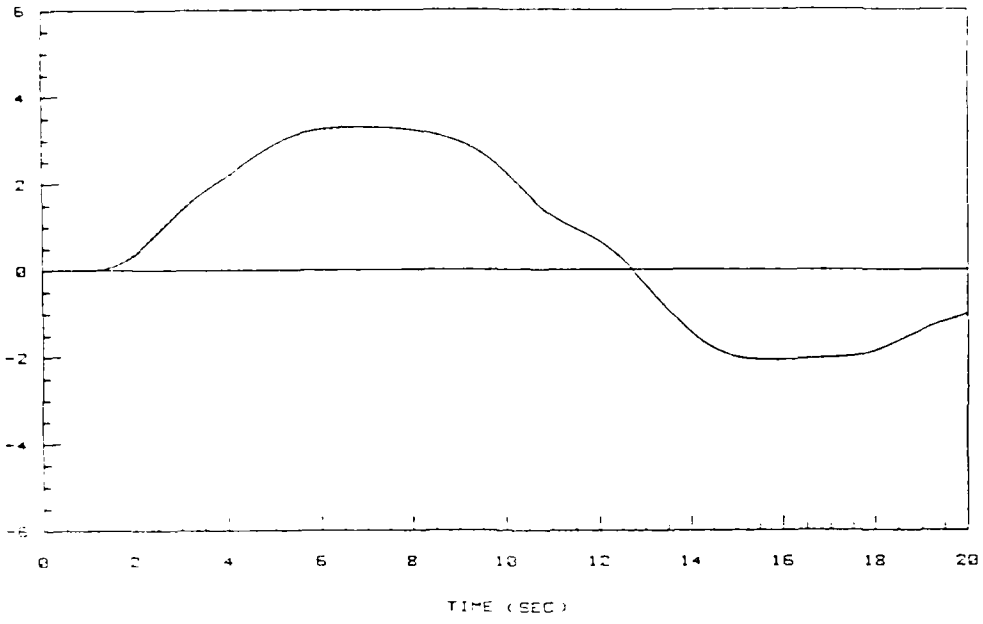

Figure 5-93. Flight path angle command and response (deg). Adaptive control law. Plant parameter change and sensor noise. (std. dev. = 0.00181 deg). Scaled algorithm (SF = 100).

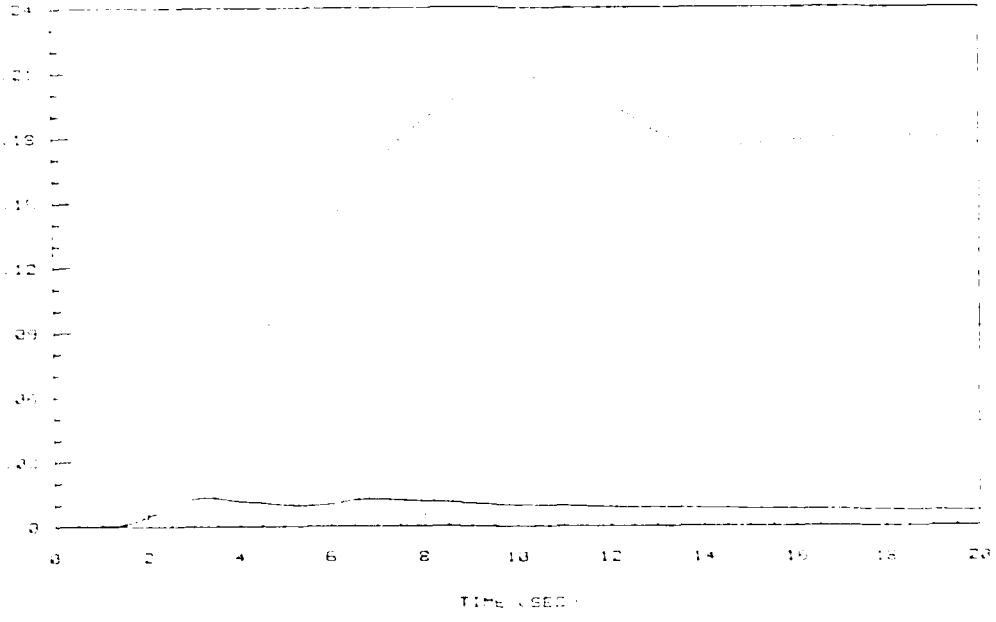

Figure 5-94. Flight path angle tracking performance index (deg). Adaptive control law. Plant parameter change and sensor noise. (std. dev. = 0.00181 deg). Scaled algorithm (SF = 100).

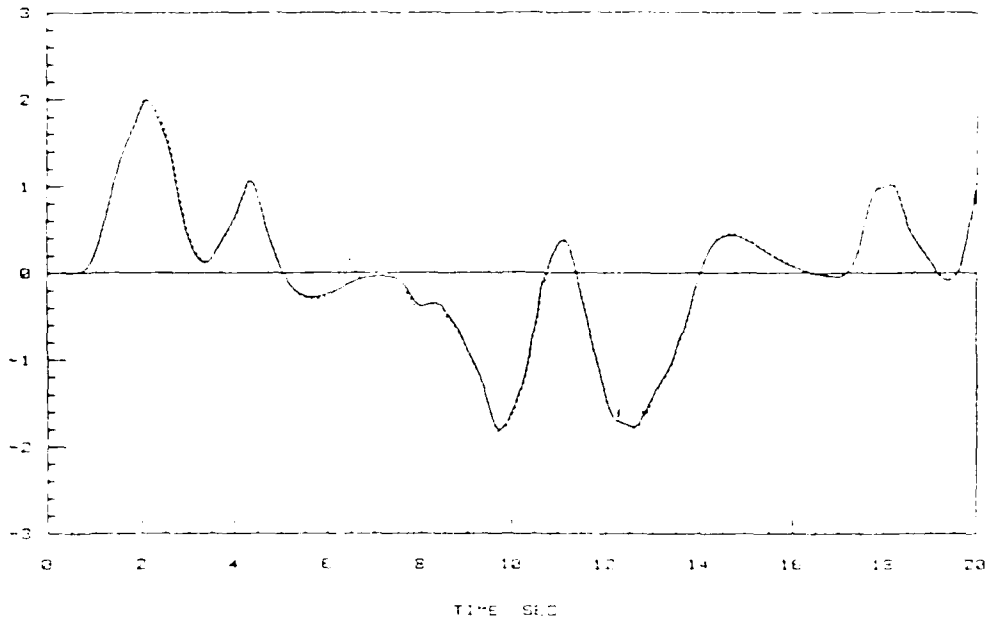

Figure 5-95. Pitch rate command and response (deg/sec). Adaptive control law. Plant parameter change and sensor noise. (std. dev. = 0.00181 deg/sec). Scaled algorithm (SF = 100).

Figure 5-96. Pitch rate tracking performance index (deg/sec). Adaptive control law. Plant parameter change and sensor noise. (std. dev. = 0.00181 deg/sec). Scaled algorithm (SF = 100).

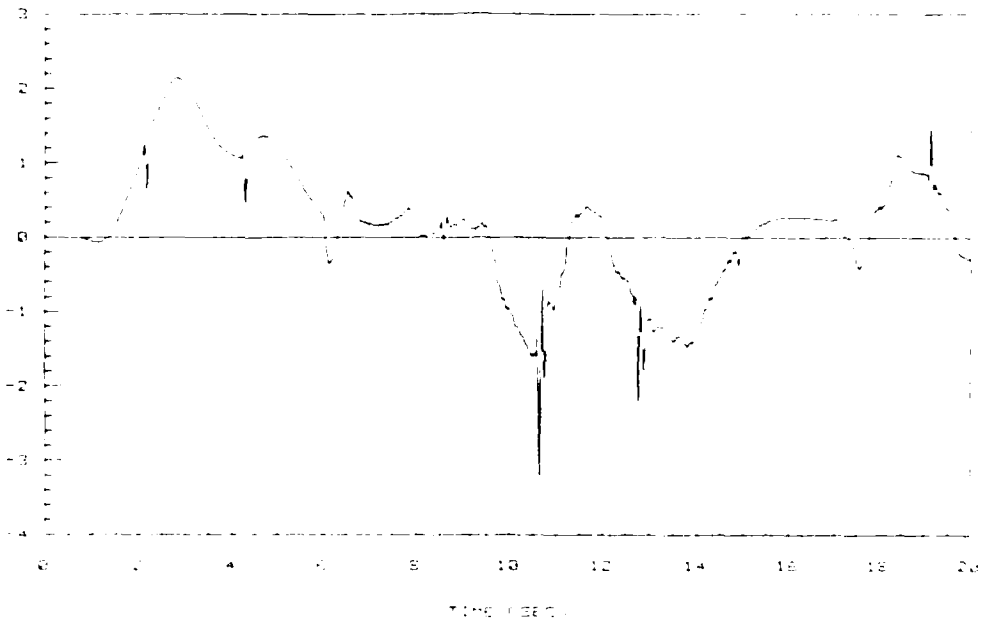

Figure 5-97. Elevator deflection (deg).
Adaptive control law. Plant parameter change and sensor noise.
(std. dev. = 0.00181 deg (deg/sec)). Scaled algorithm (SF = 100).

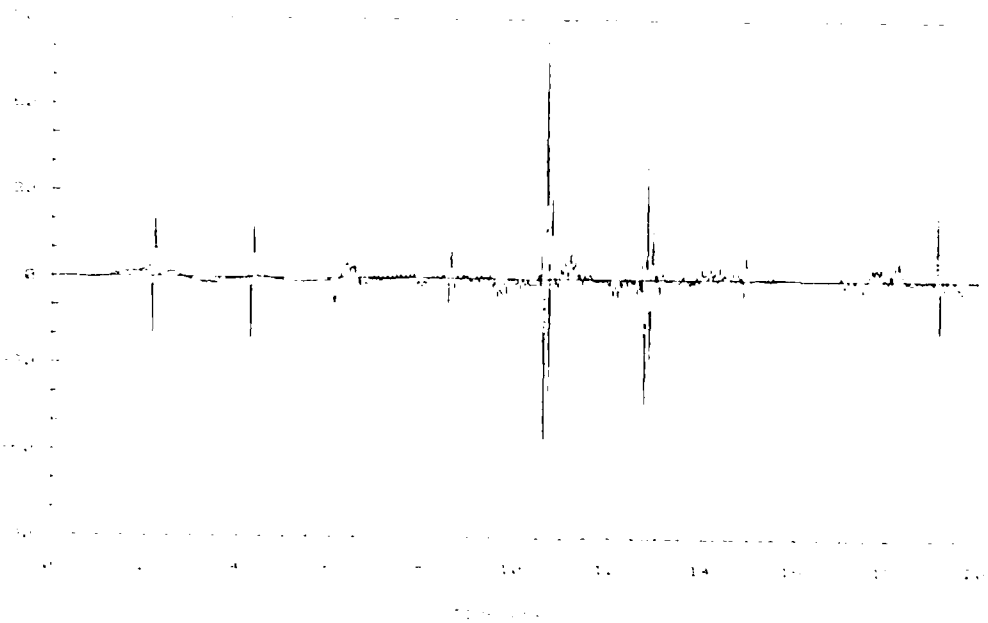

Figure 5-98. Elevator deflection rate (deg/sec).
Adaptive control law. Plant parameter change and sensor noise.
(std. dev. = 0.00181 deg (deg/sec)). Scaled algorithm (SF = 100).

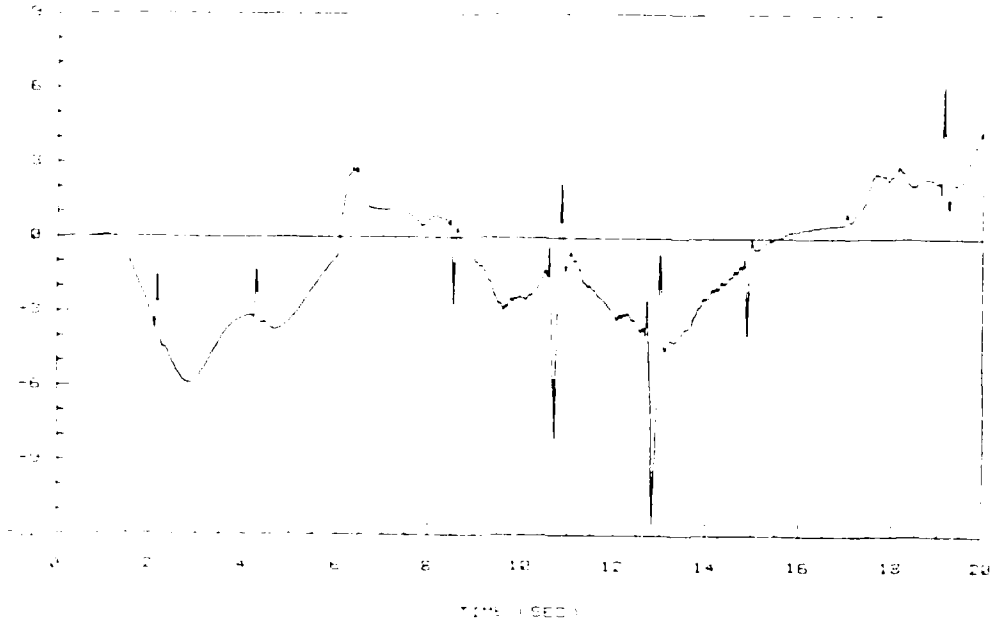

Figure 5-99. Flaperon deflection (deg).
Adaptive control law. Plant parameter change and sensor noise.
(std. dev. = 0.00181 deg (deg/sec)). Scaled algorithm (SF = 100).

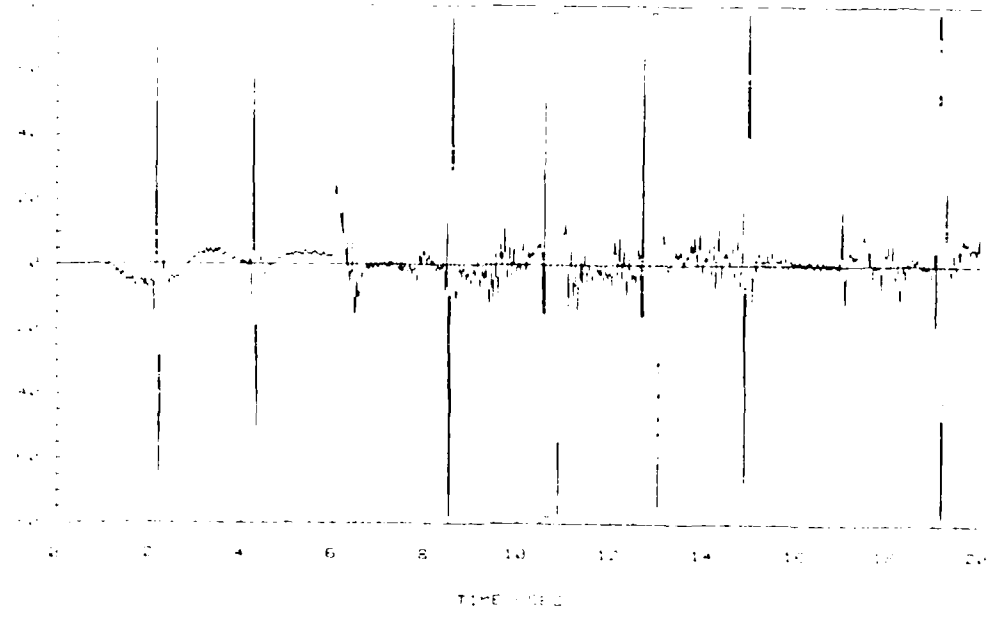

Figure 5-100. Flaperon deflection rate (deg/sec).
Adaptive control law. Plant parameter change and sensor noise.
(std. dev. = 0.00181 deg (deg/sec)). Scaled algorithm (SF = 100).

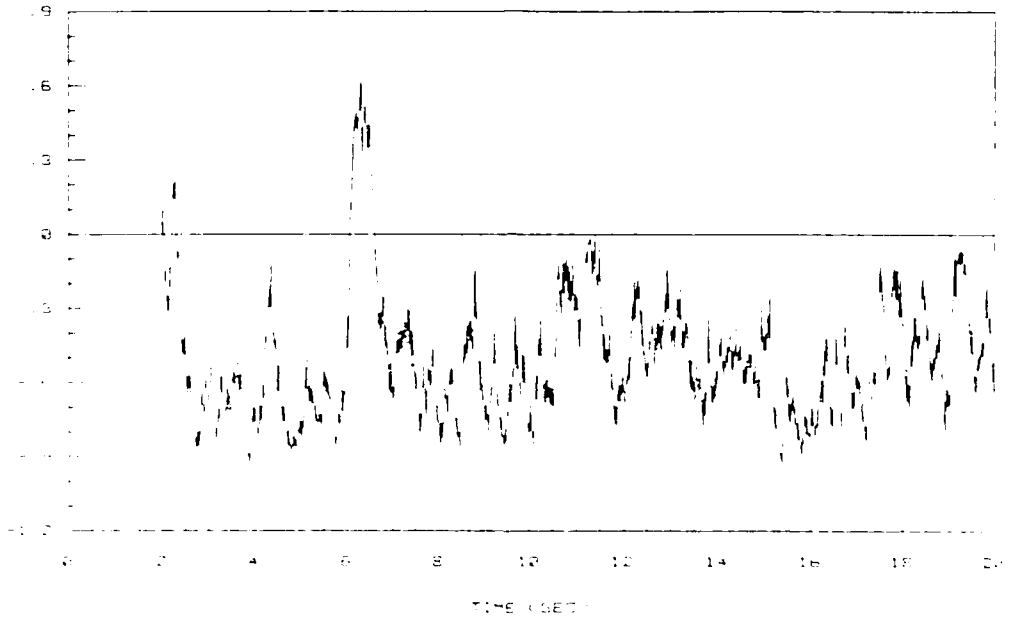

Figure 5-101. Fault detector test signal with sensor noise. (std. dev. = 0.00181 deg (deg/sec)). Scaled algorithm (SF = 100).

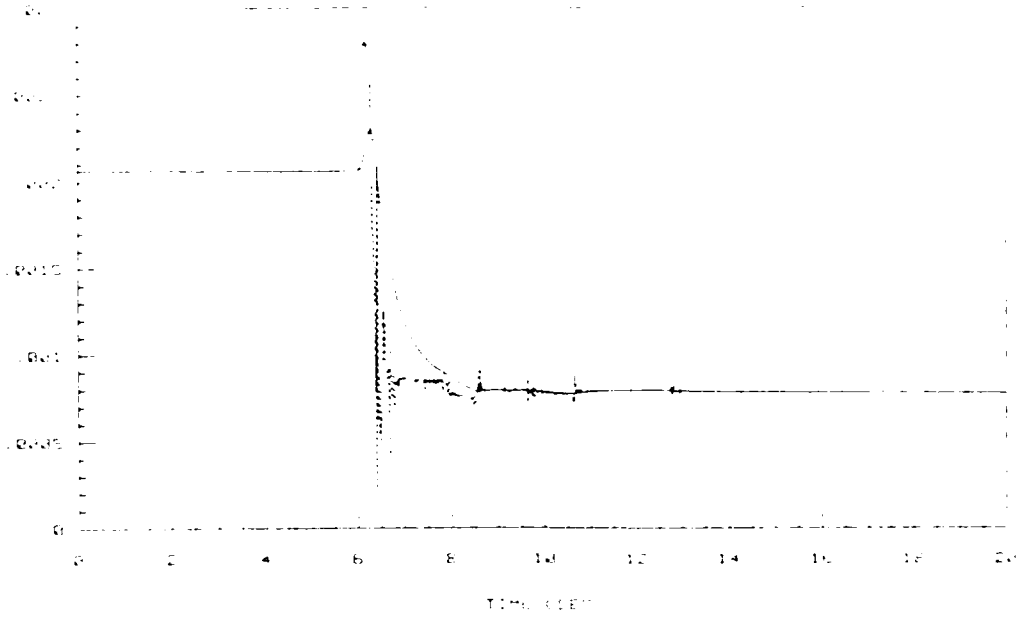

Figure 5-102. Estimate of step-response matrix element $h_{11}(kT)$ with sensor noise. (std. dev. = 0.00181 deg (deg/sec)). Scaled algorithm (SF = 100).

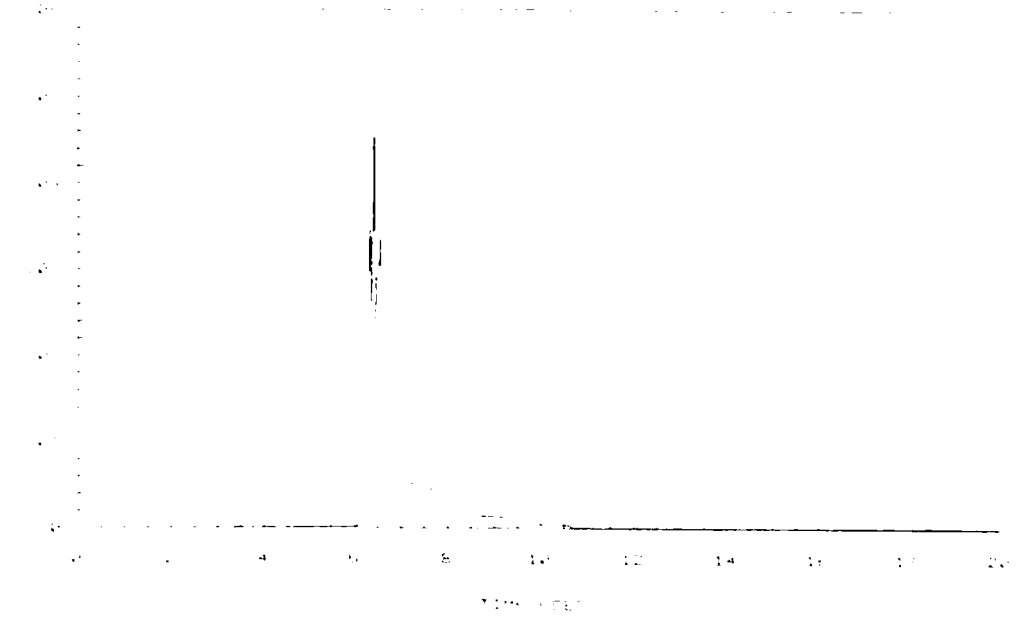

Figure 5-103. Covariance matrix element $p_{11}(kT)$ with sensor noise. (std. dev. = 0.00181 deg (deg/sec)). Scaled algorithm (SF = 100).

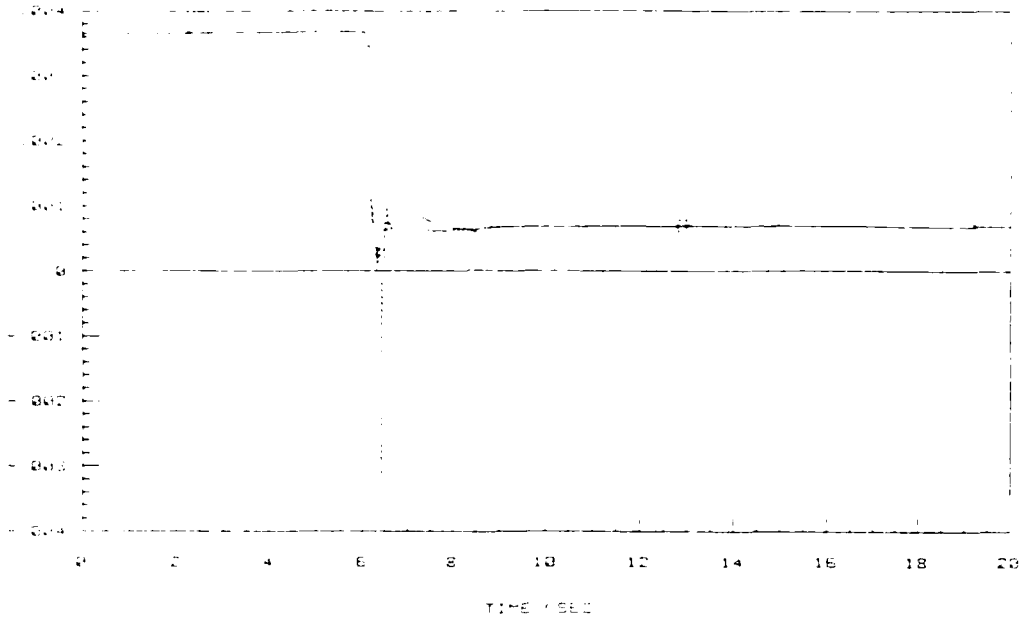

Figure 5-134. Estimate of step-response matrix element $h_{12}(kT)$ with sensor noise. (std. dev. = 0.00181 deg (deg/sec)). Scaled algorithm (SF = 100).

Figure 5-135. Covariance matrix element $p_{22}(kT)$ with sensor noise. (std. dev. = 0.00181 deg (deg/sec)). Scaled algorithm (SF = 100).

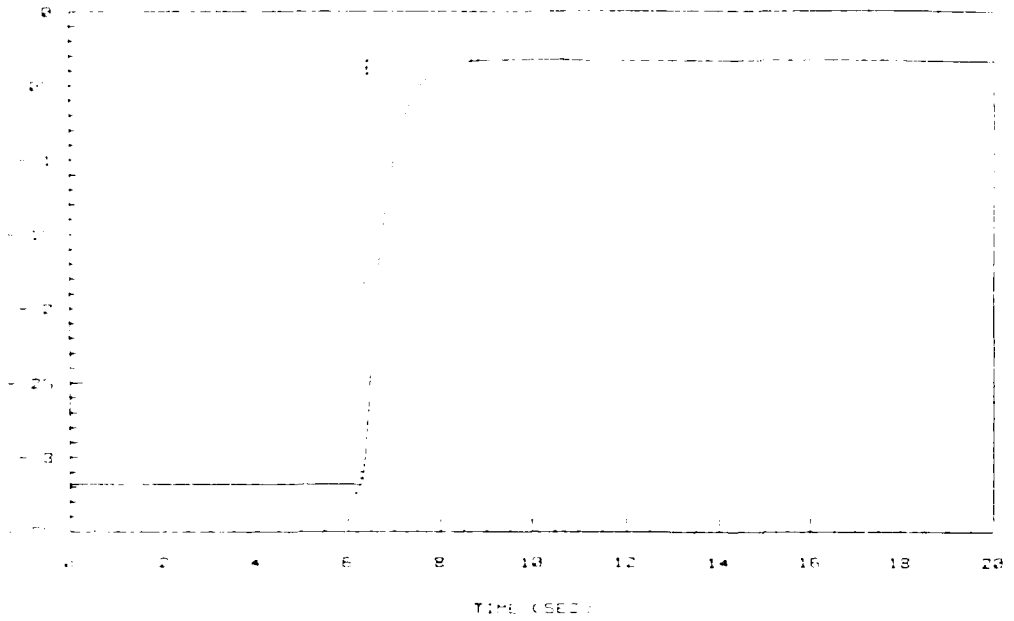

Figure 5-106. Estimate of step-response matrix element $h_{21}(kT)$ with sensor noise. (std. dev. = 0.00181 deg (deg/sec)). Scaled algorithm (SF = 100).

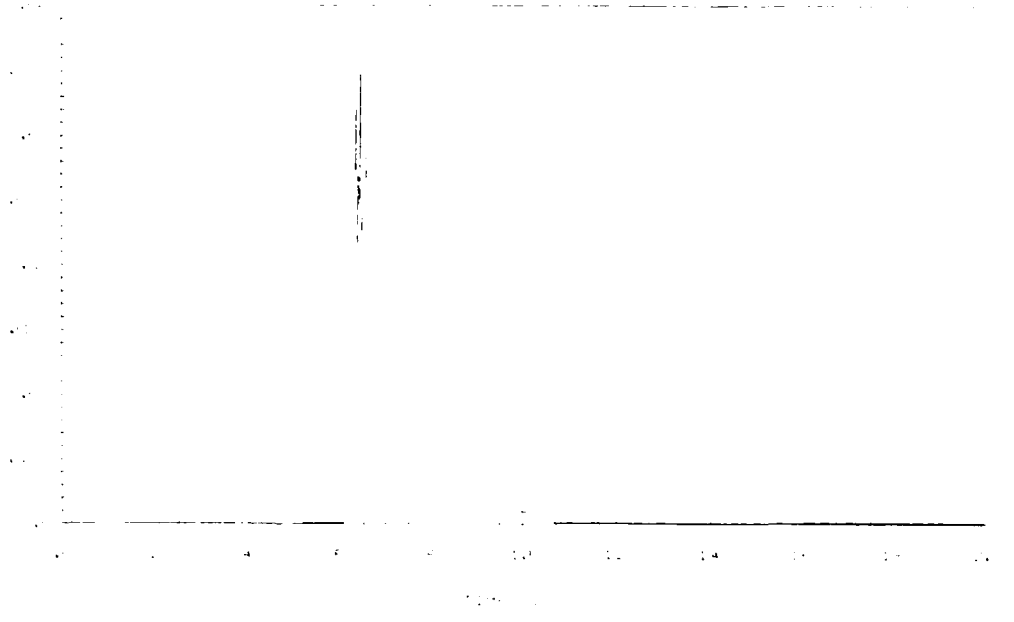

Figure 5-107. Covariance matrix element p21(kT) with sensor noise. (std. dev. = 0.00181 deg (deg/sec)). Scaled algorithm (SF = 100).

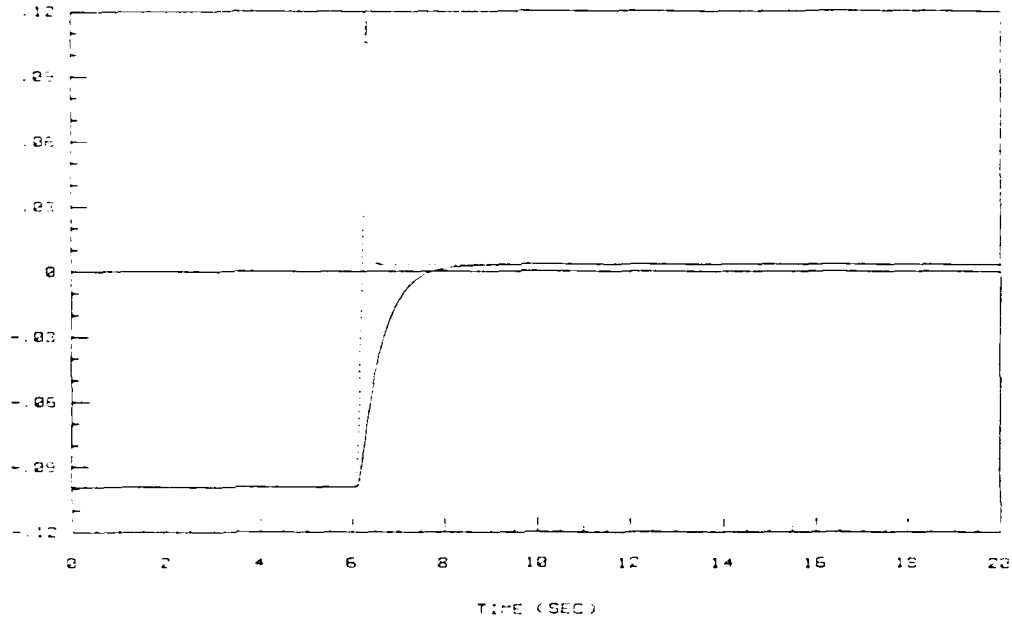

Figure 5-108. Estimate of step-response matrix element $h_{22}(kT)$ with sensor noise. (std. dev. = 0.00181 deg (deg/sec)). Scaled algorithm (SF = 100).

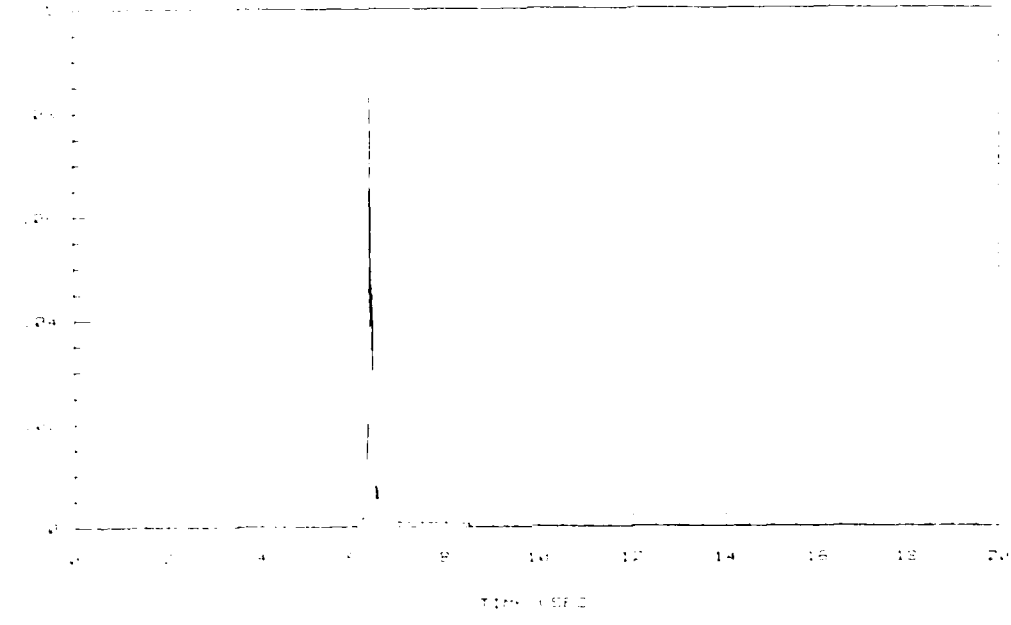

Figure 5-109. Covariance matrix element $p_{44}(kT)$ with sensor noise. (std. dev. = 0.00181 deg (deg/sec)). Scaled algorithm (SF = 100).

The closed-loop system response still exhibits a satisfactory behavior, although with noticeably higher levels of flaperon deflection rates (Figure 5-117). The bursting type of behavior shown by the flaperon deflection rate between seven and eight seconds in the simulation has its origin in the fluctuation of the filtered estimate of $h_{12}(kT)$ close to the zero axis during the same period of time. Overall, the performance of the identification algorithm is good with considerably less noise superimposed on the estimates, although the level of noise in this simulation seems to be approaching the limit for which adequate protection (against fluctuations close to the zero axis) can be provided with the scaling used (scale factor = 100 = (1/T)).

To verify if any additional beneficts can be obtained with increased scaling, a simulation was executed with a scale factor of 125. All the responses were identical from those of the simulation done with the scale factor of 100. All of the simulations executed with sensor noise seem to suggest that additional safeguards are needed in the case of step-response matrices with elements that are very close to zero.

5.3.5 Identification of Entire Parameter Vector with Full, and Reduced Order Models. As a final test of the adaptation mechanism, the estimation of the plant dynamics is carried out letting all of the elements of the parameter vector to "float" i.e. estimating all the parameters in the vector diference equation model of Eqns (3-9) and (3-10). This was done for a full order model (N = 4), and reduced order models of third (N = 3) and second (N = 2) order. All of the tests resulted in unstable aircraft responses. This is because the parameter estimates undergo large transients, particularly

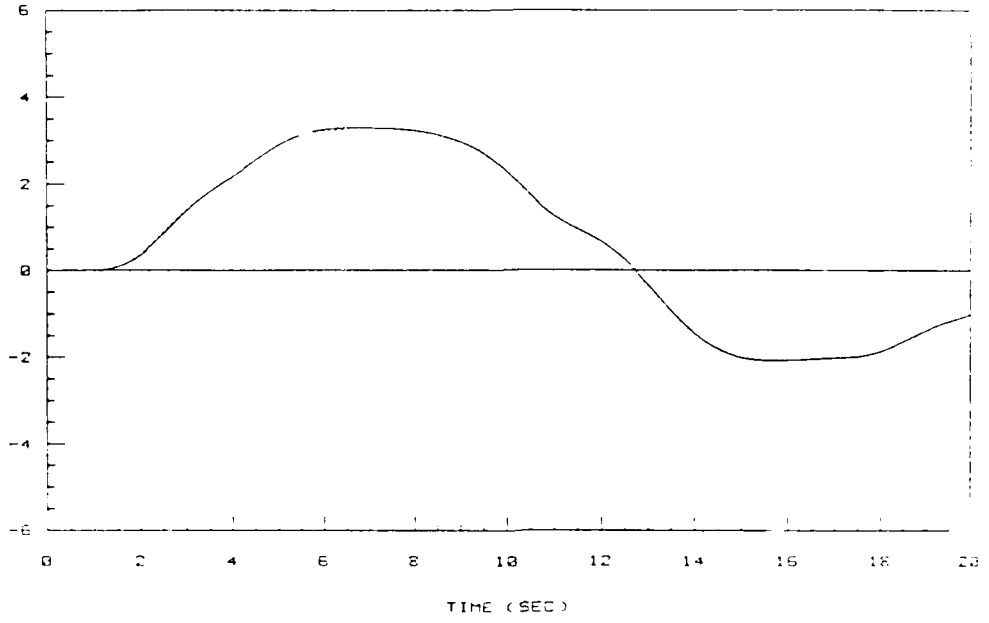

Figure 5-110. Flight path angle command and response (deg). Adaptive control law. Plant parameter change and sensor noise. (std. dev. = 0.00573 deg). Scaled algorithm (SF = 100).

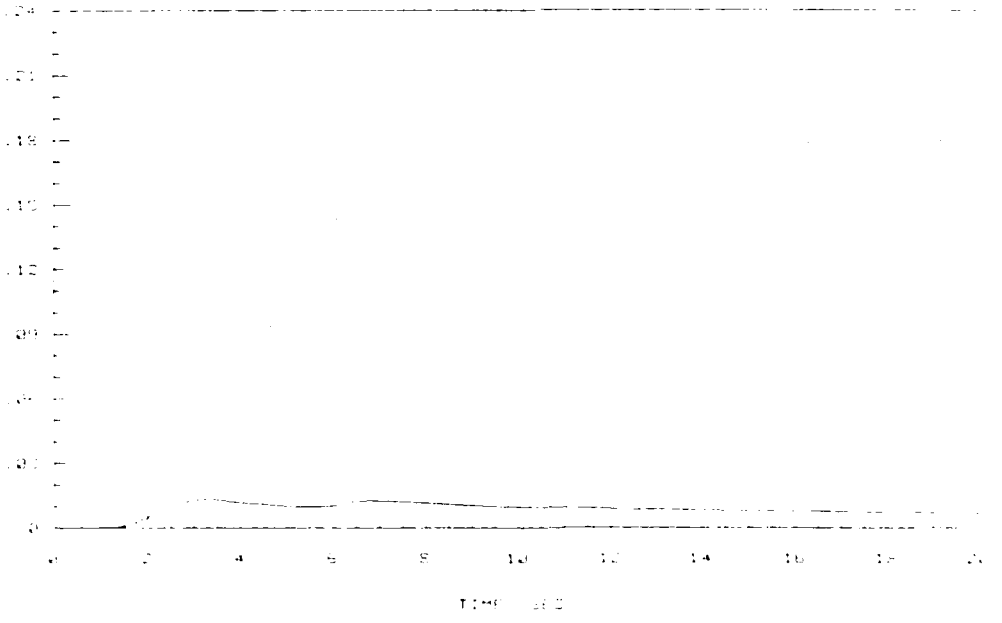

Figure 5-111. Flight path angle tracking performance index (deg). Adaptive control law. Plant parameter change and sensor noise. (std. dev. = 0.00573 deg). Scaled algorithm (SF = 100).

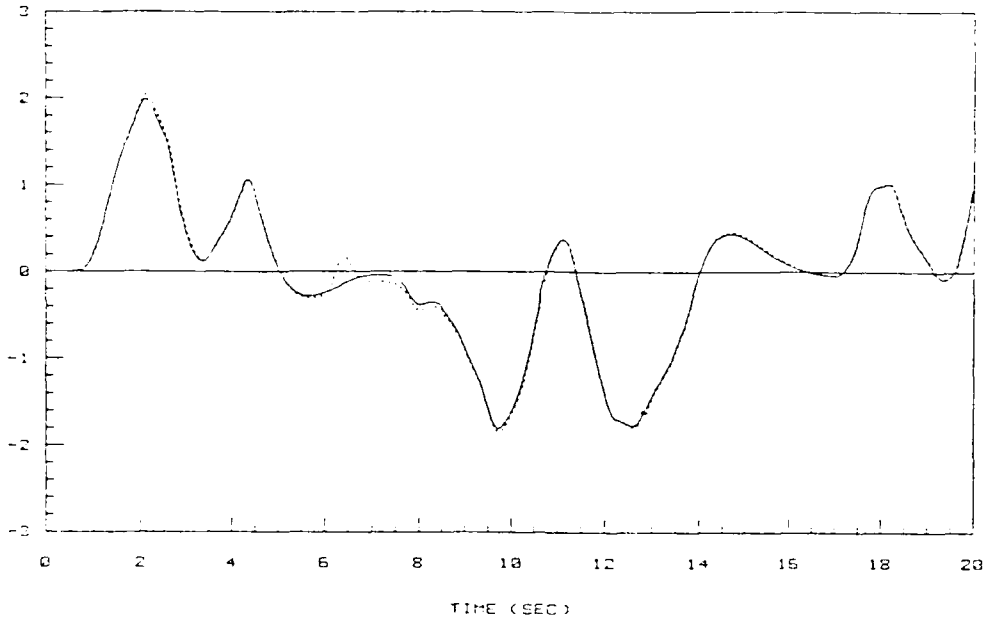

Figure 5-112. Pitch rate command and response (deg/sec). Adaptive control law. Plant parameter change and sensor noise. (std. dev. = 0.00573 deg/sec). Scaled algorithm (SF = 100).

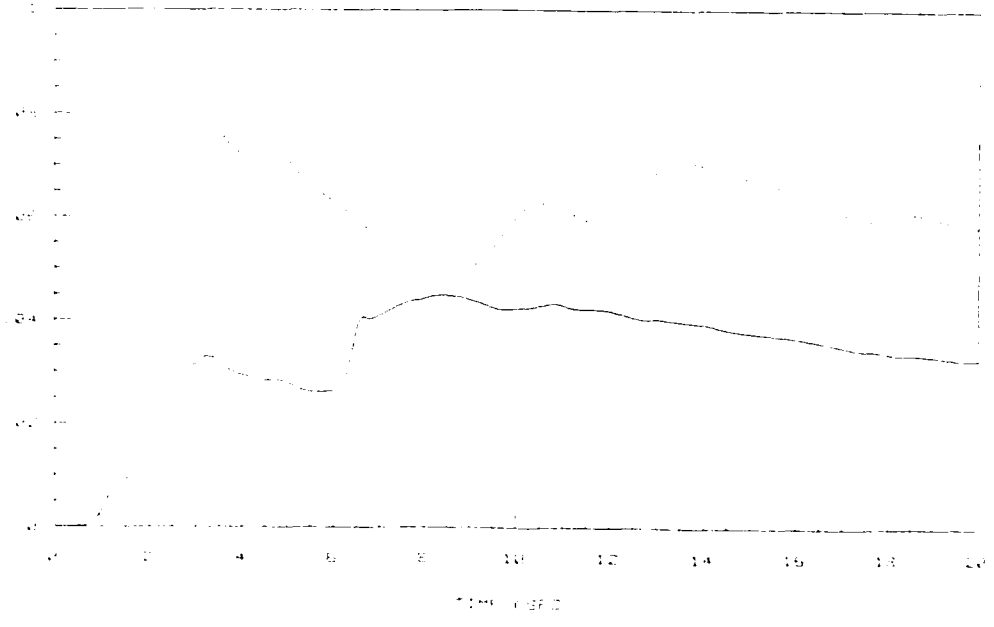

Figure 5-113. Pitch rate tracking performance index (deg/sec). Adaptive control law. Plant parameter change and sensor noise. (std. dev. = 0.00573 deg/sec). Scaled algorithm (SF = 100).

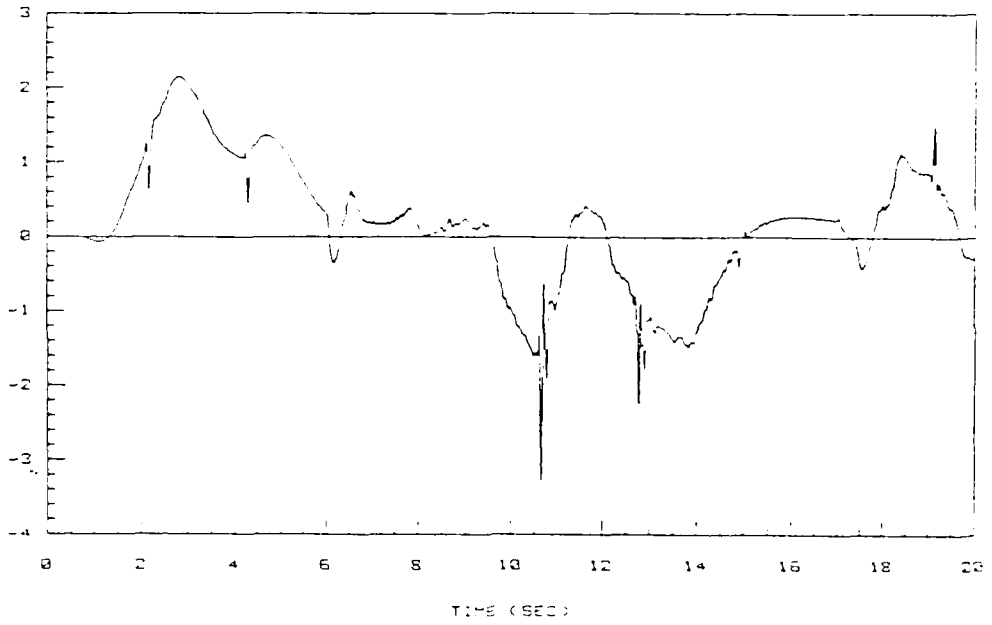

Figure 5-114. Elevator deflection (deg).
Adaptive control law. Plant parameter change and sensor noise.
(std. dev. = 0.00573 deg (deg/sec)). Scaled algorithm (SF = 100).

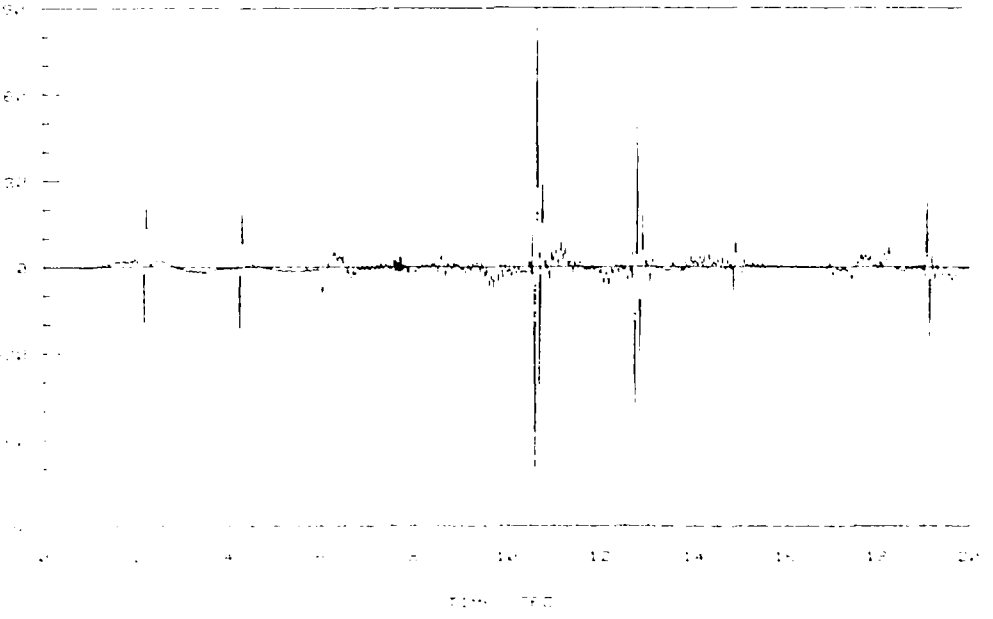

Figure 5-115. Elevator deflection rate (deg/sec).
Adaptive control law. Plant parameter change and sensor noise.
(std. dev. = 0.00573 deg (deg/sec)). Scaled algorithm (SF = 100).

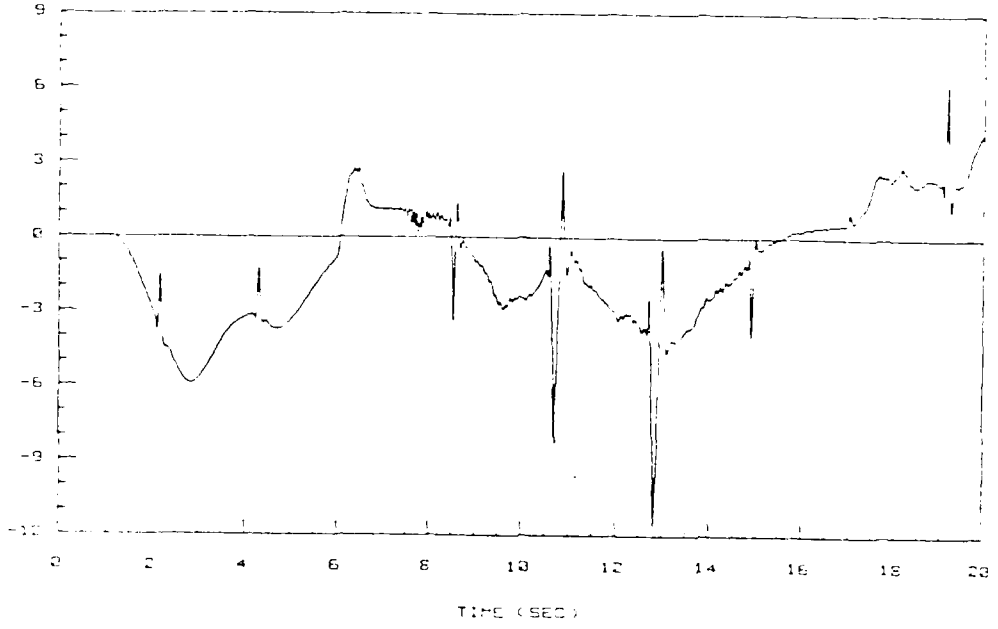

Figure 5-116. Flaperon deflection (deg).
Adaptive control law. Plant parameter change and sensor noise.
(std. dev. = 0.00573 deg (deg/sec)). Scaled algorithm (SF = 100).

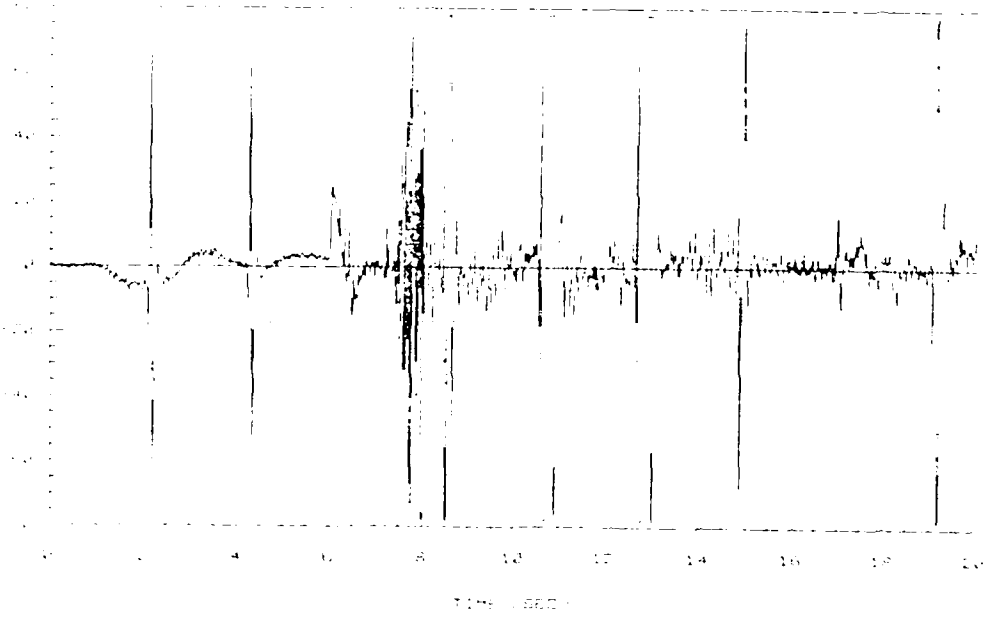

Figure 5-117. Flaperon deflection rate (deg/sec).
Adaptive control law. Plant parameter change and sensor noise.
(std. dev. = 0.00573 deg (deg/sec)). Scaled algorithm (SF = 100).

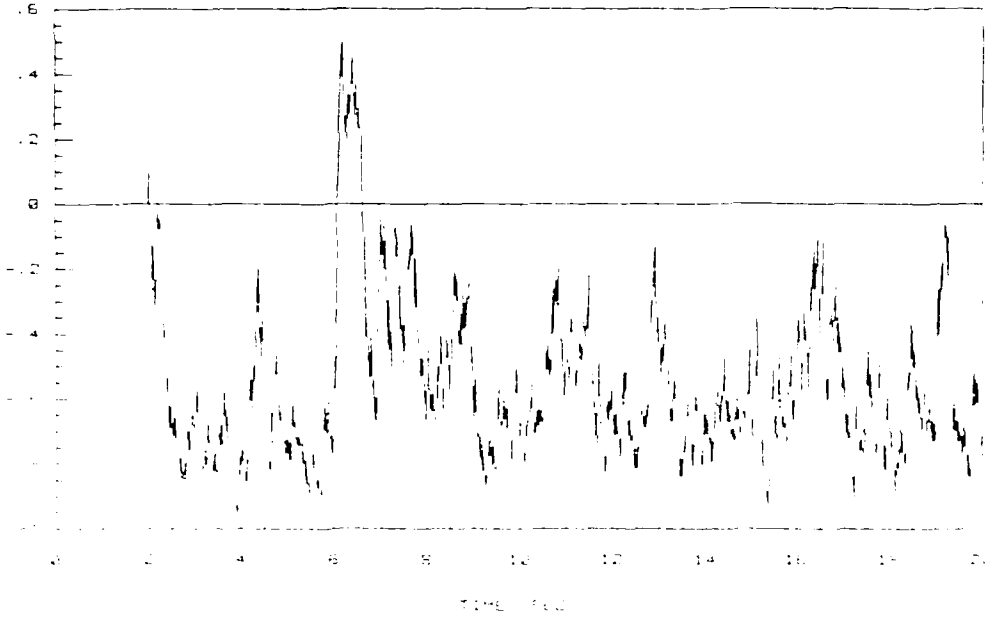

Figure 5-118. Fault detector test signal with sensor noise. (std. dev. = 0.00573 deg (deg/sec)). Scaled algorithm (SF = 100).

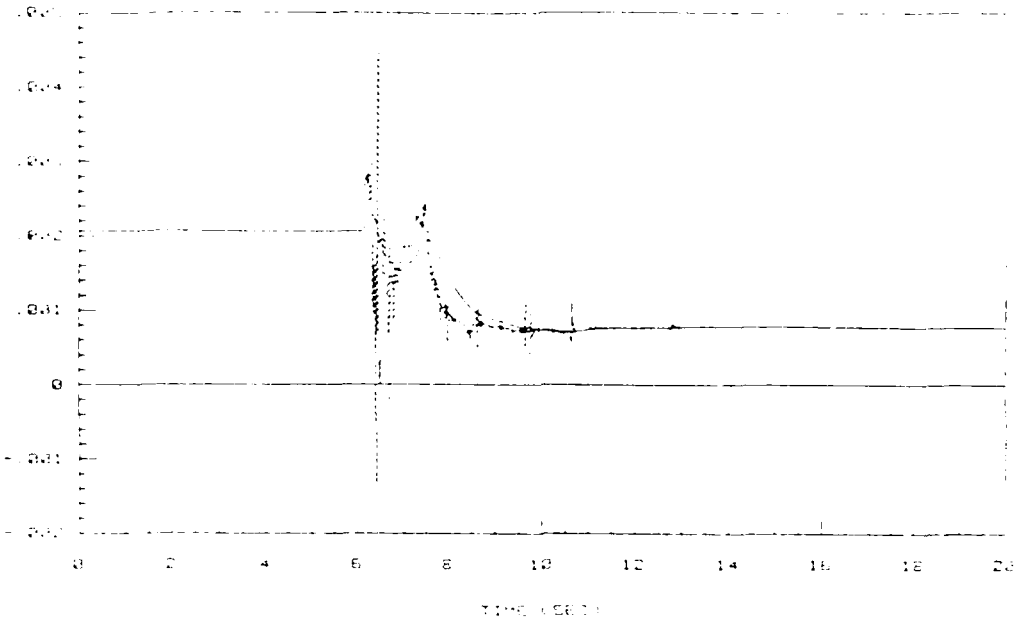

Figure 5-119. Estimate of step-response matrix element $h_{11}(kT)$ with sensor noise. (std. dev. = 0.00573 deg (deg/sec)). Scaled algorithm (SF = 100).

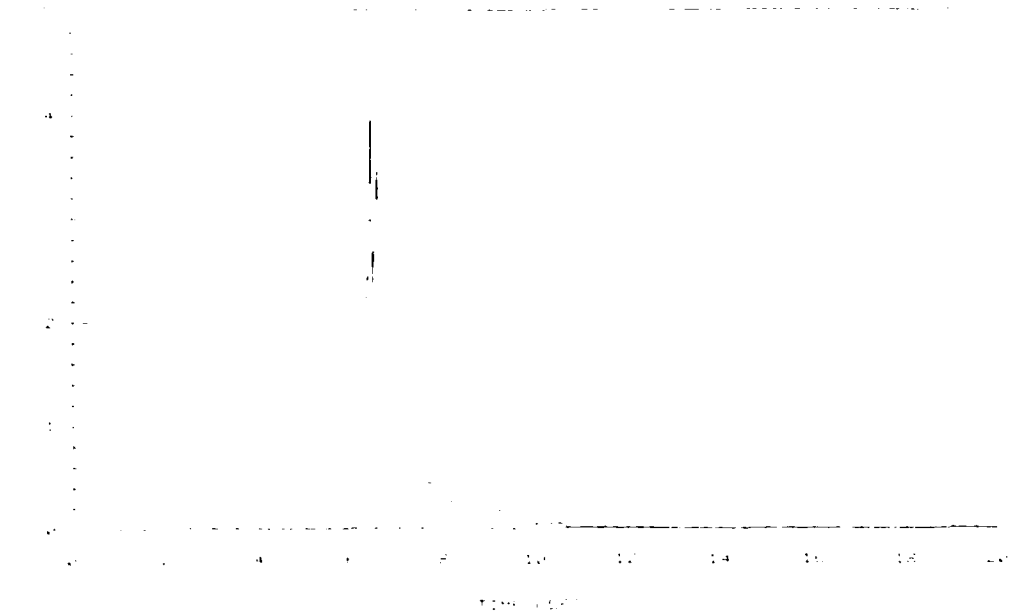

Figure 5-120. Covariance matrix element $p_{11}(kT)$ with sensor noise. (std. dev. = 0.00573 deg (deg/sec)). Scaled algorithm (SF = 100).

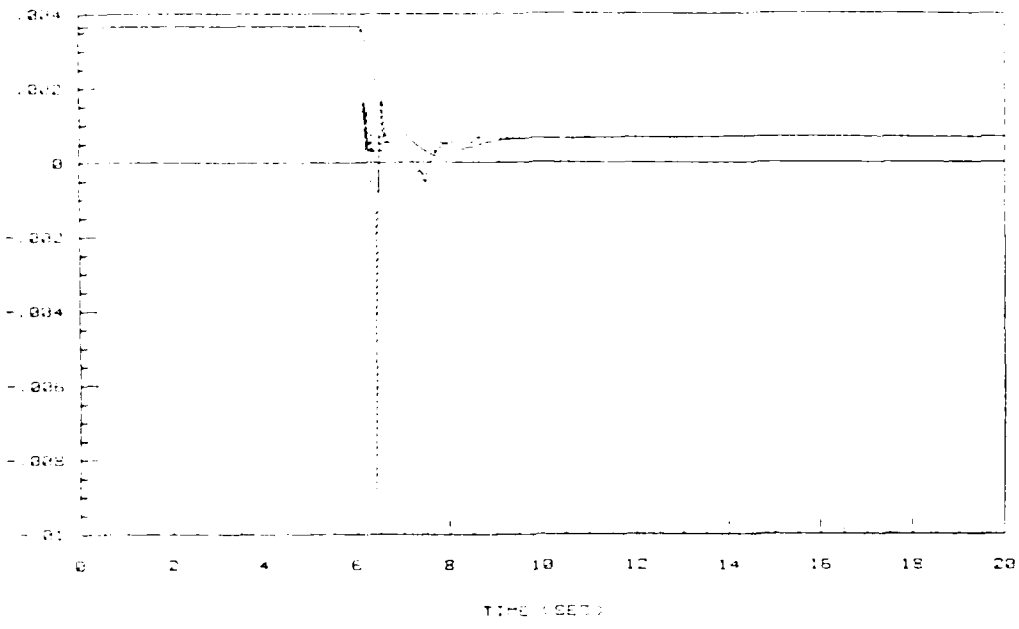

Figure 5-121. Estimate of step-response matrix element $h_{12}(kT)$ with sensor noise. (std. dev. = 0.00573 deg (deg/sec)). Scaled algorithm (SF = 100).

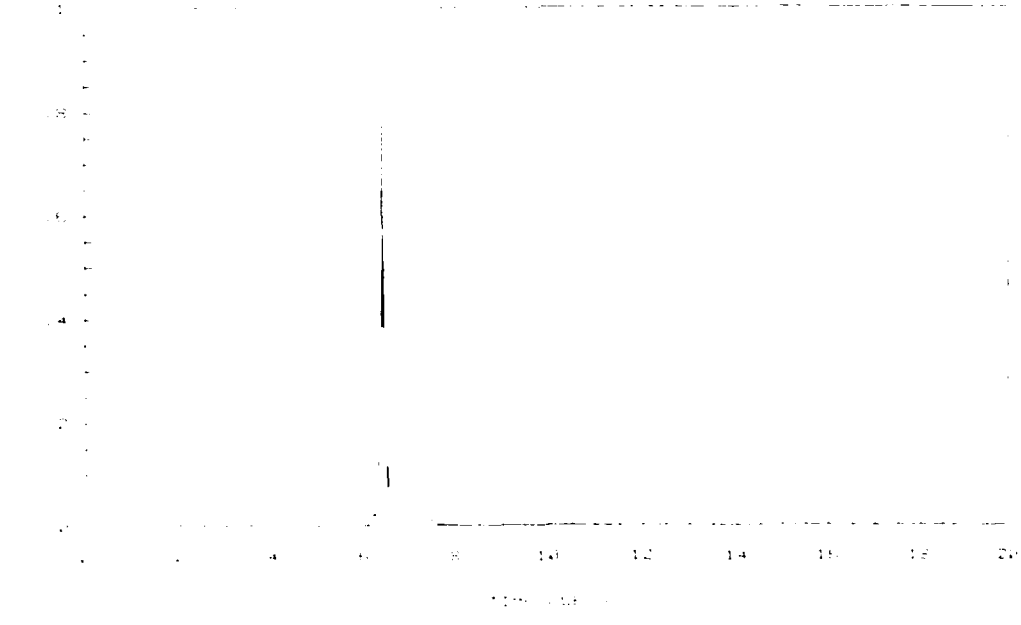

Figure 5-122. Covariance matrix element $p_{22}(kT)$ with sensor noise. (std. dev. = 0.00573 deg (deg/sec)). Scaled algorithm (SF = 100).

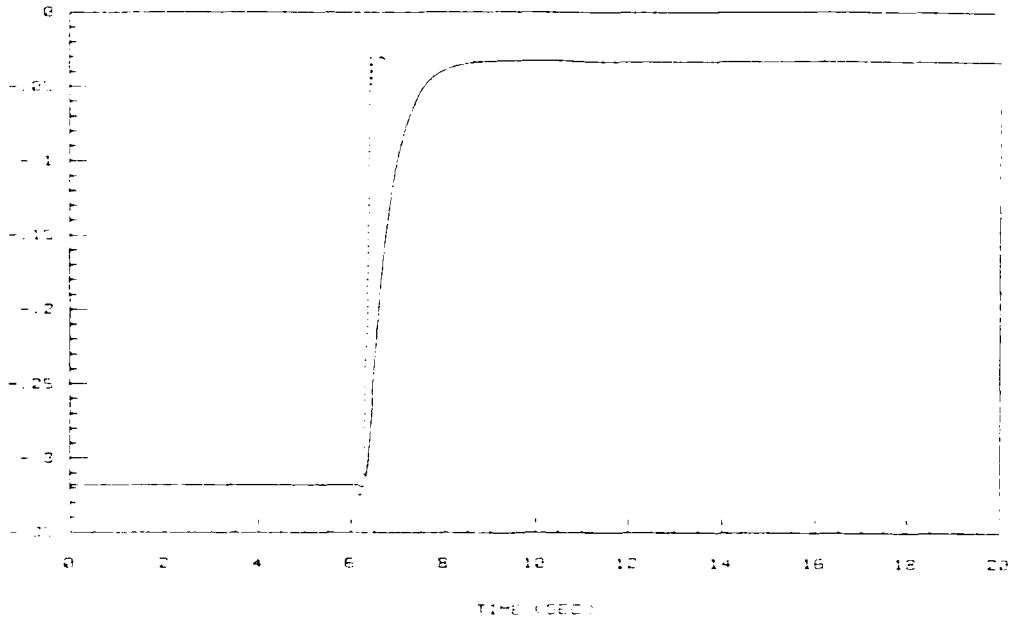

Figure 5-123. Estimate of step-response matrix element $h_{21}(kT)$ with sensor noise. (std. dev. = 0.00573 deg (deg/sec)). Scaled algorithm (SF = 100).

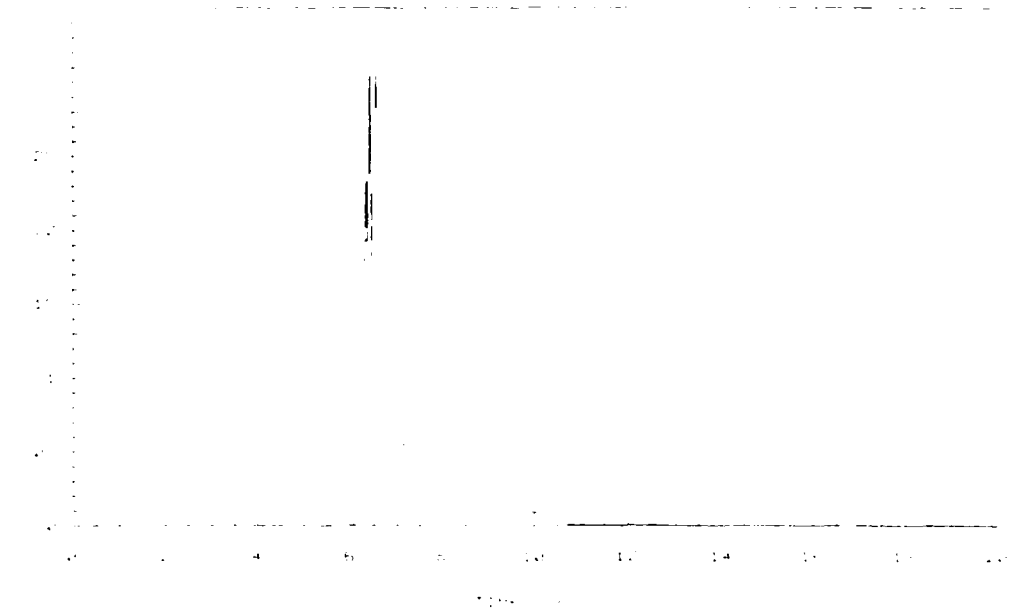

Figure 5-124. Covariance matrix element $p_{22}(kT)$ with sensor noise. (std. dev. = 0.00573 deg (deg/sec)). Scaled algorithm (SF = 100).

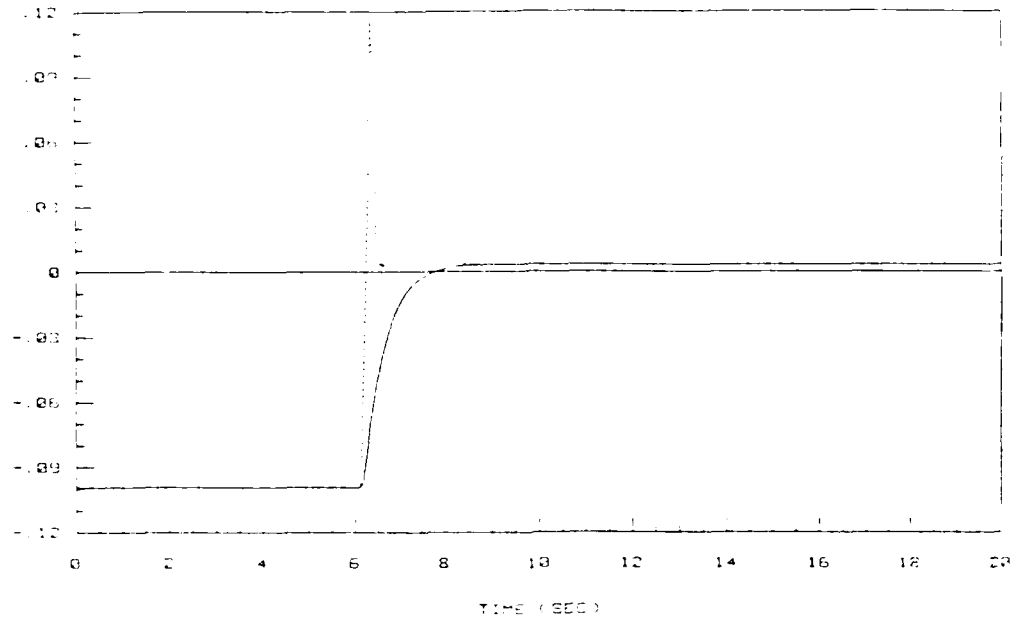

Figure 5-125. Estimate of step-response matrix element $h_{22}(kT)$ with sensor noise. (std. dev. = 0.00573 deg (deg/sec)). Scaled algorithm (SF = 100).

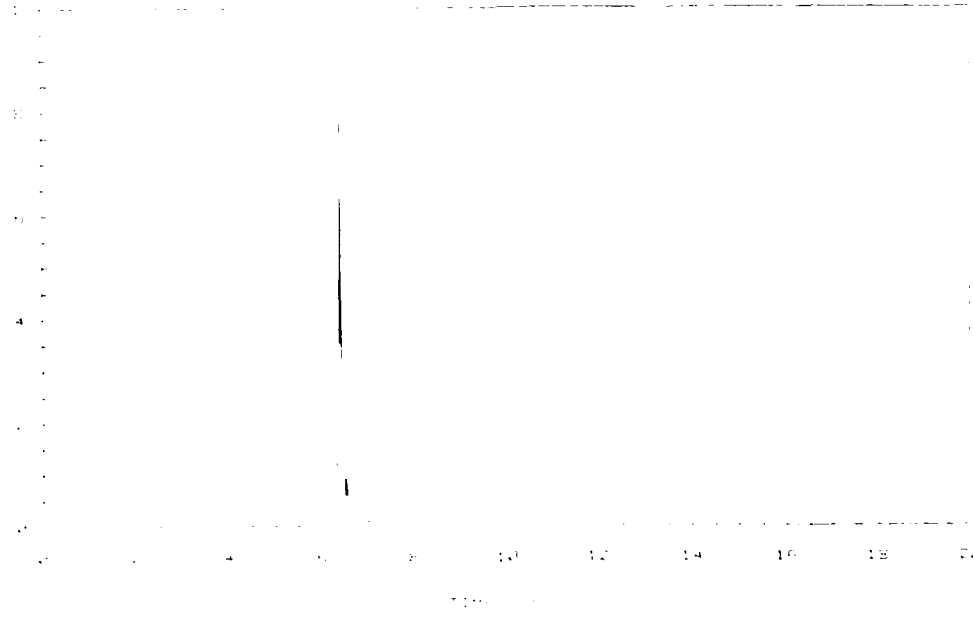

Figure 5-126. Covariance matrix element $p_{44}(kT)$ with sensor noise. (std. dev. = 0.00573 deg (deg/sec)). Scaled algorithm (SF = 100).

around zero. As explained before, these transients drive the control surfaces to their deflection rate limits for too long. This results in an excesive phase lag for the control action, and the encountering of surface deflections limits. All of these factors subsequently result in loss of control of the open-loop unstable plant.

The large transients and the seemingly long convergence time for the estimates are mainly the result of two conditions. First, the larger number of parameters to be identified puts additional demands on the level of excitation required for good identifcation to take place (see section 3.3). With an excitation level smaller than the ideal (for the particular number of parameters involved) the estimator will take a longer time to converge so that it can accumulate enough information that allows the calculation of a reasonably precise estimate.

Finally, the parametrization used for defining the input-output model suffers from so called identifiability problems emerging from pole-zero cancelation effects. When obtaining the output functions for the multi-input multi-output plant using the common denominator obtained from the tranfer matrix, the numerator polynomials may be forced to contain additional terms in order to match the form of the denominator. The introduction of these terms equates to the introduction of zeros that are not really part of the system, but rather the result of the algebra used in obtaining the input-output model. These "artificial zeros" simply cancel those poles of the common denominator that are not involved in the particular output function in question, while preserving the chosen structure of the input-output model. The resulting model is thus considered a nonminimal representation of the plant i.e. it

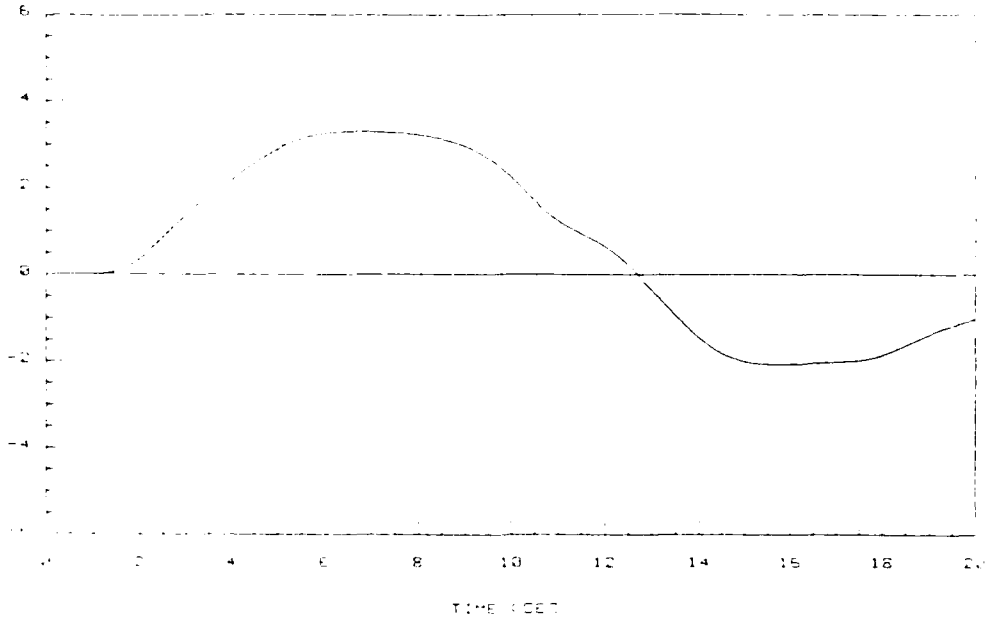

Figure 5-127. Flight path angle command and response (deg).
Adaptive control law. Plant parameter change.
Identification of full 4th order model.

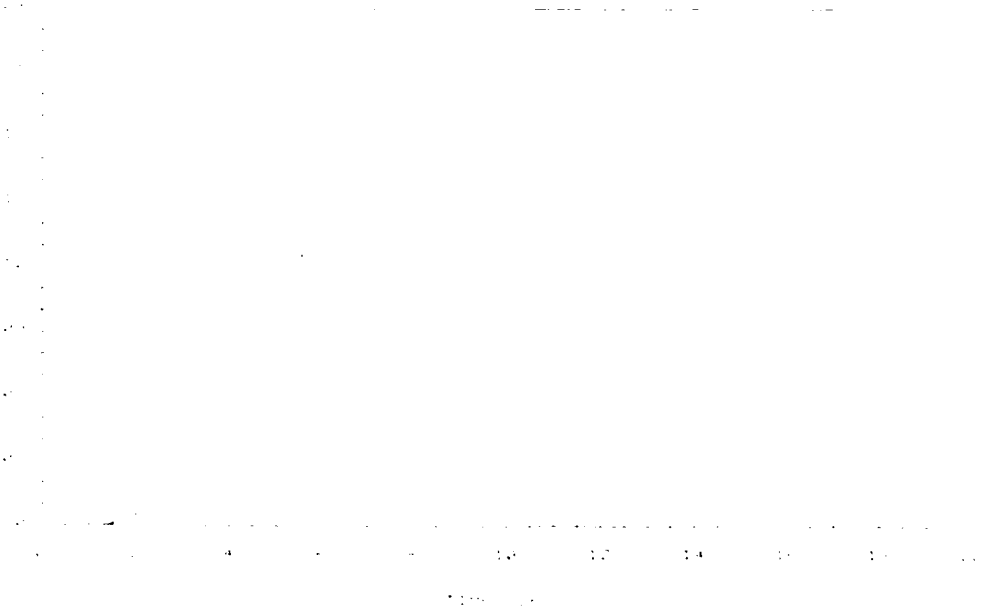

Figure 5-128. Flight path angle tracking performance index (deg).
Adaptive control law. Plant parameter change.
Identification of full 4th order model.

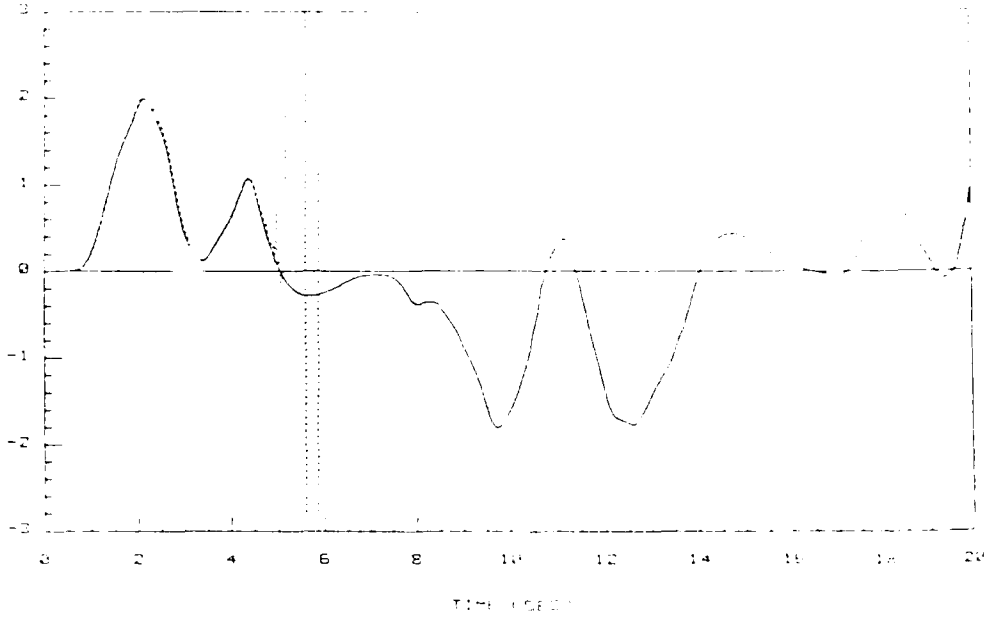

Figure 5-129. Pitch rate command and response (deg/sec).
Adaptive control law. Plant parameter change.
Identification of full 4th order model.

Figure 5-130. Pitch rate tracking performance index (deg sec).
Adaptive control law. Plant parameter change.
Identification of full 4th order model.

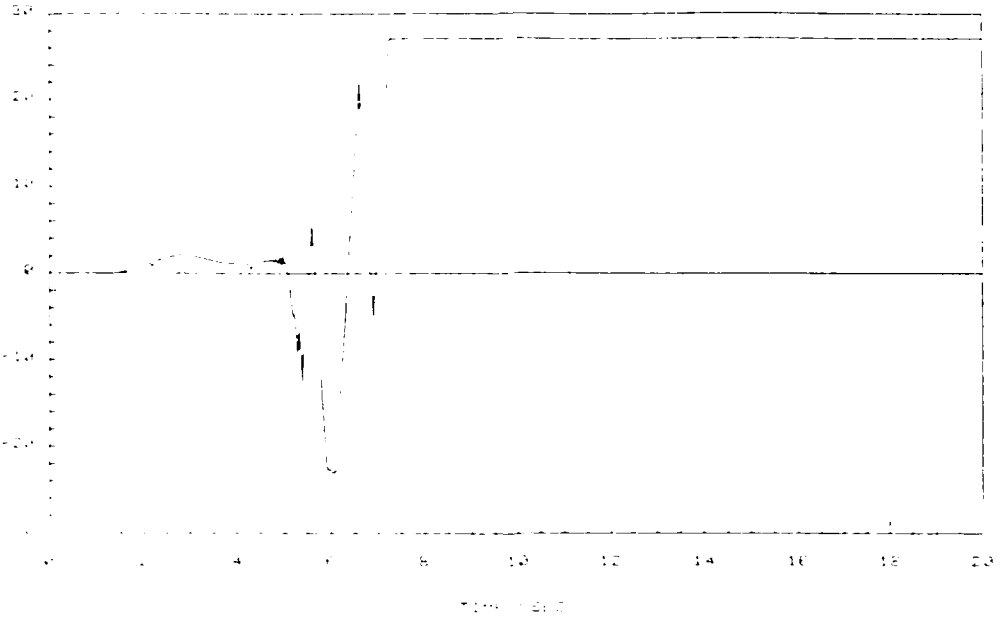

Figure 5-131. Elevator deflection (deg).
Adaptive control law. Plant parameter change.
Identification of full 4th order model.

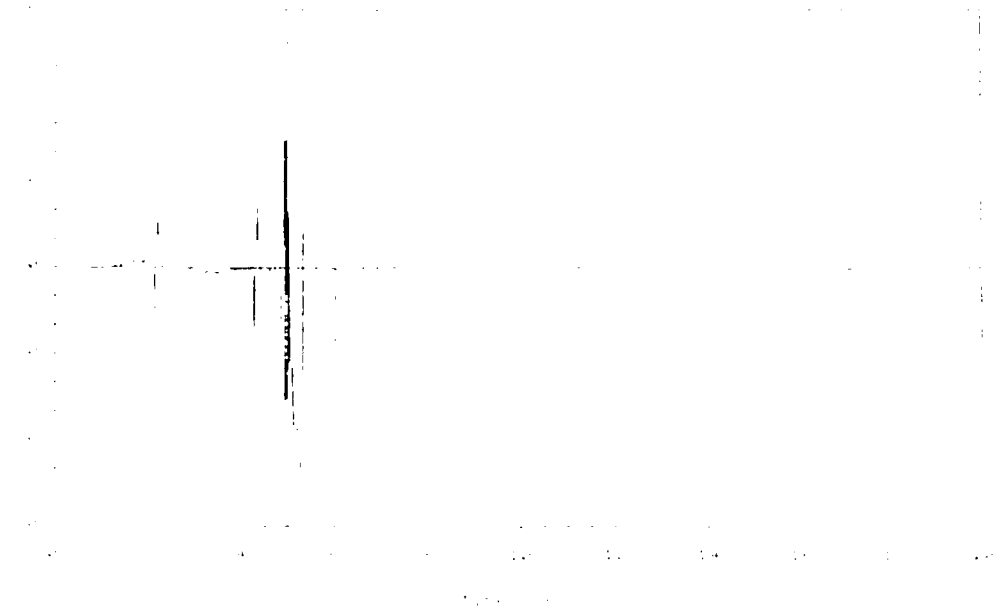

Figure 5-132. Elevator deflection (deg).
Adaptive control law. Plant parameter change.
Identification of full 4th order model.

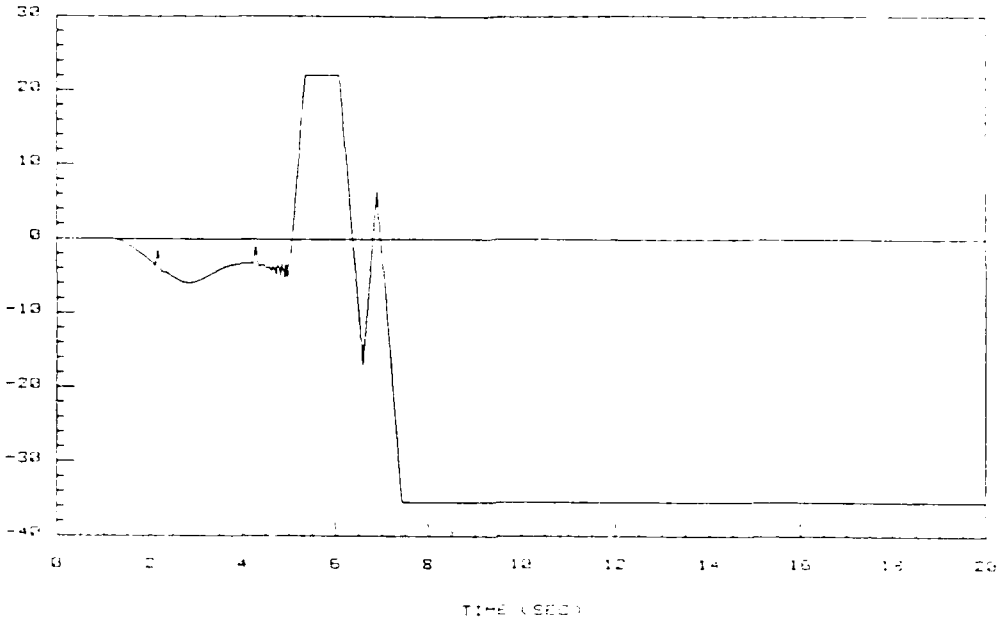

Figure 5-133. Flaperon deflection (deg).
Adaptive control law. Plant parameter change.
Identification of full 4th order model.

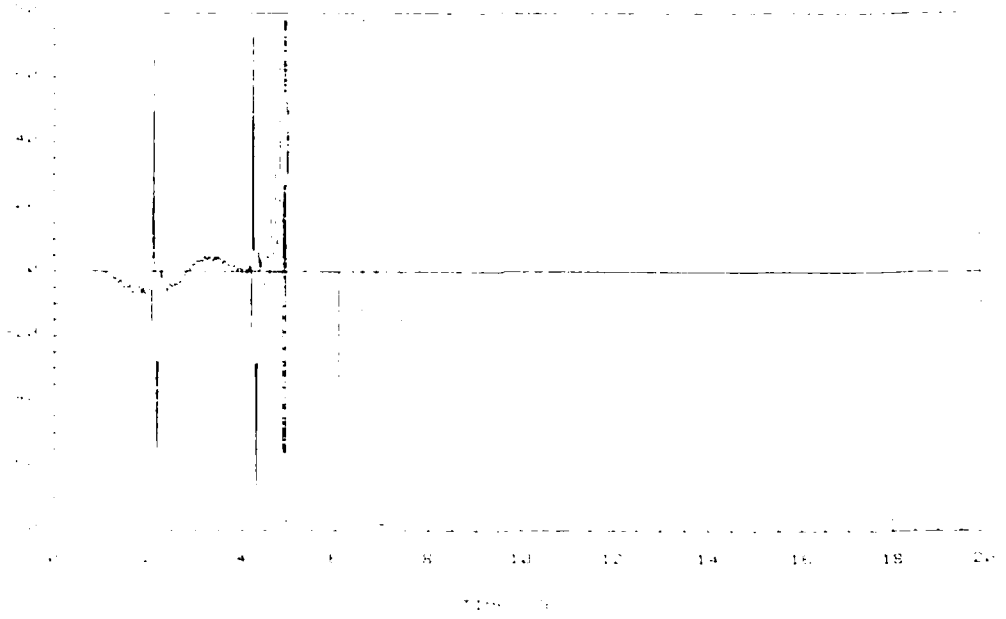

Figure 5-134. Flaperon deflection rate (deg/sec).
Adaptive control law. Plant parameter change.
Identification of full 4th order model.

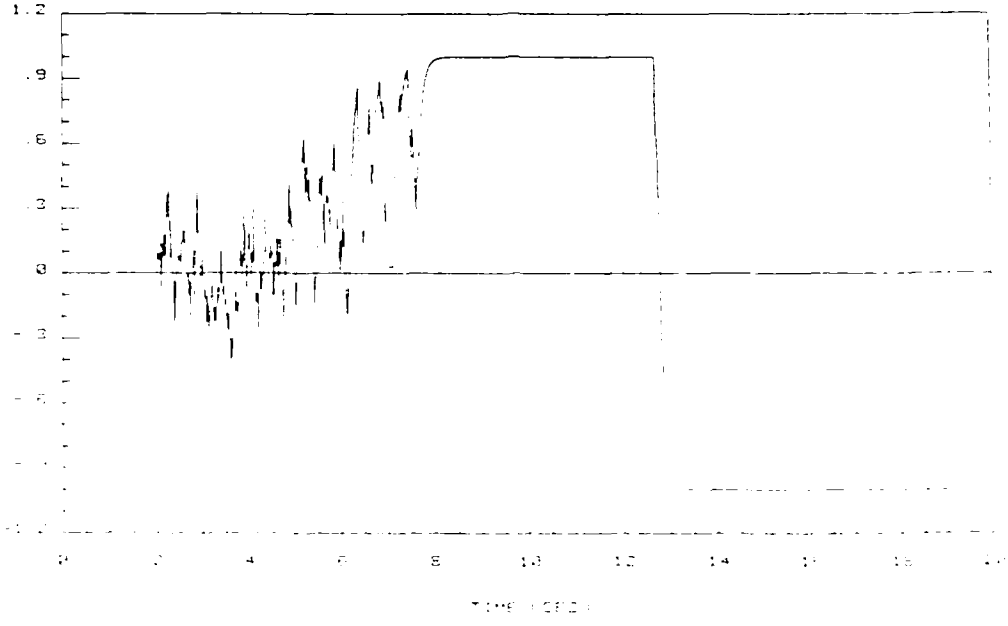

Figure 5-135. Fault detector test signal.
Identification of full 4th order model.

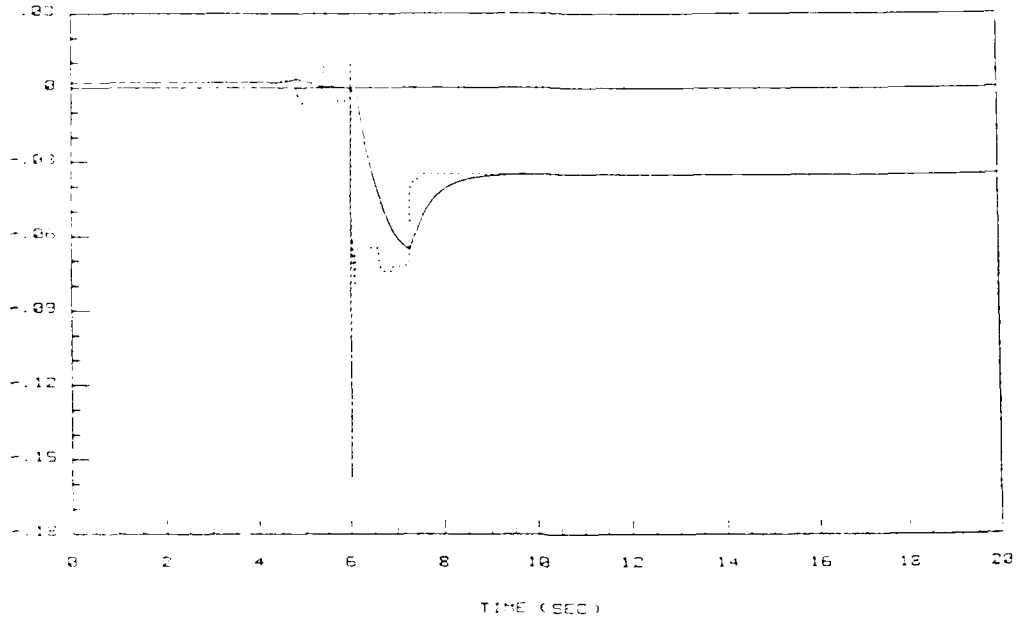

Figure 5-136. Estimate of step-response matrix element $h_{11}(kT)$ Identification of full 4th order model.

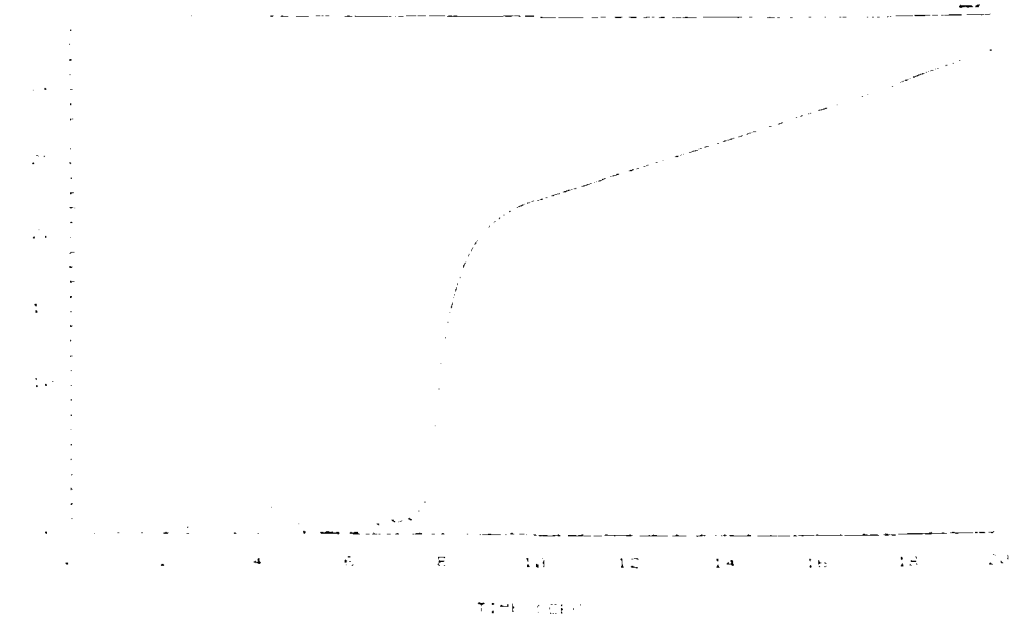

Figure 5-137. Covariance matrix element $c_{11}(kT)$. Identification of full 4th order model.

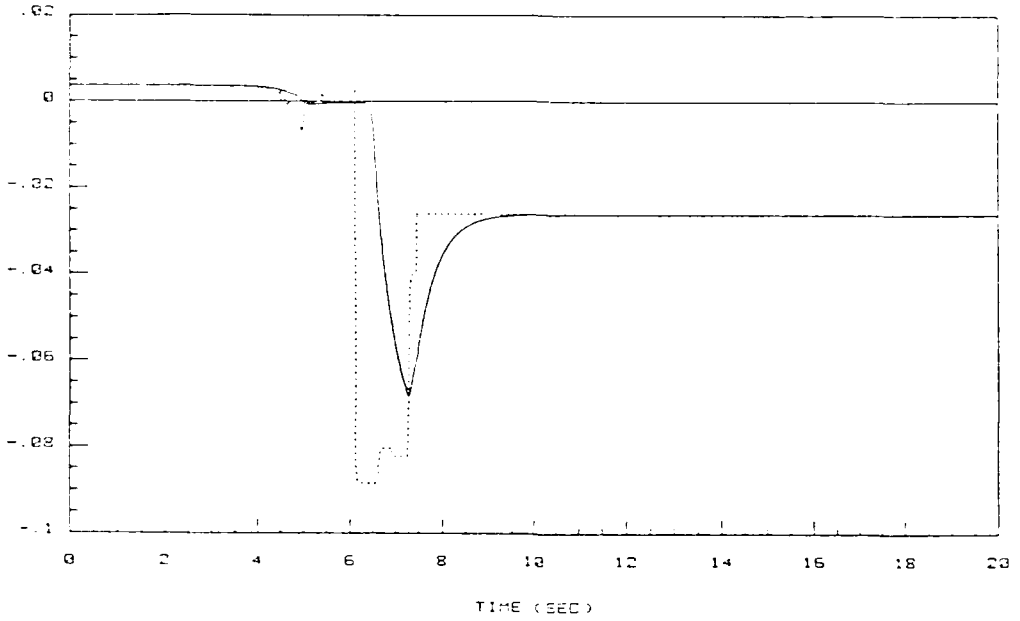

Figure 5-138. Estimate of step-response matrix element $h_{12}(kT)$. Identification of full 4th order model.

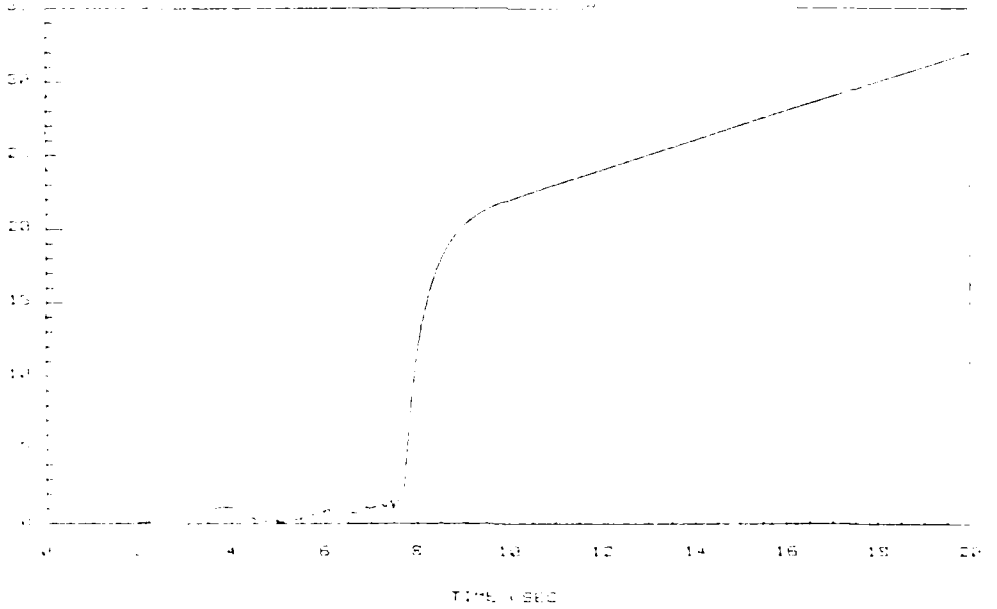

Figure 5-139. Covariance matrix element $p_{22}(kT)$. Identification of full 4th order model.

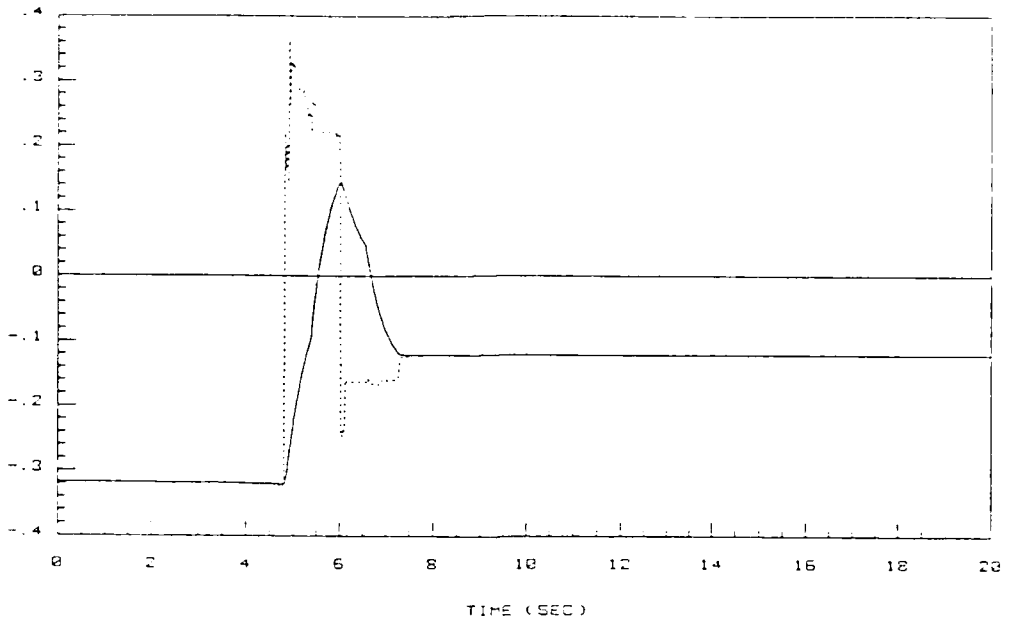

Figure 5-140. Estimate of step-response matrix element $h_{21}(kT)$. Identification of full 4th order model.

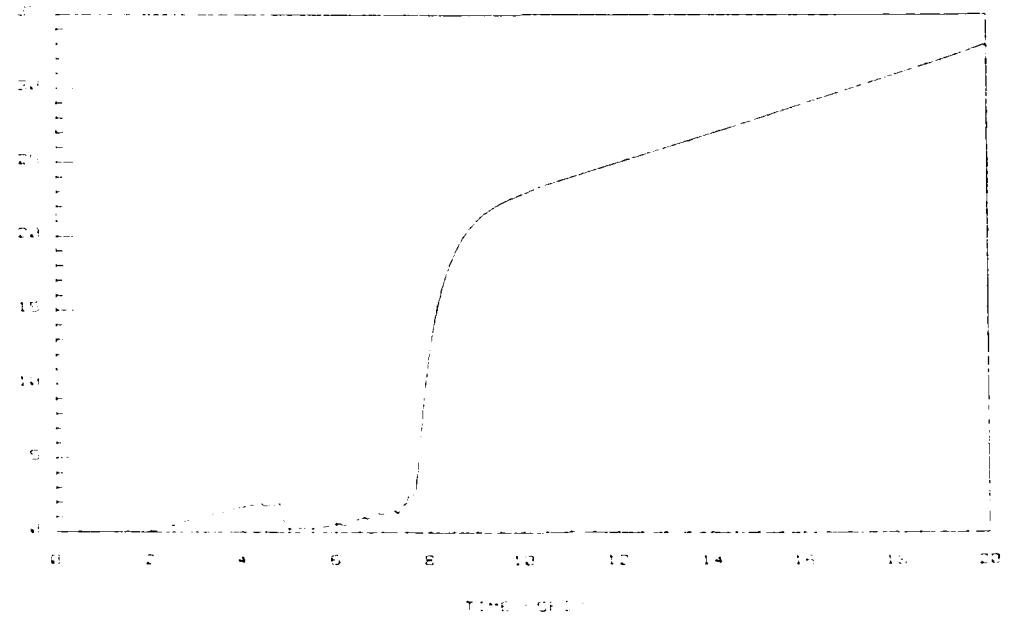

Figure 5-141. Covariance matrix element $p_{33}(kT)$. Identification of full 4th order model.

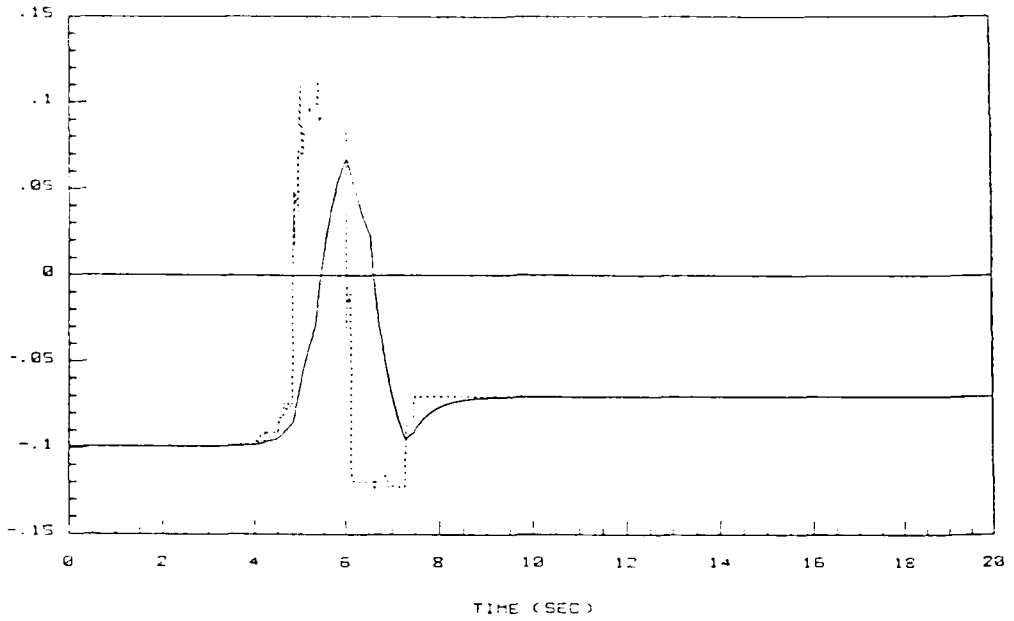

Figure 5-142. Estimate of step-response matrix element $h_{22}(kT)$. Identification of full 4th order model.

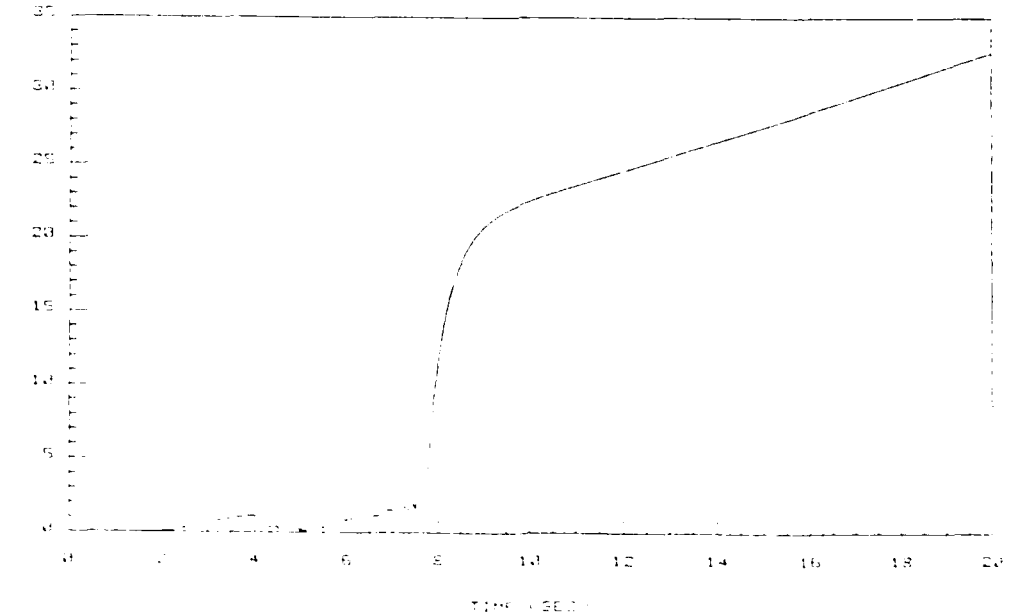

Figure 5-143. Covariance matrix element $p_{44}(kT)$. Identification of full 4th order model.

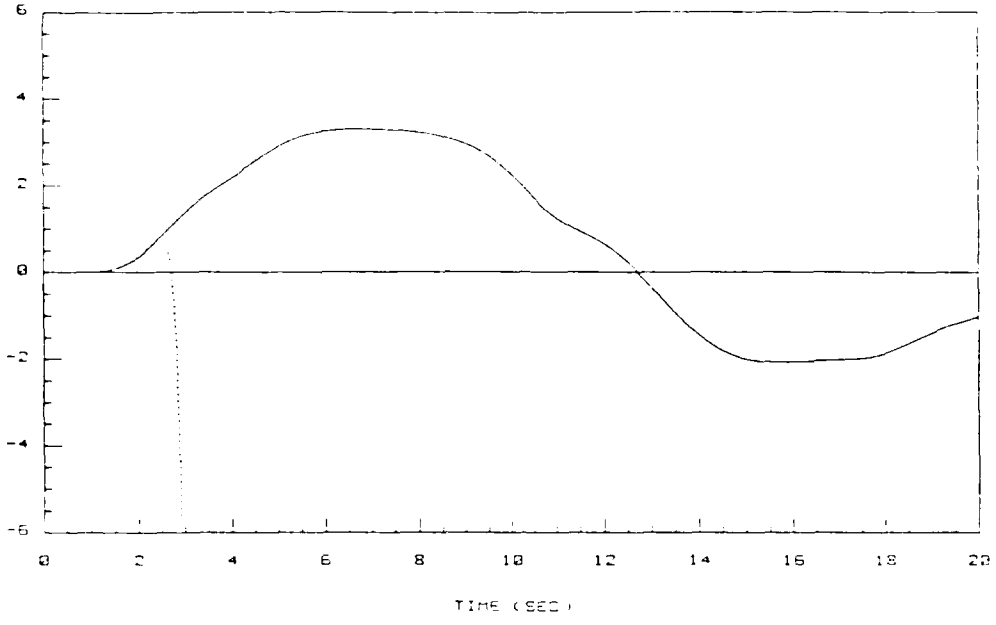

Figure 5-144. Flight path angle command and response (deg).
Adaptive control law. Plant parameter change.
Identification of full 3rd order model.

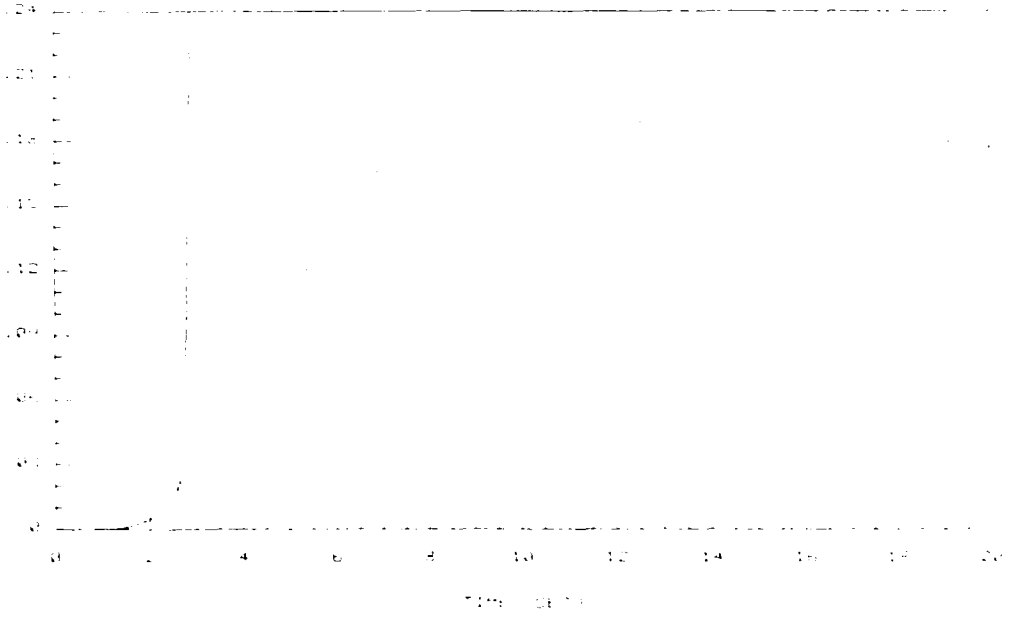

Figure 5-145. Flight path angle tracking performance index (deg).
Adaptive control law. Plant parameter change.
Identification of full 3rd order model.

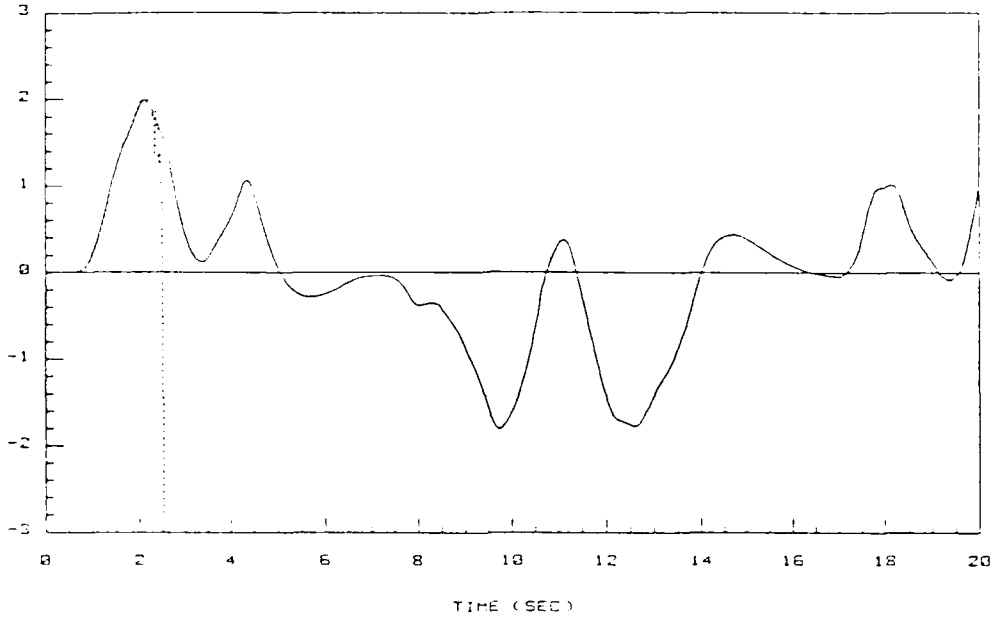

Figure 5-146. Pitch rate command and response (deg/sec).
Adaptive control law. Plant parameter change.
Identification of full 3rd order model.

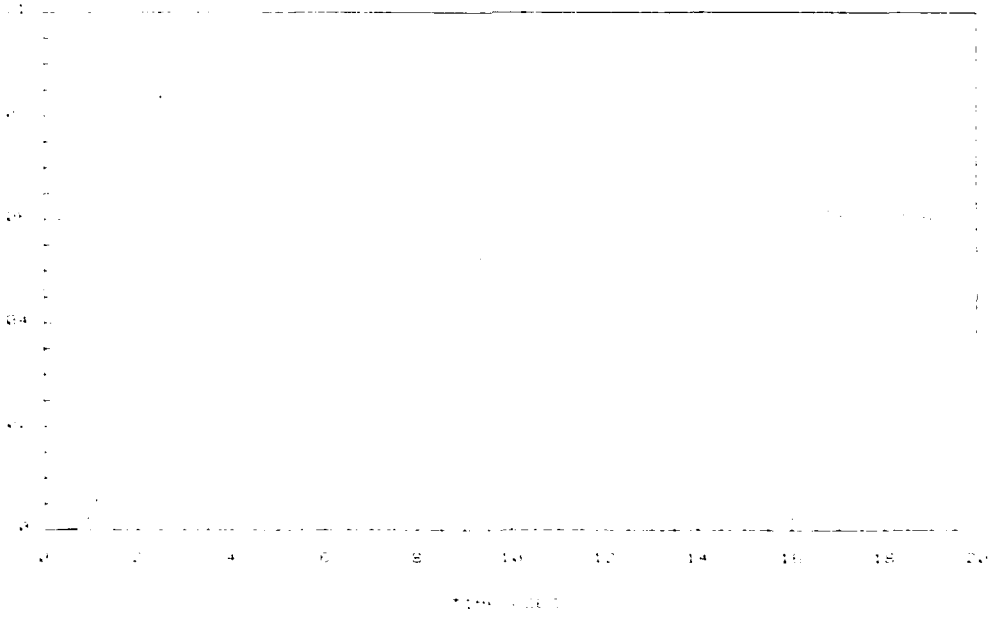

Figure 5-147. Pitch rate tracking performance index (deg/sec).
Adaptive control law. Plant parameter change.
Identification of full 3rd order model.

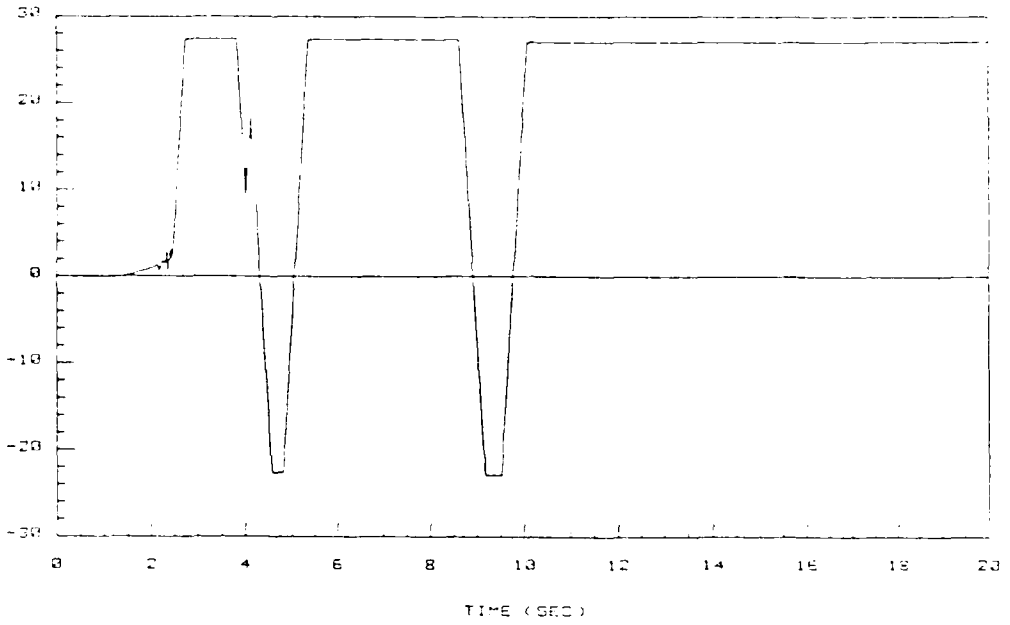

Figure 5-148. Elevator deflection (deg).
Adaptive control law. Plant parameter change.
Identification of full 3rd order model.

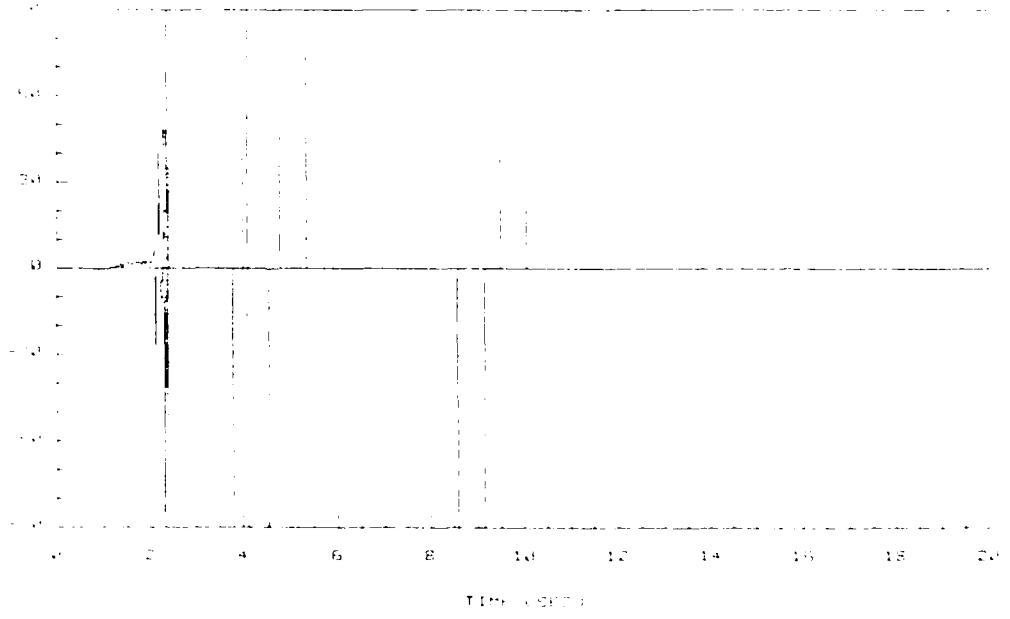

Figure 5-149. Elevator deflection rate (deg/sec).
Adaptive control law. Plant parameter change.
Identification of full 3rd order model.

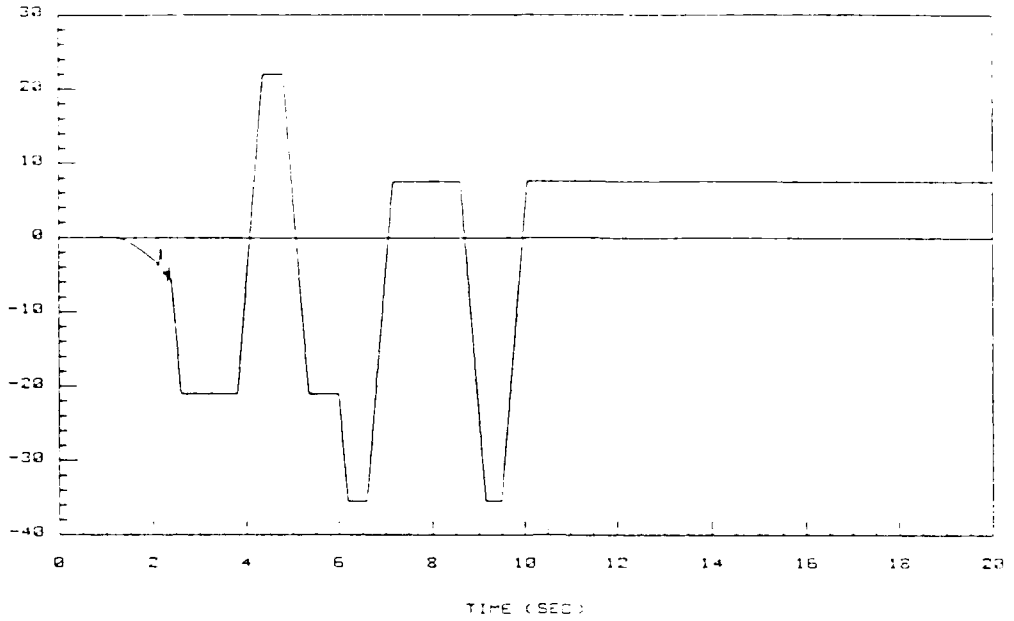

Figure 5-150. Flaperon deflection (deg).
Adaptive control law. Plant parameter change.
Identification of full 3rd order model.

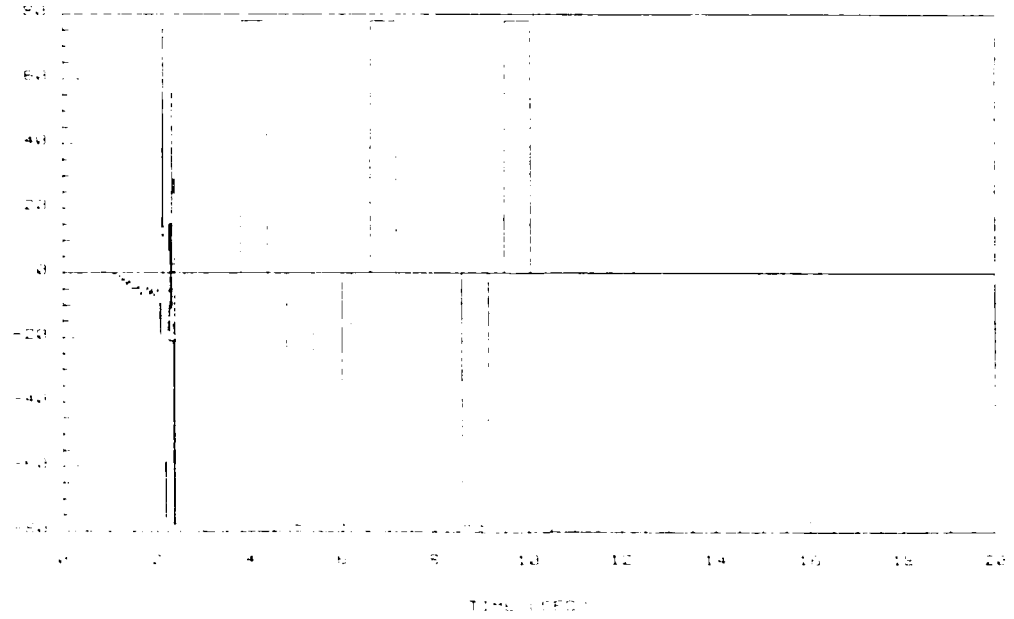

Figure 5-151. Flaperon deflection rate (deg/sec).
Adaptive control law. Plant parameter change.
Identification of full 3rd order model.

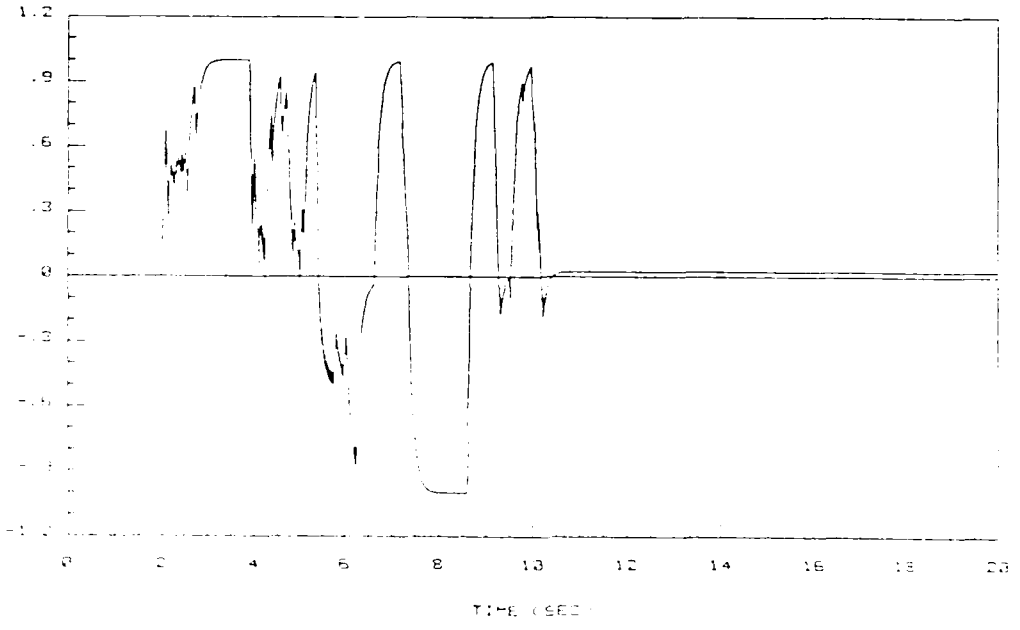

Figure 5-152. Fault detector test signal.
Identification of full 3rd order model.

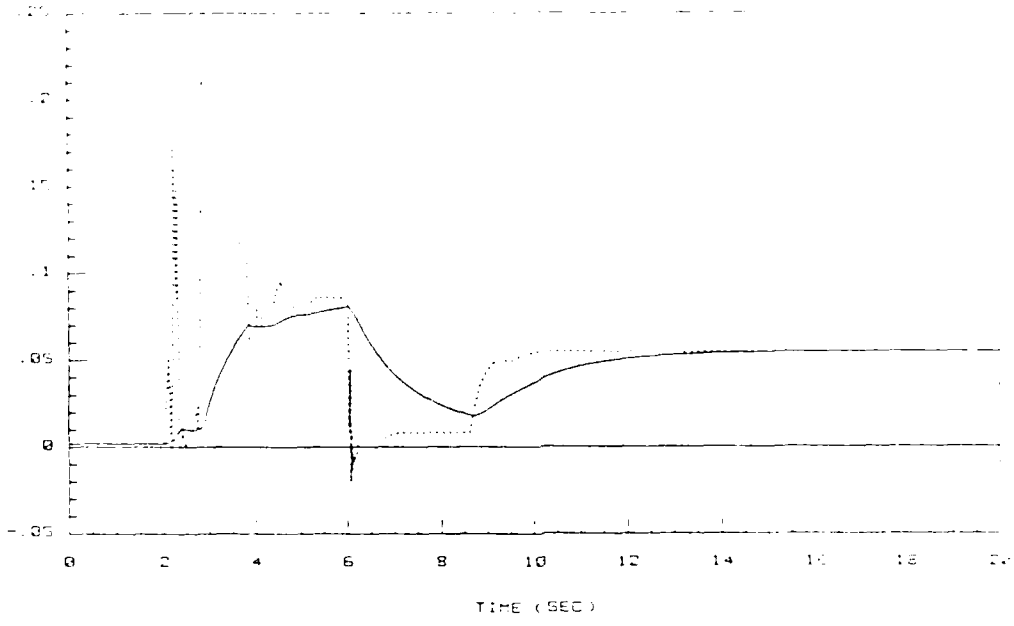

Figure 5-153. Estimate of step-response matrix element $h_{11}(kT)$ Identification of full 3rd order model.

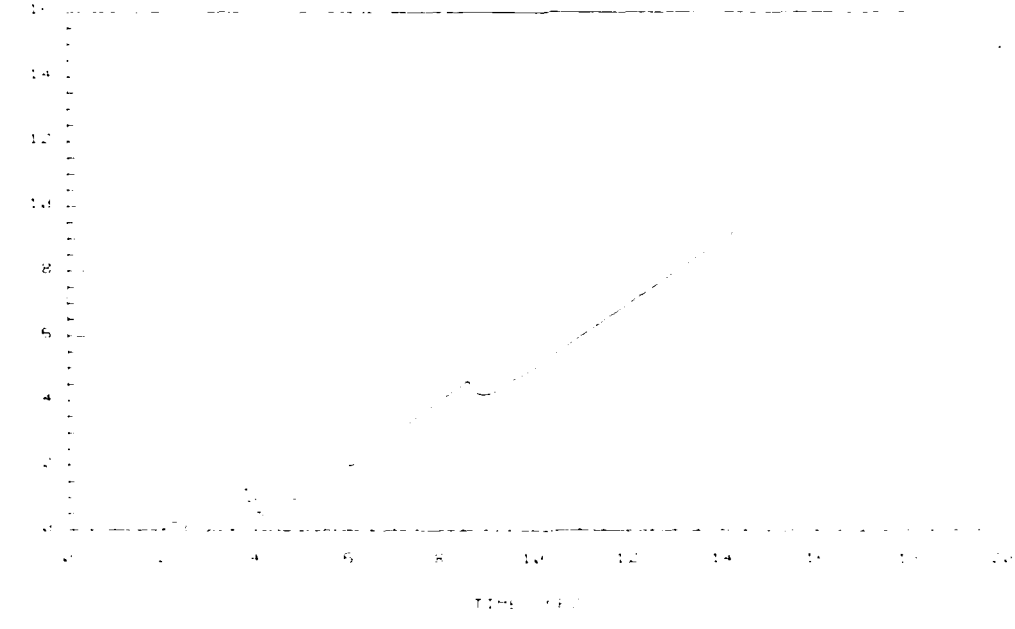

Figure 5-154. Covariance matrix element $p_{11}(kT)$. Identification of full 3rd order model.

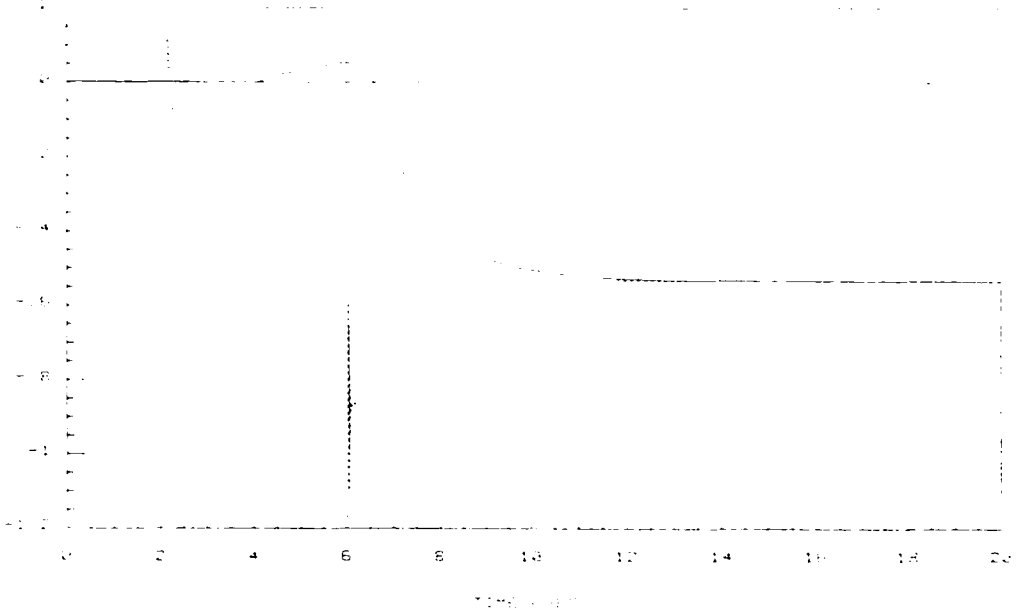

Figure 5-155. Estimate of step-response matrix element $h_{12}(kT)$. Identification of full 3rd order model.

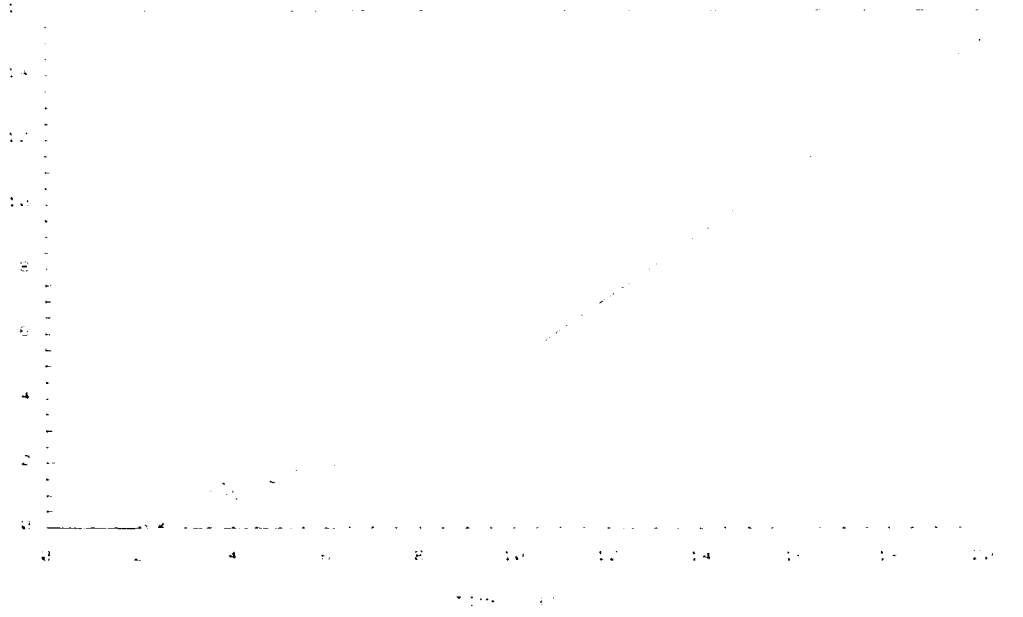

Figure 5-156. Covariance matrix element $p_{22}(kT)$. Identification of full 3rd order model.

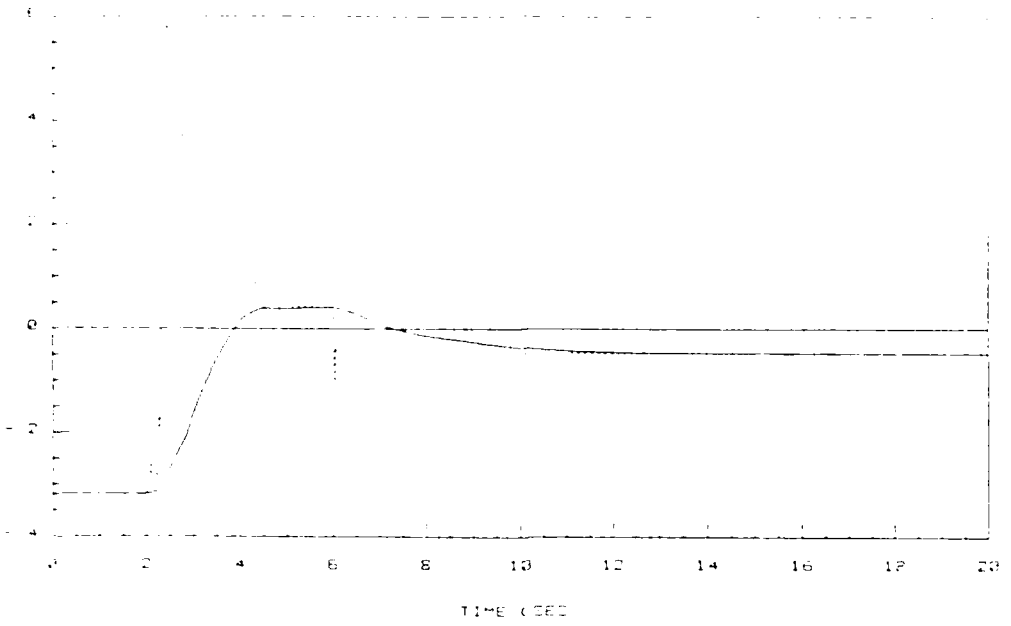

Figure 5-157. Estimate of step-response matrix element $h_{21}(\kappa T)$. Identification of full 3rd order model.

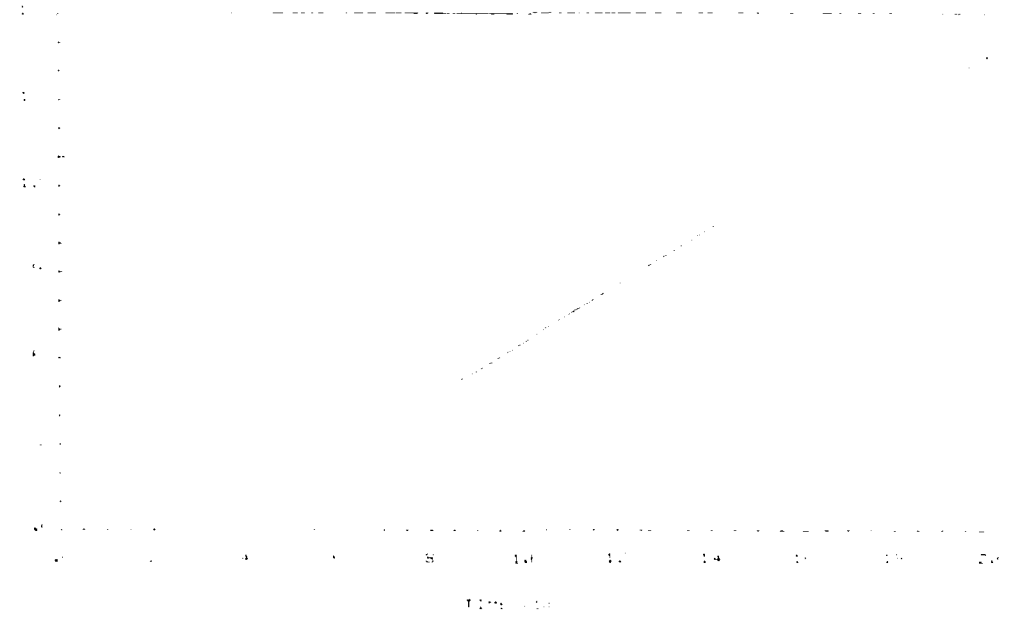

Figure 5-158. Covariance matrix element $p_{22}(\kappa T)$. Identification of full 3rd order model.

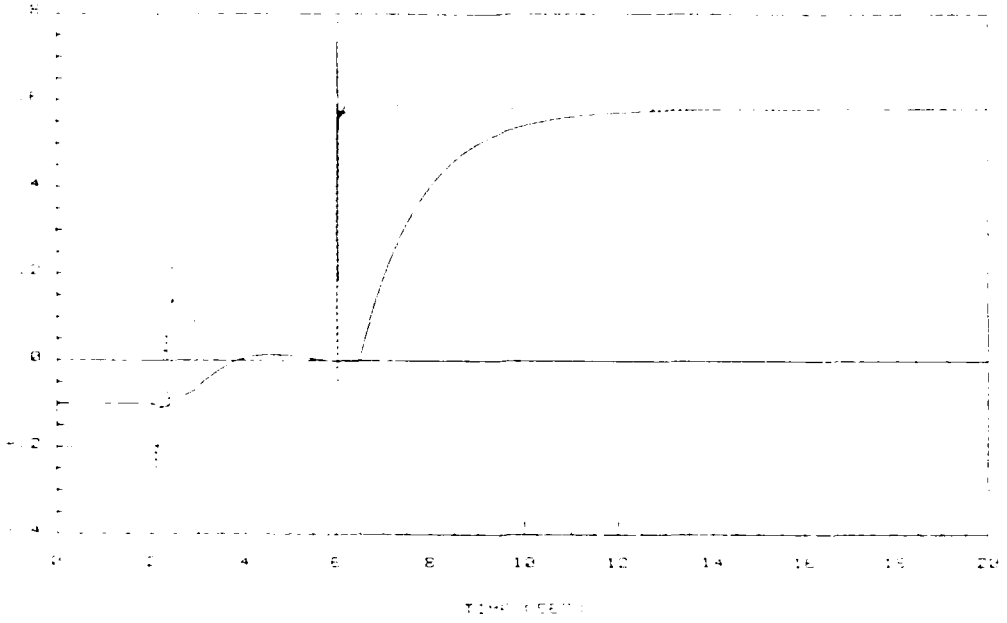

Figure 5-169. Estimate of step-response matrix element $h_{22}(kT)$. Identification of full 3rd order model.

Figure 5-170. [illegible] matrix element [illegible]. Identification of full 3rd order model.

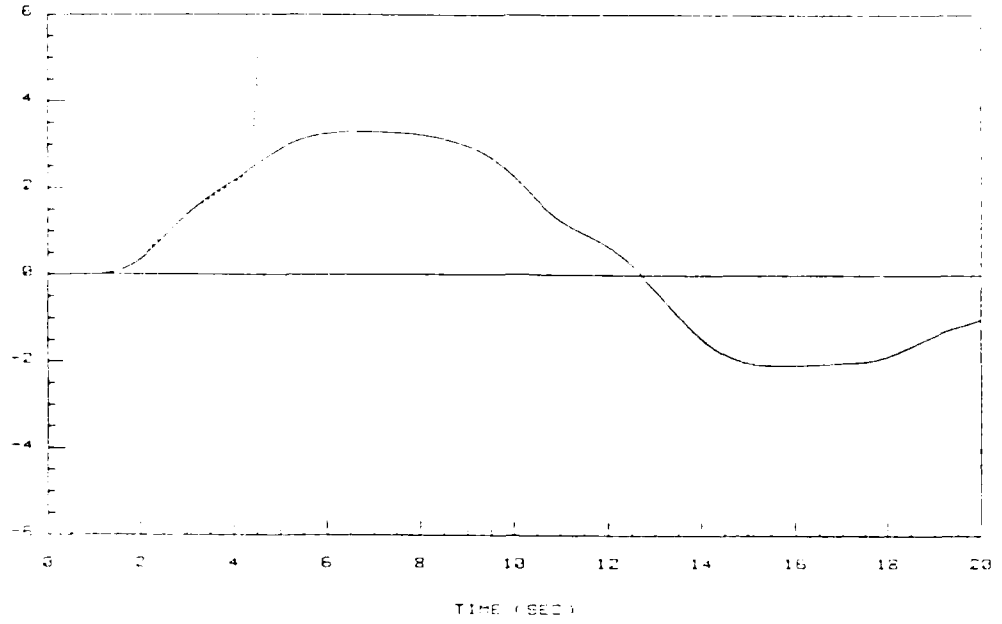

Figure 5-161. Flight path angle command and response (deg).
Adaptive control law. Plant parameter change.
Identification of full 2nd order model.

Figure 5-162. Flight path angle tracking performance index (deg).
Adaptive control law. Plant parameter change.
Identification of full 2nd order model.

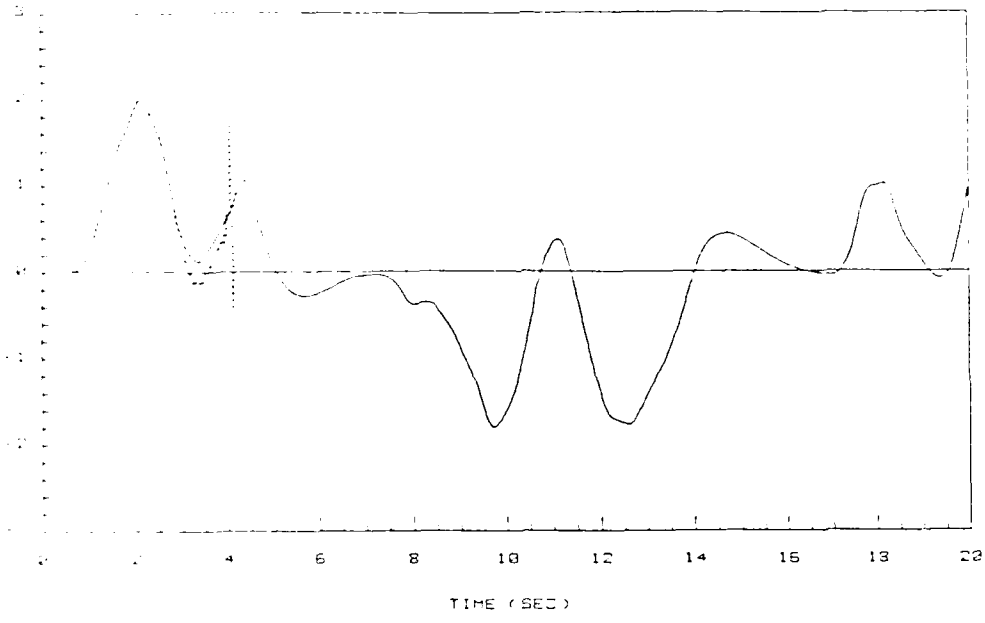

Figure 5-163. Pitch rate command and response (deg/sec).
Adaptive control law. Plant parameter change.
Identification of full 2nd order model.

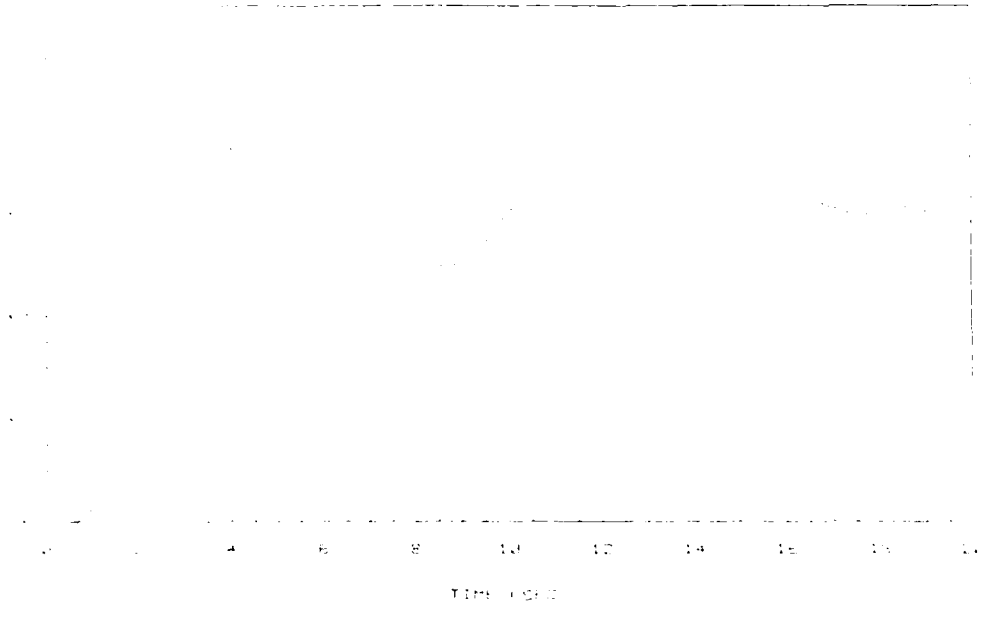

Figure 5-164. Pitch rate tracking performance index (deg/sec).
Adaptive control law. Plant parameter change.
Identification of full 2nd order model.

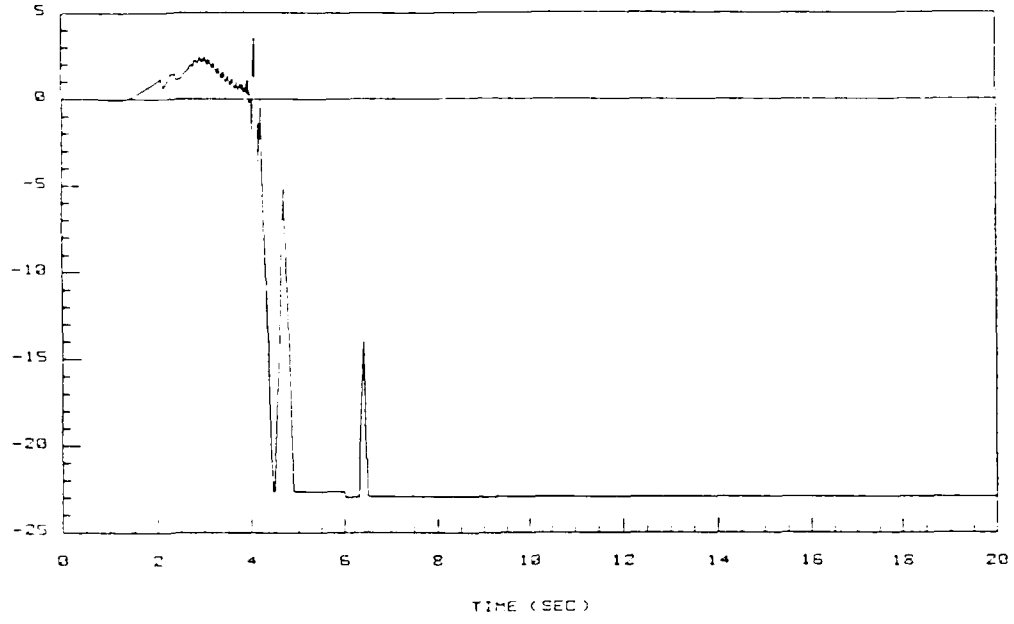

Figure 5-165. Elevator deflection (deg).
Adaptive control law. Plant parameter change.
Identification of full 2nd order model.

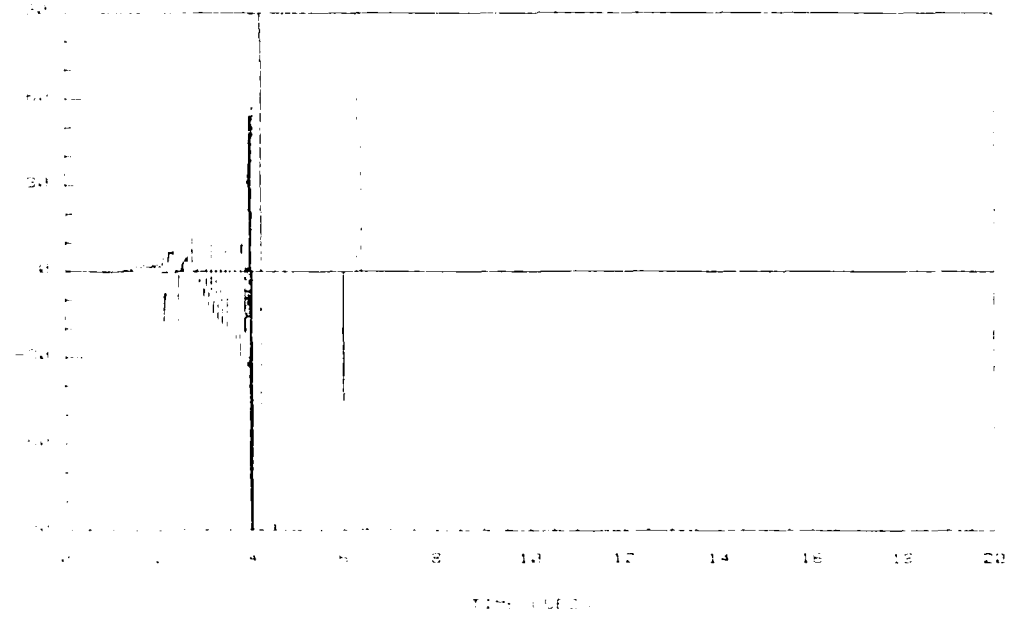

Figure 5-166. Elevator deflection rate (deg/sec).
Adaptive control law. Plant parameter change.
Identification of full 2nd order model.

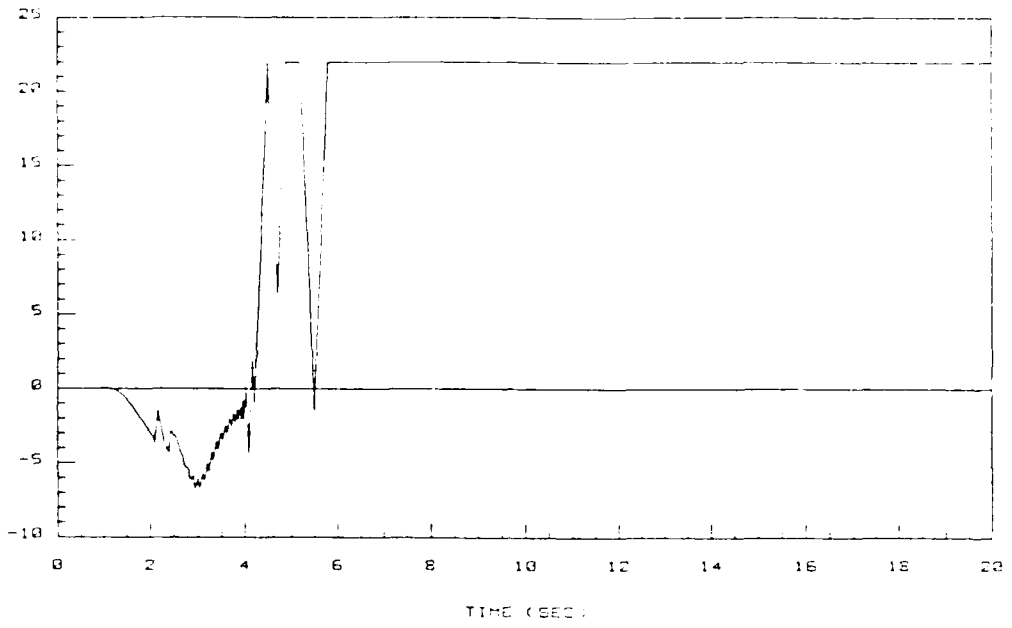

Figure 5-167. Flaperon deflection (deg).
Adaptive control law. Plant parameter change.
Identification of full 2nd order model.

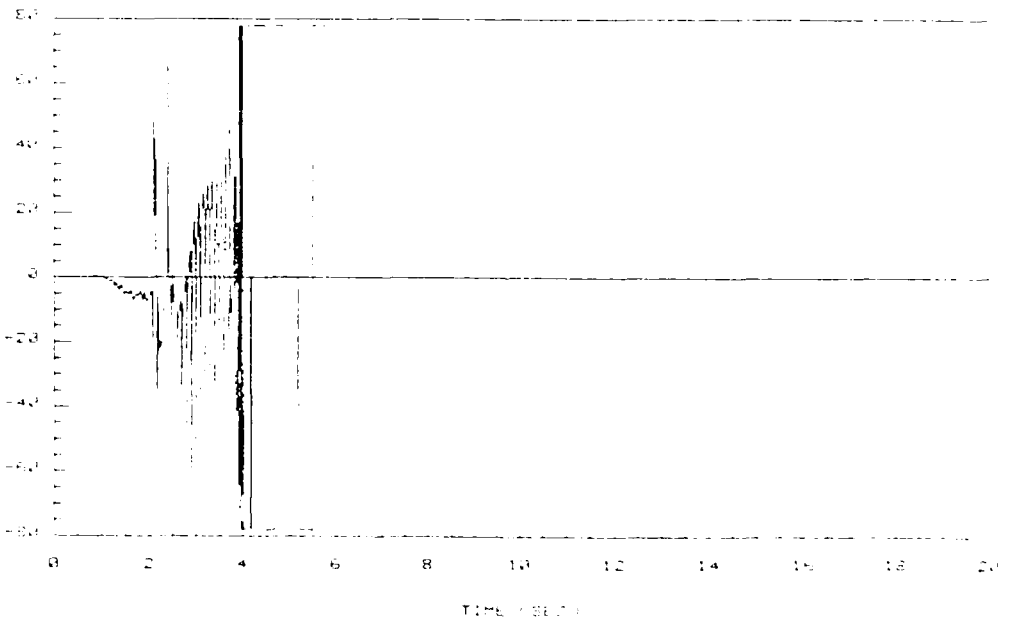

Figure 5-168. Flaperon deflection rate (deg/sec).
Adaptive control law. Plant parameter change.
Identification of full 2nd order model.

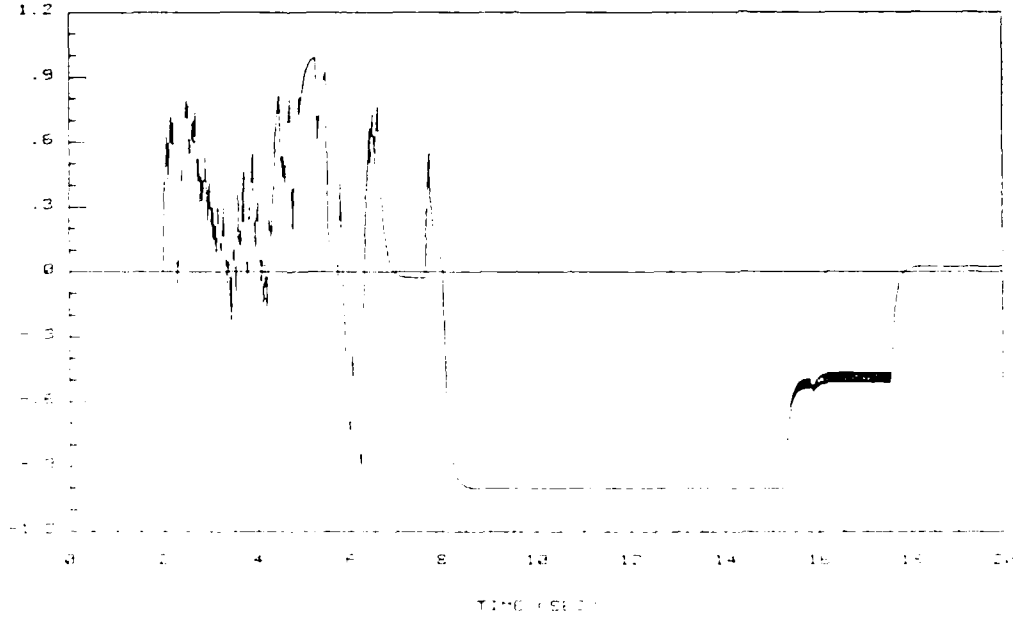

Figure 5-169. Fault detector test signal.
Identification of full 2nd order model.

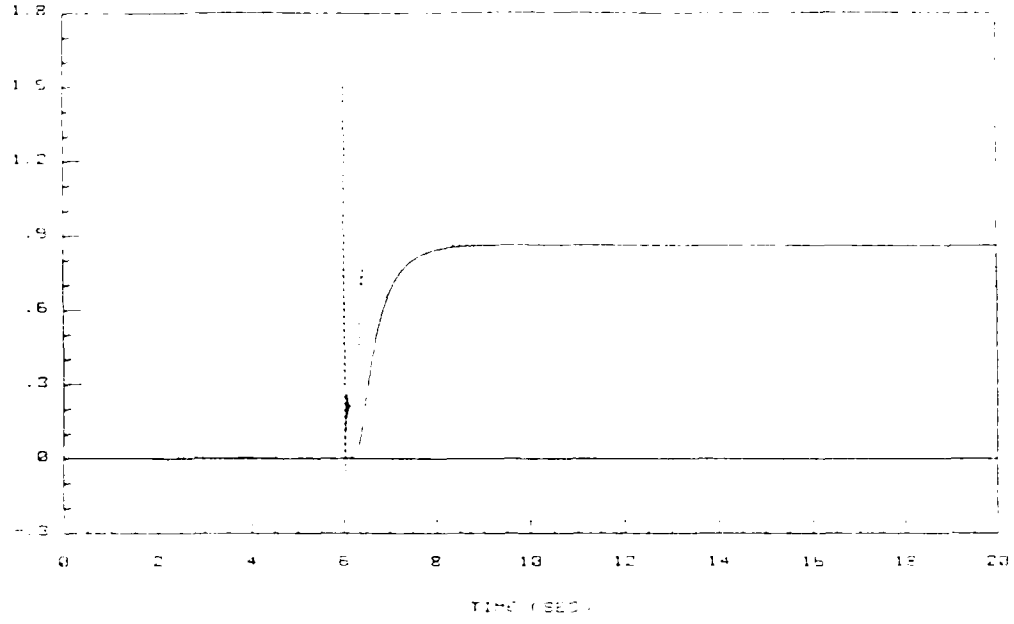

Figure 5-170. Estimate of step-response matrix element $h_{11}(kT)$
Identification of full 2nd order model.

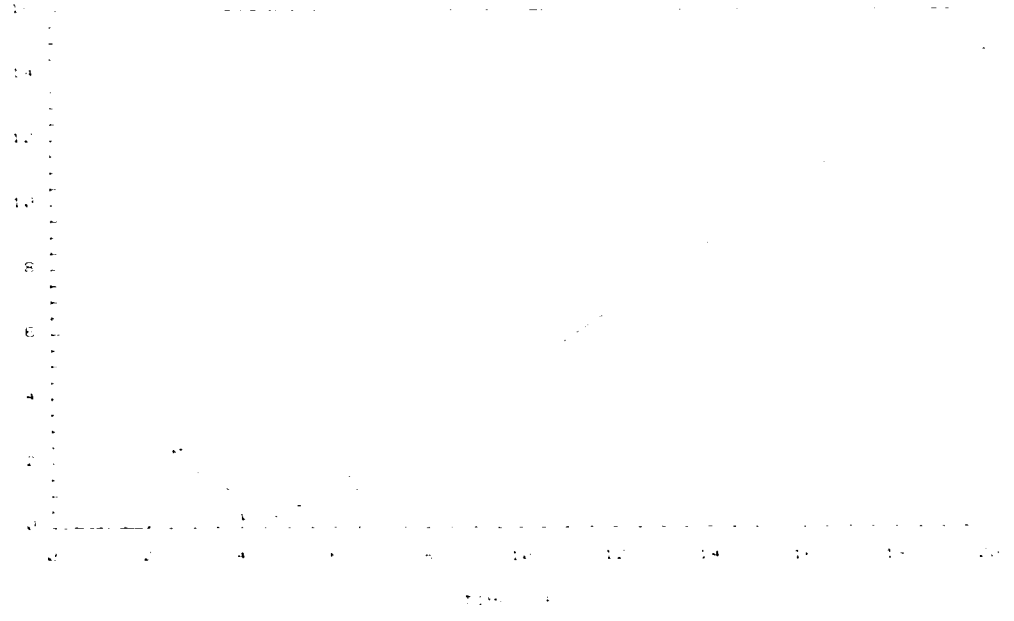

Figure 5-171. Covariance matrix element $p_{11}(kT)$.
Identification of full 2nd order model.

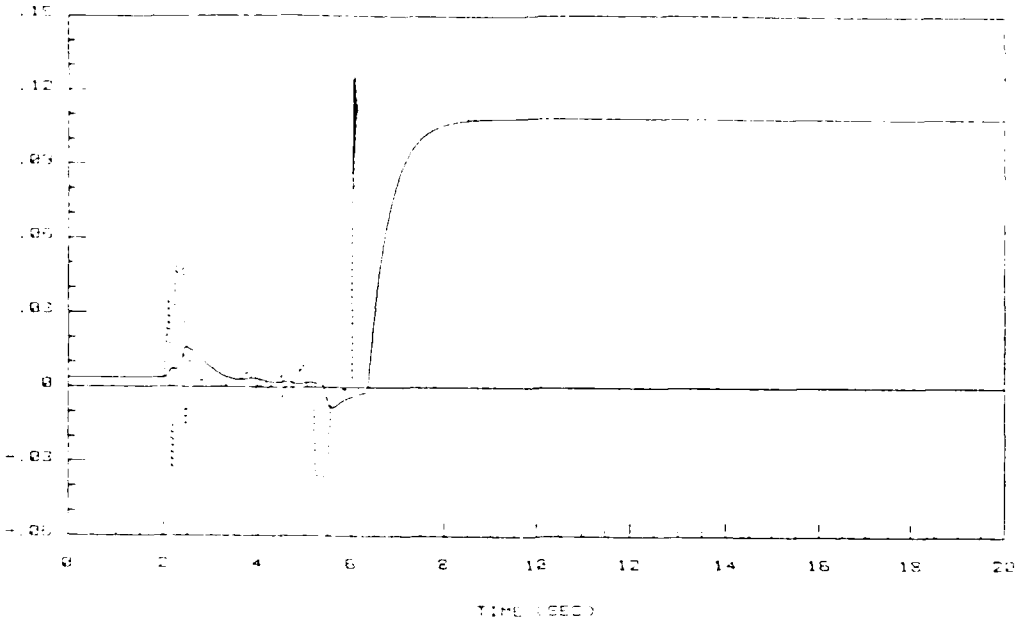

Figure 5-172. Estimate of step-response matrix element $h_{12}(kT)$. Identification of full 2nd order model.

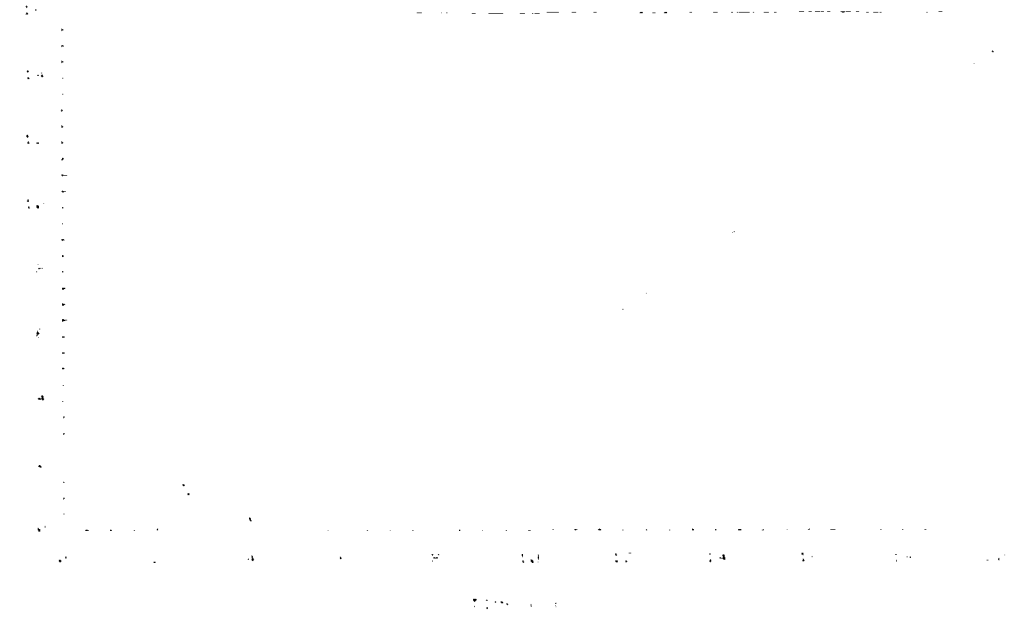

Figure 5-173. Covariance matrix element $p_{22}(kT)$. Identification of full 2nd order model.

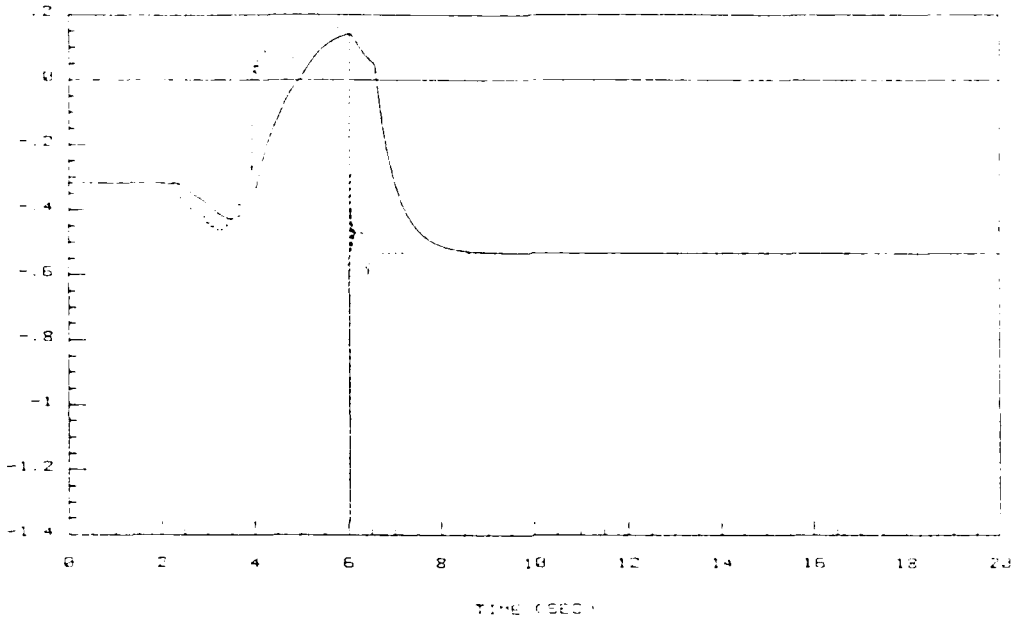

Figure 5-174. Estimate of step-response matrix element $h_{21}(kT)$. Identification of full 2nd order model.

Figure 5-175. Covariance matrix element $p_{22}(kT)$. Identification of full 2nd order model.

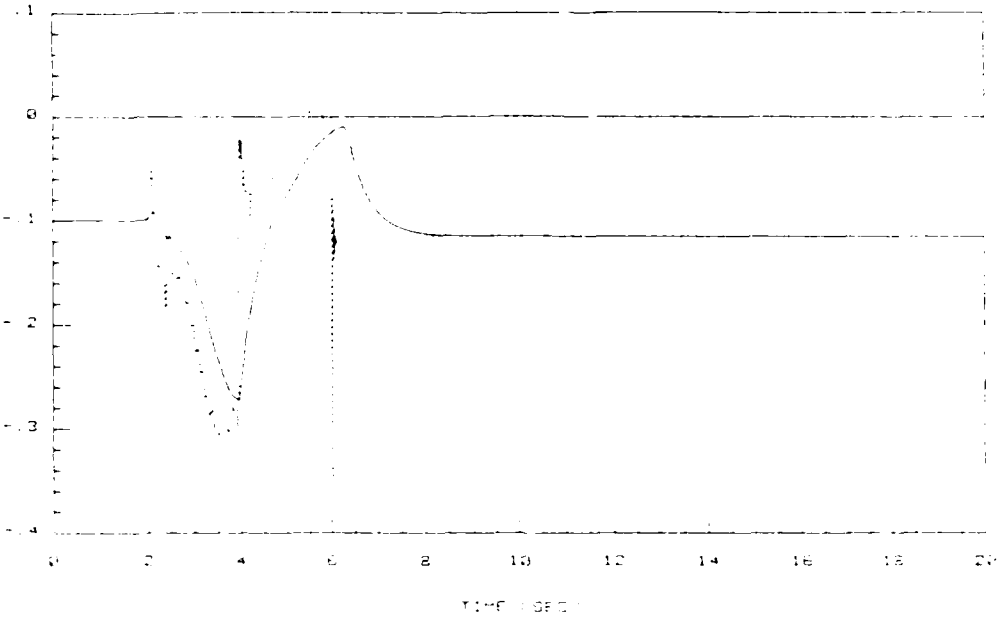

Figure 5-176. Estimate of step-response matrix element $h_{22}(kT)$. Identification of full 2nd order model.

Figure 5-177. Covariance matrix element $P_{22}(kT)$. Identification of full 2nd order model.

contains more parameters than the minimum necessary to describe it, therefore it requires considerable more excitation for proper identification. If identification of all the parameters in the model of the plant is necessary, a uniquely identifiable model form such as a canonical autoregressive moving average (ARMA) difference equation should be used (11, 17, 18). Given that the original scope of this effort was to identify only the elements of the matrix coefficient B_1, the selection of an ARMA form or a transfer matrix derived model structure is of no consequence since the B_1 coefficient is the same for both representations.

VI. Conclusions and Recommendations

6.1 Design Results

This study has evaluated the use of preliminary designs of parameter-adaptive control laws for an in-flight simulation application. It has been shown that the use of parameter-adaptive control techniques can be a highly effective way of maintaining a specified level of tracking performance by compensating for plant parameter variations. This offers the potential for increased fidelity during in-flight simulations, and good tracking performance for flight control applications in general. The effectiveness of the adaptive controller has been demonstrated by designing a digital, fast-sampling tracker controller in an explicit model-following configuration. Although much work must still be accomplished before these results are accepted in practice, the results obtained here imply that it is worthwhile to continue research in the area of adaptive flight control, particularly in the practical aspects of implementation.

6.2 Proposed Future Work

Although satisfactory responses are obtained for most of the simulations performed in this study, several modifications are presented to alleviate some of the problems encountered during the investigation. Specifically, changes are proposed to the control law to improve performance with respect to [illegible]. Modifications are also proposed for the algorithm to [illegible]

its tolerance to higher noise levels, the reduction of parameter estimate transients and their effects on closed-loop performance.

6.2.1 Control Law Modification. The simulation responses presented in Appendix D show that significant improvement can be achieved by implementing anti-windup provisions in the control law. The particular technique used in this investigation is based simply on stopping the calculation of the integral of the error in the control law whenever control surface deflection limits are reached. However, additional benefits may be obtained by modifying the controller's integral action in a different manner. Considering that Eqns (2-16) and (2-46) express the control law as a state-space system with a plant matrix $A = I$ (i.e. with open-loop poles at the unit circle), it seems reasonable to look for an alternation that would place these poles elsewhere while the control inputs are saturated. This is accomplished by expressing the control law in the following form [illegible]:

$$Z((k+1)T) = Z(kT) + T\,e(kT) + K\,[\,u(kT) - K\;Z(kT) - K\;e(kT)\,] \qquad (6\text{-}1a)$$

$$= [\,I - K\,K\,]\,Z(kT) + [\,T\,I - K\,K\,]\,e(kT) + K\,u(kT) \qquad (6\text{-}1b)$$

$u(kT) = SAT\{\,K\;Z(kT) + K$ [illegible] $\}$ (6-2)

where the function $SAT\{\,u\,\}$ [illegible]

$SAT\{\,u\,\} =$ [illegible] (6-3)

for a scalar, and

$$\mathrm{SAT}\{\,u\,\} = \begin{bmatrix} \mathrm{SAT}\{\,u_1\,\} \\ \mathrm{SAT}\{\,u_2\,\} \\ \vdots \\ \mathrm{SAT}\{\,u_m\,\} \end{bmatrix} \tag{6-4}$$

for a vector. The values u_{low} and u_{high} are chosen to correspond to the actuator limits.

While the control surfaces move within deflection limits, Eqns (6-1a) and (6-2) reduce to the standard control law given by Eqns (2-16) and (2-46). However, once a control surface (or surfaces) reach a deflection limit, the third term in Eqn (6-1a) begins to modify the integral action of the control law. Eqn (6-1b) shows that by proper selection of the matrix K, the eigenvalues of the matrix $[\, I - K K_{[illegible]} \,]$ can be assigned to lie within the unit circle thus preventing windup. Assuming that eigenvalues along the real axis are satisfactory, a simple selection for [illegible] is then

K = 1 [illegible] −1 [illegible] (6-5)

where [illegible] is a diagonal matrix with elements [illegible] ∈ (0 ... 1] (for i = 1 ... m). The elements [illegible] are adjusted [illegible] the time that the control [illegible] at the saturation [illegible] for a given maneuver is [illegible].

[illegible] in [illegible] results in [illegible] noise induced [illegible] in the parameter estimates, [illegible] with improved tolerance [illegible] by the adaptation system.

Most of the problems noted in the simulations have their root in the small magnitude of the elements of the step-response matrix (H(T)), and the inverse relationship between H(T) and the control law gain matrices. For that reason, it is imperative to avoid fluctuation of the parameter estimates when updating the control law gains since this may lead to higher control surface deflection rates and possibly instabilities.

Possible corrective measures that can be taken include the addition of supervisory type functions that monitor trends in the parameter estimates, control surface deflections, and output responses. Updating of the control law gains can be discontinued if transients in the parameter estimates exceed a certain level. If slower adaptation rates can be tolerated, the filtering of the parameter estimates may be increased thus reducing transients in the control law gains. Additional supervisory functions may provide for back-up controllers whenever the quality of the parameter estimates does not warrant satisfactory closed-loop performance.

Another possibility to avoid noise induced transients in the estimates is to move the parameters of the input-output model away from the noise level by transforming the identification problem into one of estimating larger numbers. This may be accomplished by re-arranging the structure of the input-output model from

$$u(kT) = B_1^{-1}\left[\, y(kT) + A_1\, y((k-1)T) - B_2\, u((k-2)T) + A_2\, y((k-2)T) - \ldots \right] + \ldots \qquad (k-1)$$

to

$$= B_1^{1}\, y(kT) + A_1^{1}\, y((k-1)T) - B_2^{1}\, u((k-2)T) + A_2^{1}\, y((k-2)T) - \ldots + \ldots \qquad (k-1)$$

This input-output model structure involves the estimation of B_1^{-1} which contains "large" numbers as compared with those in B_1, thus promising improved noise level tolerance, and less fluctuations in the parameter estimates for a given noise level. If necessary, scaling of the parameters and measurements may still be done in a similar manner to that described in chapter 4.

The identifiability problems, long convergence time, and large fluctuations in the parameter estimates encountered when identification of the entire parameter vevtor was considered can be reduced by employing a canonical ARMA model representation for the plant dynamics as mentioned in chapter 5. This model structure provides for the minimal number of parameters required to represent the plant, thus eliminating the pole-zero cancelation effects that occurs in the vector difference equation model derived from the transfer matrix. Also, since the number of parameters is smaller in this model representation, the ARMA canonical form requires a considerably smaller level of input excitation to the plant for proper identification to occur.

Faster identification may also occur by modifying the fault detector scheme proposed by Hagglund. In the current scheme, variations in the parameter vector cause changes in the scalar test sequences (s,T) and [illegible]. [illegible], not all the parameters change [illegible] by the same amount. However, [illegible] of the parameters are changing, as well as the relative magnitude of these changes is lost when forming a scalar test signal. [illegible] all the elements of the P matrix are increased by the same amount when a fault is detected, the estimates of the nonchanging as well as changing parameters are affected.

This increase in estimator gain may be appropriate for some parameters, but excessive for others. In cases when a large number of parameters are being identified but only a few may be changing significantly, this action may indeed slow down the identification procedure or cause unnecessary transients. It therefore seems reasonable to use a "vector" fault detector scheme that can identify changes in the individual elements of the parameter vector. Then, the appropriate elements of the P matrix can be adjusted in a manner proportional to the magnitude of the change.

To deal with the problem of measurement noise directly, the identification algorithm can be modified to employ instrumental varibles (IV) and extended least squares (ELS) techniques (28) that are better suited to handle noisy data with characteristics different from those of white Gaussian noise. These techniques include provisions that account for the shape of the noise spectrum, or correlate out the effect of noise in the parameter estimates thus reducing biases that occur when the RLS algorithm is used in a "colored" noise environment.

Further extensions to this research should consider the modifications named above, in addition to study problems such as the identification of non-linear models, command limiting schemes, control reconfiguration strategies, and the use of multiple-model moving bank estimator techniques (21). It was assumed for this investigation that the parameters for the fixed portion of the difference equation model (representative of the current flight condition) were available in an effort to reduce the number of parameters that needed to be identified. By attaching probabilistic weightings to several models, it may be

possible to select the best "fixed portion" of the parameter vector for a given flight condition. Research investigating the refinement of this technique is in progress. The use of reduced order models of a canonical ARMA structure also needs to be addressed as an alternative to multiple models scheme proposed above.

Appendix A

Aircraft Data for State Space Models

Tables A-1 through A-3 give the flight parameters, aerodynamic derivatives, and diference equation models for the flight conditions used in this thesis. The aerodynamic data was obtained from a simulation data package program for the AFTI F-16 aircraft, available at the Flight Dynamics Laboratory's Control Synthesis Branch. The difference equation models were obtained by taking the aircraft state space models and generating the tranfer matrix from their discrete time equivalent representations. This was done with the aid of $MATRIX_X$, and its model manipulation functions "DISCRETIZE" and "TFORM" (23).

TABLE A-1

AFTI/F-16 Aircraft Data

Aircraft Parameters

c (Wing Mean Aerodynamic Chord) = 11.32 ft.

S (Wing Surface Area) = 300 ft^2

b (Wing Span) = 30 ft

w (Weight) = 21,018 lbs

Moments of Inertia

I_{xx} = 14,145.68 slugs-ft^2

I_{yy} = 59,596.68 slugs-ft^2

I_{zz} = 70,887.00 slugs-ft^2

I_{xz} = 720.00 slugs-ft^2

Table A-2

Aircraft Data for 0.9 Mach, 10,000 ft

$\bar{q}$ (dynamic pressure) = 825.33 lb/in^2

V_T (trim velocity) = 969.66 ft/sec

α_T (trim angel of attack) = 1.4 deg

δe_T (trim elevator deflection) = -2.36 deg

δf_T (trim flaperon deflection) = -2.00 deg

δT_T (nominal engine thrust) = 5650.445 lb

Longitudinal Body Axis Primed Dimensional Derivatives

X'_θ = -32.1643219	Z'_θ = -.0008136	M'_θ = .0002939
X'_u = -.0157924	Z'_u = -.0000361	M'_u = -.0005463
X'_α = 44.494278	Z'_α = -2.0889177	M'_α = 5.5969896
X'_q = -23.7776337	Z'_q = .9999598	M'_q = -1.0057726
X'_{δ_e} = -.6077153	Z'_{δ_e} = -.2098655	M'_{δ_e} = -31.939163
X'_{δ_f} = 19.4285583	Z'_{δ_f} = -.3693079	M'_{δ_f} = -9.9644833

Difference Equation Model Parameters

$$A_1 = \begin{bmatrix} -3.9697145 & 0 \\ 0 & -3.9697145 \end{bmatrix} \qquad B_1 = \begin{bmatrix} .00206579 & .00365134 \\ -.3178785 & -.0992575 \end{bmatrix}$$

$$A_2 = \begin{bmatrix} 5.90880295 & 0 \\ 0 & 5.90880295 \end{bmatrix} \qquad B_2 = \begin{bmatrix} -.0062434 & -.0109394 \\ .94689976 & .29550238 \end{bmatrix}$$

$$A_3 = \begin{bmatrix} -3.90846236 & 0 \\ 0 & -3.90846236 \end{bmatrix} \qquad B_3 = \begin{bmatrix} .00622259 & .01090232 \\ -.9401651 & -.2932328 \end{bmatrix}$$

$$A_4 = \begin{bmatrix} .9693739519 & 0 \\ 0 & .9693739519 \end{bmatrix} \qquad B_4 = \begin{bmatrix} -.002045 & -.0036142 \\ .31114387 & .09698786 \end{bmatrix}$$

Table A-3

Aircraft Data for 0.3 Mach, 10,000 ft

$\bar{q}$ (dynamic pressure) = 100.02 lb/in^2

V_T (trim velocity) = 337.56 ft/sec

α_T (trim angel of attack) = 7.7 deg

δe_T (trim elevator deflection) = -2.05 deg

δf_T (trim flaperon deflection) = 12.46 deg

δT_T (nominal engine thrust) = 2538.243 lb

Longitudinal Body Axis Primed Dimensional Derivatives

X'_θ = -31.8838959	Z'_θ = -.0127706	M'_θ = .0007531
X'_u = -.0122359	Z'_u = -.0002911	M'_u = .00006
X'_α = 17.7885132	Z'_α = -.4893466	M'_α = 1.7894831
X'_q = -45.3607635	Z'_q = .9999136	M'_q = -.3870971
X'_{δ_e} = 1.6643476	Z'_{δ_e} = -.0770782	M'_{δ_e} = -3.2519884
X'_{δ_f} = -4.29844	Z'_{δ_f} = -.0691358	M'_{δ_f} = .3253066

Difference Equation Model Parameters

$$A_1 = \begin{bmatrix} -3.99131 & 0 \\ 0 & -3.99131 \end{bmatrix} \qquad B_1 = \begin{bmatrix} .000768645 & .00068963 \\ -.03246486 & .00324069 \end{bmatrix}$$

$$A_2 = \begin{bmatrix} 5.97377273 & 0 \\ 0 & 5.97377273 \end{bmatrix} \qquad B_2 = \begin{bmatrix} -.00230457 & -.0020662 \\ .097218426 & -.0097182 \end{bmatrix}$$

$$A_3 = \begin{bmatrix} -3.9736152 & 0 \\ 0 & -3.9736152 \end{bmatrix} \qquad B_3 = \begin{bmatrix} .002301487 & .0020636 \\ -.09704231 & .0097143 \end{bmatrix}$$

$$A_4 = \begin{bmatrix} .991152575 & 0 \\ 0 & .991152575 \end{bmatrix} \qquad B_4 = \begin{bmatrix} -.00076556 & -.0006870 \\ .032288744 & -.0032368 \end{bmatrix}$$

Appendix B

Equivalence Between the Step-Response Matrix and the Difference Equation Model's Matrix Coefficient B_1

In chapter 2 of this thesis we saw how the use of the step-response matrix (H(T)) provides an alternate way of defining the control law gain matrices. The use of H(T) also provides a convenient way of relating these gain matrices to the matrix coefficient B_1 of the vector difference equation used to represent the aircraft open-loop dynamics. In order to ilustrate this relationship, it is convenient to consider the significance of H(T) and how it relates to the design of the fixed-gain control law.

Consider first the solution of the matrix differential equation given in Eq (2-1), and the output relationship given by Eq (2-9). For any arbitrary input, the output response is given by (14:98-102)

$$y(t) = C \exp(A\ t)\ x(0) + \int_0^t C \exp(A\ (t-\tau))\ B\ u(\tau)\ d\tau \qquad \text{(B-1)}$$

Under the assumption of zero initial conditions for the plant ($x(0) = 0$, $y(t \leq 0) = 0$), and with the input held constant between samples by the controller, the response of the plant at $t = T$, for a given $u(0)$ is

$$y(T) = \int_0^T C \exp(A\ (T-\tau))\ B\ u(0)\ d\tau \qquad \text{(B-2a)}$$

$$= H(T)\ u(0) \qquad \text{(B-2b)}$$

Thus H(T) is the matrix multiplier that relates the input $u(0)$ to the output of the plant at t = T.

The open-loop plant may be represented by a vector difference equation form given in Eq (3-9). For the same inputs and initial conditions as before, and neglecting the zero mean equation error term, Eq (3-9) gives the following output relationship at t = T

$$y(T) = B_1\, u(0) \tag{B-3}$$

If the output in Eq (B-3) is to be the same as that of Eq (B-2), for the same arbitrary input, we must then conclude that $H(T) = B_1$.

The question of how H(T) is related to the design of the control law gain matrices can be seen simply by assuming that B remains constant between any to given sampling instants, and doing a series expansion on the matrix exponential in Eq (B-2a) as follows

$$y(T) = C \int_0^T \exp(A\ (T-\tau))\ d\tau\ B\ u(0) \tag{B-3a}$$

$$= C \int_0^T \{\ I + \frac{A\ (T-\tau)}{1!} + \frac{A^2(T-\tau)^2}{2!} + \text{H.O.T.}\ \}\ d\tau\ B\ u(0) \tag{B-3b}$$

For small sampling periods, the contribution of the terms beyond I in the series is relatively small and may be neglected. This lead to the folowing approximation for the output $y(t)$

$$y(T) \cong C \int_0^T I\ d\tau\ B\ u(0) \tag{B-4a}$$

$$y(T) \cong T\ C\ B\ u(0) \tag{B-4b}$$

Thus

$$H(T) \cong T\ C\ B \tag{B-5}$$

Recognizing that

$$H^{-1}(T) \cong -\frac{1}{T}\ [C\ B]^{-1} \tag{B-6}$$

H(T) can then be used for defining the control law gain matrices as shown in Eqs (2-46) thu (2-48).

Appendix C

Implementation Details of the Recursive Identification Algorithm

This appendix is intended to suplement the material presented in chapter 3 of this thesis by providing additional details on the implementation of the recursive identification algorithm. The first section will address the structure of the difference equation model, while section two will emphasize the actual implementation of various equations in the algorithm.

A. Structure of the Difference Equation Model

As described in Chapter 3, the difference equation model used in this thesis to represent the plant dynamics has its origin in the transfer matrix obtained from the discretized state space model of the plant. The transfer matrix representation leads to the model structure given in Eqn (3-9). In order to use the difference equation in the estimation algorithm, it must be expressed in the form of Eqn (3-10). This is done by combining all the delayed input-output measurements in the matrix $\gamma^T(kT)$, and the elements of the parameter matrices A_i and B_i $(i = 1,2,..,N)$ in the parameter vector θ. In forming the parameter vector θ we take advantage of the fact that the matrices A_i are diagonal, and are of the form a_i*I (see Appendix A), to reduce the number of elements needed in θ. The reason for the form af the matrices A_i is that the numbers a_i represent the coefficients of the characteristic equation of the discrete transfer matrix. Eqn (3-10) then assumes the form given in Eqn (C-1), which ilustrates the case for

a second order model, and where the sampling time reference has been dropped for notational convenience.

$$\begin{bmatrix} y_1(k) \\ y_2(k) \end{bmatrix} = \underbrace{\begin{bmatrix} u_1(k-1) & u_2(k-1) & 0 & 0 & -y_1(k-1) & - - - \\ 0 & 0 & u_1(k-1) & u_2(k-1) & -y_2(k-1) & - - - \end{bmatrix}}_{(k-1)} \underbrace{\begin{matrix} \\ \\ \\ \\ \\ \\ \\ \\ \\ \\ \end{matrix}}_{(k-2)} \begin{bmatrix} b_1(1,1) \\ b_1(1,2) \\ b_1(2,1) \\ b_1(2,2) \\ \bar{a}_1(1,1) \\ b_2(1,1) \\ b_2(1,2) \\ b_2(2,1) \\ b_2(2,2) \\ \bar{a}_2(1,1) \end{bmatrix} + \begin{bmatrix} \varepsilon_1(k) \\ \varepsilon_2(k) \end{bmatrix} \qquad (C\text{-}1)$$

The "blank" section of $\bar{r}^T(kT)$, underscored by (k-2), simply indicates that the arrangement of input-output data underscored by (k-1) is repeated as many times as required by the order of the difference equation.

To perform the scalar measurement update of the parameter vector, the contribution of each output is added one at a time. This is done assuming that the equation error terms in Eqn (C-1) are statistically independent from each other. This is considered a reasonable assumption since the control law used produces decoupled output responses. In that case, each output prediction and residual is generated by taking the corresponding row of $\bar{r}^T(kT)$ multiplied by the current estimate of the parameter vector θ. The scalar update of θ is then performed every time step kT by iterating through the estimation algorithm as many

times as as there are independent outputs; each time as if we were dealing with a multiple-input single-output model with the appropriate residual, output noise variance estimate, and row of $\Phi^T(kT)$ ($\Phi^T_i(kT)$) to match the particular output considered at the time.

B. Implementation of the Parameter, and Parameter Covariance Update Equations

Although the update of the parameter covariance is correctly given in Eqn (3-65), this equation needs to be modified for actual implementation. In stationary conditions, i.e. when the plant parameters have not changed and a constant level of excitation is maintained, the value of $\alpha_i(kT)$ is adjusted so that $\alpha_i(kT) = v_i^1(kT)$. This condition means that the same amount of information that enters the estimator is thrown away (see Eq (3-30)). When this happens, the denominator of the second term in Eqn (3-65) approaches infinity thus causing $P_i(kT)$ to remain at the same level. This is the desired effect, but it is hardly implementable in practice. To solve the problem, Hagglund redefined the update equations for the parameter estimates and parameter covariance (19:88) by a simple algebraic transformation that avoids the singularity condition. The resulting expressions replace Eqns (3-51) and (3-65) in the identification algorithm and are given as follows

$$\hat{\Theta}'_i(kT) = \hat{\Theta}'_{i-1}(kT) + \frac{1}{\gamma_i(kT)} P_{i-1}(kT) \Phi_i(kT) \varepsilon_i(kT) \qquad \text{(C-2)}$$

$$P_i(kT) = P_{i-1}(kT) - \frac{P_{i-1}(kT) \Phi_i(kT) \Phi_i^T(kT) P_{i-1}(kT)}{\gamma_i(kT)} \cdots \gamma_i(kT) + \alpha_i(kT) I \qquad \text{(C-3)}$$

where

$$\alpha_j(kT) = 1 - \alpha_j(kT)\, v_j(kT) \qquad \text{(C-4)}$$

$$\hat{\theta}_j(kT) = \hat{v}_j(kT) + \alpha_j(kT)\, \varepsilon_j \qquad \text{(C-5)}$$

The update equations just described are now in a form more amenable for computer implementation but further modification is still required. Kalman-filter-type update equations like Eqns (C-2) and (C-3) are renoun for having bad numerical properties, mainly because the covariance update equation may contain differences between two almost equal terms. Computer roundoff may then deteriorate the estimation.

It is often more convenient to employ factorization techniques for the update of the covariance matrix. A commonly used factorization is known as "U-D factorization" in which the covariance matrix is expressed as follows

$$P(kT) = U(kT)\, D(kT)\, U^T(kT) \qquad \text{(C-6)}$$

where $U(kT)$ is an upper triangular matrix with all diagonal elements equal to 1, and $D(kT)$ is a diagonal matrix. The updating of the covariance matrix is done by updating the U and D factors rather that updating the P matrix directly. The U-D factorization has good numerical stability and enhances the algorithm's tolerance of roundoff errors (10,28,30).

Detailed discussions on the U-D algorithm can be found in references (10), (28), (30), (41) and (42). Here we shall limit ourselves to list a segment of the FORTRAN code used to implement the parameter estimate,

and covariance matrix updates with the U-D algorithm, and a modified weighted Gram-Schmidt orthogonalization procedure (28, 42) for adding the contribution of the fault detector to the covariance matrix update. The listing is limited to those sections of code which are not implemented directly from the equations given in section 3.4.

```
**********************************************************************

      DO 26 KNOUT=1,NOUT        ! PERFORM THE UPDATE FOR EACH
                                ! OUTPUT MEASUREMENT

------------------------------------------------------------------------

         DO 30 I=2,IEND         ! IEND = TOTAL # OF PARAMETERS
            DO 30 J=1,I-1
30          UTRAN(I,J) = UTM1(J,I)  ! OBTAIN U^T_{i-1}(kT)

------------------------------------------------------------------------

         DO 35 I=1,IEND
            F(I) = 0.0          ! EVALUATE Eqn (5-60a) in (19:89)
            DO 35 J=1,I         ! f = U^T_{i-1}(kT) v_i(kT)
35          F(I) = F(I) + UTRAN(I,J)*GRADMD(J,KNOUT)

------------------------------------------------------------------------

         FTPF1 = 0.0
         DO 40 I=1,IEND
            G(I) = D(I)*F(I)    ! Eqn (5-60b) in (19:89)
            FTPF1 = FTPF1 + F(I)*G(I)  ! v^T_i(kT) P_{i-1}(kT) v_i(kT)
40          GRD(I) = GRADMD(I,KNOUT)

------------------------------------------------------------------------
```

```
CALL DELTAD(GPD,UTMI,D,IEND,A,DD,IERR)   ! Eqn (3-58)
CALL ALPH(DD,FTFI,XV(KNOUT),ALPHA(KNOUT),IERR) ! Eqn (3-62)
ZETA = 1.0 - ALPHA(KNOUT)*XV(KNOUT)  ! Eqn (C-4)
```

```
BETA(0) = XV(KNOUT)   ! Eqn (C-5), Eqn (5-60g) in (19:90)
DO 45 J=1,IEND
BETA(J) = BETA(J-1) + F(J)*G(J)*ZETA
```

```
IF (BETA(J) .EQ. 0.0) THEN        ! (19:365-366)
                                  ! Update the D(kT) matrix
   D(J) = MIN(CREG,D(J))
ELSE
   D(J) = MIN(CREG,(BETA(J-1)/BETA(J))*D(J))  ! Eqn (360h)
                                              ! in (19:90)
ENDIF
```

```
V(J) = G(J)
```

```
IF (BETA(J-1) .EQ. 0.0) THEN
   MU(J) = 0.0                    ! Eqn (5-60
ELSE
   MU(J) = -F(J)*ZETA/BETA(J-1
ENDIF
```

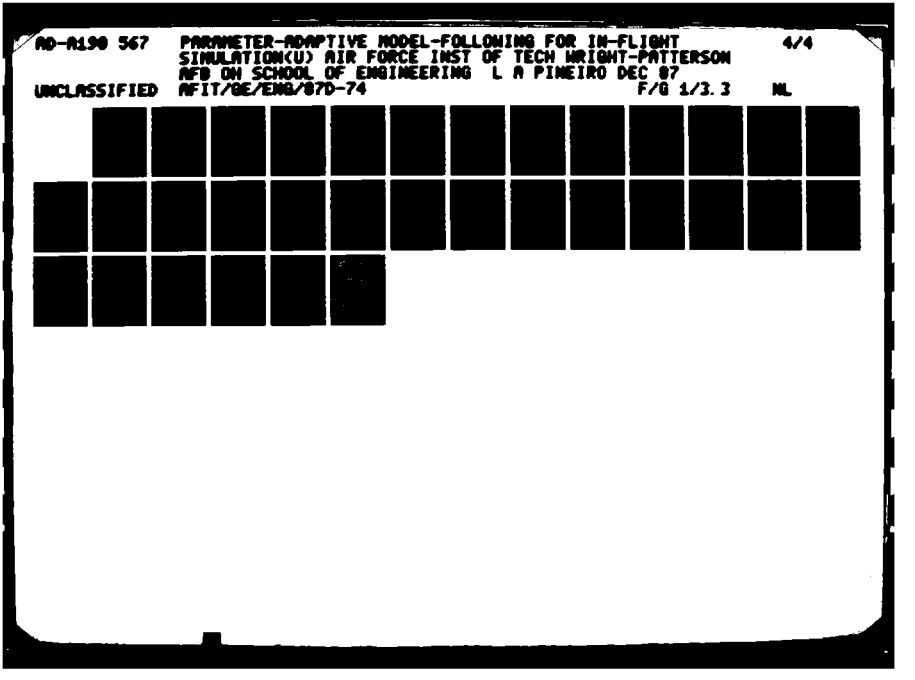
AD-A190 567
PARAMETER-ADAPTIVE MODEL-FOLLOWING FOR IN-FLIGHT SIMULATION(U) AIR FORCE INST OF TECH WRIGHT-PATTERSON AFB OH SCHOOL OF ENGINEERING L A PINEIRO DEC 87
4/4
UNCLASSIFIED
AFIT/GE/ENG/87D-74
F/G 1/3.3
NL

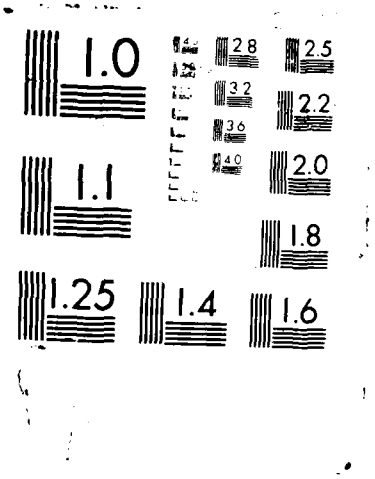
1.0
1.1
1.25
1.4
1.6
1.8
2.0
2.2
2.5
2.8
3.2
3.6
4.0

```
            IF (J .EQ. 1) THEN
               GO TO 45
            ELSE
               DO 50 I=1,J-1
               UP(I,J) = UTM1(I,J) + V(I)*MU(J) ! Eqn (5-60j) in (19:90)
                                                ! Update U(kT) matrix
50             V(I) = V(I) + UTM1(I,J)*V(J) ! Eqn (5-60d) in (19:89)
            ENDIF
```

```
45      CONTINUE
```

```
        DO 55 I=1,IEND          ! Eqn (5-60k) in (19:90)
        V(I) = V(I)/BETA(IEND)
        DELPAR(I) = V(I)*ERROR(KNOUT)    ! Calculate parameter vector
                                         ! increment
55      PARAM(I) = PARAM(I) + DELPAR(I)  ! Update parameter vector
```

.
.

Calculate β_j(kT) per Eqn (3-64) and then ....

```
        DO 68 I=1,IEND                   ! Add β from fault detector
                                         ! if fault has occured
68         BV(I) = B
        CALL MWGS(BV,IEND,UP,D,CREG,IERR) ! Use Modified Gram-Schmidt
                                          ! orthogonalization procedure
```

```
        DO 69 I=1,IEND          ! Update last U(kT) matrix
           DO 69 J=I+1,IEND
69         UTM1(I,J) = UP(I,J)
```

```
26      CONTINUE  ! with next measurement update ...
```

```
************************************************************************
************************************************************************
      SUBROUTINE MWGS(B,N,UP,D,CREG,IERR)
************************************************************************
************************************************************************

      DOUBLE PRECISION W(80,40),UP(40,40),D(40),DB(80,TEMP,
     * CREG,B(40)

                        ! See (28:333-334)
      DO 1 J=1,N

         DB(J) = D(J)

         DB(J+N) = 1.0
            DO 1 I=1,N

            W(I,J) = UP(J,I)

            IF (I .EQ. J) THEN

                W(I+N,J) = SQRT(B(I))

            ELSE

                W(I+N,J) = 0.0

            ENDIF

1     CONTINUE

------------------------------------------------------------------------

      DO 2 J=N,2,-1

         D(J) = 0.0

         DO 3 K=1,2*N

3        D(J) = D(J) + W(K,J)*DB(K)*W(K,J)

         D(J) = MIN(CREG,D(J))

         DO 4 I=1,J-1

         TEMP = 0.0

            DO 5 K=1,2*N

5           TEMP = TEMP + W(K,I)*DB(K)*W(K,J)

            IF (D(J) .EQ. 0.0 THEN
```

```
                    UP(I,J) = 0.0
                    GO TO 4
                ELSE
                    UP(I,J) = TEMP/D(J)
                ENDIF
                DO 6 K=1,2*N
6               W(K,I) = W(K,I) - UP(I,J)*W(K,J)
4             CONTINUE
2           CONTINUE
            TEMP = 0.0
            DO 7 K=1,2*N
7           TEMP = TEMP + W(K,1)*DB(K)*W(K,1)
            D(1) = MIN(CREG,TEMP)
            RETURN
            END
*******************************************************************************
```

Appendix D

Root-Locus Analysis and Time-response Checks with Regards to Functional Controlability

A. Root-Locus Analysis

Early in the design stages of this effort, concerns were brought up as for the significance and effect on the closed-loop system behavior of a transmission zero at the origin that leads to functional uncontrolability. To learn more about this condition, a root-locus analysis of the of the closed-loop system was conducted with the aircraft model corresponding to mach 0.9, 10,000 ft. This was done by individally varying the design parameters σ_1, σ_2, and ρ in the control law, and observing the location of the closed-loop system roots. To simplify the problem, actuator and sensor dynamics were not included in the analysis. A sample of the results is shown in tables D-1 through D-3. In these tables, R1 and R2 are the fast system roots and R3 through R6 represent the slow system roots. R5 and R6 correspond to the

Table D-1

Root-locus Analysis, σ_1 gain sweep ($\sigma_2 = 0.7$, $\rho = 0.8$)

roots \ σ_1	$\sigma_1 = 0.3$	$\sigma_1 = 0.4$	$\sigma_1 = 0.5$	$\sigma_1 = 0.7$
R1	.297718585951	.297714217964	.297705241223	.286779451772
R2	.687084484379	.587157197817	.487207541951	.298180935417
R3	.991868119634	.991892424014	.991908999372	.991930277332
R4	.993208391024	.993115738800	.993057794613	.992988911001
R5	.999834953500	.999834955893	.999834957328	.999834958967
R6	1.0	1.0	1.0	1.0

Table D-2

Root-locus Analysis, σ_2 gain sweep ($\sigma_1 = 0.3$, $\rho = 0.8$)

roots \ σ_2	$\sigma_2 = 0.4$	$\sigma_2 = 0.5$	$\sigma_2 = 0.7$	$\sigma_2 = 0.8$
R1	.596920647772	.497341971943	.297718585951	.197827609203
R2	.687308842456	.687155621738	.687084484379	.687070672164
R3	.991843993749	.991853164897	.991868119634	.991874333508
R4	.993793593327	.993522421431	.993208391024	.993108852556
R5	.999847457184	.999841354479	.999834953500	.999833067057
R6	1.0	1.0	1.0	1.0

Table D-3

Root-locus Analysis, ρ gain sweep ($\sigma_1 = 0.3$, $\sigma_2 = 0.7$)

roots \ ρ	$\rho = 0.6$	$\rho = 0.7$	$\rho = 0.8$	$\rho = 0.9$
R1	.295710430846	.296713062375	.297718585951	.298727026744
R2	.685130298700	.686104281008	.687084484379	.688071029587
R3	.993924862324	.992898588723	.991868119634	.990833375662
R4	.995108546177	.994161375687	.993208391024	.992249858364
R5	.999840396440	.999837226695	.999834953500	.999833244131
R6	1.0	1.0	1.0	1.0

roots introduced by the vector integrator of the control law.

As shown in these tables, the roots R1 and R2 approach the asymptotic values defined by Eqns (2-41) and (4-9) given by

$$\lambda_i = 1 - \sigma_i \qquad i = 1,2 \qquad \text{(D-1)}$$

The slow roots R3 and R4 approach those of Eqn (2-39) which by virtue of Eqn (2-44) reduces to

$$\lambda_i = 1 - T\rho \qquad i = 3,4 \qquad (D\text{-}2)$$

while the remaining slow roots R5 and R6 correspond to the roots of Eqn (2-40). In this case, R5 approaches a transmission zero of the plant located at 0.99982119878, while R6 sits on top of the transmission zero at the origin produced by the selection of pitch rate as an output quantity. It is obvious that the pole-zero cancelation occuring between the transmission zero at the origin and a pole from the vector integrator does not allow this system root to be placed arbitrarily. This situation renders the system functionally uncontrollable, however, this is to be expected given the kinematic definition used in the state-space model of the aircraft. The status of functional uncontrolability in this example does not necessarily implies that satisfactory tracking performance may not be achieved, but simply expresses the invariability of the kinematic relationship between the pitch angle and pitch rate responses. Throughout the analysis, all system roots behaved in a predictable way and remained at or within the unit circle as desired. Satisfactory tracking performance can then be achieved provided one considers the kinematic relationship just mentioned when generating the input commands to the closed-loop system.

B. Time Response Checks

Another concern regarding the issue of functional controlability was wether or not the closed-loop system was capable of following independent command inputs when that condition is not met.

Since the command inputs used throughout this thesis were not the result of decoupled motion from the AFTI/F-16, it may be argued that these signal are "related" to each other and thus not address the situation in question. To that effect, the command inputs were modified and applied to the same aircraft model of part A with the nominal control law design of chapter 4. The results are given in Figures D-1 through D-32.

Figures D-1 through D-8 present the case where the flight path angle command is temporarily "clipped" to hold a maximun value of 2 deg. while the pitch rate command remains unchanged. The responses show no noticeable tracking performance degradation.

Figures D-9 through D-16 show the responses to a flight path command of 0 deg. while the pitch rate command again remains unchanged. In this example, the control law contained no anti-windup provisions. Figures D-9 and D-10 show relatively good tracking performance for the flight path angle response. However, the pitch rate response suffers from a short period of instability caused by deflecting the flaperon to its position limit. The larger control surface deflections are attributed to the bigger demands on control action imposed by the decoupled maneuver. Aside from the instances where the flaperon is at its deflection limit, the responses exhibit good tracking behavior. Thus the condition of functional uncontrolability is not seen as the cause of the problem.

The previous maneuver was repeated, this time with the integrator limiter mentioned in chapter 4. This is to test the effectiveness of the antiwindup protection scheme. The results are shown in Figures D-17 through D-24. These ilustrate that, although the flaperon deflection

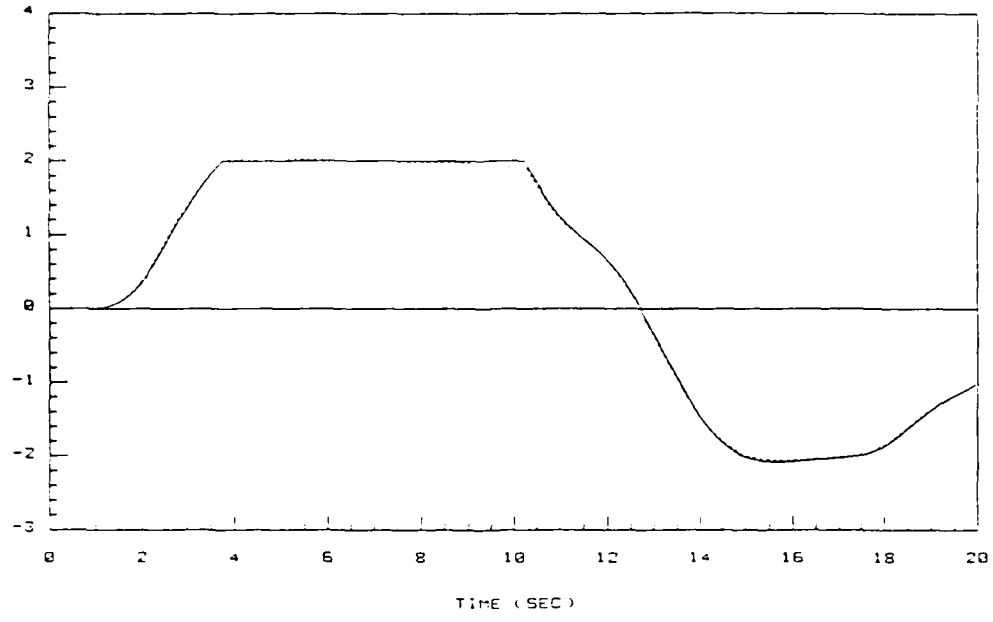

Figure D-1. Flight path angle command and response (deg). "Clipped" flight path command.

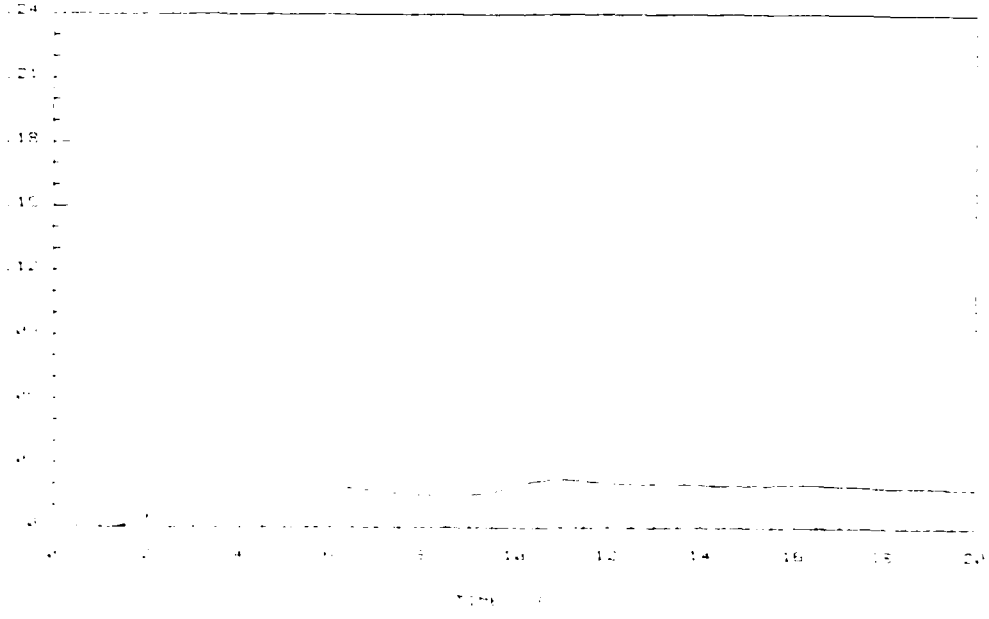

Figure D-2. Flight path angle tracking performance index (deg). "Clipped" flight path command.

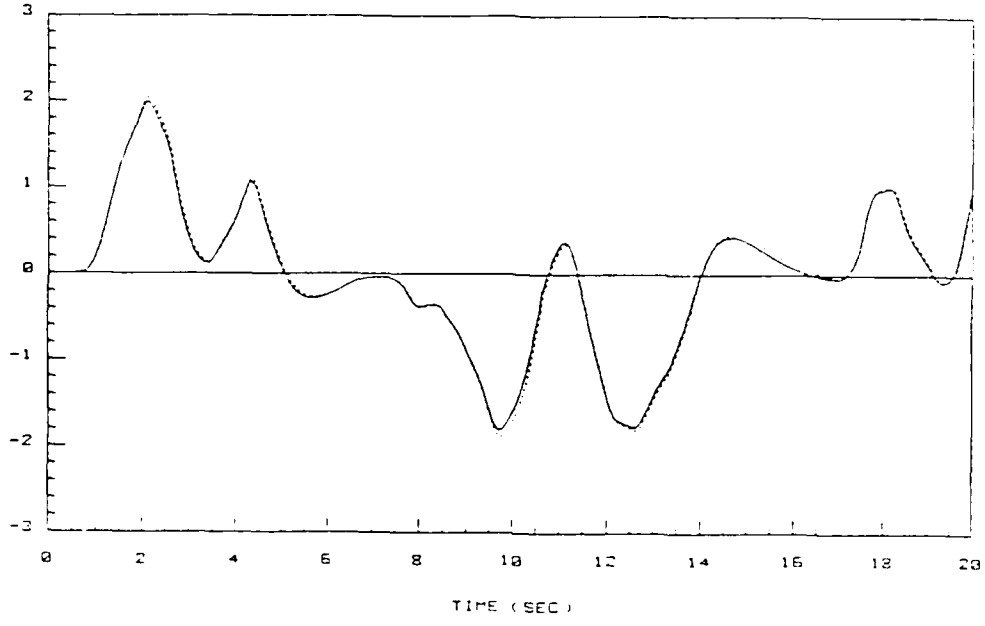

Figure D-3. Pitch rate command and response (deg/sec).
"Clipped" flight path command.

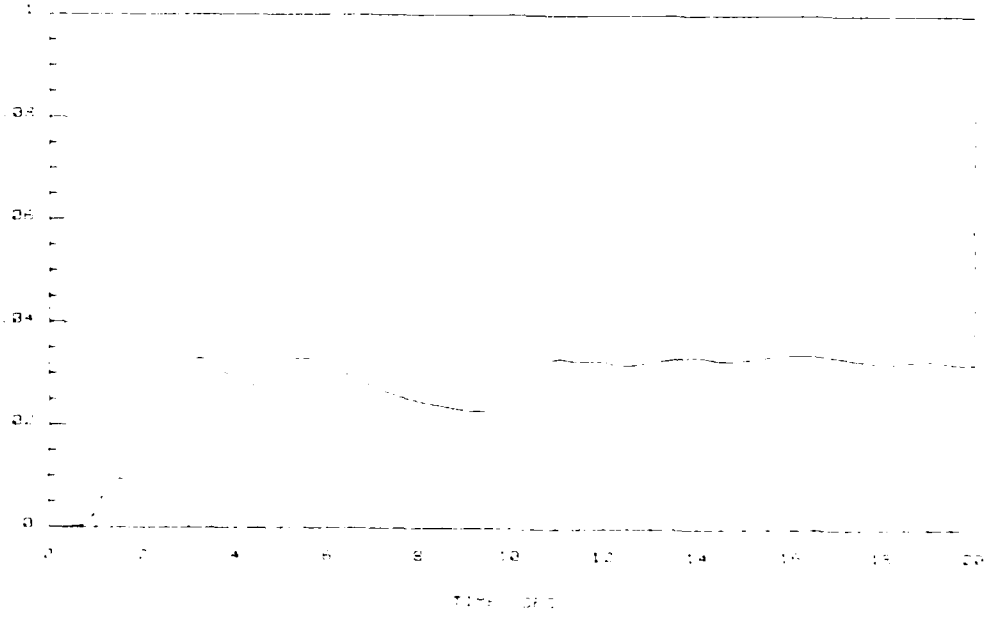

Figure D-4. Pitch rate tracking performance index (deg/sec).
"Clipped" flight path command.

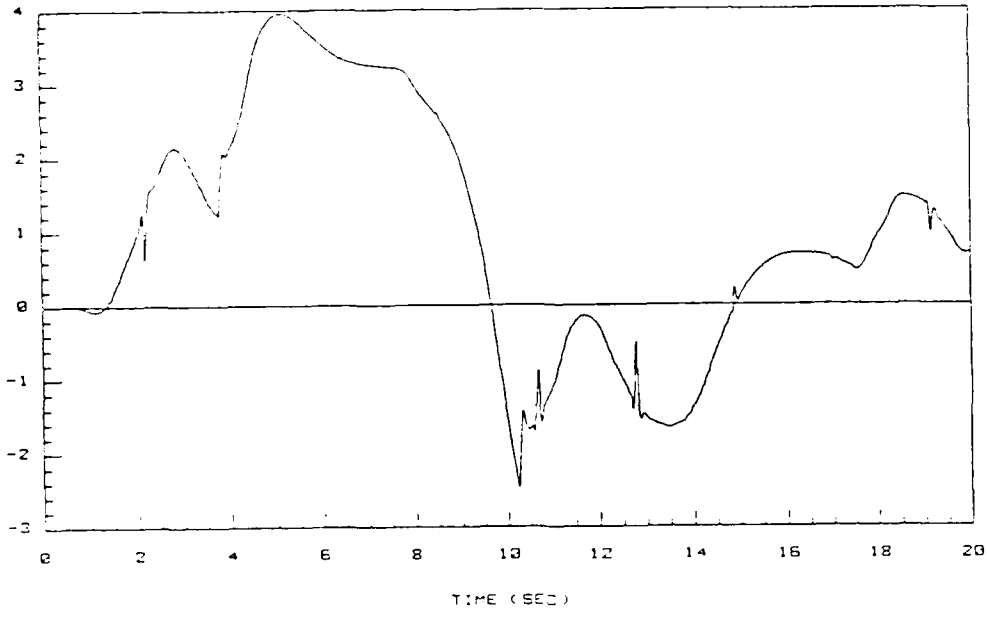

Figure D-5. Elevator deflection (deg).
"Clipped" flight path command.

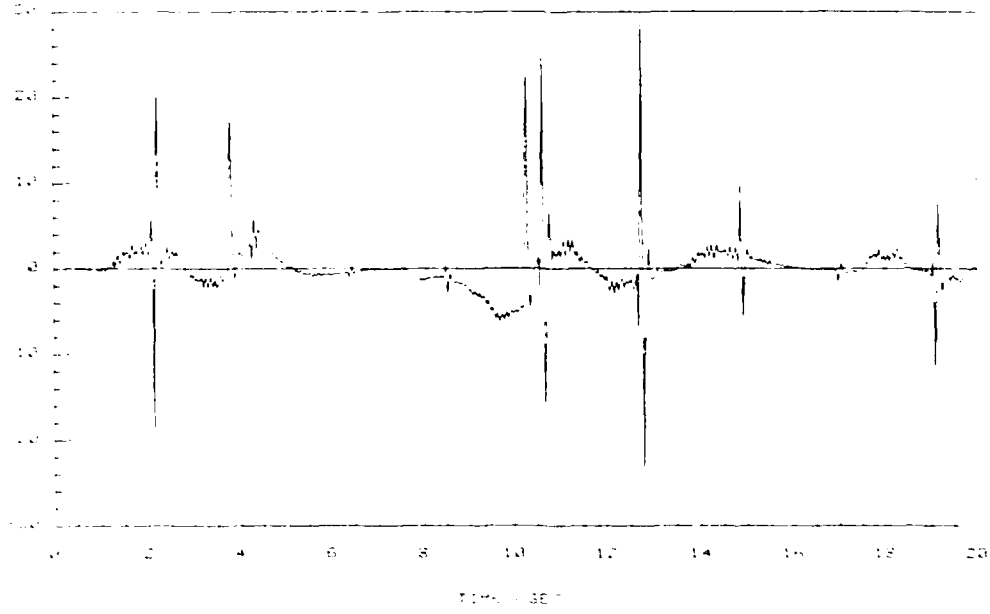

Figure D-6. Elevator deflection rate (deg/sec).
"Clipped" flight path command.

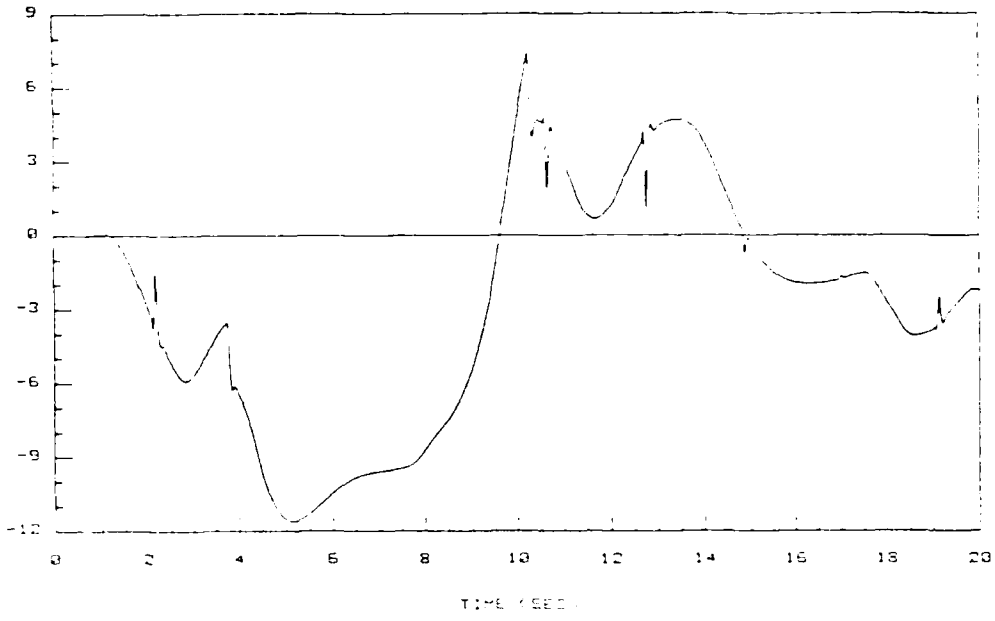

Figure D-7. Flaperon deflection (deg).
"Clipped" flight path command.

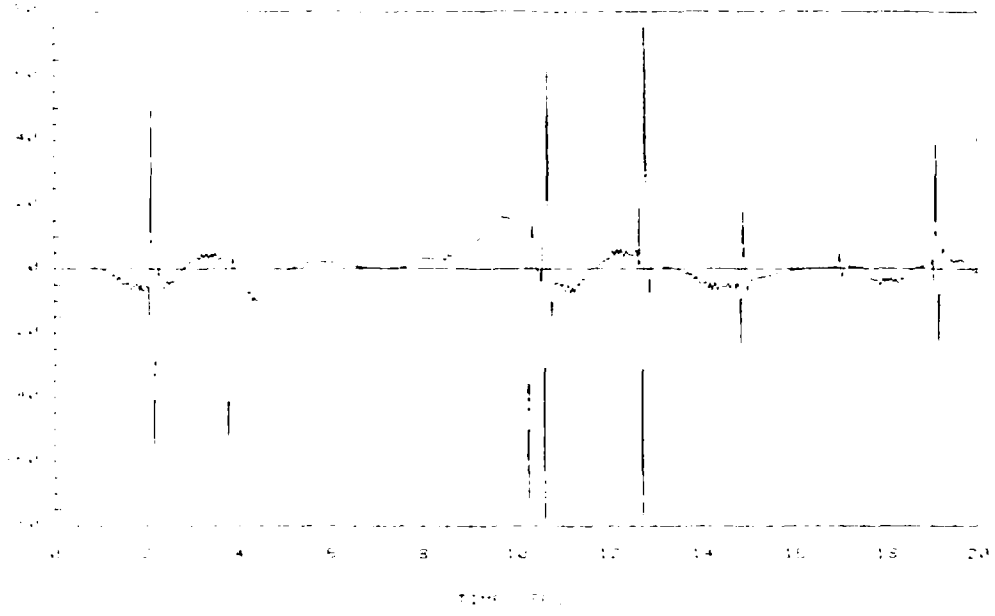

Figure D-8. Flaperon deflection rate (deg/sec).
"Clipped" flight path command.

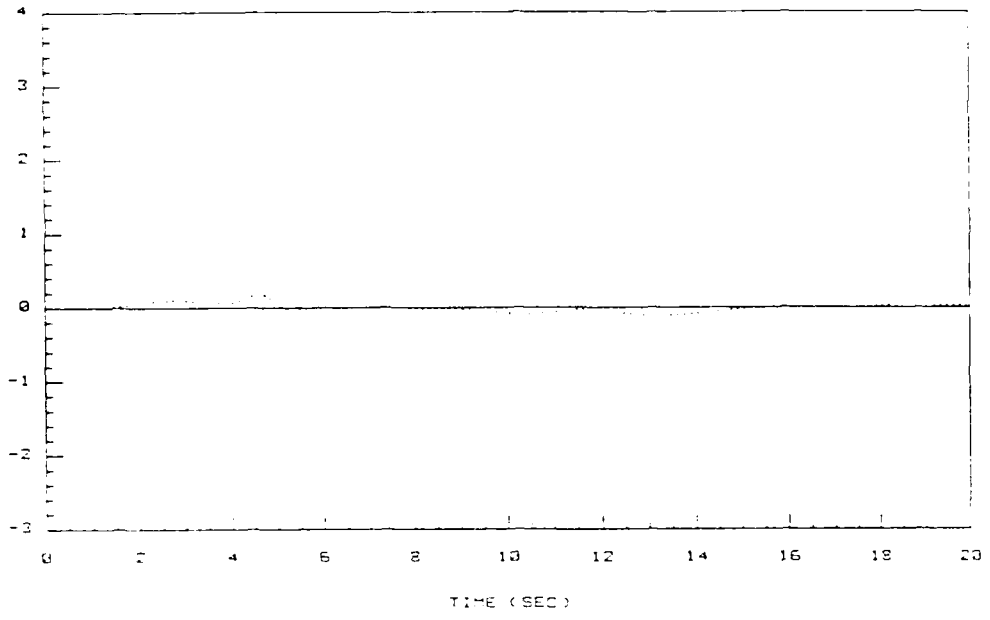

Figure D-9. Flight path angle command and response (deg).
Flight path command = 0 deg. No integrator limiter in control law.

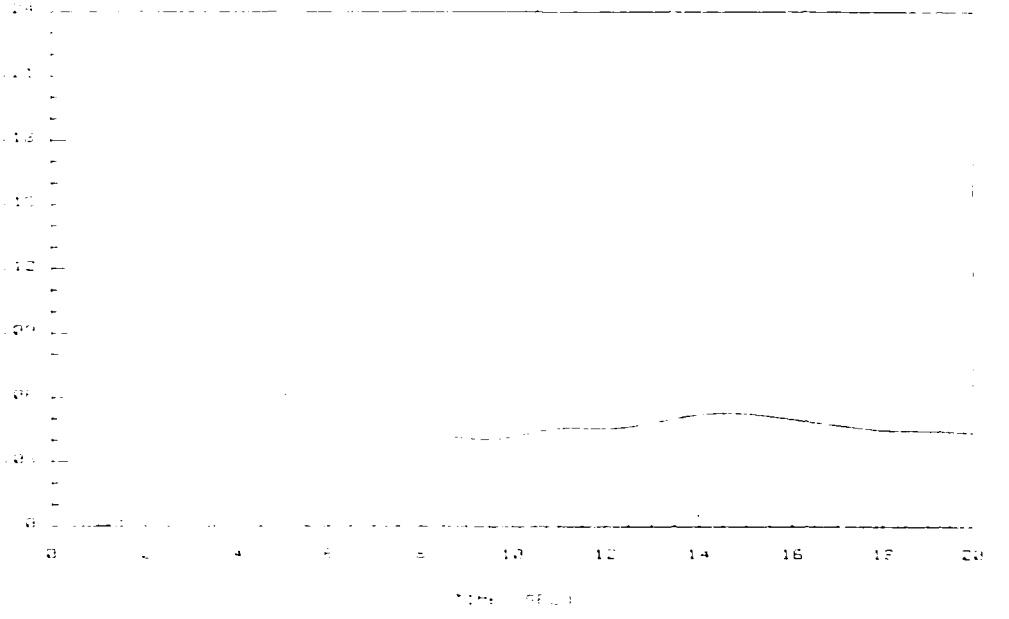

Figure D-10. Flight path angle tracking performance index (deg).
Flight path command = 0 deg. No integrator limiter in control law.

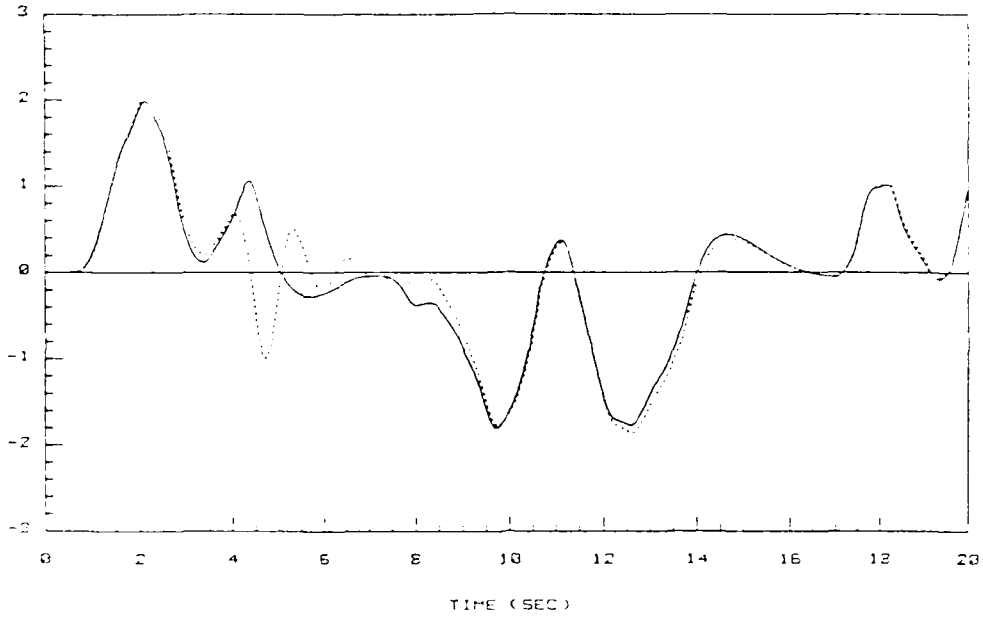

Figure D-11. Pitch rate command and response (deg/sec).
Flight path commnad = 0 deg. No integrator limiter in control law.

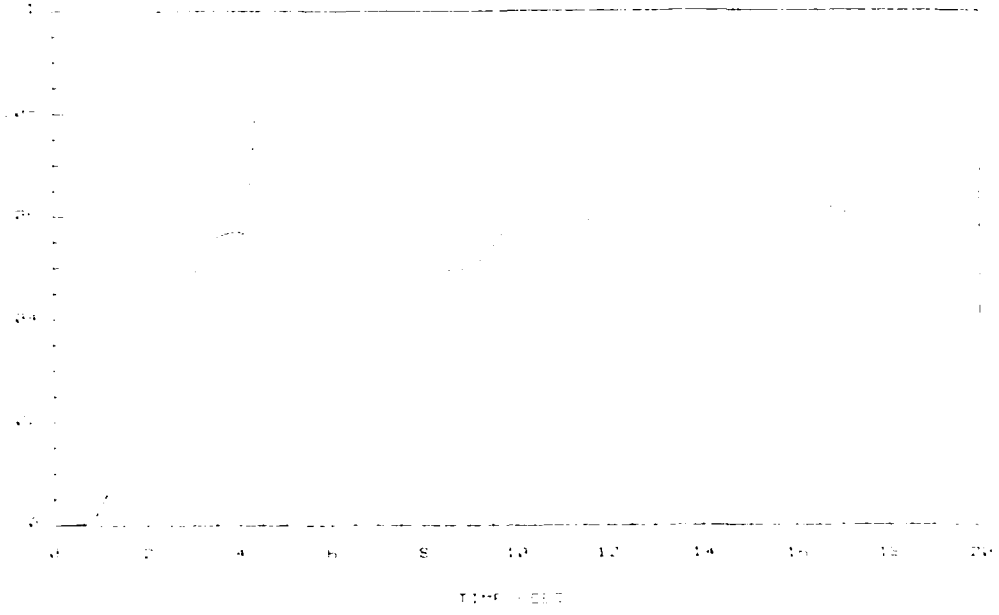

Figure D-12. Pitch rate tracking performance index (deg/sec).
Flight path command = 0 deg. No integrator limiter in control law.

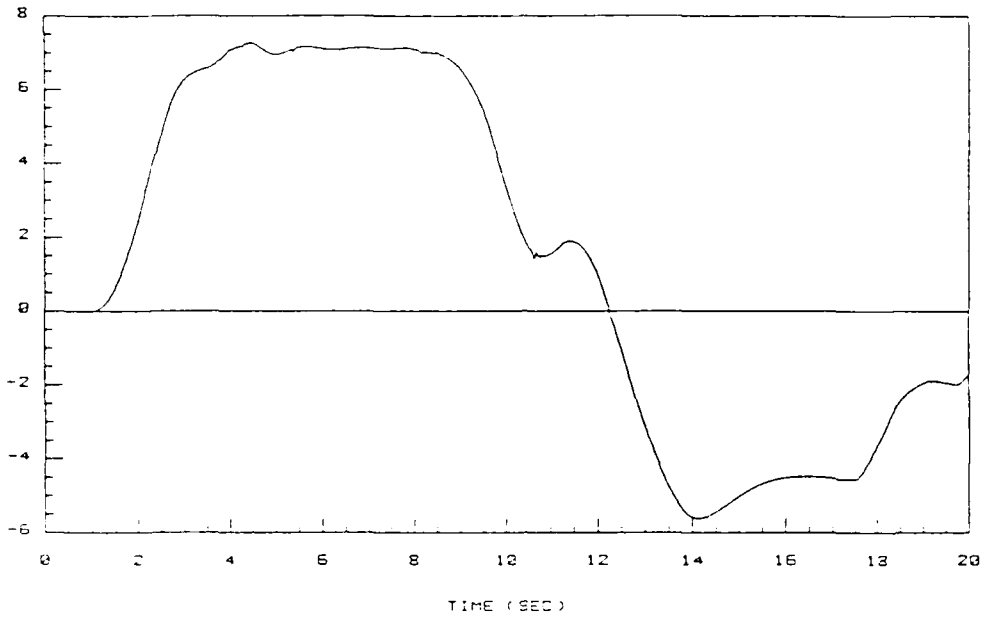

Figure D-13. Elevator deflection (deg).
Flight path command = 0 deg. No integrator limiter in control law.

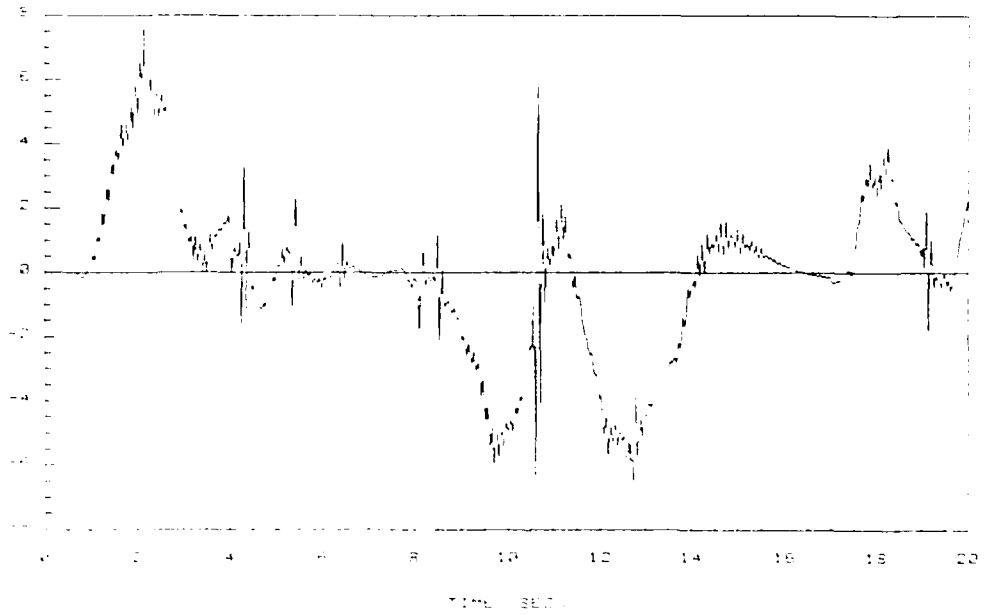

Figure D-14. Elevator deflection rate (deg/sec).
Flight path command = 0 deg. No integrator limiter in control law.

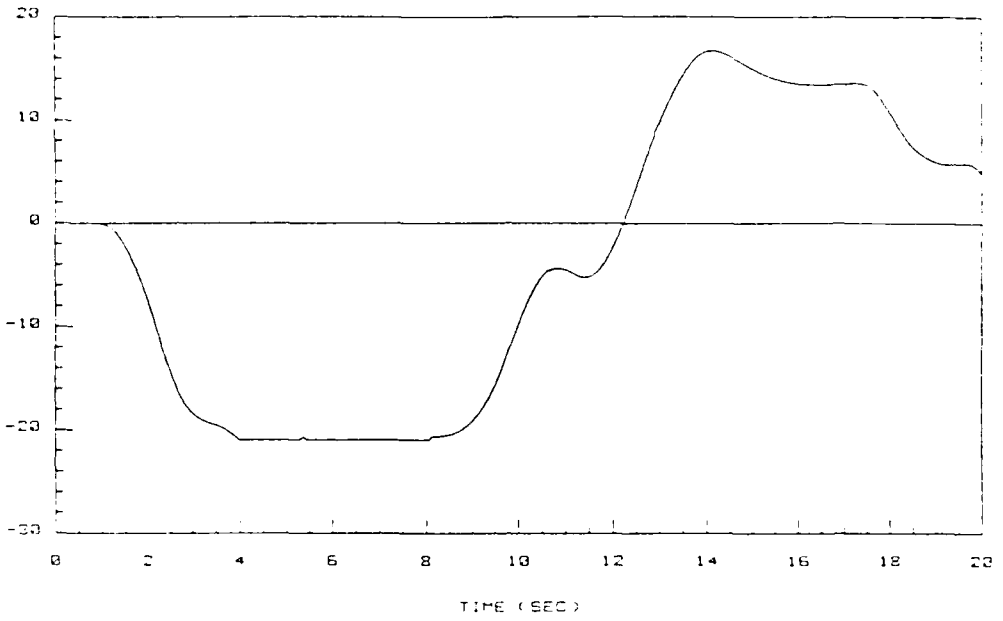

Figure D-15. Flaperon deflection (deg).
Flight path command = 0 deg. No integrator limiter in control law.

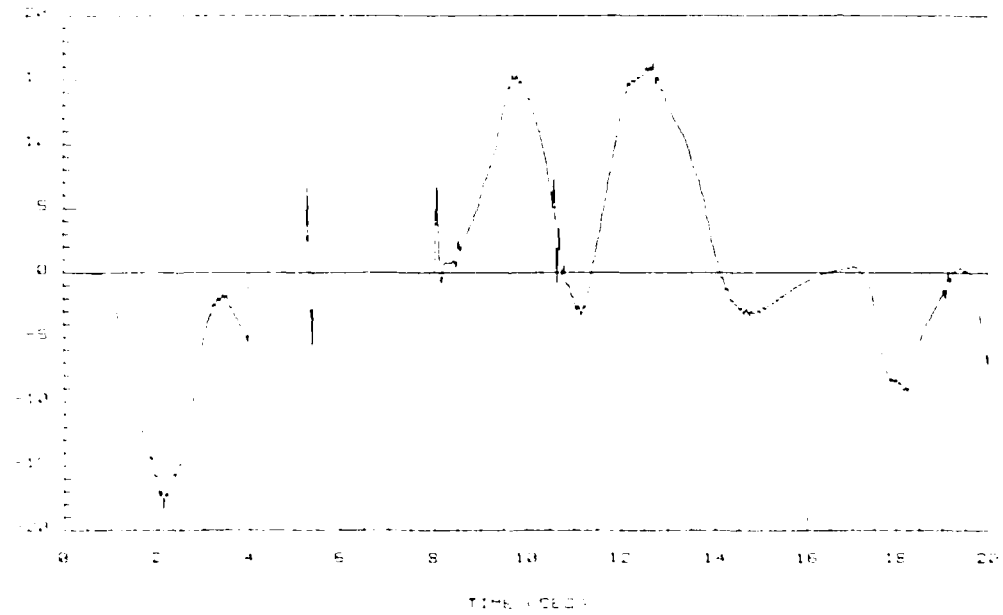

Figure D-16. Flaperon deflection rate (deg/sec).
Flight path command = 0 deg. No integrator limiter in control law.

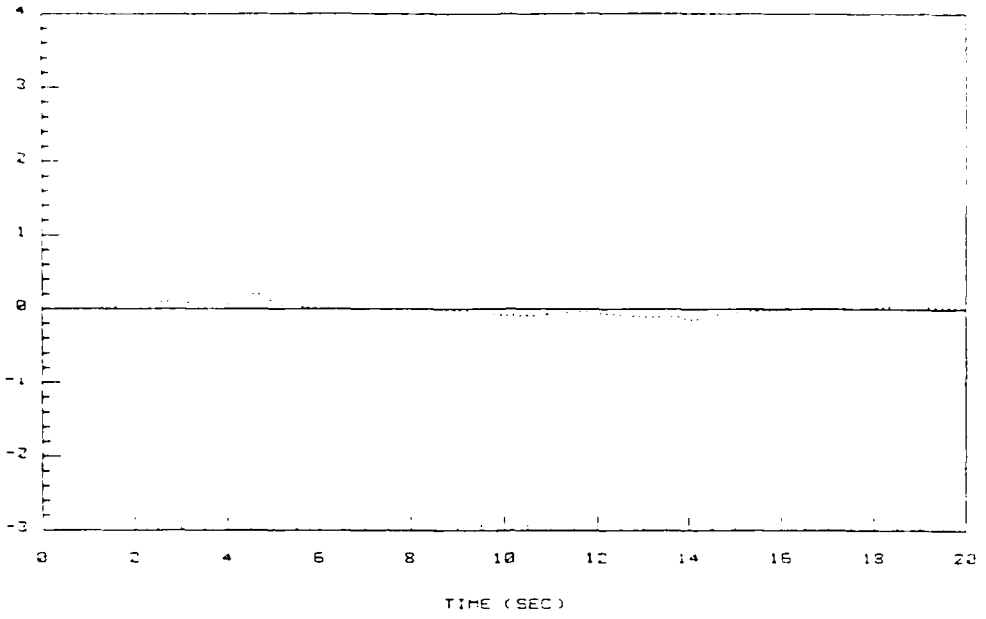

Figure D-17. Flight path angle command and response (deg). Flight path command = 0 deg. Control law with integrator limiter.

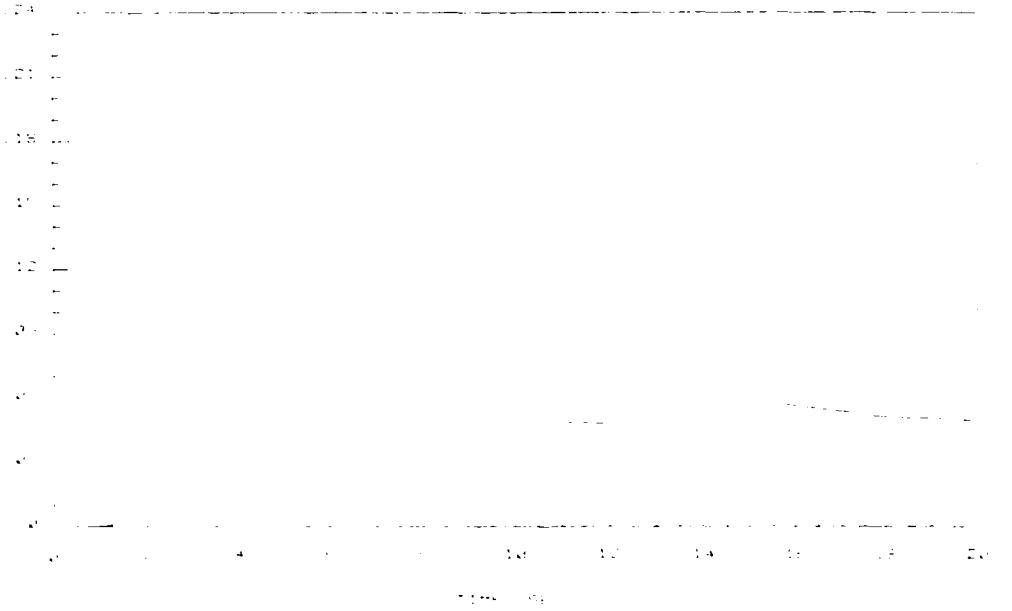

Figure D-18. Flight path angle tracking performance index (deg). Flight path command = 0 deg. Control law with integrator limiter.

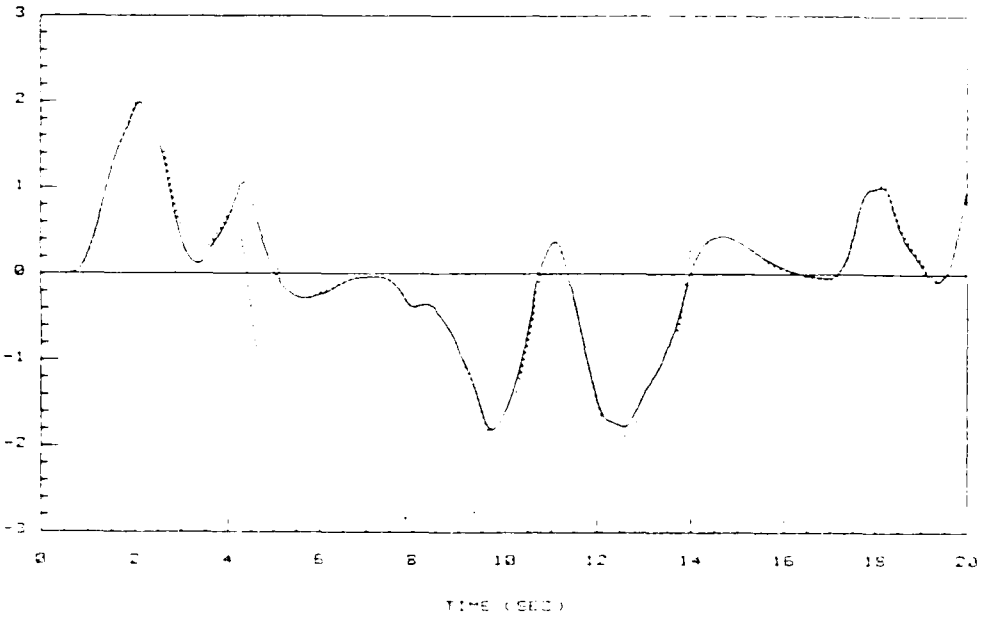

Figure D-19. Pitch rate command and response (deg/sec).
Flight path commnad = 0 deg. Control law with integrator limiter.

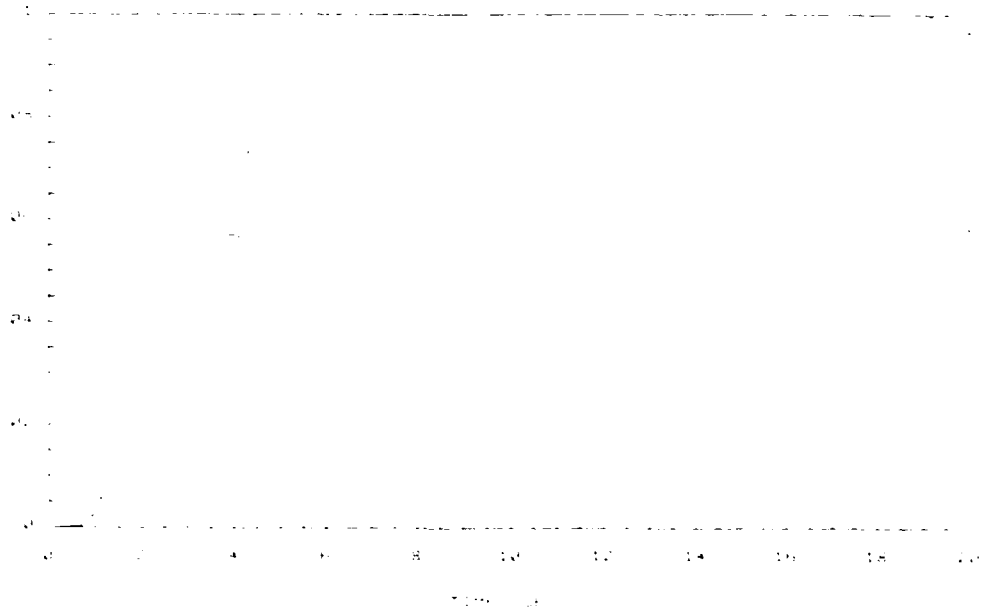

Figure D-20. Pitch rate tracking performance index (deg sec).
Flight path command = 0 deg. Control law with integrator limiter.

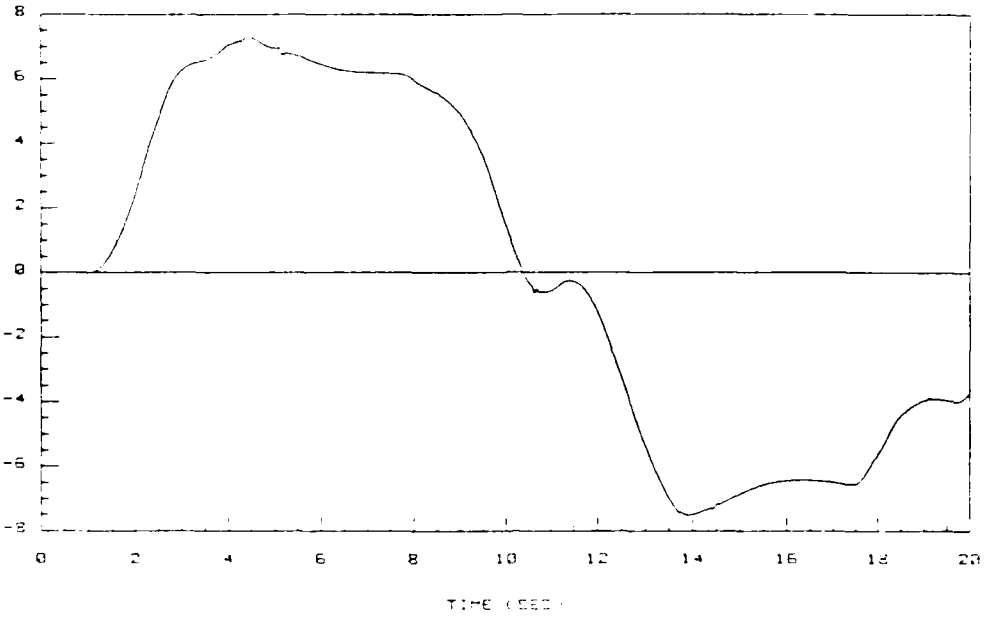

Figure D-21. Elevator deflection (deg).
Flight path command = 0 deg. Control law with integrator limiter.

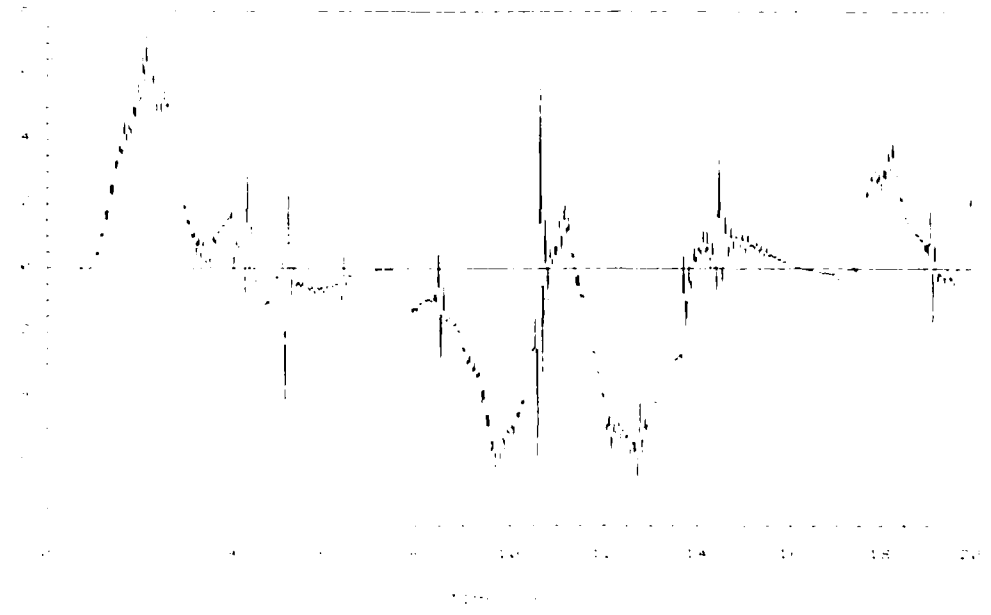

Figure D-22. Elevator deflection rate (deg/sec).
Flight path command = 0 deg. Control law with integrator limiter.

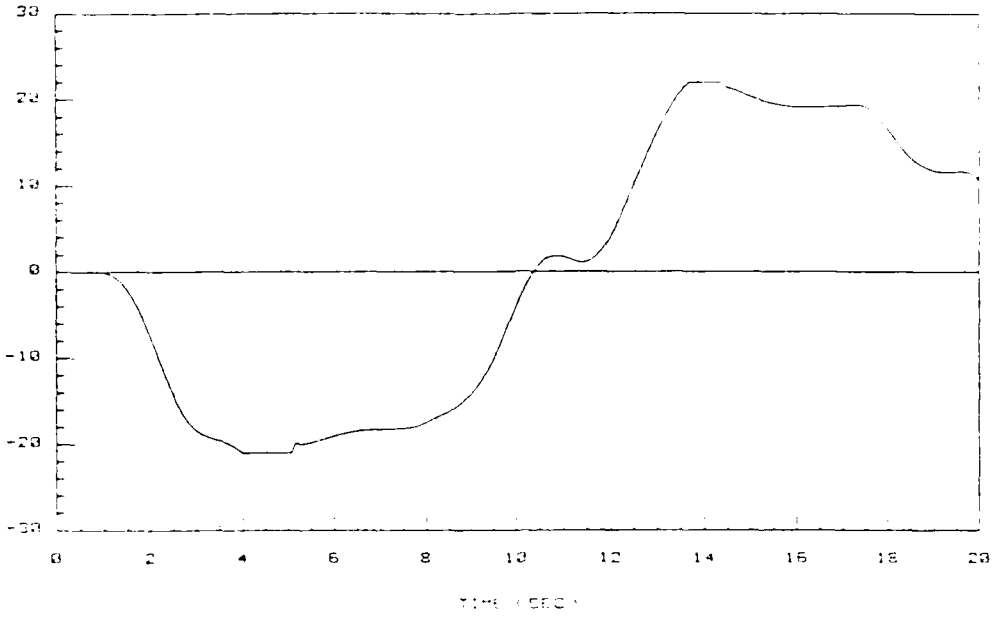

Figure D-23. Flaperon deflection (deg).
Flight path command = 0 deg. Control law with integrator limiter.

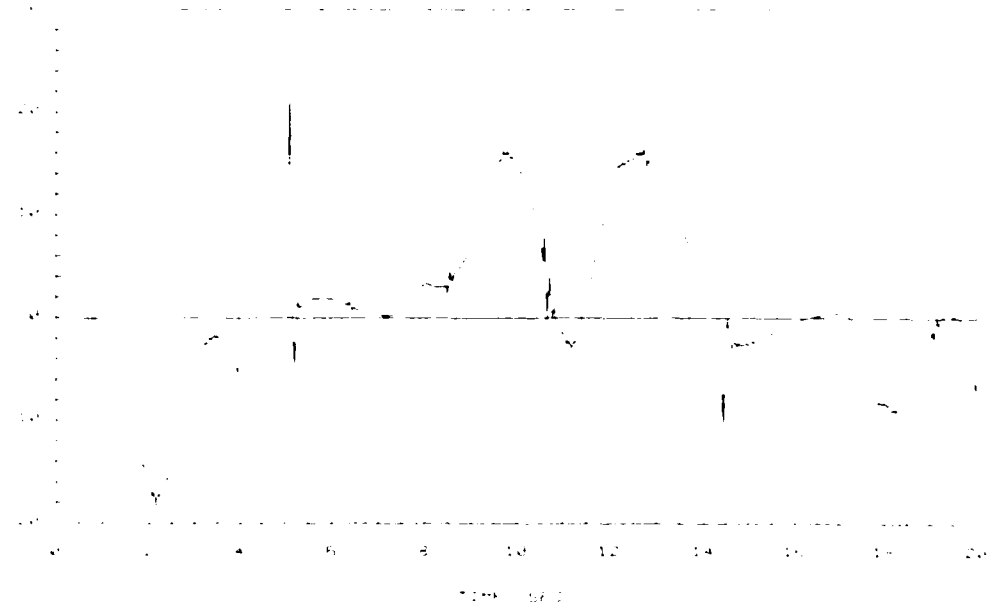

Figure D-24. Flaperon deflection rate (deg/sec).
Flight path command = 0 deg. Control law with integrator limiter.

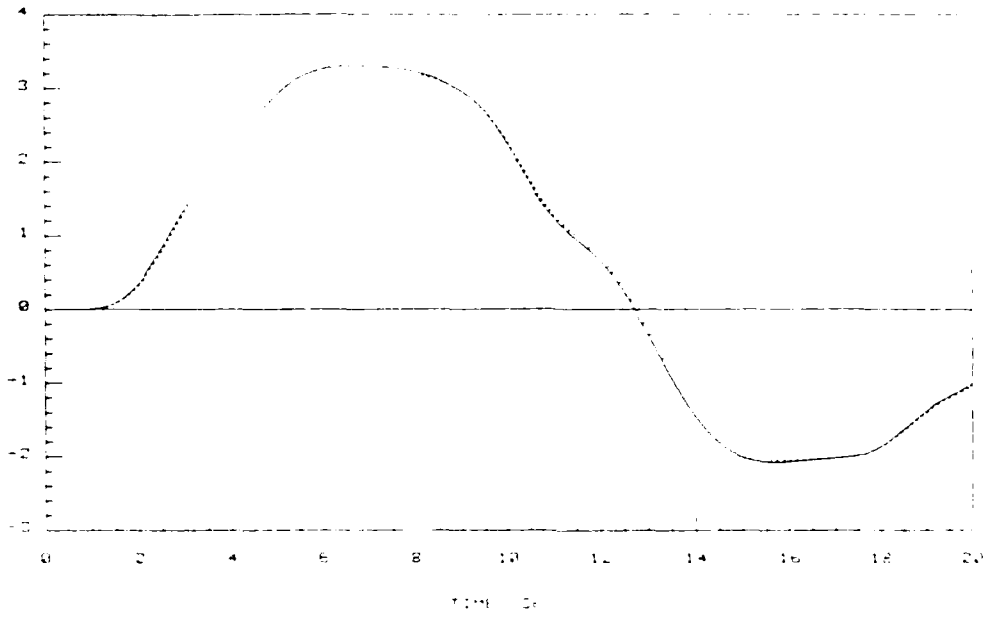

Figure D-25. Flight path angle command and response (deg).
Pitch rate command = 0 deg/sec. Control law with integrator limiter.

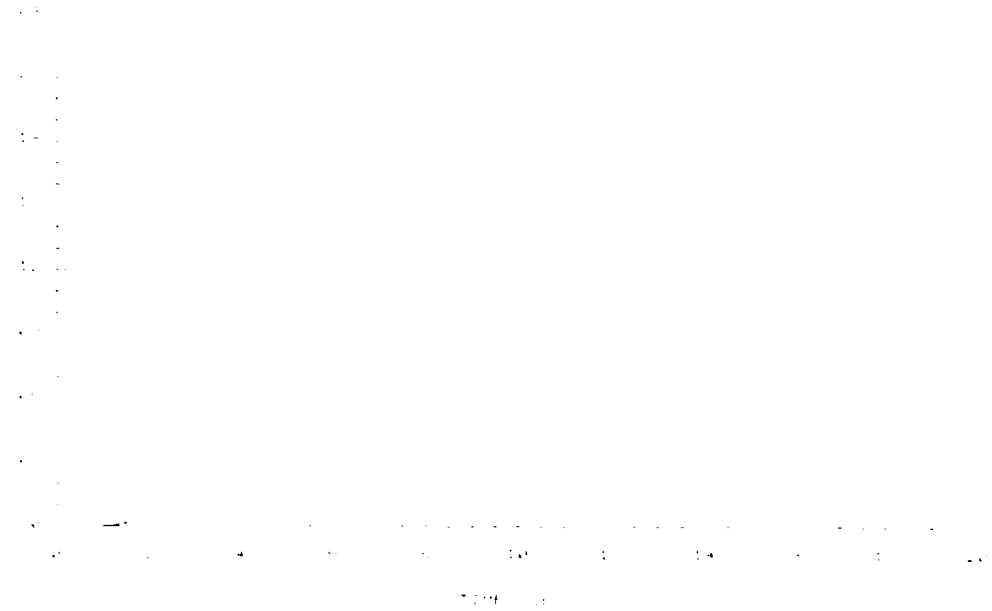

Figure D-26. Flight path angle tracking performance index (deg).
Pitch rate command = 0 deg sec. Control law with integrator limiter.

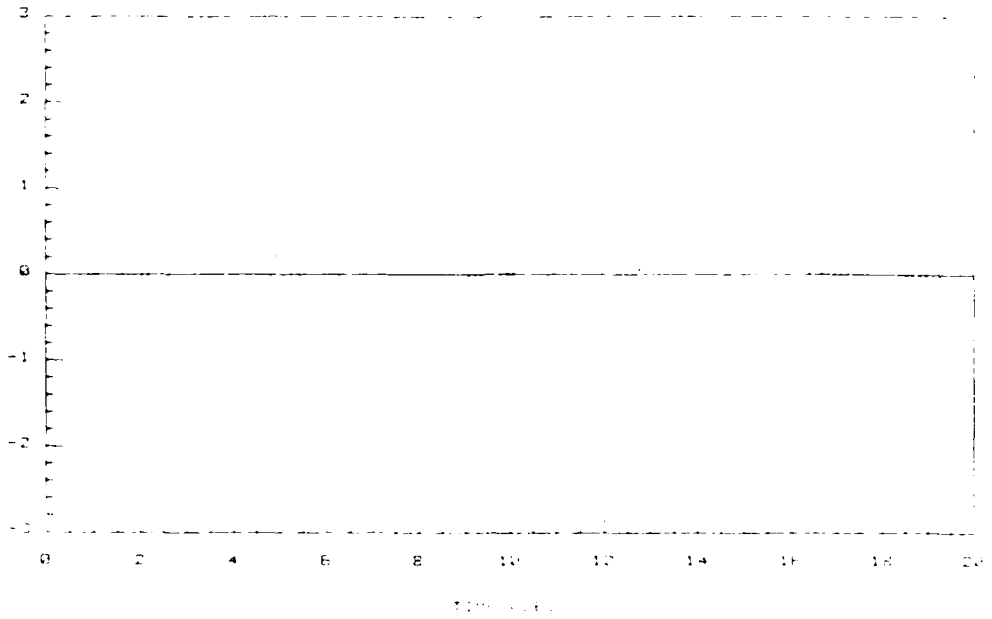

Figure D-27. Pitch rate command and response (deg/sec).
Flight path command = 0 deg. Control law with integrator limiter.

Figure D-28. Pitch rate tracking performance index (deg sec).
Pitch rate command = 0 deg sec. Control law with integrator limiter.

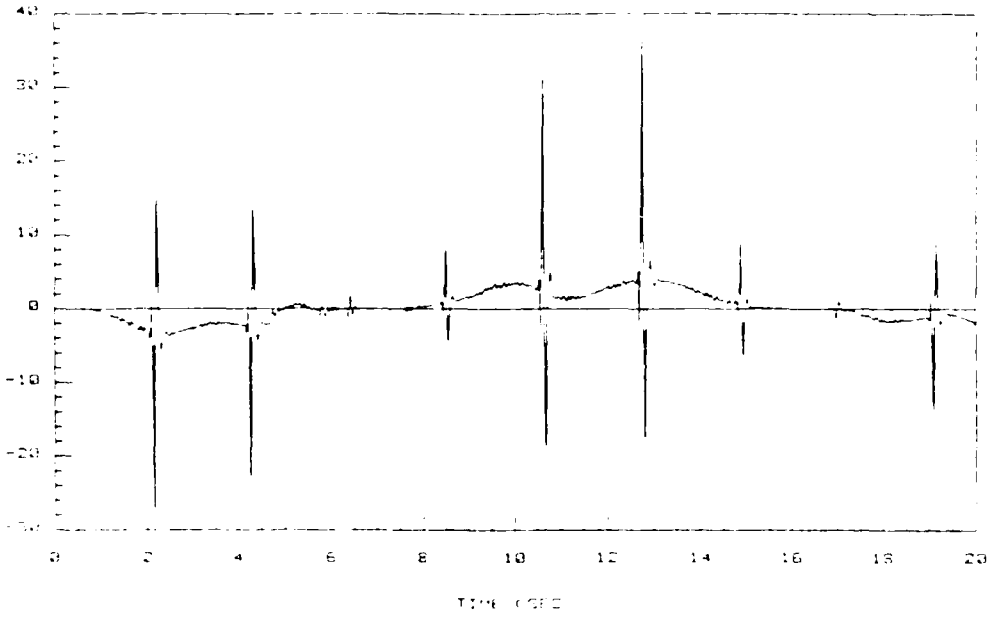

Figure D-29. Elevator deflection (deg).
Pitch rate command = 0 deg/sec. Control law with integrator limiter.

Figure D-30. Elevator deflection rate (deg/sec).
Pitch rate command = 0 deg/sec. Control law with integrator limiter.

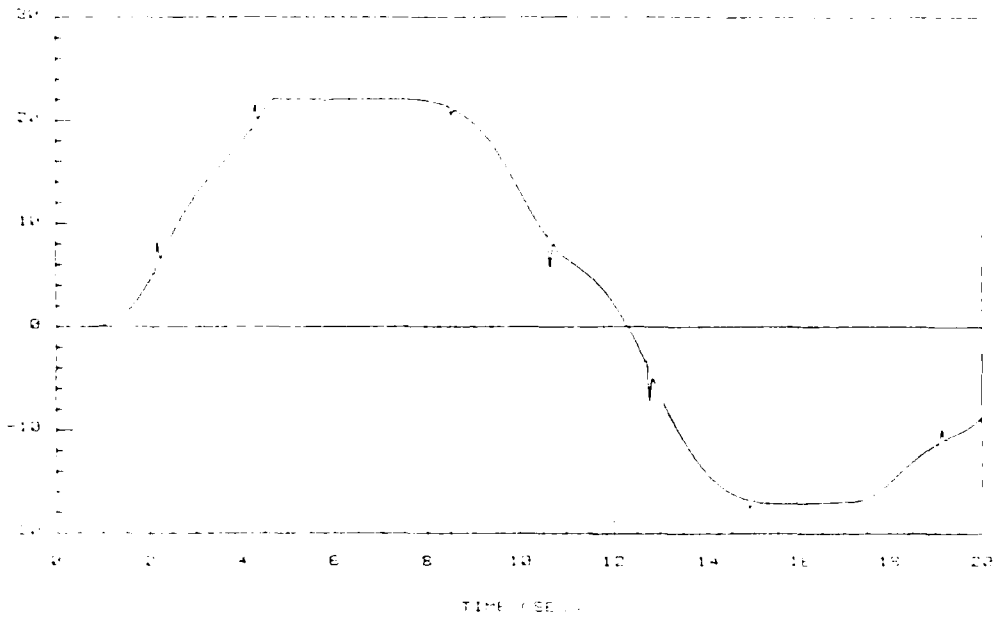

Figure D-31. Flaperon deflection (deg).
Pitch rate command = 0 deg/sec. Control law with integrator limiter.

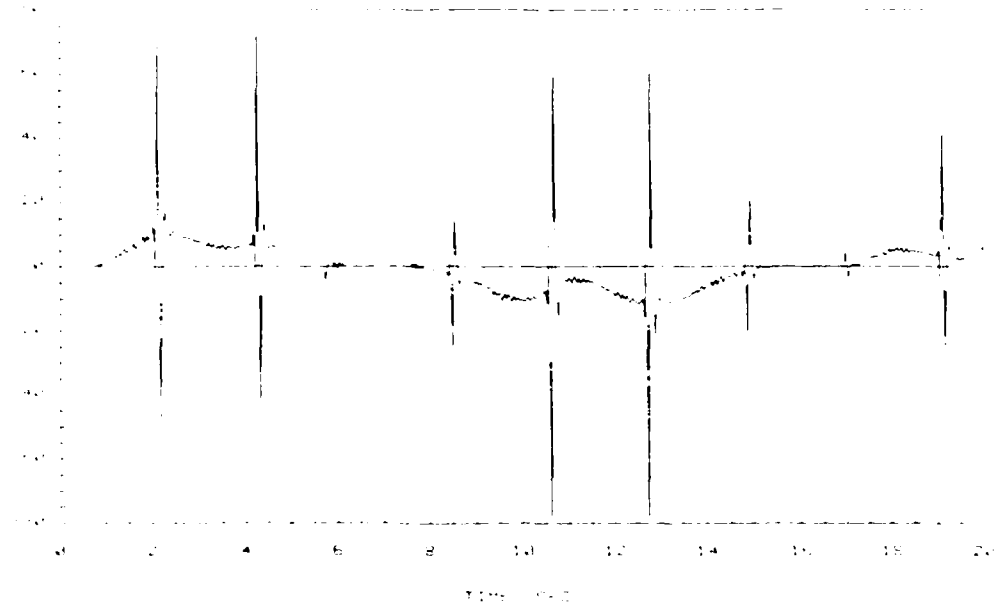

Figure D-32. Flaperon deflection rate (deg/sec).
Pitch rate command = 0 deg/sec. Control law with integrator limiter.

reaches its limit, in this occasion the amount of time that the surface remains at its maximum deflection is considerably less than in the previous simulation. Consequently, the aircraft reponses exhibit improved behavior with regards to the shorter duration of the instability, and the good tracking performance that follows once the commanded control surface deflections fall back within the given constraints for this example.

Finally, the system is tested with the pitch rate command set to 0 deg/sec, while the flight path command is set as in the original maneuver. The integrator limiter is also used in this simulation. The aircraft responses for this simulation are are presented in Figures D-25 through D-32. Tracking performance is considered good, despite the presence of a small transient in the pitch rate response caused by a brief saturation of the flaperon deflection.

Overall, these time responses indicate that given sufficient control power and command maneuvers that are within the capabilities of the host vehicle, the issue of functional uncontrolability (as it applies in this thesis) does not precludes the tracking of decoupled command inputs.

Bibliography

1. Ahmed, H. M., J. M. Delosme, and M. Morf, "Highly Concurrent Computing Structures for Matrix Arithmetic and Signal Processing," Computer, 15: 65-82 (1982).

2. Anderson, B. D. O., "Adaptive Systems, Lack of Persistency of Excitation and Bursting Phenomena," Automatica, 21: 247-258 (1985).

3. Anderson, P., Adaptive Forgetting Through Multiple Models. PhD Dissertation. Report LiTH-ISY-I-0638, Linkoping University, Linkoping, Sweden, 1983.

4. Astrom, K. J., and B. Wittenmark. Computer Controlled Systems Theory and Design. New Jersey: Prentice-Hall Inc., 1984.

5. Astrom, K. J., "Theory and Applications of Adaptive Control - A Survey," Automatica, 19: 471-486 (1983).

6. Astrom, K. J., "Stochastic Theory and Some of its Industrial Applications," Proceedings of the IFAC Symposium on Stochastic Control, Budapest, Hungary, 1974.

7. Barfield, A. F., Multivariable Control Laws for the AFTI F-16. MS Thesis, GE/EE/83S-4. School of Engineering, Air Force Institute of Technology, Wright-Patterson AFB OH, USA, 1983.

8. Barry, J., and A. E. Schelhorn, "In-Flight Simulators - Powerful Tools for Flight Research and Development," Proceedings of the IEEE National Aerospace Conference. 431-438. Dayton, OH, USA. May 1985.

9. Barry, J., and A. E. Schelhorn, "A Modest Proposal for a New Fighter In-Flight Simulator," AIAA 22nd Aerospace Sciences Meeting, Reno, Nevada, USA. Jan 1984.

10. Bierman, G. J., Factorization Methods for Discrete Sequential Estimation, New York: Academic Press, 1977.

11. Bokor, J., and L. Keviczky, "ARMA Canonical Forms Obtained from Constructibility Invariants," International Journal of Control, 45 (3): 861-873 (1987).

12. Chisci, L., and E. Mosca, "Parallel Architectures for RLS with Directional Forgetting," International Journal of Adaptive Control and Signal Processing, 1 (1): 69-88 (1987).

13. D'azzo, J. J., Lecture materials distributed in EE 7.08, Design of Linear Multivariable Feedback Control Systems. School of Engineering, Air Force Institute of Technology (AU), Wright-Patterson AFB OH, April 1985.

14. D'azzo, J. J., and C. Houpis. Linear Control Systems Analysis and Design (Second Edition). New York: McGraw-Hill, 1981.

15. Etkin, B. Dynamics of Atmosferic Flight, New York: John Wiley and Sons, Inc., 1972.

16. Fortescue, T. R., L. S. Kersherbaum, and B. E. Ydstie, "Implementation of Self Tunning Regulators with Variable Forgetting Factors," Automatica, 17: 831-835 (1981).

17. Guidorzi, R. P., "Invariants and Canonical Forms for Systams Structural and Parametric Identification," Automatica, 17: 117-133 (1981).

18. Guidorzi, R. P., "Canonical Structures in the Identification of Multivariable Systems," Automatica, 11: 361-374 (1975).

19. Hagglund, T., New Estimation Techniques for Adaptive Control. PhD Dissertation. Report LUTFD2/(TFRT-1025)/1-120/(1983), Department of Automatic Control, Lund Institute of Technology, Lund, Sweden, December 1983.

20. Hartman, U., and V. Krebs, "Command and Stability Systems for Aircraft: A New Digital Adaptive Approach," Automatica, 16: 135-146 (1981).

21. Hentz, K. P., Feasibility Analysis of Moving Bank Multiple Model Adaptive Estimation and Control Algorithms. MS Thesis, GE/ENG/84D-32. School of Engineering, Air Force Institute of Technology, Wright-Patterson AFB, OH, USA, 1984.

22. Houpis C., and G. B. Lamont. Digital Control Systems Theory, Hardware, Software. New York: McGraw-Hill, 1985.

23. Integrated Systems Inc. MATRIXx. User's Guide. Palo Alto, California, USA, 1982.

24. Isermann, R., and K. H. Lachmann, "Parameter-Adaptive Control with Configuration Aids and Supervision Functions," Automatica, 21: 625-638 (1985).

25. Isermann, R., "Parameter-Adaptive Control Algorithms – A Tutorial," Automatica, 18: 513-528 (1982).

26. Jover, J. M., and T. Kailath, "A Parallel Architecture for Kalman Filter Measurement Update and Parameter Estimation," Automatica, 22: 43-57 (1986).

27. Kokotovic, P. V., and A. H. Haddad, "Controllability and Time-Optimal Control of Systems with Slow and Fast Modes," IEEE Transactions on Automatic Control, vol AC-20: 111-113 (1975).

28. Ljung, L., and T. Soderstrom, Theory and Practice of Recursive Icentification, MIT Press, Cambridge, Mass. USA, 1983.

29. Markman, S. R., "Capabilities of Airborne and Ground Based Flight Simulation," SAE Aerospace Technology Conference & Exposition. 35-42. Long Beach, California, USA. Oct 1985.

30. Maybeck, P. Stochastic Models, Estimation and Control, Vol 1. New York: Academic Press, 1979.

31. Porter, B., Manganas, A., "Design of Adaptive Direct Digital Flight-Mode Control Systems Incorporating Recursive Step-Response Matrix Identifiers for High Performance Aircraft," Proceedings of the IEEE National Aerospace Conference, Dayton, OH, USA, May 1986.

32. Porter, B., Self-Designing Digital Control Systems. Progress and Forecast Report. Grant AFOSR-85-0208. Department of Aeronautical and Mechanical Engineering, University of Salford, Salford, England, November 1985.

33. Porter, B., A. Manganas, and T. Manganas, "Design of Fast Non-interacting Digital Flight-Mode Control Systems for High Performance Aircraft," Proceedings of the AIAA Guidance, Navigation,and Control Conference, Snowmass, Colorado, USA. August 1985.

34. Porter, B., "Design of Direct Digital Flight-Mode Control Systems for High Performance Aircraft Using Step-Response Matrices," Proceedings of the IEEE National Aerospace Conference. 507-513. Dayton, OH, USA, May, 1985.

35. Porter, B., and A. H. Jones, "Time Domain Identification of Non-Minimum Phase Characteristics of Linear Multivariable Plants," Proceedings of the IFAC Simposium on Identification and System Parameter Estimation, York, UK, 1985.

36. Porter, B., Design of high Performance Tracking Systems. Technical Report: AFWAL-TR-82-3032, Air Force Wright Aeronautical Laboratories, Wright-Patterson AFB, Ohio, USA, 1982.

37. Porter, B., Shenton, A. T., "Singular Perturbation Analysis of the Transfer Function Matrices of a Class of Multivariable Linear Systems," Internatinal Journal of Control, Vol 21, No. 4: 655-660 (1975).

38. Porter, B., and A. Bradshaw. "Design of Linear Multivariable Continuous-Time Tracking Systems," International Journal of Systems Science, Vol 5, No. 12: 1155-1164 (1974)

39. Reynolds P. A., et. al., Capability of the Total In-Flight Simulator (TIFS). Technical Report: AFFDL-TR-72-39, Air Force Flight Dynamics Laboratory, Wright-Patterson AFB, Ohio, USA, July 1972.

40. Ridgely D. B., and S. S. Banda, Introduction to Robust Multivariable Control. Technical Report: AFWAL-TR-85-3102, Air Force Wright Aeronautical Laboratories, Wright-Patterson AFB, Ohio, USA, February 1986.

41. Roy, R. H., H. A. Saberi, and R. A. Walker, Helicopter Vibration Control Design Research: ISI Report 45. Contract NAS2-11548. Integrated Systems Inc. 101 University Ave., Palo Alto, CA, USA. August 1984.

42. Rynaski, E. G., Flight Research Department, CALSPAN Corp. Memorandum on Improved Model-Following. ARVIN/CALSPAN ATC Buffalo N.Y., USA. 20 July 1984.

43. Thornton, C. L., and G. J. Bierman, "UDU^T Covariance Factorization for Kalman Filtering," In C. T. Leondes, ed.: Control and Dynamic Systems, 16: 177-248. Academic Press, New York, (1980).

44. Thornton, C. L., and G. J. Bierman, "Gram-Schmidt Algorithms for Covariance Propagation," International Journal of Control, 25: 243-260, (1977).

45. Wittenmark, B., and K. J. Astrom, "Practical Issues in the Implementation of Self-Tuning Control," Automatica, 20: 595-605 (1984).

46. Wittenmark, B., "A Two-Level Estimator for Time Varying Parameters," Automatica, 15: 85-89 (1979).

47. Wong, D., W. G. Hoefer, and M. F. Fernandez, "An Advanced Parameter Estimation Coprocessor," Proceedings of the IEEE National Aerospace Conference. 112-118. Dayton, OH, USA, May 1986.

48. Young, P., "A Second Generation Adaptive Autostabilization System for Airborne Vehicles," Automatica, 17: 459-470 (1981).

VITA

Luis A. Piñeiro is a native of Bayamon, Puerto Rico. He graduated from the University of Puerto Rico, Mayaguez campus, in 1981 with a Bachelor of Science in Electrical Engineering. He was commisioned through the Air Force ROTC program and assigned to the Aeronautical Systems Division, Deputy for Engineering, Computer Resources Branch at Wright Patterson AFB. He worked as a computer engineer in the planning of future Directorate computer facilities, and providing engineering support to the F-16 System Program Office.

In 1983 he was assigned to the Control Synthesis Branch, Flight Control Division of the Air Force Flight Dynamics Laboratory. His work involved the design of digital controllers and interfaces to ground flight simulation systems, and the development of a distributed computing simulation architechture through the use of "smart" simulation cockpits for increased simulation capability and fidelity.

Most recently, he has been assigned to the Flight Dynamics Laboratory's Advanced Development Branch were he is responsible for overseeing the flight control and simulation systems design on the Variable stability In-flight Simulator Test Aircraft (VISTA) program. He is also working towards and advanced degree at the Air Force Institute of Technology, Wright Patterson AFB, Ohio.

REPORT DOCUMENTATION PAGE

Form Approved
OMB No 0704-0188

1a. REPORT SECURITY CLASSIFICATION: UNCLASSIFIED	1b. RESTRICTIVE MARKINGS
2a. SECURITY CLASSIFICATION AUTHORITY	3. DISTRIBUTION/AVAILABILITY OF REPORT: Approved for public release; distribution unlimited.
2b. DECLASSIFICATION/DOWNGRADING SCHEDULE	
4. PERFORMING ORGANIZATION REPORT NUMBER(S): AFIT/GE/ENG/87D-74	5. MONITORING ORGANIZATION REPORT NUMBER(S)
6a. NAME OF PERFORMING ORGANIZATION: School of Engineering; 6b. OFFICE SYMBOL (If applicable): AFIT/ENG	7a. NAME OF MONITORING ORGANIZATION
6c. ADDRESS (City, State, and ZIP Code): Air Force Institute of Technology, Wright-Patterson AFB OH 45433	7b. ADDRESS (City, State, and ZIP Code)
8a. NAME OF FUNDING/SPONSORING ORGANIZATION: Flight Dynamics Lab.; 8b. OFFICE SYMBOL (If applicable): AFWAL/FIGX	9. PROCUREMENT INSTRUMENT IDENTIFICATION NUMBER
8c. ADDRESS (City, State, and ZIP Code): Wright-Patterson AFB OH 45433	10. SOURCE OF FUNDING NUMBERS: PROGRAM ELEMENT NO; PROJECT NO; TASK NO; WORK UNIT ACCESSION NO

11. TITLE (Include Security Classification)

PARAMETER-ADAPTIVE MODEL-FOLLOWING FOR IN-FLIGHT SIMULATION

12. PERSONAL AUTHOR(S)

Luis A. Pineiro Aponte, B.S.E.E., Captain, USAF

13a. TYPE OF REPORT	13b. TIME COVERED	14. DATE OF REPORT (Year, Month, Day)	15. PAGE COUNT
MS Thesis	FROM _____ TO _____	1987 December	284

16. SUPPLEMENTARY NOTATION

17. COSATI CODES			18. SUBJECT TERMS (Continue on reverse if necessary and identify by block number)
FIELD	GROUP	SUB-GROUP	Multivariable Control, Flight Control System, Digital Control System, Adaptive Control System.
01	03		

19. ABSTRACT (Continue on reverse if necessary and identify by block number)

Thesis Advisor: Col. Daniel J. Biezad

Approved for Public Release: IAW AFR 190-1
Lynn Wilson 24 Feb 88
Dean

20. DISTRIBUTION/AVAILABILITY OF ABSTRACT: ☒ UNCLASSIFIED/UNLIMITED ☐ SAME AS RPT ☐ DTIC USERS	21. ABSTRACT SECURITY CLASSIFICATION
22a. NAME OF RESPONSIBLE INDIVIDUAL: John J. D'Azzo, Professor	22b. TELEPHONE (Include Area Code): (513)-255-3576 / 22c. OFFICE SYMBOL: AFIT/ENG

DD Form 1473, JUN 86 — Previous editions are obsolete — SECURITY CLASSIFICATION OF THIS PAGE

Abtract

In-flight simulations are normally accomplished by using model-following control laws which depend on accurate knowledge of the stability derivatives of the host aircraft. Degraded simulation performance may result if the stability derivatives deviate considerably from their presumed values. Gain scheduling is often employed to compensate for plant parameter variations, but this form of open-loop compensation usually requires extensive flight testing for proper fine tuning.

This thesis implements an adaptive, fast-sampling control law to compensate for changing aircraft parameters. The step-response matrix which is required for this implementation is identified recursively using a recently developed technique which does not require special "test" signals and which automatically discounts old data depending on the input excitation detected. Tracking fidelity is maintained despite parameter changes which occur either abruptly or slowly. Simulations are conducted, using a model of the AFTI/F-16 aircraft and the control design package $MATRIX_X$, to test the resulting adaptive system. Actuator position and rate limits are discussed. The performance of the resulting system is excellent and demonstrates the relative advantages of adaptive controllers for in-flight simulation. Recommendations are made for future analysis including the use of moving-bank estimators.

END
DATE
FILMED
4-88
DTIC